POAC

PROCEEDINGS

Volume 3

The 15th International Conference on Port and Ocean Engineering under Arctic Conditions

M-241

POAC'99

PROCEEDINGS OF THE 15TH INTERNATIONAL CONFERENCE ON PORT AND OCEAN ENGINEERING UNDER ARCTIC CONDITIONS

Espoo, Finland, August 23-27, 1999

VOL. 3

Jukka Tuhkuri and Kaj Riska, editors

Helsinki University of Technology
Ship Laboratory

Teknillinen korkeakoulu
Laivalaboratorio

Espoo 1999

Distribution:
Helsinki University of Technology
Ship Laboratory
P.O.Box 4100
FIN-02015 HUT, Finland
Tel. +358 9 451 3501
Fax +358 9 451 4173
E-mail: leila.silonsaari@hut.fi

ISBN 951-22-4619-8
ISBN 951-22-4620-1
ISSN 1456-3045

Tummavuoren Kirjapaino Oy
Vantaa 1999

PREFACE

This volume is the third of the three volumes of the Proceedings from the 15th International Conference on Port and Ocean Engineering under Arctic Conditions held at the Helsinki University of Technology, Finland, in August 1999. This Volume 3 contains 17 reviewed papers, 2 keynote lectures presented at the conference, lists of evaluators and conference participants, and also the final list of sponsors of the POAC'99 conference. Volumes 1 and 2 contain altogether 94 scientific papers, so the POAC'99 proceedings contain in total 111 reviewed papers. Volume 1 contains also description of the POAC'99 conference organisation. The photographs from different social events shown at the end of this volume were kindly provided for publication by Ms. Sharon Jeffers.

October 1999

Jukka Tuhkuri
Kaj Riska

TABLE OF CONTENTS

VOLUME 3

ACKNOWLEDGEMENTS

The POAC'99 conference was financially supported by the following organisations:

Academy of Finland
Aker Finnyards Oy
City of Espoo
Elomatic Oy
European Commission, DG XII
Finnair
Finnish Institute of Marine Research
Finnish Maritime Administration
Finnish Maritime Foundation
Fortum Oil and Gas Oy
Geological Survey of Finland
Helsinki University of Technology
ILS Ltd.
Kamewa Finland Ltd.
Kvaerner Masa-Yards Inc.
Technical Research Centre of Finland

PREVIOUS POAC CONFERENCES

1st	1971	Trondheim	Norway	
2nd	1973	Reykjavik	Iceland	
3rd	1975	Fairbanks	USA	
4th	1977	St. John's	Canada	
5th	1979	Trondheim	Norway	
6th	1981	Québec City	Canada	(jointly with IAHR)
7th	1983	Helsinki	Finland	
8th	1985	Narssarssuaq	Greenland	
9th	1987	Fairbanks	USA	
10th	1989	Luleå	Sweden	
11th	1991	St. John's	Canada	
12th	1993	Hamburg	Germany	
13th	1995	Murmansk	Russia	
14th	1997	Yokohama	Japan	(jointly with OMAE)
15th	1999	Helsinki	Finland	

PARTIAL LIST OF EVALUATORS

Abdelnour, R.
Aksenov, Y.
Alexandrov, V.
Appolonov, E.
Ash, J.
Belyashov, V.
Bond, J.
Brigham, L.
Brubaker, D.
Cavanie, A.
Cole, D.
Dempsey, J.
Daley, C.
Doble, M.
Edelman, G.
Eichen, H.
Eranti, E.
Eronen, H.
Ettema, R.
Evensen, G.
Flett, D.
Fransson, L.
Frederking, R.
Gagnon, R.
Gill, R.
Glen, I.
Goldstein, R.
Grönvall, H.
Haapala, J.
Haas, C.
Hanhirova, K.
Hansen, E.
Heinonen, J.
Hellmann, J-H.
Herlevi, A.
Herzen v., R.
Hirayama, K-I.
Hopkins, M.
Hyyppä, J.
Håkansson, B.
Häkkinen, S.
Hänninen, H.
Höyland, K.
Izumiyama, K.
Jalonen, R.
Jones, S.
Juurmaa, K.
Kalliosaari, S.
Kamesaki, K.
Karavanov, S.
Kato, K.
Kendrick, A.
Kitagawa, H.
Kivimaa, S.
Kloster, K.
Koivumäki, P.
Kovacs, A.
Koskinen, P.
Kostiainen, K.
Kujala, P.
Kämäräinen, J.
Kärnä, T.
Köhler, P.
Lahtinen, J.
Lampela, K.
Larmi, M.
Lehmus, E.
Lensu, M.
Leppäranta, M.
Lindroos, H.
Lozowski, E.
Lundqvist, J-E.
Løset, S.
Makkonen, L.
Manninen, T.
Maslowski, W.
Matusiak, J.
Mikkola, M.
Moore, J.
Mulherin, N.
Multala, J.
Mäkynen, M.
Mälkki, P.
Määttänen, M.
Nevel, D.
Nortala-Hoikkanen, A.
Nyman, T.
Okko, O.
Ovsienko, S.
Palmer, A.
Partanen, T.
Pedersen, L.
Pulliainen, J.
Riska, K.
Rytkönen, J.
Saarnisto, M.
Salonen, E-M.
Sandqvist, J.
Sandven, S.
Santaoja, K.
Sayed, M.
Schulson, E.
Schwarz, J.
Seinä, A.
Shen, H.
Similä, M.
Sinha, N.
Sodhi, D.
Soininen, H.
Stepanov, I.
St.John, J.
Strübing, K.
Takeuchi, T.
Timco, G.
Tsoy, L.
Tucker, T.
Tuhkuri, J.
Tunik, A.
Uto, S.
Uuskallio, A.
Valanto, P.
Valeur, H.
Veitch, B.
Vihma, T.
Vironmäki, J.
Wadhams, P.
Weiss, J.
Wilhelmson. M.
Wilkman, G.
Willmott, A.
Yerusalimskij, A.
Zhang, J.

POAC-Conference
Helsinki 23.8.1999.
Mr. Alpo Kuparinen
Deputy Director General
Ministry of Trade and Industry
Finland

A NORTHERN DIMENSION FOR THE POLICIES OF THE EUROPEAN UNION

Starting point

The European Council in Luxembourg took note of the Finnish proposal concerning a Northen Dimension of the EU in December 1997. The European Council requested the Commission to prepare a report which was submitted to the European Council in Vienna in December 1998.

The Conclusions of the EU-presidency at the Vienna European Council have been described as a political break-through as regards the Northern Dimension in the policies of the European Union. The European Council welcomed the report submitted by the European Commission. In doing so the European Council emphasised the need for further exchange of views with all countries concerned on the development of the concept. The European Council underlined the importance of the Northern Dimension for the internal policies of the Union as well as its external relations, in particular towards Russia and the Baltic Sea region.

Thus the European Council welcomed the report and invited the Council of the European Union to specify guidelines for action in related areas, based on the Commission's Interim Report. These guidelines were adopted at the General Affairs Council in May 1999. They were given a political "blessing" at the European Council in Cologne in June 1999.

Objectives

The Northern Dimension is part of EU policies for external relations with a specific aim to raise the Union's profile in Northern Europe. It is conceived as a way of working with the countries of Europe's northern regions to increase prosperity, strengthen security and resolutely combat dangers such as environmental pollution, nuclear risks and cross-border crime.

The concept of the Northern Dimension addresses challenges and embraces opportunities that exist in these regions. It is a means of identifying the interests of the EU in the North and establishing a consistent line of action there. One of its main objectives is to create favourable conditions for EU enlargement without creating new dividing lines on the European continent.

The geographic focus of the Northern Dimension concept is understood to be on the countries bordering the Baltic Sea and on the Northwest Russian regions, as well as Kaliningrad. More specifically, the Northern Dimension covers the following geographical area: from Iceland in the west across to Northwest Russia, from the Norwegian, Barents and Kara Seas in the north to the southern coast of the Baltic Sea. Hence, it forms itself along the border of the EU zone and across it.

Working Mechanisms

The Northern Dimension builds upon the existing framework of contractual relationships, financial instruments and regional organisations. No additional financial instruments are needed in the EU for this purpose. The dialogue takes place within the context of the Europe Agreements as regards Estonia, Latvia, Lithuania and Poland, that of the Partnership and Cooperation Agreement (PCA) as regards Russia and that of the European Economic Area (EEA) as regards Norway and Iceland.

The Northern Dimension is thus not primarily a programme intended for public-sector support. The main thing is to create the preconditions for private investment in sectors of strategic importance for the economy. EU programmes and actions on a bilateral and Nordic basis must promote economic co-operation in which the public and private sectors are responsible for their own contributions. At the same time, there is a strong focus on co-operation and co-financing between private investors, international investment institutions and public programmes.

The implementation and further development of the Northern Dimension should be done by fully utilising regional bodies, such as the Council of the Baltic Sea States (CBSS) and the Barents Euro Arctic Council (BEAC). The Commission could also consider contacts with the Arctic Council. However, the Northern Dimension itself should not be seen as a new regional initiative.

The Northern Dimension encourages intensified cooperation and increased interaction between all actors of the region, including the EU member states, the Commission, the partner countries and the regional bodies. Correspondingly, it tries to improve the interoperability of EU programmes as well as national programmes with a view to creating synergies between them.

Key principles: positive interdependence and added value

In accordance with the Union's founding principles, the Northern Dimension is designed to contribute to the reinforcement of positive interdependence between the European Union, Russia and the other states in the Baltic Sea region. Economic interdependence is conceived as an asset for security, stability and sustainable development in Northern Europe. Its significance has recently been strengthened for several reasons:

- due to the northern enlargement of the Union in 1995 by Austria, Finland and Sweden, the Union has attained a 1,300 km long border with Russia. The significance of the common EU-Russia border will only grow with the future enlargement;

- increasing demand for energy and raw materials in Europe underscores the strategic importance of Northwest Russia's reserves;
- environmental problems in the region are closely related to the economic exploitation of oil and gas, minerals and forests, while their impacts are of transboundary nature. The already heavily burdened Baltic Sea will become an internal waterway of the EU.

As the list above suggests, interdependence has both positive and negative manifestations. In these same areas, expected value added is high. The EU considers that the promotion of a Northern Dimension concept should take place where there is clear added value through better coordination and increased synergies. Such sectors are given priority in the implementation of the Northern Dimension. The Council discerns the following priority sectors:

- infrastructure, including transport, energy, and telecommunication ,
- natural resources, environment, nuclear safety,
- education, training, research and human resources development,
- public health and social administration,
- cross-border cooperation, cross-border trade and investment, fight against crime, in particular cross-border crime.

The main added value of the Northern Dimension concept lies in its ability to create favourable preconditions for private investment in sectors of strategic importance for the region's economy. The Northern Dimension is not a massive public sector endeavour. Participation of the private sector and international financing institutes is essential for its realisation.

Particular interests to this conference

The north of Europe offers great potential for business and industry in the next millennium. If co-ordination of Union activities in northern Europe is intensified, international finance can be more effectively channelled into concrete projects and programmes in the area.

Of special interest to this conference is the exploiting and utilisation of natural resources in North-West Russia, especially gas and oil. These deposits are enormous, actually nobody knows how large they really are. Anyway, it has been estimated that for example Russia holds about a third of

the world's gas resources. The market for gas and for Russia's gigantic other natural resources lies in Europe. Today, two-thirds of Russia's exports to EU countries comprise energy, and in the future the EU will be even more dependent on imported energy as its own output declines and the Union enlarges.

There is one common feature concerning these resources; they are extremely difficult to exploit. The cold climate and other hard natural conditions are extraordinary demanding. New technologies have to be developed for exploiting and transporting these resources. Also the infrastructure needed must be built starting from practically zero point. All this will be a challenge of millenium to the participants of this conference.

Also the pollution in western and north-western parts of Russia and in the Baltic directly affect extensive regions of the Union and future member countries, and indeed the Union as a whole. It is a common concern of Russia and the Union. Of extraordinary importance is co-operation on the development of the water and sewage sector in St Petersburg but also in other parts of the Baltic.

One issue that has aroused special attention in development of the Northern Dimension is nuclear safety. The crucial issue of nuclear waste management in the Kola peninsula and of increasing the operational safety of Russia's nuclear power plants demand more effective international co-operation. Since both matters relate to nuclear safety they are of global importance, and are thus an extremely suitable subject for co-operation between the EU, Russia, the United States and Norway.

Economic growth in northern Europe and Union enlargement both call for better transport connections, a more developed traffic infrastructure, the construction of extensive new traffic networks in Europe, and the modernisation of telecommunications.

How the Northern Dimension emerged in the European Union

With regard to the future development of the Northern Dimension, attention should be paid to two items in the Presidency Conclusions of Cologne. First, the European Council welcomed the incoming Presidency's intention of holding a Foreign Minister Conference on the Northern Dimension in

November 1999. Second, the European Council stated that it is time to bring about closer involvement of the acceding countries concerned, the Russian Federation, Norway and Iceland in the process as it unfolds.

A Northern Dimension Conference on foreign minister level will be organised in Helsinki on November 12 next fall. All partner countries in northern Europe , while greeting favourably the Vienna conclusions, have reminded the Union of their will to be considered not as objects, but rather as equal partners. While individual dialogue with the partners is valuable , providing a common forum for the Union and the partners will be politically beneficial in view of the aim of promoting co-operation and positive interdependence in the region.

On the basis of the results of the conference, the European Council would be able, in December in Helsinki, to decide on any subsequent measures to make the content of the Northern Dimension more tangible. This, in our wiew, could include a decision by the European Council to request the Commission to prepare an Action Plan on the Northern Dimension.

Unlike the Common Strategy on Russia, which is based on the Treaty of Amsterdam, the Northern Dimension lacks such a judicial and institutional basis. It rests on political conclusions of the European Council.

Finnish Presidency: Foreign Minister Conference and Finland's Goal-Setting

The Foreign Minister Conference on the Northern Dimension on 11-12 November 1999 in Helsinki will offer an important opportunity for the Union, its member states and partners to further discuss the concept and elaborate concrete ideas to advance it.

Finland has set the following goals for its Presidency as regards to the Northern Dimension:

- to consolidate the position of the Northern Dimension concept on the EU agenda,
- to support the Commission in the implementation of the Northern Dimension,

- to consider the possibility of drawing up an action plan for the Northern Dimension at the European Council in Helsinki,
- to increase cooperation on northern issues between the EU, the US and Canada within the framework of the Transatlantic cooperation.

Ladies and Gentlemen

In this introduction I have tried to shortly cover main sectors mentioned as priority areas in the Northern Dimension for the policies of the Union. It should have become clear that military security issues are not included in the concept. However, the ultimate goal of this initiative is to promote stability and peace through integration and economic co-operation.

EUROPEAN RESEARCH STRUCTURES IN THE STUDY OF THE ARCTIC SEAS
institutional or ad hoc progress ?

Pentti Mälkki
Finnish Institute of Marine Research

1. Introduction

The topic of my speech focuses on two aspects: European and Arctic Seas. In order to cover this, I have, however, to go beyond both. This is due to the fact that we cannot consider the issue without discussing the overlapping of some activities found in other fora. My intention is, therefore, to speak about the existing international organisations - not all of them - and consider whether their activities have or will be contributing to the study of Arctic Seas.

The interest to the Arctic has been considered to be of limited value for many decision making bodies. Those benefiting from activities there have been local people, seal and whale hunters a century ago, in this century military and defence people, offshore mining and transport activities and, earlier as well as today, those considering seriously sea connection between the Atlantic and Pacific through the Arctic Seas. Although we here find these things important, that is not the case among many decision makers in various countries. This is reflected also in the international organisation of cooperation. The bodies considered in this presentation form an interesting mix of national contributors to polar research.

2. The organisations

The organisations dealing with cooperative Arctic science issues in any form are either nongovernmental: poor and run by science motives, and the governmental organisations which have applications in mind and usually also means for implementing their ideas. The Arctic - including the Arctic Seas - cannot be treated without consideration of circumpolar activities and, therefore, purely European cooperative science organisations are few in number. If one considers those without any other mission, there is only one, the European Polar Board (1995-). Arctic is, however, one focus in truly powerful bodies, such as the ESA Earth Observation Programme and European Union Fourth Framework Programme, in particular the MAST III programme. In addition to these, I will consider the International Arctic Science Committee (1990-), the Arctic Ocean Sciences Board (1984-), Arctic Monitoring and Assessment Programme and the Barents Euro-Arctic Council (1993-).

EUROPEAN POLAR BOARD (1995-)
Parent organisation: ESF
Members: Nominated by national research councils

The principal objective is to be the European voice for, and to facilitate cooperation between, European organisations in polar science. Together with its sister organisation European Marine Board it has a joint secretariat (common acronym EMaPS) and joint Executive Committee. The original statement of objectives consisted of seven main objectives and six further objectives. They were intended to be common for both Boards, thus covering a wide range of topics. Interestingly, already in 1995 the Marine Board considered the polar seas to belong to the interest of the Polar Board. This, needless to say, certainly has had some implications in the MAST programme development, to be discussed later.

The EPB is a very young organisation for seeing results immediately. It has been a discussion forum, the objective to have an European voice for polar science would not have been implemented without EPB. It has not been able to promote sharing of research facilities or joint activities according to original ideas and objectives. The EPB has made proposals for inclusion in FP5, partly of policy nature. Part of those have come from other fora and, therefore, were known already.

The EPB went through an international evaluation in 1998, jointly for EBP and EMB. The evaluators noted the above and, in addition that

- The board lacks a structure of working groups which could widen its active participation.
- The Evaluation Committee found the concept viable but needs exist for fundamental changes in operation
- EPB has been a good discussion forum, its influence in polar science has been indirect.
- Prior to EPB, its predecessor ECOPS (European Committee for Ocean and Polar Sciences) had launched the idea of "Grand Challenges", two of which dealt with polar research (EPICA on ice core drilling in Antarctic and AOGC, A.O. Grand Challenge.) The evaluation committee found ECOPS having been oligarchic and stated that " .. the idea of grand projects provides an important rationale for European cooperation and makes it possible to define research needs in a context that fits with the "think big" process by which the EU is formulating its priorities....Meanwhile, the failure to actually implement...shows that such priorities are not easily implemented (nor funded) by collective initiative from the top" and ....."Support for bottom-up research initiatives and commitments by individual scientists cannot be expected to reflect wider European interest any more than merely the specific interests and specialities of the most successfully competitive scientists."

This and similar statements elsewhere neglected the fact that for each grand challenge preparatory conferences had been organised and a large Euroconference, in which state representatives, in most cases from ministries of member countries had committed to active support of the grand challenges.

As a consequence of the evaluation and the debate following that, objectives of the EPB were reduced to more realistic, consisting of :

- Forum to bring members together to share information, find common problems and solutions, to cooperate and to seek collective positions and endeavours for European polar science.
- Strategy to identify and prioritise scientific and technology issues of strategic importance, where relevant in close association with European Commission.
- Voice to express a collective vision for the future European Polar science and technology in relation to developments in Europe and world-wide and to improve the public understanding of science in these fields.
- Harmonisation to give European added value to the EPB members' national programmes, as well as being consistent with programmes of relevant international organisations, and to interact with any relevant international scientific organisations, and to facilitate the shared use of research facilities.

What will be the value of EPB in future, remains to be seen.

INTERNATIONAL ARCTIC SCIENCE COMMITTEE (1990-)

Parent organisation: applied to ICSU membership
Members: nominated by nat. res. councils

Structure:

Consists of the Council (all member countries' representatives, presently 17 countries) and the Regional Board (8 charter Arctic countries). Regional Board deals with issues which have connection with governmental authorities, such as permissions to conduct research on respective areas, as well as other issues of common interest of the arctic countries.

Modus operandi:

Non-governmental international organisation to encourage and facilitate cooperation in all aspects of arctic research, in all countries engaged in arctic research and in all areas of the arctic region. Mission: To encourage, facilitate and promote the full range of basic and applied research encouraging cooperation and integration of human, social and natural sciences concerned with the Arctic at a circumarctic or international level; and to provide scientific advice on arctic issues.

Achievements:

An international review was carried out after 5 years of operation, with questionnaire to some 450 scientists, leading to improved structure and activities. Today, IASC has clear project selection structure, a number of projects either in implementation phase (e.g. Barents and Bering Seas impact studies) or with completed plans with starting funding (e.g. Feedback of Arctic Ecosystems, Effects of UV-radiation increase). Funding of all these studies goes through national or international funding agencies. The IASC has been very active in efforts to reencourage the Russian Arctic research,

with its efforts to launch a number of programs in the Russian Arctic. So far, these programs do exist as plans without implementation and funding.

IASC involvement in Arctic Ocean studies is somewhat unclear: On one hand it has decided to focus mainly on interdisciplinary issues, on the other hand it has taken under its umbrella such projects as geophysical mapping of the Arctic Ocean, deep sea drilling in the Arctic Ocean, bathymetric mapping in the Arctic Ocean and land-ocean interaction. Part of these, such as the deep sea drilling project, did already exist, waiting only for suitable umbrella. Part of these, such as the mapping, is carried out mainly by others (in this case IHO/Canada), part of these only exist as plans.

IASC has established an Arctic Operators Forum, to act in a similar way as its counterpart in the Antarctic. This forum is still in very formative phase.

One can say that the IASC has a niche which it fits. IASC acts as an official scientific adviser for example for the Arctic Council. Lack of substantial funding makes IASC, as other non-governmental organisations mainly discussion fora, which may add seeding good cooperation provided somebody will fund it.

ARCTIC OCEAN SCIENCES BOARD (1984-)

Parent organisation: none
Members: Nominated by research councils/polar research organisations

Among the Arctic research organisations, this is the one which is least formal. Its membership consists of either people nominated by national funding agencies (UK, Canada, US, Sweden, Denmark), or from national polar research organisations (Germany, France, Finland, Japan, Norway, Russia).

The operational principle in AOSB is expressed in the mission and strategy documents, accepted in 1992:

The Mission of AOSB is to facilitate Arctic Ocean research by the support of multi-national and multidisciplinary natural sciences and engineering programs.

The Strategy consists of providing added value by
1. encouraging and supporting science-led programs by offering planning, coordination, and access to funding and logistics;
2. cosponsoring international activities and encouraging cooperation between various programs;
3. ensuring that information on Arctic Ocean research is exchanged between nations and disseminated to Arctic Ocean scientists in each nation;
4. providing networks for Arctic Ocean scientists, for example, on access to facilities/logistics and access to data;
5. establishing telemail interconnections for information exchange;
6. establishing means of initiating and maintaining long term capture systems (via moorings, buoys, satellites etc.);
7. establishing means of initiating and maintaining systems for long term archiving, cataloguing and exchanging arctic oceanographic data;

8. ensuring that there is interaction, when appropriate, between the international Arctic Ocean science community and those concerned with arctic policies; and
9. promoting symposia and educational activities.

AOSB has mainly focused on single, specified science issues: During 1986-93 the Greenland Sea Project, after that International Arctic Polynya Programme (IAPP), recently plans for Arctic fresh water balance studies, both on paleorecords and on summarising the knowledge in symposium monograph. Funding of these programs has been almost entirely on national basis.

The AOSB projects have been surprisingly successful, having had good planning, initially accepted basic funding of logistics, and little formalities. The Greenland Sea Project has had as a follow up two major European projects: ESOP I and II on the study of Greenland Sea dynamics, and VEINS to study exchanges of water, heat and mass between the Atlantic, sub-Arctic and the Arctic Ocean. The IAPP started with substantial study of polynya in NE Greenland coast, followed by a similar topic at the end of the Baffin Bay.

ARCTIC MONITORING AND ASSESSMENT PROGRAMME (AMAP, 1990-)

Parent organisation: Governmental
Members: nominated by Ministries of Environment

AMAP is a consequence of ministerial negotiations at the end of 1980's to protect the Arctic environment. It consists of several subactivities, the Arctic Ocean and its living resources having a substantial part on it. In itself, AMAP is not a science program, but recent development has involved a wide range of scientists in particular to the evaluation phase. The outcome of AMAP is a very comprehensive report on the state of the Arctic, covering all aspects and all areas. Following the assessment, high level political decisions have been made for continuation and new focus on monitoring of the Arctic environment.

AMAP has served as an instrument, which is needed for more concrete action for the sustainable development of the Arctic. The measures to be taken require political initiatives, which in the setting of international organisations belong to the recently established Arctic Council. How this will proceed, depends on all actors, not the least those in the country which hold the chair of the Council.

BARENTS EURO-ARCTIC COUNCIL (1993-)

Parent organisation: Governmental

Barents Euroarctic Council has been established to enhance the development of the Barents region, covering northern parts of Norway, Sweden, Finland and Russia substantial parts of the Arctic seas. It is mainly an political and economical organisation, having 7 member countries and 9 observers. It has as main activities: economy, trade, science and technology, tourism, infrastructure, educational and cultural exchange and improvement of indigenous peoples in the North. Science issues are dealt within each of the above activities. Needless to say, the Arctic seas

research falls within the range of oil and gas exploitation, development of infrastructure and environment.

The Barents Council has made a comprehensive analysis of actions to be implemented in the region, those remain still in the phase: "to be implemented".

MARINE SCIENCE AND TECHNOLOGY PROGRAMME (1989-1998)
Parent organisation: European Union
Members: None, funding in DG XII 1991-98

The European Union science programme, called Framework Programme (FP), has become an important instrument in European science policy. Although it covers only a fractional part of total science funding in Europe, its role has exceeded this fraction substantially, partly because the national funding in EU projects often exceeds the common share. FP IV, which nominally ended 1998, contained in its subprogramme MAST III a number of elements dealing with the Arctic seas.

In MAST III work programme one particular emphasis was to study the extreme marine environments, including the ice covered seas in the northern hemisphere (Arctic and sub-Arctic seas). The scientific issues to be covered included a.o. the following:

"Objective
To understand the functioning of ecosystems in extreme marine environments and to determine their role in the global environment by studying their characteristic physical, chemical, biological and geological processes.

Research tasks
The ice-covered seas in the northern hemisphere:
Physical dynamics of sea ice, including interaction with man-made structures; deep water formation; large-scale circulation, eddies and shelf processes in the Arctic; biological dynamics of sea ice system and their particular role in the Arctic food webs, life cycle strategies of marine organisms in Arctic sea; energy and mass exchange between sea ice and both the water column and atmosphere; vertical biogeochemical transfer processes and the impact of variability in pack ice coverage on the sea floor communities; sediment formation in ice-covered regions and the geological record as indicator of long-term ice cover change."

Within MAST-programme, there also was a technological subprogramme. This has been much less productive in obtaining viable applications than the purely scientific part. Part of the reason obviously has been that it was primarily concerning scientific instrumentation technology, and commercial interest to this branch R&D is very limited.

Out of the total 230 MECU funding of MAST III, some 12 MECU has been spent on this group of studies. The funding includes Ice State and Loleif, also reported here, and the studies ESOP 2 and VEINS, mentioned earlier in connection of AOSB. Within the FP IV Climate programme, studies of the Barents Sea response as well as some other climate and remote sensing studies have been funded.

Looking at the number of projects funded within the FP IV, one cannot but note that the interest of EU DG XII has not been particularly encouraging. I feel myself unable to analyse the result, having been in this particular case on both sides of the fence.

EARTH OBSERVATION PROGRAMME
Parent organisation: European Space Agency
Members: None, funding and operational programme

The European Space Agency has during the past decades increased its earth observation component. Jointly with other space agencies, the observation programme is already rather comprehensive. As far as Arctic observation is concerned, we are still far away from the situation in meteorology, where operational weather satellites cover the needs daily. For the land/sea surfaces, this can be expected to be the case when ENVISAT 1 satellite becomes operational.

Looking at the achievements of ESA, we can note that the EO-programme has during 1972-97 funded some 3.3 E+9 Euros (some 12 % of total spending), fraction of which on polar remote sensing. The importance of ESA's activities is not only in the availability of the satellite data, it is also in the substantial development of interpretation and other R&D-activities ESA has supported during the years. If we consider that in this conference, close to 15 % of all papers have some reference/relation to satellite data, it is easy to state the importance of the active Earth Observation Programme for the Arctic research.

3. Reflections on the above

Out of the above, some conclusions can be drawn:

A. There is considerable flora of international organisations (outside POAC) dealing with marine research in the Arctic.

B. Some of them have been fairly progressive in contributing to the progress of Arctic Ocean understanding in different ways:
ESA with successful funding in remote sensing
AMAP in producing excellent status report of the Arctic environment
AOSB in implementing successful projects in both subarctic and high arctic

C. Some of them have not so far proven their potential, e.g. the European Polar Board and the Barents Euro-Arctic Regional Council, partly also IASC.

D. There is considerable overlapping in the structure of the organisations, this deals in particular the non-governmental bodies, such as EPB, IASC and AOSB.

E. It seems to be hard to establish even European research policy towards the Arctic marine research, there are strong lobbies against emphasis into the North.

4. Institutional or ad hoc progress ?

Returning now to the original question set in the title of the lecture, we have to consider the issue from different angles.

As far as basic science is concerned, the question is, do the above mentioned institutions contribute to the research strategy which is important in the Arctic Ocean? Similarly, do the funding agencies respond positively to concerns of importance?

For applied science, who defines the research strategy (if anybody) ? What is the role of the above institutions in design, implementation or funding ?

The following table represents my personal view on the answers to these questions:

	Basic research		Applied research	
organisation	strategy	funding	strategy	funding
EPB	no	no	no	no
IASC	somewhat	no	no	no
AOSB	yes	partly	no	no
AMAP	no	no	yes	yes
EU MAST III	no	little	no	little
ESA EOP	no	yes	yes	yes
BEAR	no	no	no	no

One can see, that EPB has not so far achieved any results, AOSB within its project oriented approach has succeeded well, IASC has proceeded to some extent, without substantial implementation. Among the governmental organisations there is clear division to reactive (MAST, BEAR) and proactive (AMAP, ESA). The latter have contributed, the former can be considered as disappointments from purely Arctic marine research point of view.

In comparison to what is the national contribution in each country plus the importance of bilateral agreements on research, the above contributions can be stated to be minor. So, the final answer to the title question is: ad hoc progress. This does not exclude the importance of national strategies, which has made the ad hoc progress possible.

THE METHOD FOR REFINEMENT OF ANALYTIC MODELS OF SHIP HULL/ICE IMPACT INTERACTION BASING ON THE STATISTIC ANALYSIS OF MODEL AND FULL SCALE EXPERIMENTS

E.M. Appolonov, A.B. Nesterov and Yu. A. Zimnitsky
Krylov Shipbuilding Research Institute, St.Petersburg, Russian Federation

ABSTRACT

The analytic relationships of the hydrodynamic model of solid body/ice impact interaction are investigated in the light of model and full scale experiment results obtained in the nineties, as well as by special ARCDEV-project experiments of spherical bodies dropping. The method for model refinement based on introducing an empirical coefficient of ice load localization is proposed. Perspects of further improvement of solid body/ice impact interaction analytic models are considered.

1. INTRODUCTION

The hydrodynamic model (HDM) of solid body/ice impact interaction (Kurdumov and Kheisin, 1976) used for 30 years in the Russian methodology for definition of ice loads on hulls of Arctic ships and icebreakers, was based on a series of experimental investigations consisting of spherical bodies dropped on the ice (Likhomanov and Kheisin, 1971). In these experiments, called Drop Ball Tests (DBT), direct pressure measurement was not carried out. Therefore, the smooth (parabolic) pressures distribution in the contact resented by the authors area was not confirmed experimentally.

In the West experiments researching ice failure during interaction with a solid body through a DBT (Timco and Frederking, 1990, 1993), penetration of medium-scale indentors, (MSI Tests - Frederking, Jordaan and McCallum, 1990), as well as the results of full-scale ship testing in ice (Masterson and Frederking, 1993), unambiguously identified a pronounced peak character in the ice pressures pattern. The discrepancy of the western experimental data with the HDM smooth law of pressure distribution in the contact area is understand to be the main reason that Western experts' have not fully embraced the HDM.

To investigate the above mentioned discrepancy in the HDM, a special experimental apparatus was developed by Krylov Shipbuilding Research Institute for running DBT in full-scale ice conditions. After testing in the ice of the open basin in Krylov Institute, the apparatus was performed during an Arctic voyage in April-May 1998 as part of the ADCDEV-project. At the moment of preparation of this material the theoretic analysis of the complex experiments performed within the ARCDEV project was not complete. Therefore, that HDM refinement presented below is of preliminary character.

2. DESCRIPTION OF THE EXPERIMENTAL APPARATUS FOR THE DBT

The DBT apparatus (Fig.1) is a truss structure consisting of three columns rigidly connected between each other that are installed on the ice or another stiff foundation. A stationary plate,

designed for installation of a lifting device (that is a manual pulley block) is attached rigidly to the upper ends of the columns. Stability of the apparatus truss on the ice is ensured with the help of three additional angular supports. Between the truss columns, a movable plate is located. Semi-spheres with pressure gauges, weights and acceleration gauges are attached rigidly to the movable plate. The movable plate together with the weights and a semi-sphere can move free between the columns in the vertical direction allowing to imitate a process of dynamic ice failure at plate dropping. The unit structure allows to vary

- geometrical shapes and sizes of an element interacting with the ice by their substitution on the movable plate;
- speed of structures collision with the ice by variation of the drop height;
- the mass of the dropped structure by installation of additional weights.

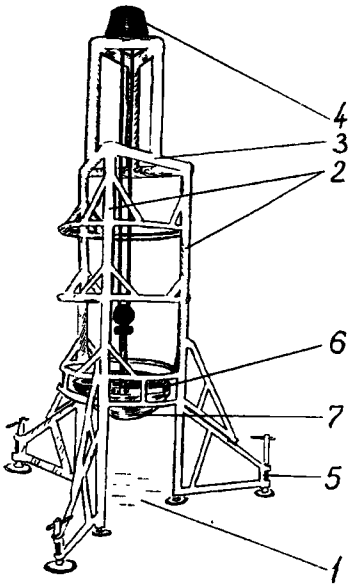

1 - stiff foundation (ice),
2 - columns,
3 - stationary plate,
4 - lifting device,
5 - additional angular supports,
6 - movable plate,
7 - semi - sphere.

Figure 1. General view of the experimental unit for DBT

During the tests performed within the program ARCDEV, the unit was furnished with two semi-spheres of diameters 498 mm and 350 mm correspondingly. They could be dropped from any height in the range from 100mm to 1500mm and therefore provided collision speed variation in the range from 1 m/sec. to 5m/sec. The mass of the semi-spheres could be varied with the addition of weights within the following range

from 70 to 250 kg with a step ~ 20 kg for the semi-sphere with the diameter 490 mm;
from 40 to 140kg with the step ~ 20 kg for the semi-sphere with diameter 350 mm.

Lifting the movable plate with an installed semi-sphere was carried out with the help of the manual 20-fold pulley block. Using such a lifting device has provided for the possibility of performing DBT both in laboratory and field conditions.

For convenient transportation, the unit structure has several joints. In particular, the truss structure is divided into three blocks; the additional angular supports are also separate blocks.

During the DBT tests, the following physical magnitudes were measured:

- the contact pressures occurring at semi-sphere interaction with the ice;
- the speeds and accelerations characterizing the semi-sphere movement during its interaction with the ice;
- the depth of semi-sphere indentation in the ice.

3. MODIFICATION OF THE HDM ANALYTIC RELATIONSHIPS BASED ON THE DBT RESULTS

The HDM analytic relationships (Kurdumov and Kheisin, 1976) contain the following expression for the pressure pattern in the area of spherical weight contact with the ice:

$$p(r) = a_p^{sph} V^{0.25} \left(\frac{r_0}{\alpha}\right)^{0.5} \left(\alpha^2 - r^2\right)^{0.25}, \tag{1}$$

where p is the pressure;

a_p^{sph} is the parameter of dynamic strength of the ice (PDSI);

V is the operational speed;

r_0 is the radius of the area of the sphere-ice contact;

$r = \dfrac{r}{r_0 / \alpha} \le 1$ is a dimensionless coordinate;

r is the distance from the contact area center (radius);

$\alpha = 1.05 \div 1.08$ is a numerical coefficient taking into account flaking on the contact area edges that were observed during the 1971 DBT.

It should be noted that the introduction of the coefficient α does not change the pressure pattern shape, but limits the area of the body-ice force contact. Actually, (1) can be presented in the following form:

$$p = \begin{cases} p_0 \left(1 - \left(\dfrac{r}{r_0}\right)^2\right)^{0.25} & at \quad r \le r_{ef} \\ 0 & at \quad r > r_{ef} \end{cases} \tag{2}$$

where $p_0 = a_p^{sph} V^{0.25} r_0^{0.5}$ is the pressure in the pattern center;

$r_{ef} = \dfrac{r_0}{\alpha}$ is the effective radius of the area of sphere-ice force contact.

The ice load parameters are found from the solution of the following equation of sphere motion at its penetration into the ice

$$MV\frac{dV}{d\xi} = -\int_{Aef} pdA_{ef} \tag{3}$$

where ξ is the depth of body indentation into the ice;

A_e is the effective contact area;

M is the sphere mass.

In compliance with (2), integration in (3) is performed over the effective contact area limited by the circle of radius r_{ef}.

Kurdumov and Kheisin obtained the solution of equation (3) using a constant value for the coefficient α at

$$\alpha = 1.06 = const \tag{4}$$

The influence of α is relatively small and its introduction has a more theoretical sense than a practical one.

The experimental research works for justification of the HDM (Likhomanov and Kheisin, 1971) did not include the direct measurement of the pressures in the contact area with the ice, so that relationship (1) was not directly verified by an experiment. The analysis of the DBT results performed within the ARCDEV-project has shown that the pressure pattern in the area of sphere contact with the ice has a peak character; i.e. it does not conform to (1). To improve the HDM agreement with the experiment an approach consisting of α interpreted as another empirical coefficient (along with a_p^{sph}) in the HDM relationships which takes into account the peak character of the pressure pattern can be used. In this case satisfactory agreement of the theoretic relationships with the experimental data (Fig. 2) can be reached with α variation in a narrow range; $\alpha = 1.89 \div 2.05$.

The obtained result $\alpha \approx 2$ testifies to the high level of pressure pattern peakness for the DBT conditions. In this connection the following considerations seem very important. At the DBT, flakes influence on the contact area edges is minimum. Therefore, the flakes cannot explain occurrence of the pattern peakness. At consideration of inclined side interaction with the ice edge, the more intensive process of flake formation is observed. Nevertheless, the analysis of the results of ice load measurements in full-scale conditions (Masterson and Frederking, 1993, for example) has permitted to assess the value of the ice load peakness parameter in case of ship hull/ice interaction as follows:

$\alpha_{ship} \approx 2$

Reconciliation of the peakness parameters for the DBT and at ship hull impacts against the ice permits to advance the following preliminary considerations.

(i) The reasons of the load pattern peakness are caused not by flakes formation, but by another more complicated process (possibly, the nature of this process is connected with development of micro cracks in the direction from the contact area center to the edges).

(ii) Carrying away the finely disperse layer and formation of larger fragments are two visual demonstration of the ice failure process.

(iii) Prevailing of flakes formation is not a sign of the increased peakness of the ice load pattern.

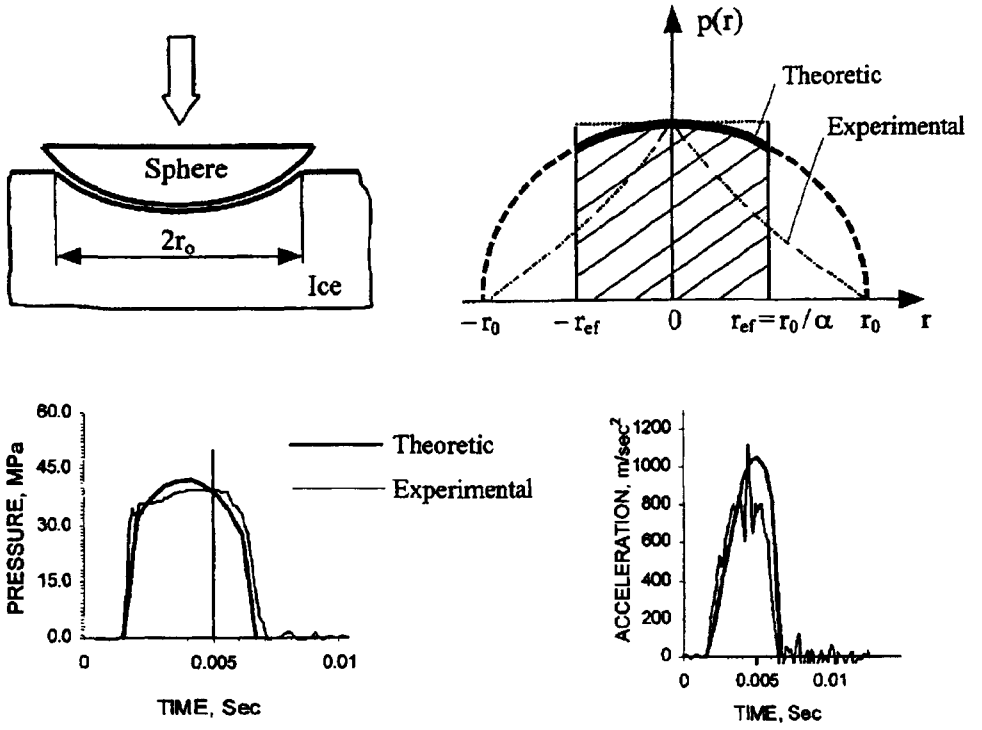

Figure 2. Improvement of the theoretical and experimental results conformity at interpretation of magnitude α as a parameter defined from the experiment

4. PERSPECTIVES OF IMPROVEMENT OF APPROACHES TO THE DESCRIPTION OF SHIP/ICE INTERACTION

The detailed analysis of the HDM, as well as study of works by Daley, 1991, Kujala, 1994, Sayed and Frederking, 1992, Savage, Sayed and Frederking, 1992, on description of the process of expelling failed ice as a Coulomb – Mohr's material, leads to the conclusion that generation of a non-contradictory theoretic model of ice failure is highly difficult at the present stage. A semi-empirical approach, based on quantitative and qualitative generalization of experimental investigation results, seems rational.

From these positions, the possibilities of refinement of the spherical body/ice interaction analytic model can be formulated, based on some statements justified both experimentally and theoretically that are valid both for DBT and the case of ship hull impact against the ice as follows:

(i) At solid body penetration into the ice, in all points of the contact area the following regularity of pressures time history is observed: growth from zero to a certain maximum and further fall to zero in the moment of body stop.

(ii) Maximum for the impact pressure in an arbitrary point depends on this point distance to the impact center.

The mentioned regularities can be explained within the HDM that gives a relationship of pressure in a point versus the degree functions of speed simultaneous values and contact area dimensions, as well as a function of point distance to the impact center.

$$p(t,r) \sim V^{0.25}(t) \quad r_0^{0.5}(t)\left(1-\frac{r}{r_0(t)}\right)^{0.25} \tag{5}$$

In the initial moment $p = 0$ because $r_0(0) = 0$. During the impact $r_0(t)$ increases, and $V(t)$ decreases that results in appearance of the $p(t)$ maximum. In the end of the impact at $t = t_0$, $V(t_0) = 0$, and $p(t_0) = 0$ correspondingly.

According to the DBT analysis, relationship (5) gives the speed influence slightly too high; we may assume that the speed influence has a probabilistic nature. The description of function $p(r)$ needs essential correction (to take into account the pattern peakness). Therefore, the structure of the function for the simultaneous pressures can be accepted as an attempt to realize the proposed above semi-empirical approach:

$$p(t,r) \sim V^a(t) \cdot r_o^b(t) \cdot f(\bar{r}) \tag{6}$$

where $f(\bar{r}) = \left(1-\bar{r}^c\right)^d$, $\bar{r} = r / r_0(t)$;

a, b, c, d are empirical coefficients.

In order to develop the proposed semi-empirical approach, research works on the following main directions are supposed:

- continuation of the DBT to refine relationships (6);
- performing drop tests with ellipsoid weights to study the character of pressure distribution at the contact area prolate in one direction;
- performing drop tests with flat weights dropped on the ice field in the form of a prolate wedge to refine the influence of flakes formation upon the pressure pattern peakness;
- application of the obtained results to the analysis of laboratory tests of larger scale (type of MSI tests) and ship and icebreakers testing in Arctic ice.

5. CONCLUSION

Therefore, by introduction of an empirical coefficient of ice load peakness α the conformity of the hydrodynamic model to the experimental data is improved essentially. Nevertheless, the problem of improving the analytic models of ship impact against the ice still, as with all the familiar models has drawbacks. In order to resolve this problem, equally with continuation of the theoretic research works, generation of semi-empirical functions based on the experimental data analysis and convenient for practical use at ship hull ice loads regulation is expedient. With the object of extending the experimental investigations, drop tests with ellipsoid and flat weights dropped on the ice wedge are expedient.

6. ACKNOWLEDGMENT

This work is a part of the project «Arctic Demonstration Voyage» (contract No WA-97-SC.2191) supported by the European Commission, DG Vll, through Sea Transport Programme. The Project is co-ordinated by FORTUM OIL AND GAS OYJ, FI. From European Union member countries following companies and institutions participle: Earth Observation Sciences Ltd, GB; Helsinki University of Technology, Ship Laboratory, FI, Hamburg Ship Model Basin Ltd, DE; Institute of Ship Operations, Sea Transport and Simulation, DE; Kvaerner Masa Yards, FI; Lloyd's Register of Shipping, GB; Aker-MTW Shipyard, DE; Nansen Environmental and Remote Sensing Center, NO; Remtec Systems Ltd, FI; Tecnomare S.p.A., IT; and Shell Vankor Development, NL. Russian Partners in ARCDEV Project are: The Russian Federation Ministry of Transport, Administration of the Northern Sea Route; State Research Center of the Russian Federation Arctic and Antarctic Research Institute; Arctic Shipping Services; Central Marine Research and Design Institute; State Research Center of the Russian Federation Krylov Ship Research Institute; and Murmansk Shipping Company.

REFERENCES

Daley, C. 1991. Ice Edge Contact. A Brittle Failure Process Model. Acta Polytechnica Scandinavica, Me 100, Helsinki, 92 p.

Frederking, R.M.W., Jordaan I.J. and McCallum J.S. 1990. Field Tests of Ice Indentation of Medium Scale Hobson's Choice Ice Island, 1989. Proceeding of the 10th IAHR Ice Symposium, Espoo, Finland, Aug.20-23, 1990, Vol. II, pp. 931-944.

Kujala P. 1994. On the Statistics of Ice Loads on Ship Hull in the Baltic. Acta Polytechnica Scandinavica, Me 116, Helsinki, 98 p.

Kurdumov, V.A. and Kheisin, D.E. 1976. Hydrodynamic Model of the Impact of a Solid on Ice. Prikladnay Mechanica, Vol. 12, No 10, Kiyev, pp. 103-109.

Likhomanov, V.A. and Kheisin, D.E. 1971. Experimental investigation of solid body impact on ice. Problemy Arctiki i Antarctiki, Leningrad, Vol. 38, pp. 128-136.

Masterson, D.M. and Frederking, R.M.W. 1993. Local contact pressures in ship/ice and structure/ice interactions. Cold Regions Science and Technology, Elsevier Science Publishers B.V., Amsterdam, Vol. 21, pp. 169-185.

Savage, S.B., Sayed, M. and Frederking, R.M.W. 1992. Two-dimensional extrusion of crushed ice. Part 2: analysis. Cold Regions Science and Technology. Elsevier Science Publishers B.V., Amsterdam, Vol. 21, pp. 37-47.

Sayed, M. and Frederking R.M.W. 1992. Two-dimensional extrusion of crushed ice. Part 1: experimental. Cold Regions Science and Technology. Elsevier Science Publishers B.V., Amsterdam, Vol. 21, pp. 25-36.

Timco, G. W. and Frederking, R.M.W. 1990. Drop impact tests on freshwater ice: spherical head. Proceeding of the 10th IAHR Ice Symposium, Espoo, Finland, Aug. 20-23, 1990, Vol. II, pp. 776-787.

Timco, G. W. and Frederking, R.M.W. 1993. Laboratory impact tests on freshwater ice. Cold Regions Science and Technology. Elsevier Science Publishers B.V., Amsterdam, Vol. 22, pp. 77-97.

SIMULATING RIDGE KEEL FAILURE BY FINITE ELEMENT METHOD

Jaakko Heinonen
Helsinki University of Technology, Finland
Laboratory for Mechanics of Materials

ABSTRACT

Ridge keel failure in a punch test is simulated by using the elastic plastic theory based on the Mohr-Coulomb yield criterion. In the punch test a circular plate is pushed vertically downwards until the ridge keel collapses. The problem is solved numerically by using a finite element method (FEM). Simulations are used for determining the material parameters from the experiments. A simplified model gives knowledge about how the failure is proceeding inside the keel and how the values for the material parameters affect the load capacity of rubble.

The main material parameters determining the failure in rubble are cohesion and friction. Several simulations have been done with different values for cohesion and friction. Both cohesion and friction affect almost linearly the load capacity in the punch test. The failure develops almost conically downwards.

1. INTRODUCTION

Several studies of the mechanical properties of ice rubble exist. Some of them describe ice block interactions determining macroscopical behaviour like cohesion and friction (Ettema and Urroz, 1989 and Ettema and Urroz-Aguirre, 1991). Experiments are mainly done in laboratories resulting in some values for the material properties (Azarnejad and Brown, 1998). Also, studies from field experiments exist (Leppäranta and Hakala, 1989 and 1992, Croasdale etc., 1997, Heinonen, 1998). It is known that properties in nature differ considerable from the laboratory results (Leppäranta and Hakala, 1989 and 1992, Croasdale etc., 1997). There are several reasons for that. In the laboratory, tests are always performed in the smaller scale and ice rubble is artificially manufactured causing different ice fragment shape and size. Therefore, texture and porosity of rubble is different from that in nature. Also, a different temperature history and salinity affect freeze bounds and consolidation by freezing.

In the LOLEIF project, several punch tests for first year ridge keels have been performed in Gulf of Bothnia during winters 1998 and 1999. In the punch test a circular plate is pushed vertically downwards until the ridge keel collapses. The problem is how to interpret results, especially how to separate cohesive and frictional strength of rubble from the measured load capacity.

Traditionally the easiest way to simulate ridge keel failure is using the limit load theory based on plasticity. The aim of this paper is to introduce a finite element model to simulate ridge keel failure. Results can be used when determining the mechanical properties of the ridge keel from the experiments. Because the Mohr-Coulomb yield criterion includes two material parameters, cohesion and friction, they cannot be defined by a single test when the peak load is applied as

a measure of the load capacity. Having several test sets, simulated test results can be compared with the experimental ones. The material model parameters can then be chosen so that the simulated results fit the experimental ones.

2. SIMULATED TEST

A principle of a punch test is shown in Figure 1. This experimentally performed test is now simulated numerically. The sail is removed and a circular plate of the consolidated layer is cut free from the surrounding solid ice field. The ridge keel is then loaded vertically by pushing the circular plate downwards. Therefore, only the rubble in the keel is loaded.

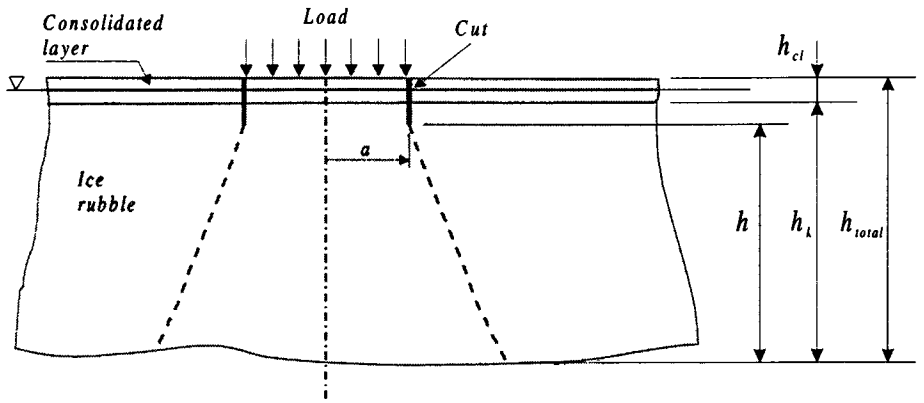

Figure 1. Punch test: The ridge keel is pushed vertically downwards.

3. FEM-MODEL

Numerical simulations for the following model, shown in Fig. 2, are done by using a commercial finite element program ABAQUS/Standard 5.8. The geometry of the ridge keel and the consolidated layer is simplified and modelled by using axisymmetric solid elements. Due to the axial symmetry, only one half the cross section is modelled. The keel is divided into two layers. The upper one contains the consolidated layer and the level ice, both behaving like an elastic material having same values for material parameters. In the second layer, rubble, the block size is assumed to be small compared with the thickness of the rubble. Therefore, rubble is approximated to be homogeneous having a constant value for the parameters through the thickness.

Rubble is assumed to behave like an elastic perfectly plastic material. The yielding depends on both cohesion and friction. The yield criterion is written according to the Mohr-Coulomb constitutive law as

$$|\tau| = c - \sigma \tan\phi \qquad (1)$$

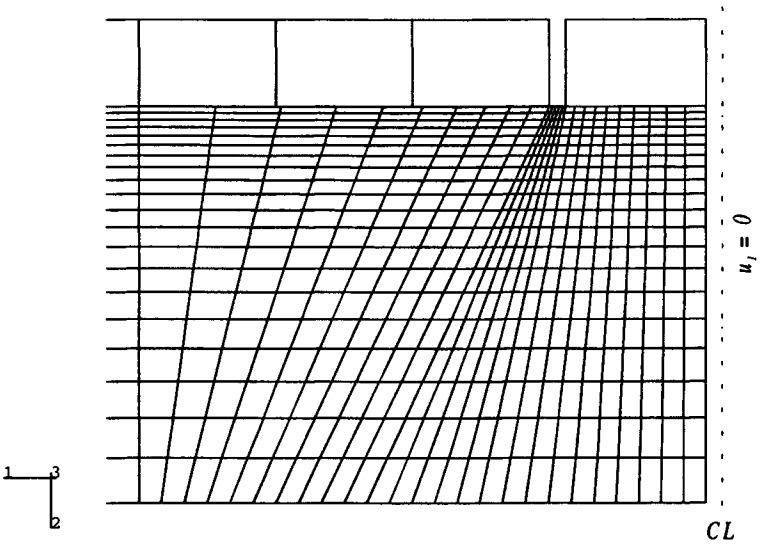

Figure 2. Finite element model of the ridge keel punch test. The element mesh and the boundary conditions are shown. Only one half the cross section is modelled due to the axial symmetry. (u_1 is the displacement to the direction 1).

in which τ is shear strength and σ is the normal stress. c is cohesion and ϕ is the angle of internal friction; both of them are assumed to be constant. Because of the discontinuity of the gradients of the yield surface, the numerical program smoothens the corners of the yield surface (Hibbit, Karlsson & Sorensen, Inc., 1998).

The element mesh contains 520 elements for rubble and five elements for the consolidated layer as shown in Fig. 2. The far end boundary conditions are modelled by using infinity elements (CINAX4). Otherwise, linear four node elements (CAX4) are used. Symmetric boundary conditions are applied at the centre line.

The analysis contains two steps. The first step is done for solving the initial stress state inside the keel. The second step is for adding the external load. In the first step, a buoyancy load for rubble is added. The upper surface of the consolidated layer is fixed to avoid displacements in the first step. The average volume force γ due to buoyance in the ridge keel is

$$\gamma = (\rho_w - \rho_i)(1 - e)\, g \tag{2}$$

where ρ_w is density for water and ρ_i is density for the ice blocks. e is the relative volume of water pockets in the ridge keel (porosity). g is the gravitative acceleration ($g = 9.81$ m/s^2).

In the second step, the circular plate is moved downwards incrementally (displacement controlled).

An error always exists when using this kind of discretisation, because the load will cause a singular stress state at the edge of the platen pushed downwards. Thus, the results are dependent on the element mesh.

Several analyses have been done by using different strength values in the yield criterion (eq. (1)). The following values have been used in the simulations:

- the cohesion c varies between 2.0 - 8.0 kPa
- the friction angle ϕ varies between 15° - 45°

The dimensions of the keel geometry are shown in Table 1. They are chosen according to the field tests (Heinonen, 1998). Values for the other material parameters are shown in Table 2. Usual values are chosen. The value for porosity of the keel is chosen to be 0.4. Keel porosity in Gulf of Bothnia is found round 0.3 - 0.4 (Kjestveit, 1999). The numerical estimate for the load capacity is not sensitive for the elastic properties of rubble (Young's modulus). It mainly affects the magnitude of deformations. Therefore, a choice of the unknown value is not important in this type of analysis.

Table1 Dimensions of the ridge keel.

a	radius of the platen	1.3 m
$h = h_k$	keel depth	3.7 m
h_{cl}	consolidated layer thickness	0.8 m
h_{total}	total keel depth	4.5 m

Table 2 Values for the material parameters.

		Consolidated layer	**Rubble**
E	Young's modulus	9.0 GPa	50.0 MPa
ν	Poisson value	0.3	0.3
ρ_w	density of water	1000 kg/m^3	
ρ_i	density of ice	917 kg/m^3	
e	porosity of the keel	0.4	

4. RESULTS

4.1 Load capacity

The calculated results with various values for cohesion and friction are shown in Figures 3 and 4. Fig. 3 shows the load versus the displacement. The load will be almost constant after the limit value is reached. The slip line is then activated through the keel. Unfortunately the elastic perfectly plastic material model cannot estimate what is happening after the peak load.

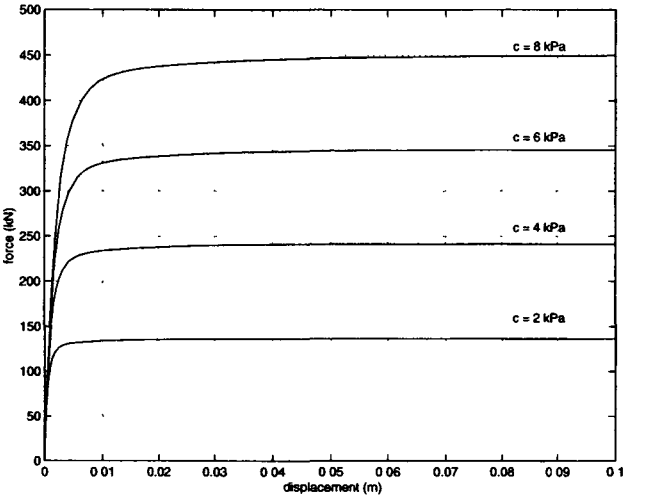

Figure 3. Force vs. displacement of the platen with different values for cohesion. The friction angle is 25°.

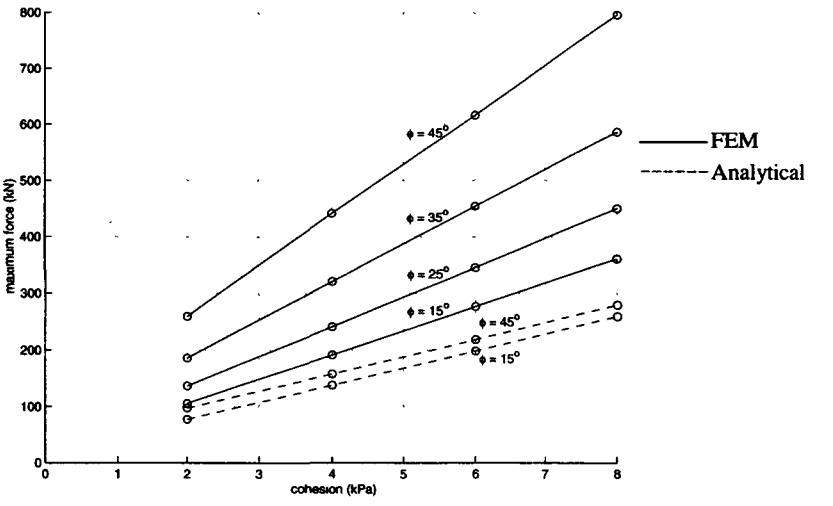

Figure 4. Maximum load capacity vs. cohesion with different values for the friction angle.

Figure 4 shows the maximum load capacity versus the cohesion with different values for the friction angle. According Fig. 4 the maximum load capacity is linearly dependent on cohesion. This effect is also found analytically, for example by using the limit load model. Using the lower bound theory, the plastic load capacity for the cylindrical failure mode can be found as

$$F = 2\pi ahc + \pi ah^2\gamma\tan\phi + \gamma\pi a^2 h \qquad (3)$$

where the maximum load F is divided into three parts: the first term is the cohesive part, the second is the frictional part and the last one is the buoyancy load. It is noteworthy that in the analytical model, the external load does not affect the normal stress state inside the keel.

The load capacity from the FEM analysis is much higher than the one found from eq. (3) as shown in Fig. 4. A difference is mainly due to the frictional part of strength. The reason is that the normal stress distribution inside the keel due to the external load is not taken into account in the limit load model. The normal stresses inside the keel due to the external load are much higher than the initial stresses due to the buoyancy. Therefore, pressure in the keel caused by the external load gives much more frictional strength. So friction has a more important role than eq. (3) shows, where the elastic behaviour is neglected.

According to eq. (3) cohesive strength and frictional strength are totally separated. However, Fig. 4 shows that the slope is dependent on friction, i.e. $\partial F/\partial c$ is function of friction. This feature is not included in the analytical result. The load capacity is more sensitive of cohesion with higher friction angles, when the difference between the numerical and the analytical result is bigger.

The conclusion is that in this case the traditional limit load model based on plasticity underestimates material load capability because it avoids the elastic behaviour. The normal stress distribution inside the keel due to the external load should be taken into account. However, the FEM calculations may overestimate the load capability, because the maximum pressure is not limited in the yield criterion (eq. (1)). Therefore, the effect of friction is too high.

4.2 Failure zone

Figure 5 shows how the plastic zone develops through the keel. The failure line differs from the vertical line. The direction for the failure line is dependent on the friction angle. Analytical studies show that in pure shear stress state, the angle should be about $\phi/2$. The angle is also dependent on the element mesh used, especially the direction of the elements near the edge of the platen. However, the slip angle is not directed according to the element column near the edge of the platen. There is also dependence between the plastic zone width and the mesh direction. All these features will be studied in future.

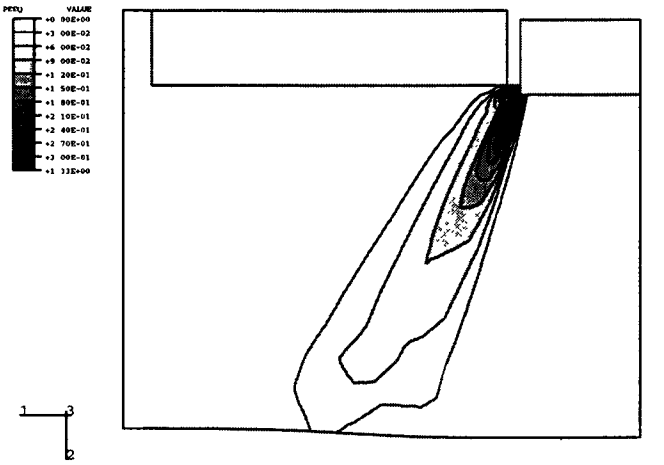

Figure 5. Contour plot of the equivalent plastic strain at deformed state, when the displacement of the platen is 0.1 m. c = 6 kPa, $\phi = 25°$.

5. CONCLUSIONS

The finite element analyses give reference data for comparing the limit load results. It also gives ideas about how the material parameters affect the load capacity. Also, it gives knowledge about where the failure proceeds, a location and a shape for the fracture plane, which supports development work for the advanced theories of the ridge keel failure. The load and displacement histories are simulated reliably until the peak load is reached, but the post peak behaviour cannot be simulated correctly with the elastic perfectly plastic material model.

The FEM simulations give higher load capacity than the analytical limit load calculations due to increase of the pressure resulting from the elastic solution. The results show that the limit load model underestimates the effects of friction. Therefore, frictional strength of rubble has an important role for the load capability.

6. REFERENCES

Azarnejad, A. and Brown, T.G. 1998. Observations of ice rubble behaviour in punch tests. Proc. Of the 14th International Symposium on Ice, Vol. 1, Clarkson University, Potsdam, New York, USA, pp. 589-596

Croasdale & Associates Ltd., In Situ Ridge Strength Measurements Local & Global 1998, Proposal for a Joint Industry-Government Project, 1997, 24 p.

Ettema, R. and Urroz, G.E., On Internal Friction and Cohesion in Unconsolidated Ice Rubble, Cold Regions Science and Technology, 16(1989), pp. 237-247

Ettema, R. and Urroz-Aguirre, G.E, Friction and Cohesion in Ice Rubble Reviewed, Proc. 6th Int. Speciality Conf., Cold Regions Engineering, 1991, pp. 316-325

Heinonen, J., Ridge Loading Experiments, Field Experiments in Winter 1998, Unpublished report for the LOLEIF Project, 1998, 25 p.

Hibbit, Karlsson & Sorensen, Inc. 1998, ABAQUS/Standard User's Manual, Vol. 1, ver. 5.8

Kjestveit, G., Investigation of Mechanical Properties of Ice Ridges, Norwegian University of Science and Technology, Department of Structural Engineering, Master Thesis, 1999, 46 p.

Leppäranta, M. and Hakala, R. 1989, Field Measurements of the Structure and Strength of First-year Ice Ridges in the Baltic Sea, 8th International Conference on Offshore Mechanics and Arctic Engineering Vol 4, pp. 169-174

Leppäranta, M. and Hakala, R., The Structure and Strength of First-year Ice Ridges in the Baltic Sea, Cold Regions Science and Technology, 20(1992), pp. 295-311

FIELD EXPERIMENTS ON UNIAXIAL COMPRESSIVE STRENGTH OF SEA ICE IN THE WEDDELL SEA, ANTARCTICA

Seppo Kivimaa, Research Scientist
VTT Manufacturing Technology, Maritime and Mechanical Engineering
Espoo, Finland

ABSTRACT

The field experiments on Antarctic sea ice physical properties were performed in the Weddell Sea during the two Finnish Antarctic Expeditions (FINNARP-89/90 and -91/92). Altogether 86 ice cores were drilled from 19 test sites including shorefast ice and pack ice floes. The temperature, salinity and density distributions in the ice cores were measured. Ice thin sections were prepared and photographed through crossed polaroids to study the ice structural characteristics. The unconfined uniaxial compressive strength of ice was tested with 217 samples in the ambient temperatures of the examined ice floes. The tests were made in the brittle range with high strain rate in-situ or in the cold laboratories of the research vessels. Typical profiles of ice salinity, density, temperature and uniaxial compressive strength in the ice floes are presented. The results of structural classification of ice samples are given. Ice unconfined uniaxial compressive strength versus ice total porosity is illustrated.

1. INTRODUCTION

Antarctic sea ice undergoes a large seasonal variation annually. The extent of the total sea ice cover in the Antarctic Ocean varies from the austral summer minimum of 3 x 10^6 km^2 to the austral winter maximum of 20 x 10^6 km^2 (Zwally et. al, 1983). Most of Antarctic sea ice is drifting pack ice. At its peak extent in late winter fast sea ice covers roughly an area of 0.55 x 10^6 km^2 (Panov & Fedotov, 1979). The Weddell Sea is the main source of pack ice formation in Antarctica. It is estimated that the pack ice area affected by Weddell Sea processes is 8 - 10 x 10^6 km^2 (Ackley, 1979). Every year a polynya starts to open on the eastern coast of the Weddell Sea in November-December. It widens towards the west up to the mid February, when the ice cover is smallest. An unmelted ice massive remains over the austral summer in the southwestern part of the Weddell Sea on the coast of the Antarctic Peninsula. This ice mass drifts northwards by the influence of the Weddell Gyre.

The ice research presented here was conducted in austral summer ice conditions during two Finnish Antarctic Expeditions (FINNARP) in the Weddell Sea. The first expedition FINNARP-89/90 was made on board a Finnish R/V Aranda from 8th December, 1989 to 27th February, 1990 (Mälkki et. al, 1990). The second expedition FINNARP-91/92 was made on board a Russian R/V Akademik Fedorov from 6th November, 1991 to 5th March, 1992. Fig.1 presents the routes of the research vessels in the Weddell Sea during the expeditions. There can be seen that R/V Aranda operated in the marginal ice zone of the eastern Weddell Sea. R/V Akademik Fedorov operated also in the central part of the Weddell Sea during the foundation of the American-Russian ice station Weddell-1, which was the first drifting research station on the pack ice in the Antarctic Ocean.

The main targets of the sea ice research in the FINNARP-89/90 and -91/92 expeditions involved collecting basic data on ice physical properties, ice strength, pack ice formations and ice mass balance in the Weddell Sea. This kind of ground data are needed for basic geophysical investigations, remote sensing, development of sea ice mathematical models and ship ice navigation. This paper concentrates to the sea ice research made by analysing ice cores drilled from the ice fields with a CRREL-type ice coring auger (core diameter 10.5 cm). The examined ice properties were the unconfined uniaxial compressive strength, ice crystal structure, temperature, salinity and density. The properties were determined as vertical profiles in the studied ice floes. The basic idea in the compressive strength tests was to obtain the ice strength in the ambient temperatures of the ice floes.

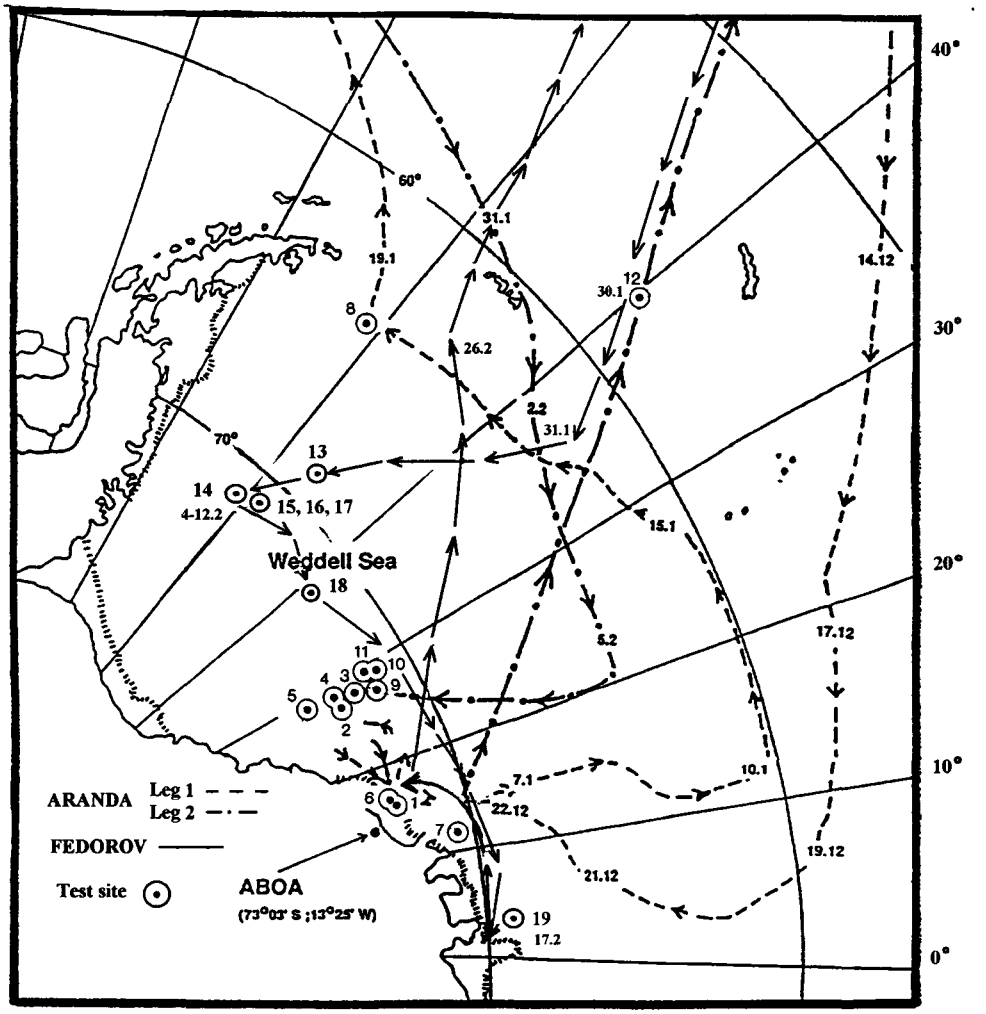

Fig. 1. The routes of R/V Aranda during FINNARP-89/90 and R/V Akademik Fedorov during FINNARP-91/92 expeditions in the Weddell Sea.

The ice cores were collected altogether from 19 test sites. In Table 1 are presented the positions of the test sites, date and ice floe description. The main part of the samples were collected in the pack ice zone of the eastern and central Weddell Sea. Three test sites located at the shorefast ice zone on the coastline of the Queen Maud Land and a couple samples were picked up in the western Weddell Sea. Most of the ice floes consisted of firstyear sea ice. The measured thickness of the level part of the floes varied from 0.6 metres to 3.5 metres. A few samples were taken from multiyear floe and a growler of glacial ice. In the course of the expeditions altogether 86 ice cores were collected.

Table 1. The positions and types of the examined ice floes.

SITE	DATE	LAT	LON	Ice floe type	Thickness [m]
S1	24-26.12.89	72° 23' S	16° 19' W	Shorefast, level	1.3 - 1.5
S2	31.12.89	72° 49' S	27° 32' W	Pack ice	0.8
S3	1.1.90	72° 32' S	28° 46' W	Pack ice, ridged	> 1.3
S4	1.1-2.1.90	72° 51' S	28° 33' W	Pack ice, ridged	> 1.5
S5	3.1.90	73° 50' S	28° 43' W	Pack ice	2
S6	4.1.90	72° 26' S	16° 29' W	Shorefast, ridged	3
S7	5.1.90	70° 33' S	11° 42' W	Pack ice	0.9 - 1.0
S8	18.1.90	64° 28' S	51° 56' W	Pack ice	N.A.
S9	8.2.90	72° 01' S	28° 22' W	Pack ice	1.2 - 1.4
S10	8.2.90	71° 40' S	29° 06' W	Pack ice, ridged	1.8 - 2.3
S11	9.2.90	71° 42' S	29° 02' W	Pack ice, ridged	2.3 - 3.5
S12	20.2.90	57° 30' S	39° 32' W	Drifting growler	1.0
S13	2.2.92	68° 49' S	47° 35' W	Pack ice	1.0-1.2
S14	5.2-12.2.92	71° 35' S	50° 02' W	Pack ice, ridged	2.1
S15	6.2.92, 10.2.92	71° 45' S	48° 50' W	Pack ice	1.4
S16	13.2.92	71° 20' S	49° 20' W	Pack ice	0.6
S17	13.2.92	70° 53' S	48° 18' W	Pack ice	0.8
S18	14.2.92	72° 09' S	39° 37' W	Pack ice	0.9
S19	18.2.92	70° 07' S	01° 30' W	Shorefast	> 3.3

2. SAMPLING AND ANALYTICAL TECHNIQUES

2.1 Ice temperature, salinity, density and uniaxial compressive strength measurements

The temperature profile of the ice cores was measured both in FINNARP-89/90 and in FINNARP-91/92 with FLUKE 50 k/j Thermometer in-situ immediately after the cores were lifted on the ice field. The distance between measurement points was 10 cm. The ice cores to be used to determine the salinity distribution were sawed to 10 cm thick pieces, put into plastic bags or boxes and transported to the research vessel. There they were melted and the salinities were measured by the Guildline Autosal 8400 salinometer in FINNARP-89/90 expedition and by the YSI 33 salinometer in FINNARP-91/92 expedition.

The temperature profile of the ice cores, which were used in the compressive strength tests was measured first in-situ. After that the ice cores were packed in plastic bags and transported in thermo boxes to compressive strength tests. The sample temperature was measured also just before the compressive strength test in order to obtain the correlation to the ice field temperature. The weigths of the samples were measured to determine the ice bulk

density. In addition, salinities of the tested compressive strength samples were analysed. The ice unconfined uniaxial compressive strength tests were made with a electro-hydraulic testing machine in-situ (Site1) immediately after sampling or in the cold laboratories of the research vessels (Sites 2-19) approximately 2 hours after the drilling of the ice cores. The diameter of the cylindrical samples was 10,5 cm and sample lengths varied from 20 cm to 25 cm. The compression axis was parallel to the vertical axis of the ice cores and loading strain rate was high being approximately 10^{-3} 1/s. Altogether 217 uniaxial compressive strength samples were tested during the two expeditions.

2.2 Ice structure characterization

Ice texture was studied only during the FINNARP-89/90 expedition. The texture ice cores were cut to approximately 0.5 metres long pieces, packed in plastic bags, put in styrox boxes, and transported immediately to the freezers in the cold laboratory container on board R/V Aranda. There vertical thick sections were made with a band saw and further thin sections were prepared with a microtome. The rest of the samples were stored in the freezers and used later to prepare horizontal thin sections. Every thin section was photographed between crossed polaroids. Altogether 130 thin sections were examined during FINNARP-89/90 expedition.

The ice was classified by using the thin sections into two main classes: the genetic and the textural class. The genetic classes describe the oceanographic conditions when the ice was formed. The genetic classification consisted of frazil and congelation ice. The frazil ice is formed in upper part of water column by surface accumulation of frazil slush. The congelation ice is formed by congelation of seawater at the ice-water interface under stable conditions (tranquil congelation) resulting in formation of columnar ice texture or it is formed of seawater at the ice-water interface under unstable conditions (distributed congelation), resulting in formation of intermediate columnar/granular ice texture.

The textural class was recognised on the basis of the grain size and the shape of the brine inclusion, similar way as Eicken and Lange (1989). They divided samples into five distinct classes at the textural level: granular, columnar, intermediate columnar/granular, mixed columnar/granular and platelet ice. Further distinction was made between polygonal granular and orbicular granular ice.

3. TYPICAL PROFILES OF THE EXAMINED SEA ICE PROPERTIES

3.1 Shorefast ice field

This sampling site S1 (72° 23' S, 16° 19' W) located few nautical miles from the continental ice shelf. The ice cores were drilled and tested there 24th-26th December, 1989. Ice field thickness was 130 - 151 cm having a snow cover of 22 - 27 cm. This shorefast ice field was composed mainly of gongelation ice. The texture ice core consisted 76,5 % of congelation ice and 23.5 % of frazil ice. The top 21 cm of the ice core had orbicular and polygonal granular ice texture. Below this layer began 114 cm thick intermediate columnar/granular ice layer. At the bottom of the core there was 14 cm thick layer of platelet ice. From the depth 120 cm to the bottom there was a brown algae layer. Some ice crystals which thickness was 1-2 mm and diameter 20-40 mm were attached to the the bottom of the ice core. Similar loose ice crystals

were found also in the coring holes. The thickness of this sub-ice platelet layer below the ice cover was 50-70 cm.

The uniaxial compressive strength tests were performed on this shorefast ice field in-situ. The results of seven ice cores are presented in Fig.2. The ice field temperature Tf was -3.0 °C in the surface layer and it increased rather linearly towards the bottom of the ice field to -1.5 °C. The testing temperature Tt of the samples followed closely to the ice field temperature Tf. The average ice field temperature was -2.3 °C. In the salinity ice core the minimum salinity 2.2 ppt (parts per thousand) was recorded close to the centre part of the core at 80-90 cm and the maximum salinity 7.3 ppt at the bottom of the the salinity core at 140-151 cm. The average salinity of the salinity core was 5.2 ppt. The compressive strength sample salinities in Fig. 2 varied between 3.0 ppt and 7.7 ppt. The average ice density was 0.885 g/cm^3. The maximum unconfined uniaxial compressive strength was 4.50 MPa. The compressive strength profile shows clearly a stronger layer in the centre part of the floe (70-90 cm), which can be explained by ice microstructure. The microstructure of this strong layer was classified as intermediate columnar/granular. The average compressive strength of the tested samples, which describes the overall ice field strength, was 2.4 MPa.

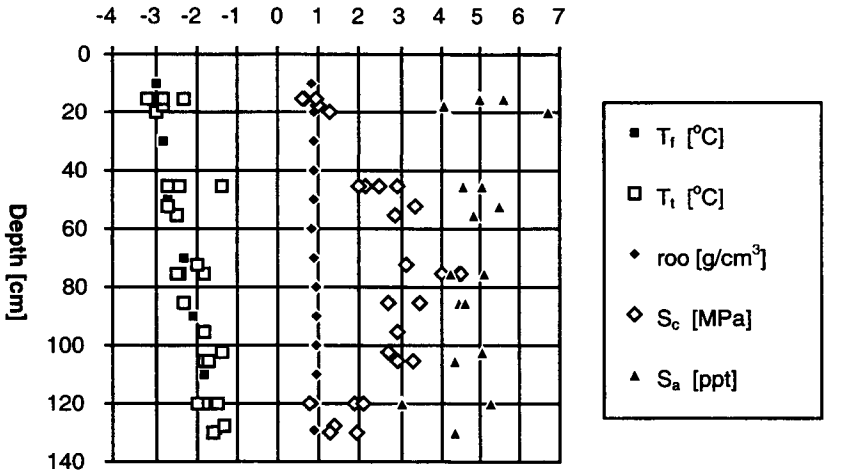

Fig. 2. The unconfined uniaxial compressive strength Sc, ice field temperature Tf, testing temperature Tt, salinity Sa and density roo profiles by seven ice cores in the shorefast ice field at the site S1.

3.2 Pack ice floe

The sampling site S4 (72° 51' S, 28° 33' W) is introduced as an example of the examined pack ice floes. The measurements were made there 1st -2nd January, 1990. The floe included many pressure ridges which were formed of rafted ice sheets. The ice sheet thickness was 150 cm on the level part of the floe, but close to the pressure ridges the thickness of the floe exceeded five metres. There was great brine drainage in the top layer of the floe, where the minimum salinity was only 0.2 ppt. The maximum salinities were measured in the bottom part of the salinity ice core. The average salinity was 2.6 ppt. The texture ice core included granular, intermediate columnar/granular, mixed columnar/granular and columnar structures in thin

layers altering each other. The contents of frazil and congelation ice were correspondingly 45.1 % and 54.9 %.

The compressive strength, density and temperature profiles from the site S4 are illustrated by Fig. 3. The ice field temperatures were high through the examined ice cores. In the surface layers temperatures were close 0.0 °C and the minimum temperature -1.6 °C was measured 90-110 cm below the surface. The average temperature was -0.9 °C. The minimum uniaxial unconfined compressive strength of 0.36 MPa was measured in the top layer. The maximum compressive strength 2.58 MPa was obtained in a sample 65-94 cm below the surface. The average uniaxial compressive strength of this pack ice floe was 1.35 MPa. The average density was 0.861 g/cm^3. The ice floe was porous and clearly in melting condition. However, this pack ice floe was so thick that it did not not melt during the season. The installed Argos buoy in an other FINNARP-89 project (Launiainen & al., 1991) was operating on the floe still on the 3rd of September, 1991 which means that the ice floe survived at least one summer season after the expedition. So it became actually a multiyear ice floe.

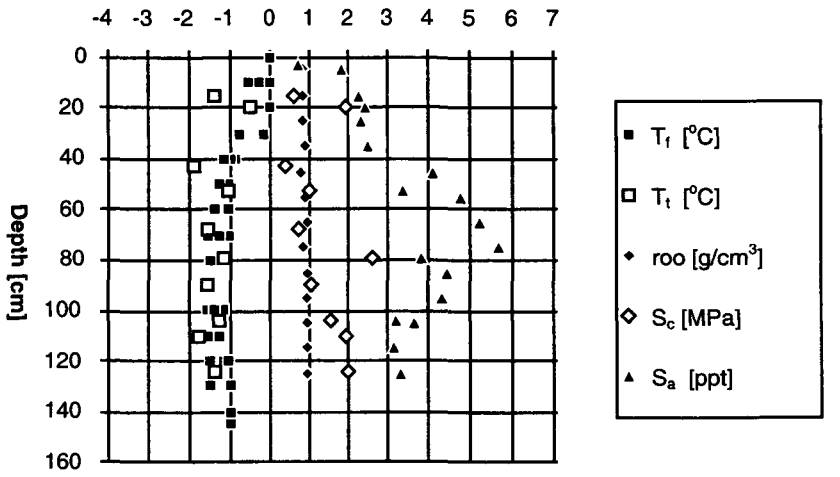

Fig. 3. The uniaxial unconfined compressive strength Sc, ice field temperature Tf, testing temperature Tt, salinity Sa and density roo profiles by four ice cores in the pack ice field at test site S4.

3.3 A growler

On the 20th of February, 1990 a small freely drifting growler of glacial ice was picked up on board R/V Aranda by a grane. The dimensions of the growler were approximately 3 m x 3 m x 1 m. An interesting feature was that the temperature of the growler was very low despite the small size being from -5.1 °C to -3.8 °C inside. Altogether 13 compressive strength samples were prepared from the growler. The compressive strength varied between 1.2 MPa and 6.1 MPa and the average strength was 3.2 MPa. The densities of the measured samples were from 0.882 g/cm^3 to 0.921 g/cm^3.

4. SUMMARY OF THE RESULTS

4.1 Ice salinity and temperature

In Table 2 are presented the measured minimum, maximum and average values for ice salinity and ambient temperature in different ice floes. The salinity results were rather similar compared to those of Gow et. al (1987). The average salinities varied at different test sites from 2.2 ppt to 5.7 ppt. The salinity range of the measured samples was from 0.2 ppt to 7.6 ppt. In some ice cores rather great brine drainage was detected in the top layer. The average salinity in the growler was 0.6 ppt.

The ambient temperatures of the tested floes were high reflecting the midsummer conditions in the Weddell Sea. The ice floe temperatures varied from -3.0 °C to 0.0 °C. Three typical temperature distributions were obtained. In the shorefast level ice field close to the continental ice shelf the vertical temperature distribution was linear between the surface and the bottom. In the thin level ice fields rather constant temperature distributions were measured, where the temperature was close to the sea water temperature. In the thick pack ice floes the surface layer temperature was close to the air temperature. Typically the middle layer of these floes was coldest and the bottom layer temperature was close to the seawater temperature. The average temperature of the growler was -4.5 °C.

Table 2. Minimum, maximum and average salinities and ambient temperatures of the different ice floes

SITE	Salinity [ppt]			Temperature [°C]		
	Min.	Max.	Ave.	Min.	Max.	Ave.
S1	2.2	7.3	5.2	-3.0	-1.5	-2.3
S2	1.3	5.0	4.1	-1.7	-1.1	-1.4
S3	3.2	3.2	3.2	-1.3	-0.6	-0.9
S4	0.2	4.0	2.6	-1.6	0.0	-0.9
S5	0.4	5.7	3.6	-2.0	-0.4	-1.1
S6	2.8	5.4	4.1	N.A.	N.A.	N.A.
S7	1.4	5.1	4.4	-2.3	-1.0	-1.9
S8	1.7	2.5	2.2	N.A.	N.A.	N.A.
S9	2.7	4.7	3.4	-1.3	-0.5	-0.9
S10	2.4	5.1	3.6	-1.7	-0.1	-1.0
S11	2.5	5.1	3.6	-1.9	-0.2	-1.3
S12	0.5	0.8	0.6	-5.1	-3.8	-4.5
S13	2.1	4.1	3.4	-2.7	-0.6	-2.0
S14	1.1	5.9	3.2	-1.7	-2.7	-2.3
S15	1.7	4.9	3.2	-2.7	-1.2	-2.0
S16	4.7	7.1	5.7	-1.6	-1.4	-1.5
S17	1.7	5.8	3.5	-2.4	-1.8	-2.1
S18	1.1	4.9	3.3	-2.1	-0.9	-1.5
S19	0.3	7.6	3.9	-2.3	-0.4	-1.5

4.2 Ice internal structure

Genetically congelation ice was the dominat component in the ice cores: 62.1 % of the total length of the texture ice cores was composed of congelation ice and 37.9 % was frazil ice. The percentage of frazil was typically higher in the heavily ridged ice floes compared to the

more level floes. The content of congelation ice was clearly higher in the examined ice cores during FINNARP-89 expedition than the results from other expeditions in the Weddell Sea, presented in Table 3. The reason for the difference to the former expeditions may be explained by the spatial variation of different ice types. Intermediate columnar/granular ice was the dominant component in the crystal structure: 35.8 % of the examined material was intermediate columnar/granular ice and 22.4 % of the analysed ice had clear columnar structure.

Table 3. Observed sea ice growth during a number of expeditions into the Weddell Sea.

Expedition	Observed growth		Reference
	frazil, %	congelation, %	
PolSea	57.4	42.6	Gow et al., 1987
WWSP-1	57.1	42.9	Lange et al., 1989
WWSP-2	51.7	48.3	Eiken and Lange, 1989
EPOS-I	63.8	36.2	Lange, 1989
WWGS	41.9	58.1	Lange, 1989
FINNARP-89	37.9	62.1	

PolSea=Polar Sea Expedition, WWSP = Winter Weddell Sea Project (Leg 1 and 2), EPOS-I = The European Polarstern Study (Leg 1), WWGS = Winter Weddell Gyre Study

4.3 Ice unconfined uniaxial compressive strength

The applied procedure to make the compressive strength tests immediately in the ambient ice field temperatures was different from the previous compressive strength tests for Antarctic sea ice by Urabe and Inoue (1986). They stored ice samples for a long time in a temperature of approximately - 20 °C and tested them after the expedition in different temperatures. Urabe and Inoue (1986) examined only shorefast sea ice. During the FINNARP-89/90 and -91/92 expeditions the test temperatures of the ice samples were very close to the original ice field temperatures of both the shorefast and pack ice floes.

A summary of the measured ice unconfined uniaxial compressive strengths and average densities of the ice floes is given in Table 4. In general the measured strengths were rather low reflecting the midsummer conditions, where temperatures of the floes are high and the ice structure is porous. In the shorefast ice fields the destruction of ice had not proceeded as far as in the pack ice floes. The maximum unconfined uniaxial compressive strengths of the shorefast ice and pack ice were correspondingly 4.50 MPa and 3.99 MPa. The highest uniaxial compressive strength of 6.09 MPa was measured in the growler of glacial ice. In the tested pack ice floes no clear difference could be noticed between the strength results measured in the beginning of January compared to those measured in the beginning of February. The average density of the floes varied from 0.761 g/cm^3 to 0.900 g/cm^3. In the growler the average density was 0.911 g/cm3.

In Fig. 4 are presented the measured unconfined uniaxial compressive strengths in the pack ice floes as a function of total porosity of the tested samples. The porosity of ice is an important physical quantity in determing ice mechanical properties. The porosity of sea ice contains both gas (va) and brine volumes (vb). These are difficult to measure directly. Here the method of Cox and Weeks (1983) has been applied in order to calculate the total porosities of the ice samples from measurements of salinity, temperature and density in the

uniaxial compressive strength tests. In Fig. 4 can be seen that the uniaxial compressive strength decreases as the total porosity of the samples increases.

Table 4. A summary of the measured ice compressive strengths and average ice densities.

	Uniaxial	compressive	strength	Density
Site	Min	Max	Ave.	Ave.
	[MPa]	[MPa]	[MPa]	[g/cm^3]
S1	0.59	4.50	2.35	0.885
S2	0.34	1.91	1.04	0.790
S3	0.81	1.59	1.25	N.A.
S4	0.36	2.58	1.35	0.861
S5	0.89	2.73	1.70	0.857
S6	1.09	3.14	2.15	0.887
S7	0.77	2.41	1.58	0.840
S8	3.85*	6.98*	5.42*	0.877
S9	0.33	3.49	1.64	0.880
S10	0.35	2.89	1.31	0.884
S11	0.38	2.39	1.17	0.873
S12	1.21	6.09	3.19	0.911
S13	N.A.	N.A.	N.A.	0.863
S14	0.37	2.55	1.17	0.900
S15	0.23	3.99	1.57	0.852
S16	1.11	1.11	1.11	N.A.
S17	0.56	0.88	0.72	0.761
S18	0.65	1.99	1.03	0.806
S19	1.25	3.29	1.99	N.A.

* The uniaxial compressive strength was tested approximately at -5 °C lower temperature than the ambient temperature of the ice floe.

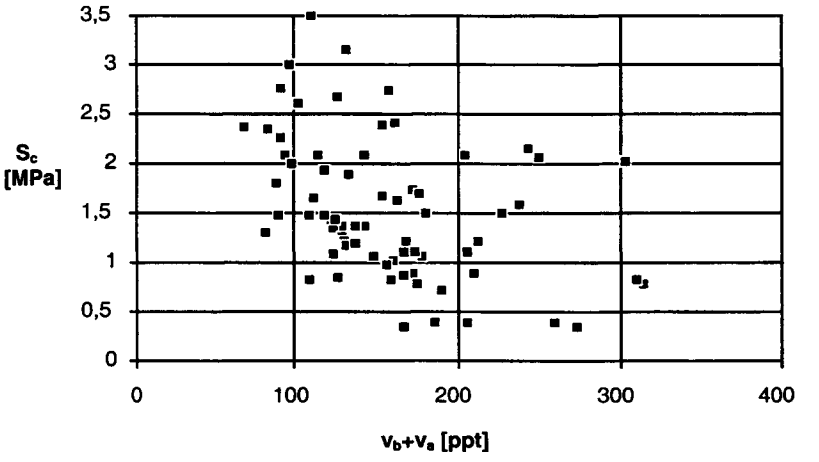

Fig. 4. The unconfined uniaxial compressive strength Sc of the samples in pack ice versus the ice total porosity vb+va.

5. CONCLUSIONS

A large body of new field data was obtained on the properties of the ice floes in the Weddell Sea, Antarctica during the FINNARP-89/90 and -91/92 expeditions, where the sea ice crystal structure, porosity and compressive strength research were combined together.

The amount of frazil ice in the analysed ice cores was smaller than that reported by other expeditions in the Weddell Sea, Antarctica. The overall frazil ice content obtained, 37.9% is still high compared to the amount of frazil ice reported from the Arctic Ocean. The dominant component (35.8%) in the crystal structure of the ice cores was intermediate columnar/granular ice.

The measured uniaxial compressive strengths in the ambient conditions of the ice fields in the Weddell Sea were rather low reflecting the summer ice conditions. A parabolic strength distribution was found in the shorefast level ice, in which the middle layer of the floe had the highest strength. The maximum measured ice strengths were 4.5 MPa and 4.0 MPa correspondingly in the shorefast ice and in the pack ice floes. A clear decrease in the ice uniaxial compressive strength as ice total porosity increased was found. The potential hazard of growlers for ship ice navigation was demonstrated by high compressive strength values.

REFERENCES

Ackley, S.F. 1979. Drifting buoy measurements in Weddell Sea pack ice, Antarctic Journal of the United States, 16(5), 106-108.

Cox, N., & Weeks, W. 1983. Equations for determining the gas and brine volumes in sea ice samples, Journal of Glaciology, Vol. 29, No. 102.

Eicken, H. & Lange, M.A. 1989. Development and properties of sea ice in the coastal regime of the southeastern Weddell Sea, Journal of geophysical research , 94 (C6), 8193-8206.

Gow, A. J., Ackley, S. F., Buck, K. R. & Golden, K. M. 1987. Physical and structural characteristics of Weddell Sea pack ice. CRREL Report 87-14.

Lange, M.A., Ackley, S.F., Wadhams P., Dieckman G.S. & Eicken, H..1989. Development of sea ice in the Weddell Sea, Antarctica, Annals of Glaciology, 12, 92-96.

Lange, M. A.1989. Sea ice properties, Report on Polar Research 62, Alfred-Wegener-Institute, Bremerhaven, 85-97.

Launiainen, J., Vihma, T. & Rantanen, K.1991. Air-sea interaction experiment in the Weddell Sea, Antarctic Reports in Finland No 2. Ministry of Trade and Industry, Helsinki, Finland.

Mälkki, P., Niemistö, L. & Aro, E. 1990. R/V Aranda on the Weddell Sea on season 1989-90, Symposium on Antarctic Logistics and Operations, Sao Paulo, Brazil.

Panov, V.V. & Fedotov, V.I.1979. Physical conditions of fast ice formation in East Antarctica, Polar Geogr. Geol., III (1), 1-15.

Zwally, H.J., Comiso, J.C., Parkinson, W.J., Campbell, F.D., Carsey, F.D. & Gloersen, P. 1983. Antarctic Sea Ice, 1973-1976; Satellite Passive-Microwave Observations. Washington D.C. National, Aeronautics and Space Adminstration (NASA SP-459).

Urabe, N. & Inoue, M. 1986. Mechanical properties of Antarctic sea ice, Proceedings of Offshore Mechanics and Arctic Engineering Symposium, ASME, Tokyo, Japan, Vol. IV, pp. 303-309.

ICE LOAD MEASUREMENTS ONBOARD MT UIKKU DURING THE ARCDEV VOYAGE

K. Kotisalo and P. Kujala
Helsinki University of Technology, Ship Laboratory, Espoo, Finland

1. ABSTRACT

During the Arctic Demonstration and Exploratory Voyage (ARCDEV) from Murmansk to the Ob Bay and back during the spring of 1998 ice load measurements were carried out onboard the tanker Uikku. The aim of these measurements was to study the ice induced loads on the ship hull when the ship navigates in various ice conditions. The hull of M/T Uikku was instrumented so that ice induced loads and stresses on shell plating could be studied at various locations along the ship hull both in the longitudinal and vertical directions. The measuring system gathered time histories and maximum values on 20 minute periods 24 hours/day. Some propulsion quantities were also recorded.

The collected database and conducted statistical analysis of 20 minute extreme values form a good basis for the evaluation of safety of ships navigating along the Northern Sea Route (NSR). The results of these measurements may also used in the development of unifield requrements for polar ship structures for International Association of Classification Societies (IACS) and in understanding and validating the ice load calculation methods on which the rules are based.

2. INTRODUCTION

The Arctic Demonstration Voyage to the Russian Arctic demonstrated the viability of year-round marine transportation in this area, linking Siberia to Europe. The project took advantage of gasoil transport from the experimental production site Sabeta, located on the Yamal Peninsula at the northwestern shore of the Ob Bay, to the port of Rotterdam. This sea transport was conducted by the product tanker M/T Uikku in April and May 1998.

One important task of the work conducted during the voyage was to measure the ice induced loads on the hull and the propulsion devices of M/T Uikku. The hull of M/T Uikku was instrumented so that ice induced loads and stresses on the shell plating could be studied at various locations both in longitudinal and in vertical directions along the ship hull. Longitudinal bending stresses at two locations on the hull and ship vertical accelerations were measured to study the global ship behavior when hitting e.g. heavy ice ridges. (Kotisalo & Kujala 1999)

These results are to be used in the ARCDEV-project to assess the load level encountered in various ice conditions and operating modes navigating in the western part of the NSR. Further, the loading data is to be used to determine the required strength level.

3. THE SHIP

The motor tanker Uikku is a double hull ice breaking tanker with eight cargo tanks and two slop tanks. The ship is owned by Neste Shippings and Kvaerner Masa-Yards' joint venture company Nemarc The ship's main particulars are presented in Table 1.

Table 1. Main particulars of M/T Uikku

Length O.A.	164.4 m
Length B.P.	150 m
Breath moulded	22.2 m
Depth moulded	12 m
Corresponding deadweight	15748 tons

The ship is classified by Det Norske Veritas as class +1 A 1 Tanker for Oil, and by the Finnish Board of Navigation as ice class 1 A super. The ship was built in 1976 at Werft Nobiskrug Gmbh, and Kvaerner Masa-Yards conducted an Azipod conversion in 1993. Normal tensile steel (σ_y=235 Mpa) is used except in the longitudinally framed area at midbody region where high strength steel (σ_y=360 Mpa) is applied. The ship has a diesel electric propulsion system with four diesel generators. The ship's maximum propulsion power is 11.4 MW.

4. THE MEASURING SYSTEM

The aim of the measurements was to study the ice induced loads on the ship hull and the ship accelerations at the bow when the ship navigated in various ice conditions. Time histories of almost all signals were recorded during the whole period in the ice. Maximum values of each signal were recorded on 20 minute periods. The period was kept short so that, later in the analysis, the maximum values could be related to the prevailing ice conditions.

The measurements included the following items onboard M/T Uikku:

- Load on the shell transverse frame at bow area (#196.5), at bow shoulder area (#175.5), at midbody area and at aftship area (# 52.5 and #38.5) (measured by shear strain gauges).
- Load on the shell longitudinal frames at midbody area (#63.5-65), (measured by shear strain gauges).
- Stresses on the shell plating and frames at the waterline at bow area (#196.5), at bow shoulder area (#175.5), at midsbody area (#63.5-65) and at aftship area (# 52.5 and #38.5).
- The longitudinal bending stresses on deck at midbody (#120).
-Vertical accelerations at the bow and stern of the ship and longitudinal acceleration at bow.
-Steering angle of the Azipod and power, torque and r.p.m. of the propulsion motor.

4.1 Instrumentation

VTT Manufacturing Technology conducted the instrumentation as a sub contractor to Helsinki University of Technology (HUT). The measuring system consists of 61 strain gages, which were connected as 42 sensors. The detailed locations of the instrumentation are presented on Figure 1.

The ice loads were evaluated by measuring shear strains at the neutral axis of the frame. The approach of recording shear strains on the web of a frame was chosen because the loads

experienced by frames are the main interest of the present study. The method to determine ice induced loads through shear strains was earlier used on full scale measurements in the Baltic Sea area (Riska et al. 1983). Shear strain gauge pairs are connected so that the load between gauges could be measured by using one recording channel. From each instrumented frame loads were measured separately from the upper, middle and lower part of the frame.

Accelerations at two points of the hull were also measured at the bow and at the aft of the ship.

The signals from the sensors were amplified with DC-amplifiers. In addition, low pass filters were used to filter high frequency noise from the measured signals.

4.2 Calibration of the load measuring system

The influence coefficients for the load-measuring (FFR) system are based on the assumption that the entire ice load from the plating goes through the frames. So after the shear stress distribution at the ends of the frames is determined, the load applied on the frame between these locations can be calculated. For each instrumented frame the shear stress distribution was calculated analytically and also by using finite element models.

5. DESCRIPTION OF THE VOYAGE

M/T Uikku started in ballast condition from the port of Murmansk on 26th of April 1998. Draughts in ballast and cargo condition are presented in Table 2.

Due to the heavy ice conditions and the east wind the passage through the Kara Gate was blocked and the convoy –M/T Uikku and IB Kapitan Dranitsyn- entered the Kara Sea using the northern route. The north edge of Novaya Zemlja was passed on 29th of April and the nuclear icebreaker Rossiya joined to the convoy. The route of the convoy is presented in Figure 3

While the convoy was proceeding through the Kara Sea the IBN Vaygach broke a channel through the fast ice of the Bay of Ob to the town of Sabeta. The convoy reached the entrance of this channel on 3rd of May, when the IBN Rossiya left the convoy. M/T Uikku and IB Kapitan Dranitsyn proceeded on their own to Sabeta, and the convoy reached the sub-ice loading terminal on 4th of May.

Loading was completed on 8th of May and the convoy proceeded back to the Kara Sea. When the convoy reached the Kara Sea the draught of M/T Uikku was increased by taking on ballast water. On the Kara Sea IBN Rossiya joined the convoy and assisted the convoy through the Kara Gate to the Barents Sea, where the convoy arrived on 12th of May. After light ice conditions and open water were reached M/T Uikku proceeded independently to Murmansk, where she arrived on 13th of May.

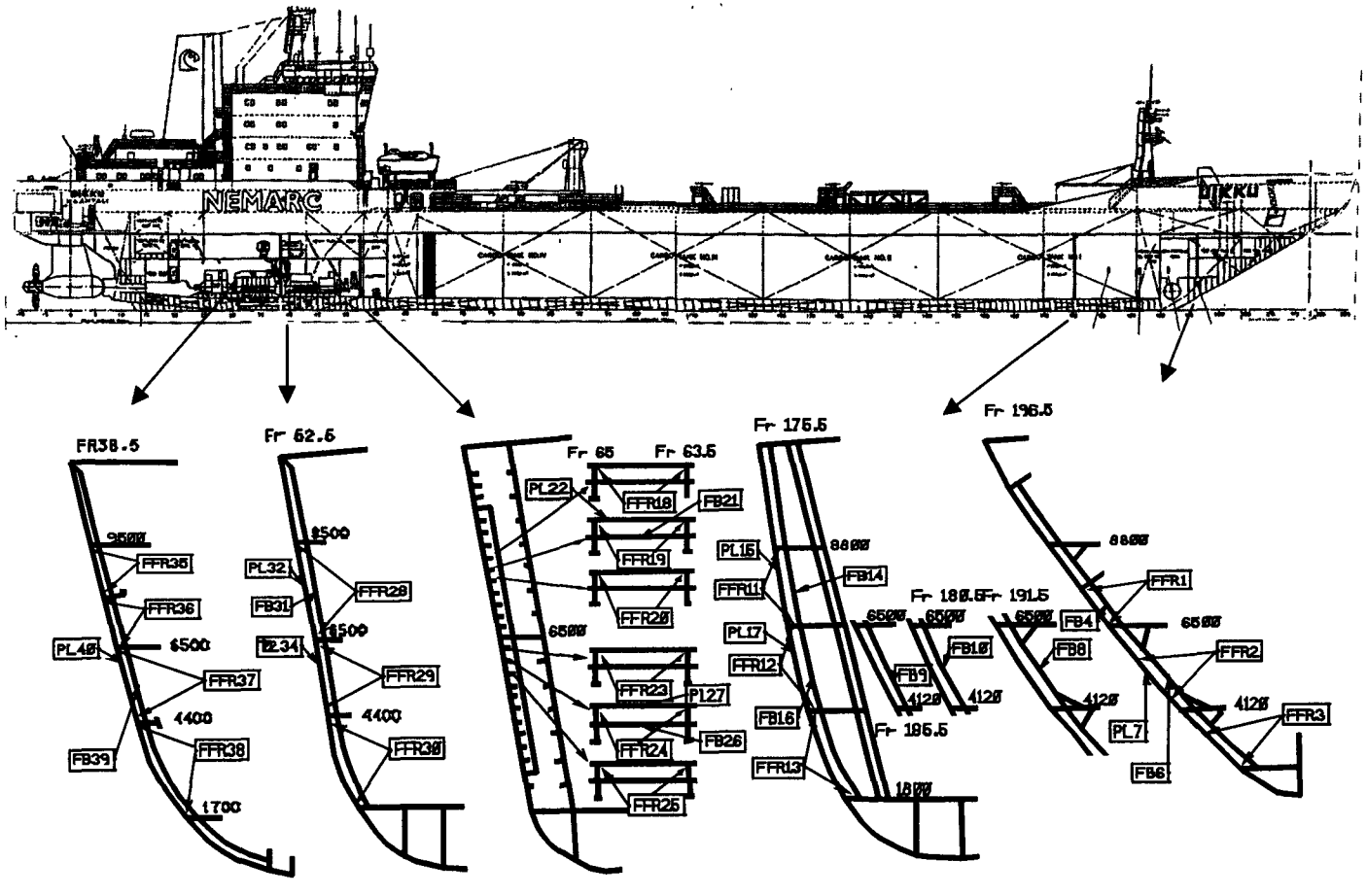

Figure 1: Instrumentation of M/T Uikku

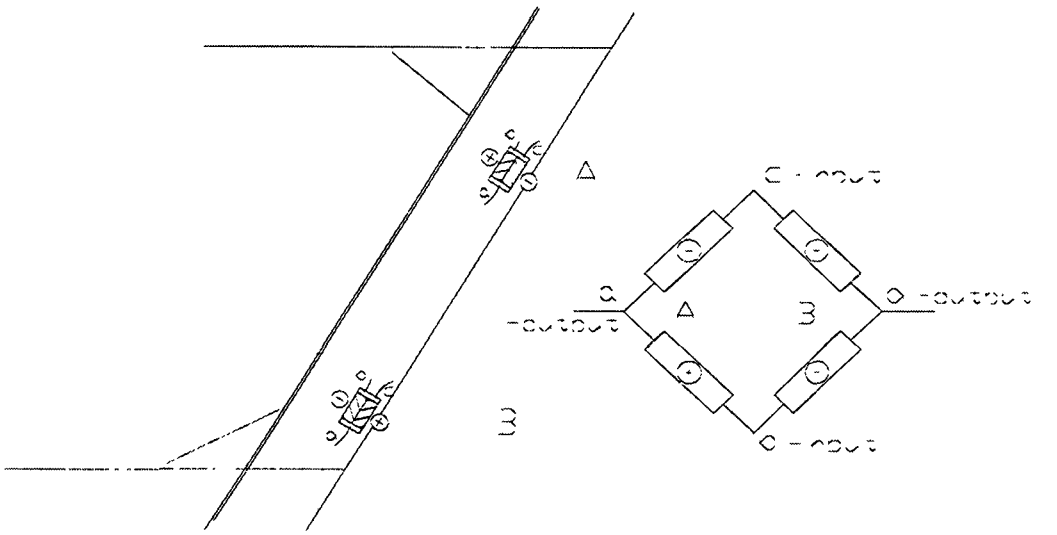

Figure 2: Arrangement to measure load from the frame (picture not to scale).

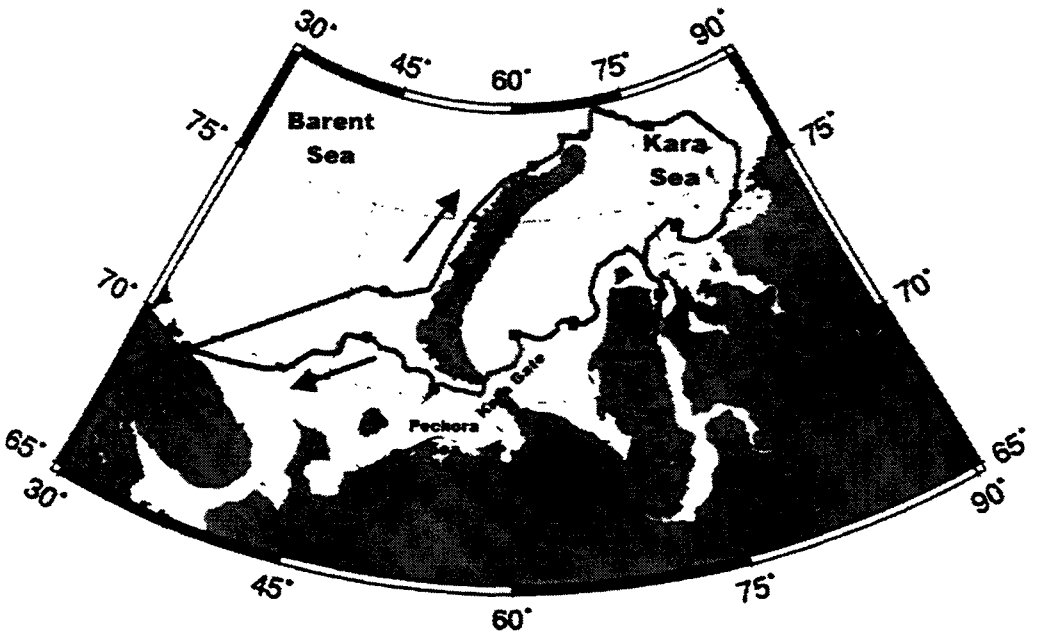

Figure 3: Route of the convoy (http://arcdev.neste.com 1998).

Table 2: Draughts of the M/T Uikku during the voyage [m].

Draughts of the ship		
	T_a	T_f
Ballast condition (from Murmansk to Sabeta)	6.8	5.8
Cargo condition (from Sabeta to Kara Sea)	8.5	7.9
Cargo condition (from Kara Sea to Murmansk)	9	8.3

6. MEASUREMENTS CONDUCTED DURING THE VOYAGE

During the voyage three parallel 32 channel recording systems were used. A PC based recording system was used to collect maximum, minimum and average values during each 20 minute period. This system collected extreme values automatically during the voyage. Another PC based recording system was used to record time histories. Altogether, there were 55 periods with a duration of 10 minutes recorded with this PC based recording system during ballast condition and 58 during cargo condition. 27 of these were analysed more carefully. 256 Hz/channel was used as a digitizing frequency on both PC based recording systems. Signals were also recorded continuously 24 hours/day with a digital 32 channel tape recorder. A digitizing frequency of 600 Hz/channel was used in the tape recorder.

Loads are presented using kN/m, where the length used is the frame spacing for the transverse frames and length along the frame for the longitudinal frames. Time, which is used with extreme values, is the ending time of the 20 minute period. (Kotisalo & Kujala 1999)

7. RESULTS OF THE MEASUREMENTS

The observed ice induced load and stress level on the hull was fairly high. This is shown by some permanent deflections of various parts of the hull. Most of them were so small that sensors could be balanced after the event without any loss of sensitivity of the sensor.

Relative maximum loads on various hull areas of the ship divided according to sea area and type of operation are presented in Figure 4. The highest loads were measured from the bow shoulder area except when the ship was towed by the icebreaker.

The relative maximum loads are plotted on Figure 5 as a function of the maximum ice thickness during the measuring period while ship was navigating on the Kara Sea with IB assistance. Used load scale is equal with scale used on Figure 4. Presented ice thickness are based on visual observations made onboard M/T Uikku. Maximum ice thickness is divided into five classes (<10, 10-30, 30-70, 70-120, >120 cm), these classes are presented in Figure 5 by using the maximum value of each class.

The highest loads are frequently connected with special kinds of operation such as approaching and attaching to the loading terminal or tight turns. The radius of turning has a remarkable influence on the loads especially on the aft and midbody areas. The relation between the angle of the Azipod and loads on mid and aft ship areas can clearly be seen from figures Figure 6 and Figure 7.

Another factor of operation of the ship, which has an effect on the loads, is used propulsion power. The relation between power and the 20 minute period maximum loads was found to be strongest when the ship was assisted in the level ice field, presented in Figure 8.

Figure 9 gives the distribution of the 20-minute maximum loads in the vertical direction on various parts of the hull when the ship was navigating through the Kara Sea. The presented distance is measured from the midspan of each instrumented part of the frame to the waterline.

The level of the measured loads can be checked by comparing the measured loads (FFR2, FFR12, FFR29 and FFR37) with the measured bending stresses at midspan (FB6, FB16, FB33 and FB39) as shown in Figure 10. This figure also shows the calculated relationships between loads and stresses at the midspan of the frames. Calculations are made by using FEM and by following the Finnish-Swedish ice rules (1985). FEM calculations are made by using two different kinds of boundary conditions, the frame is fully fixed at both ends in the lower relation and the upper relation is calculated so that the frame is simply supported. From the Finnish-Swedish ice rules formulas for continuous frames between several decks or stringers (m=5.7) were used to calculate the relation between the load and stress.

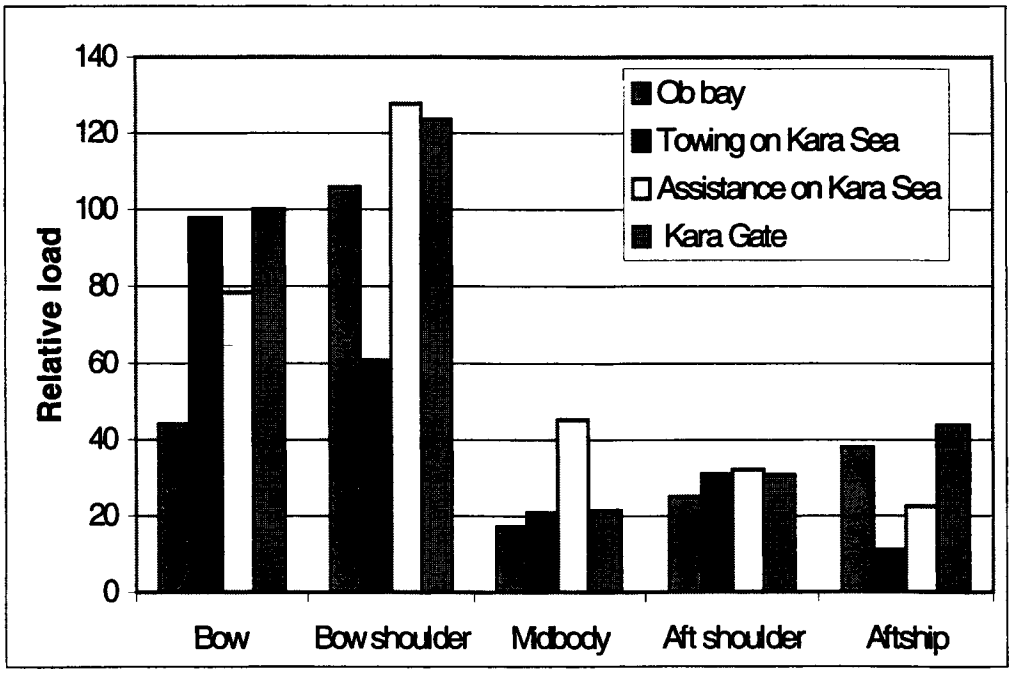

Figure 4: Relative maximum loads on different hull areas of M/T Uikku.

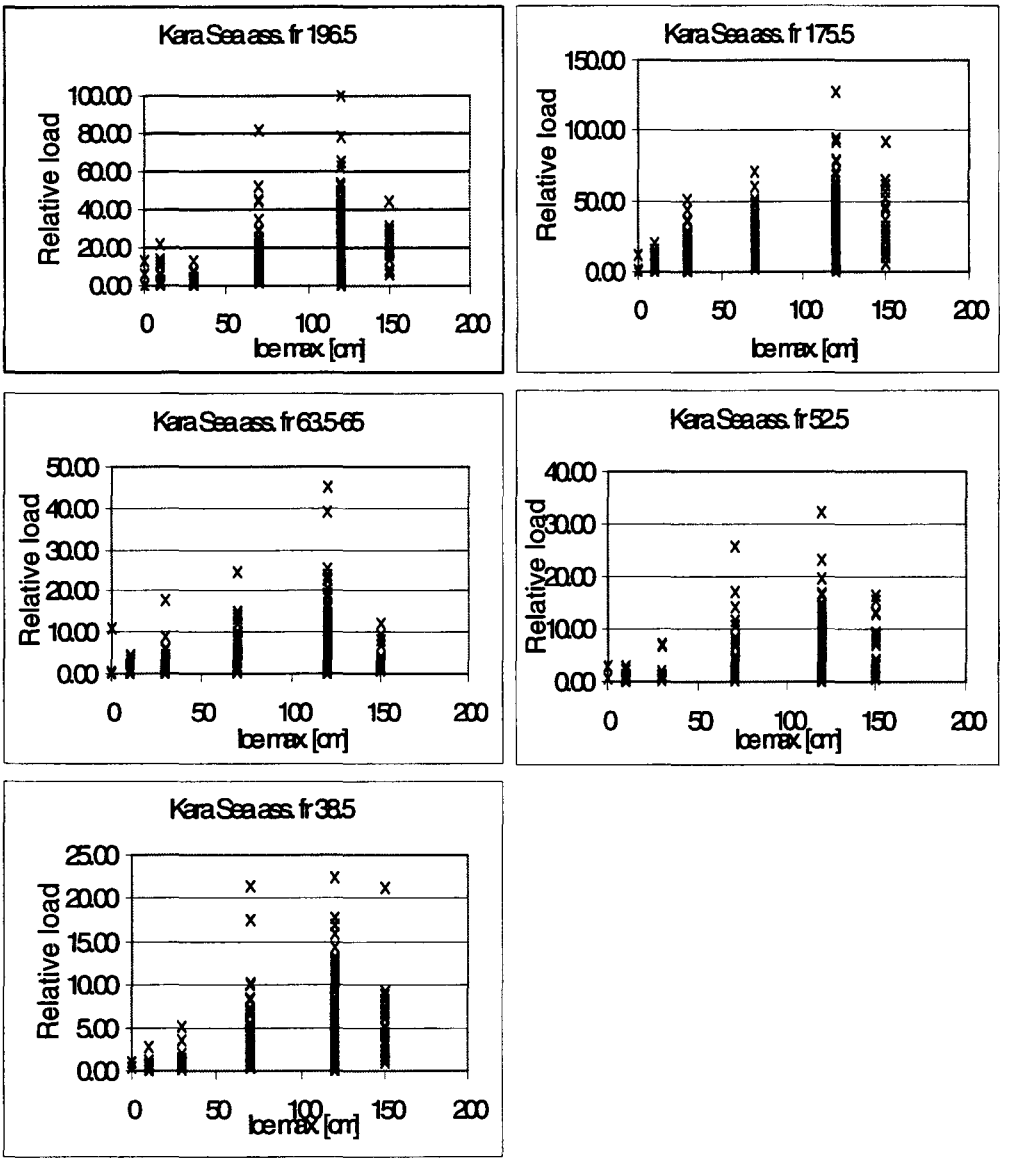

Figure 5: Maximum loads of 20 minute periods as a function of maximum level ice thickness while the ship was navigating on the Kara Sea with IB assistance.

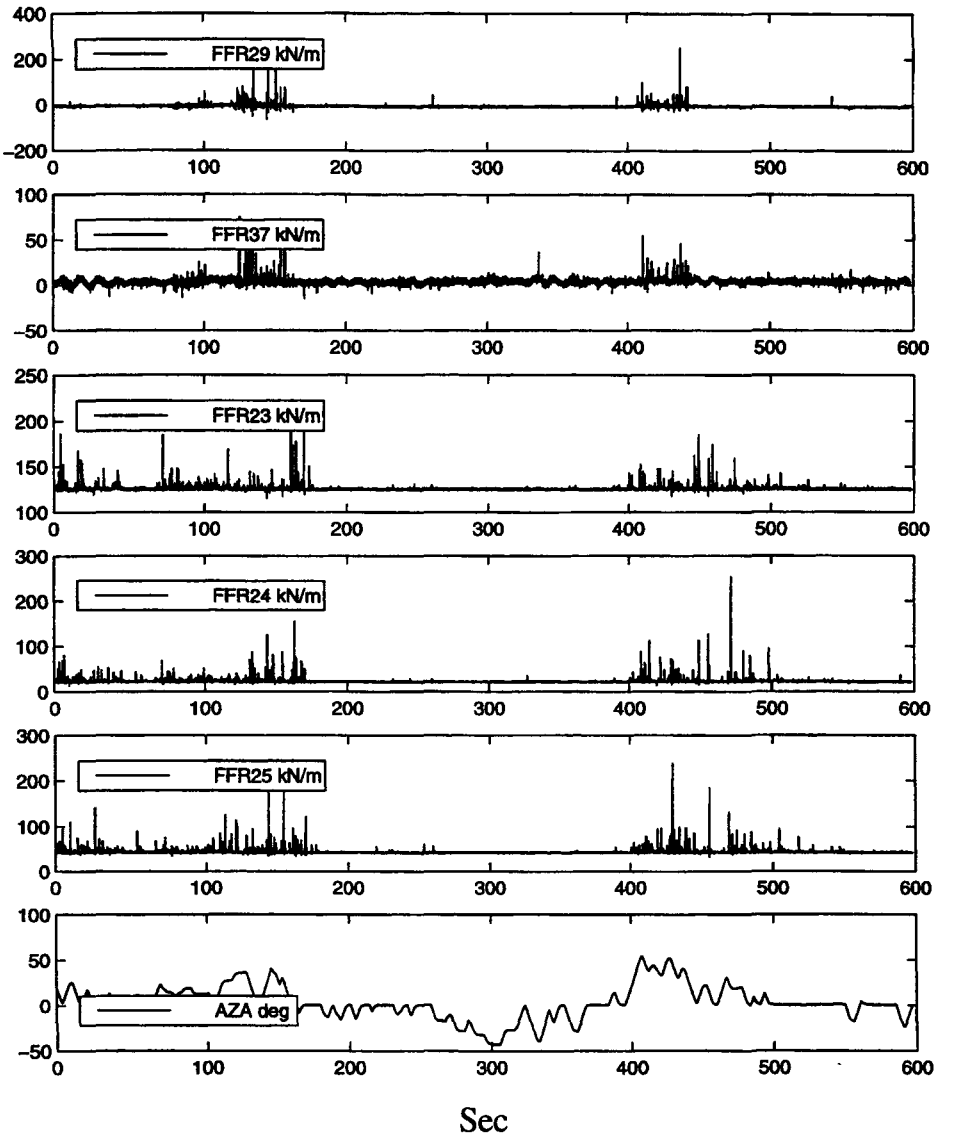

Figure 6: Example of the relation between positive (clockwise) angle of azipod and loads on the starboard side of the ship.

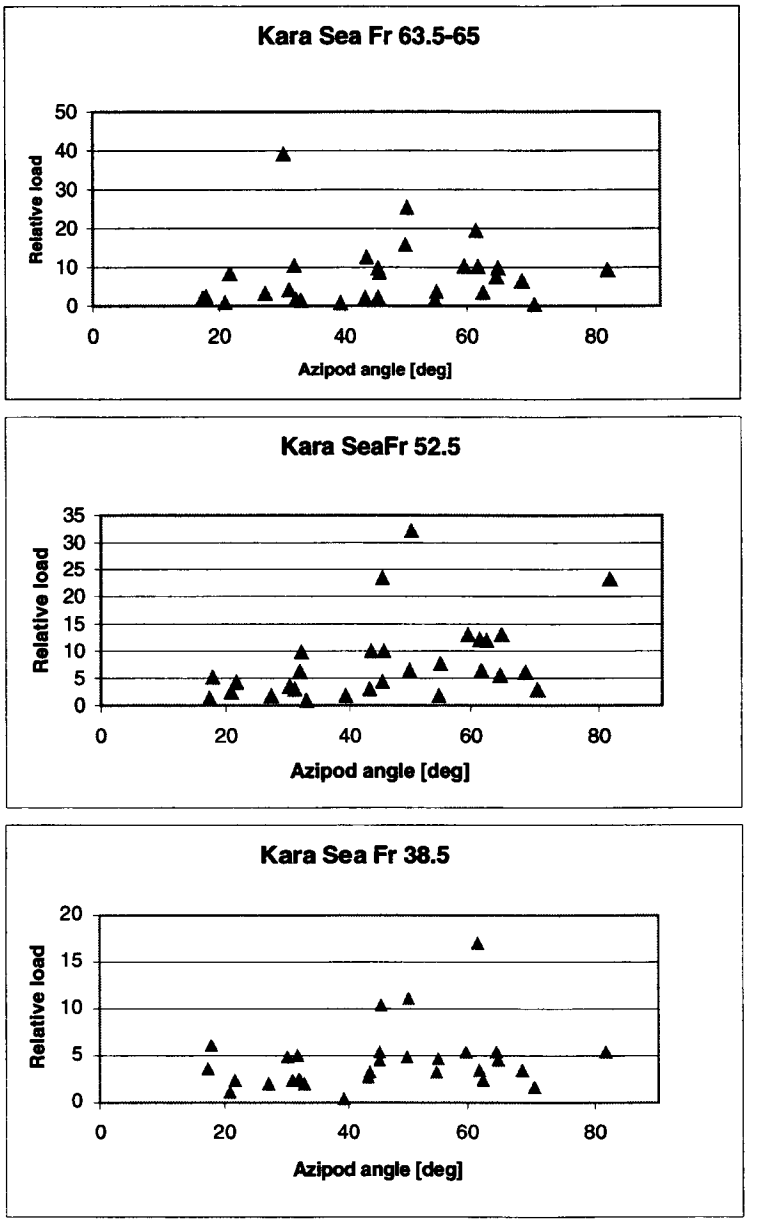

Figure 7: Maximum loads on the starboard side of the as a function of maximum angle of azipod (clockwise), when the maximum speed during the period was 5-10 kn and maximum ice thickness 70-120 cm.

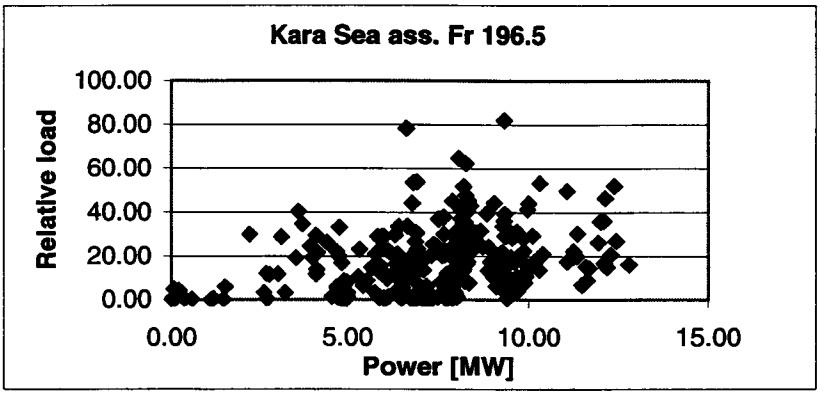

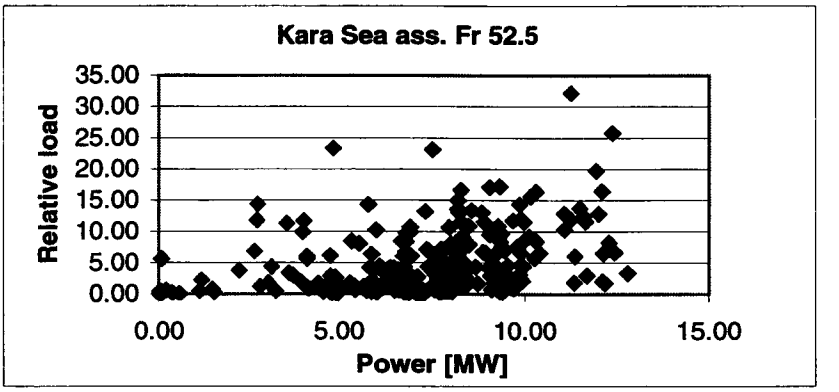

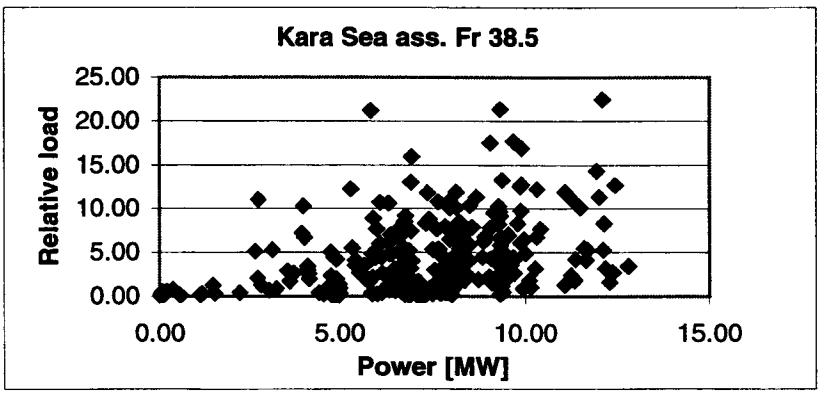

Figure 8: Maximum loads on different areas of the hull as a function of propulsion power.

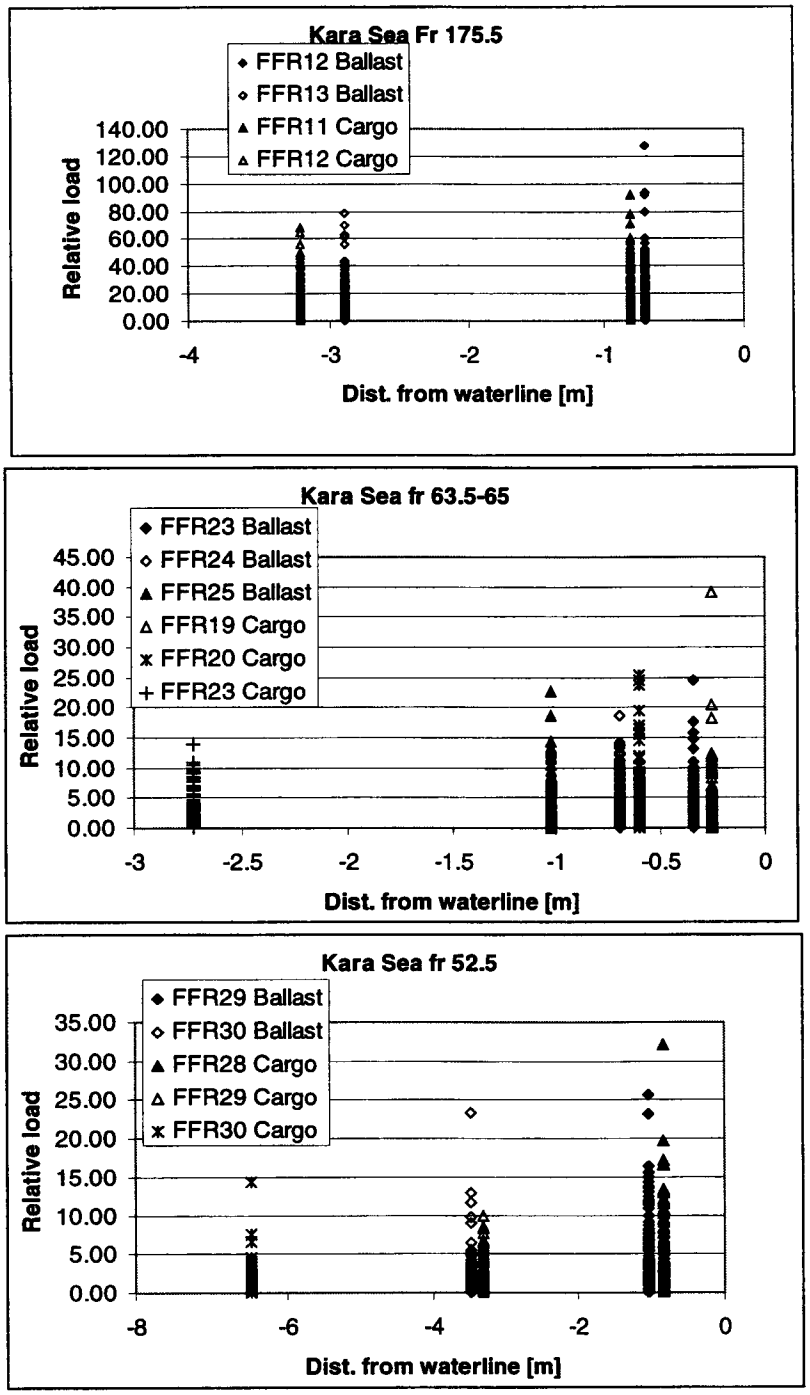

Figure 9: Load distribution in vertical direction.

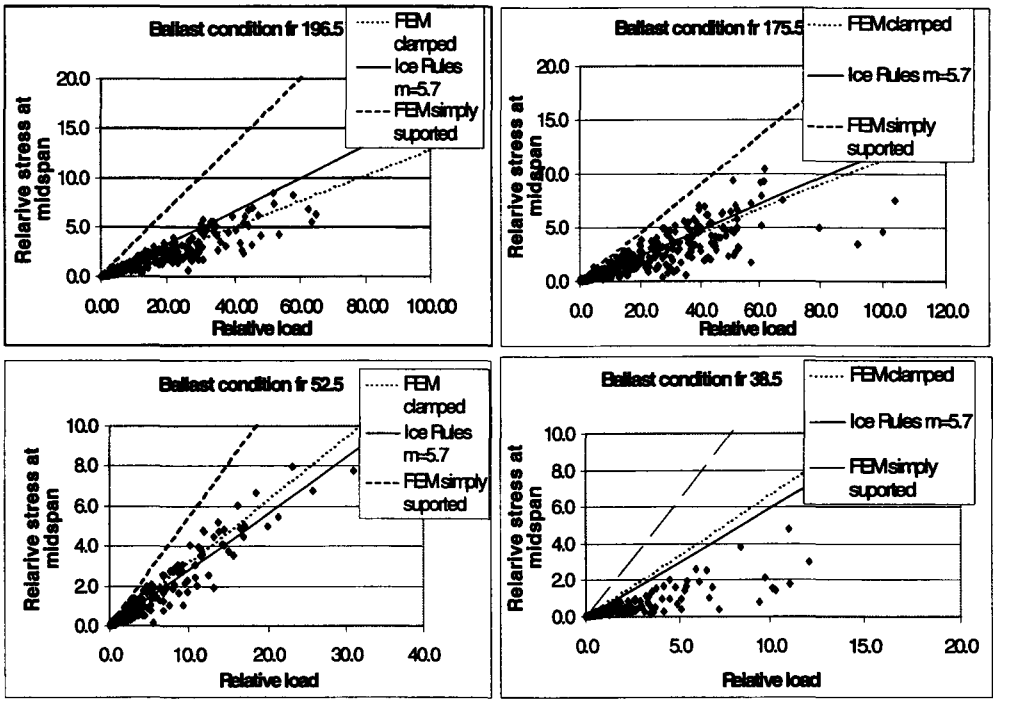

Figure 10: Comparison of the measured loads and stresses on the midspan. Also the calculated relations are given.

8. CONCLUSIONS

The measuring system installed onboard M/T Uikku worked well throughout the voyage. The database gathered consists of time histories of all the instrumented channels and maximum, minimum and average values observed on 20 minute periods monitored 24 hours/day.

The database gathered shows a wide scatter of ice induced loads. This variation can be explained by the statistical nature of the ice loads due to the large amount of factors that have an influence on the magnitude of the loads.

In addition to the existing ice conditions, the ship operation profile has a significant influence on the ice induced loads. Highest load values were often connected to some special kind of operation of the ship. The angle of the azipod has a clear effect on the loads on the aft part of midbody and aftship areas. The effect of the used engine power can be seen on the measured maximum values on all the measured areas.

The database shortly illustrated here forms a good basis for analysing the ice-induced loads in various ice conditions and operations of the ship. Clear indications for the proper level of ice strengthening for ships navigating in these ice-conditions also can be achieved from the database.

9. ACKNOWLEDGEMENTS

This work is a part of the project "Arctic Demonstration Voyage" (contract No WA-97-SC.2191) supported by the European Commission, DG VII, through Sea Transport Programme. The project is coordinated by the Neste OYJ. From European Union member countries following companies and institutions participate: Earth Observation Sciences Ltd, GB; Helsinki University of Technology, Ship Laboratory, FI; Hamburg Ship Model Basin Ltd., DE; Institute of Ship Operation, Sea Transport and Simulation,DE; Kvaerner Masa Yards, FI; Lloyds Register, GB; Aker - MTW Shipyard, DE; Nansen Environmental and Remote Sensing Center, NO; REMTEC Systems Ltd., FI; Tecnomare S.p.A, IT; and Shell Vankor Development, NL. The Russian partners in the ARCDEV project are: State Research Center of the Russian Federation Arctic and Antarctic Research Institute; Arctic Shipping Service; Central Marine Research and Design Institute; State Research Center of the Russian Federation Krylov Ship Research Institute; and Murmansk Shipping Company

10.REFERENCES

Finnish-Swedish ice class rules 1985. Board of Navigation, Helsinki. 43p.

http://arcdev.neste.com/voyage.html. 1998.

Kotisalo, K. & Kujala, P., 1999, Ice load measurements onboard M/T Uikku. ARCDEV-project. Helsinki University of Tehnology, Ship Laboratory, Report D-47. 200 p. Not published.

Riska, K. et al., 1983, Ice load and pressure measurements on board I.B. Sisu, POAC 83, porc. vol. 2, Helsinki, Apr. 5-9, 1983. Publ. Technical Research Centre of Finland (VVT), Espoo 1983. VVT Symposium 28. Pp. 1055-1069.

SYMMETRIC AND ASYMMETRIC FLAKING PROCESSES

Tuomo Kärnä and Erkki Järvinen
VTT Building Technology

ABSTRACT

This paper discusses some key problems related to the development of dynamic ice-structure interaction models. Emphasis is placed on brittle and transitional ice failure phenomena that occur in the near field area of an ice sheet acting on a vertical structure. The paper shows that the ice failure process may consist of both symmetric and asymmetric flaking (spalling) at the ice edge. It is proposed that asymmetric flaking (spalling) is typical for high rates of indentation whereas symmetric flaking can be anticipated for low rates of interaction. The influence of interfacial friction on changes between these types of flaking is discussed.

1. INTRODUCTION

1.1 A persistent problem in predicting ice loads

This paper considers some features of the dynamic interaction between level ice and a vertical faced structure. Figure 1 shows a proposed universal curve for uniaxial crushing and indentation (Michel 1978, Sanderson 1988). We are interested in the decrease of the "uniaxial/indentation strength", which occurs at a transitional loading rate. This decrease in ice strength was seen first by Peyton (1966) in laboratory indentation tests, in field tests as well as in direct compression tests on large samples of sea ice. A similar decrease in ice strength was reported by Schwarz (1970), Carter and Michel (1971), Hirayama et al. (1975), Michel and Toussaint (1977), Määttänen (1981), Sodhi and Morris (1984), Tsuchiya et al. (1985) and Tuhkuri (1995). The detailed studies of Wu et al. (1976) indicate that the transitional rate with the decreasing indentation pressure depends on the ice temperature.

Results of laboratory studies on ice indentation with compliant indenters have been reported by Sodhi (1991, 1997, 1998a), Muhonen et al. (1992), Kärnä et al. (1993) and Kamesaki et al. (1995). These studies show that the decrease in the apparent ice strength, which occurs in the transitional loading rate is associated with a change from almost simultaneous ice failure into non-simultaneous ice failure in front of the indenter.

The universal curve shown in Fig. 1 compiles data from both uniaxial compressive tests and indentation tests. Therefore, both kind of data are traditionally described in terms of ice crushing strength. However, it should be appreciated that for indentation tests the strength was obtained by dividing the measured global load by a nominal contact area. The inference is that the measured decrease in the apparent crushing strength (named here as "negative pressure gradient") is not necessarily a pure ice property. In fact, the laboratory indentation tests

mentioned above show that this feature is relevant for the global ice load and is associated with a change in the ice failure mode.

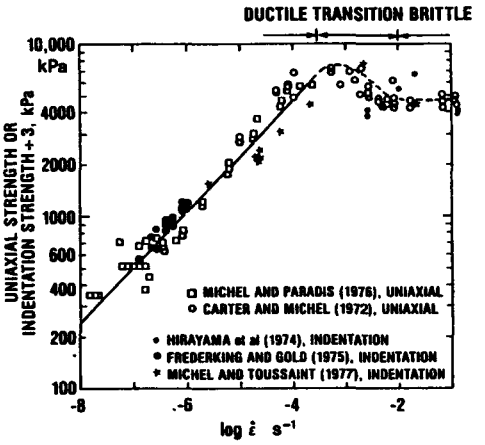

Figure 1. Universal curve for uniaxial crushing and indentation of sea ice(Michel 1978, Sandersson 1988).

Sodhi (1998a) explains this change by noting that for low indentation velocities, a large zone of microcracks appears in the ice sheet adjacent to the structure. The associated deformations of the ice sheet result in almost simultaneous failure of the ice sheet and into highest global loads. During high-speed indentation, the zone of microcracks remains small. Therefore, failure of the ice takes place by successive flaking of ice from small zones of microcraked ice. Daley et al. (1998) describe further details of the ice failure process by summarising various ways that solid ice can fail and become pulverised ice.

1.2 Consequences

The negative gradient discussed above has two significant consequences in predicting the ice effects on offshore structures. First, steady-state vibrations may arise due to this phenomenon. Models capable of predicting ice induced vibrations [e.g. Määttänen 1978, Kärnä et al. 1994b, 1997, 1999] are based on the assumption that the indentation pressure and/or the global load exhibit a negative gradient at a transitional region of indentation rate. The mass forces that arise during steady-state vibrations may cause a significant magnification in the internal stresses within the structure.

It has been proposed that ice induced vibration is a resonant phenomenon, which can be modelled using a characteristic frequency for ice (Sodhi et al. 1984, 1988). This parameter is defined using a damage length d_s (Fig. 4), which is the distance of ice movement between two adjacent events of ice failure. This damage parameter is not a pure ice property but depends also on the stiffness of the structure (Kärnä et al. 1993). Therefore, it is not likely that ice induced vibration can be modelled as a resonant phenomenon.

The second consequence of the negative gradient is depicted in Fig. 2. Kamesaki et al. (1996) studied data of several series of laboratory indentation tests. They showed that the

quasi-static peak loads on compliant structures can be 50% to 150% higher than the load on a rigid structure. Therefore, we can see (Fig. 2) that the structure's compliance and the contact area exert approximately equal influences on the global load. The present design practice considers the effect of the nominal contact area (Sandersson 1988) or the contact width (Blanchet 1996). The omission of the influence due to the compliance is clearly a major reason for the prevailing lack of consensus on the magnitude of ice loads on vertical structures.

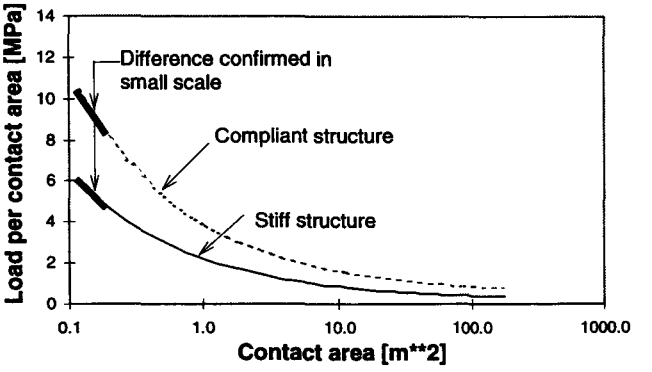

Figure 2. Influence of contact area and structure' s compliance on the global load.

2. THE NEGATIVE PRESSURE GRADIENT

The physical reasons for the negative pressure gradient are not clear at present. A plausible explanation is that ice failure mode at each cross section, adjacent to the ice edge changes as the rate of interaction changes. Timco & Frederking (1995) and Daley et al. (1998) provide overviews of the present understanding of the ice failure at a cross-section of the ice edge interacting with a structure. The global load on a wide structure is the sum of all cross-sectional local forces. Therefore, cross-sectional studies of the ice failure can not provide a full explanation for the negative pressure gradient. We should study also the correlation between the local forces. Experiments show that the abrupt decrease of the global load at a transitional indentation rate is related to a change in the correlation between the local forces. In particular, it is widely accepted that the negative pressure gradient is caused by a change from almost simultaneous ice failure at low indentation rate into non-simultaneous failure at high rate [Sodhi 1991, 1997, 1998; Kärnä et al. 1993].

The basic reasons for a change from simultaneous into non-simultaneous ice failure are not fully understood. A further problem is that this phenomena provides only a qualitative explanation for the negative pressure gradient. More fundamental concepts are needed for numerical modelling of the ice loads.

A few scenarios are discussed below to explain the basic physical reasons for the negative pressure gradient. Let us consider situations where a structure penetrates into an ice sheet (Fig. 3). The changes in the relative velocity between the structure and the ice edge are an essential part of our study. Therefore, we will consider both stiff and compliant structures.

During each loading phase the global load increases because the structure and the ice edge are in contact and move against each other (Fig. 4). The peak load is obtained at an event of ice failure. Due to the ice failure, the structure rebounds at a high velocity against the ice edge. The length (d_c in Fig. 4) of this transient motion is short if the structure is stiff. In the case of compliant structures the transient displacement can be significantly larger than the displacement during the loading phase.

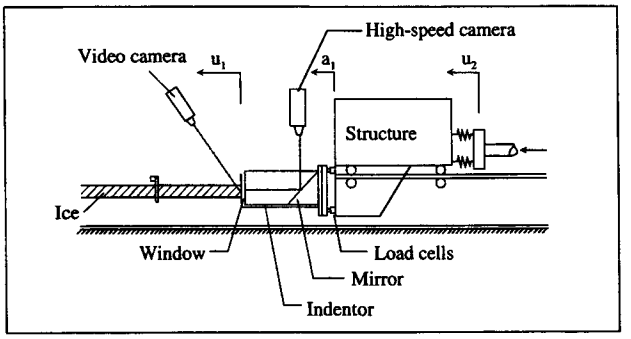

Figure 3. Test set-up in a series of indentation tests (Muhonen et al. 1992).

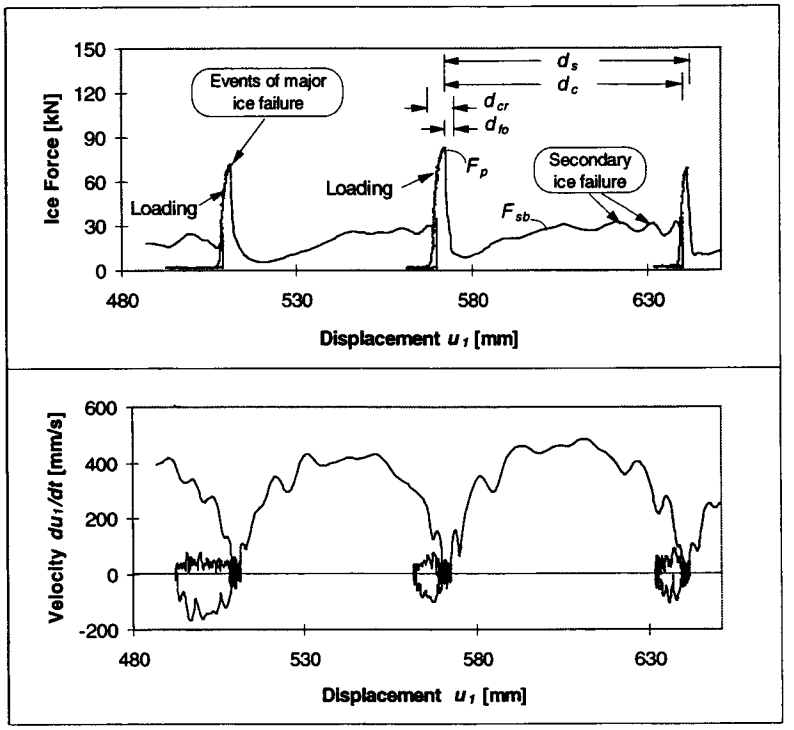

Figure 4. The global force- and the velocity signals in an indentation test with a compliant structure (Time window of test No 69, Muhonen et al. 1992).

2.1 Symmetric and asymmetric flaking

In indentation tests with compliant structures, the major peak forces occur at the event of a major ice failure as shown in Fig. 4 and Fig. 5(A). Horizontal cracks depicted in Fig. 5 play an important role in the failure process as discussed in Sect. 2.3. A study of the records taken by the high speed camera shows (Muhonen et al. 1992; Kärnä et al. 1993) that during each loading phase the crushed ice is stationary between the indenters and the ice edge. No flow of the crushed ice is visible through the window that was fixed at the indenter. After the ice failure, the crushed ice is extruded simultaneously upwards and downwards as depicted in Fig. 5 (A). The ice failure is simultaneous over the whole contact area. Therefore, the structure looses its contact with an intact ice at all points of the ice edge. This kind of ice failure is characterised here as symmetric flaking (or spalling). Kamesaki et al. (1997) saw a similar symmetric flaking in tests with a compliant indenter.

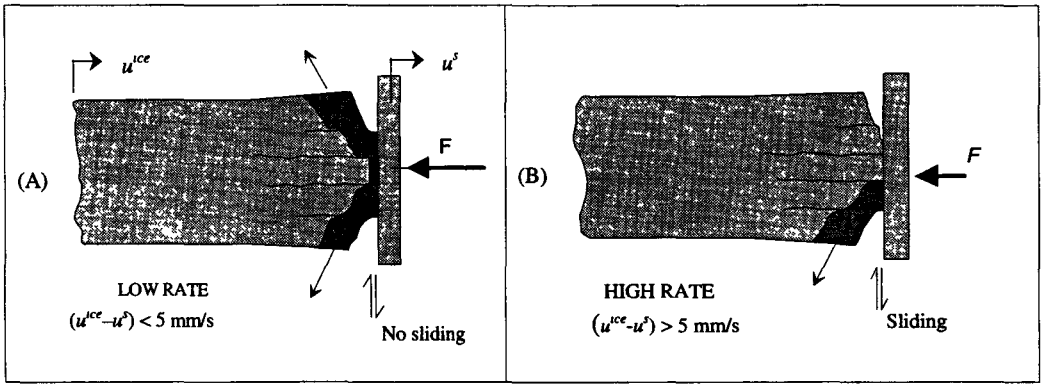

Figure 5. (A) Major event of ice crushing in an asymmetric flaking failure mode; (B) Secondary crushing in an asymmetric flaking failure mode.

During ice extrusion the structure moves against the new boundary of intact ice by a distance d_{fo}, shown in Fig. 4. This parameter (finite ice failure depth) as well as the total depth of crushing and flaking d_{cr} are convenient parameters in numerical models as measures of the ice that is lost from the ice edge during the loading and unloading (Kärnä 1994a).

Figure 4 shows that minor force peaks may occur while the structure is experiencing its high-speed transient motion after the major crushing events. Detailed studies of the video records show that these peaks are associated with secondary crushing and non-simultaneous ice failure (Kärnä et al. 1993). High speed camera records are not available for these events. However, we believe that the ice crushing at these minor force peaks can be characterised as asymmetric flaking as depicted in Fig 5(B). Daley (1992) analysed the test records of Joensuu and Riska (1989) and developed a model for sequential and asymmetric flaking. An essential feature of this kind of failure is that the structure maintains a contact with intact ice at all times. Accordingly, the finite ice failure depth parameter d_{fo} is not relevant for this failure mode.

Gagnon (1998) studied the records of a test series carried out at the Hobson's Choice Island and found evidence on asymmetric failure modes. Sodhi et al. (1998b) describe the results of medium-scale indentation tests that were carried at a constant velocity. The records show that the contact was "line-like" flaking in tests where the constant velocity was in the range of 3 mm/s to 30 mm/s. Furthermore, the failure at different zones of the ice edge occurred non-simultaneously. There are indications that the ice failure at each zone occurred as symmetric flaking at the event of first ice failure (Takeuchi et al. 1997) and as asymmetric flaking for the subsequent events of failure.

The data discussed above indicates that the conditions of almost simultaneous ice failure are usually associated with symmetric flaking whereas non-simultaneous failure occurs as asymmetric flaking. There is no consensus on the reasons for a change from symmetric into asymmetric flaking. Further studies are needed on this subject because this change is apparently connected with conditions that lead to maximum global loads on a wide offshore structures.

2.2 Velocity dependent friction

While trying to explain the mechanism that leads to the negative pressure gradient and changes between symmetric and asymmetric flaking, we may raise the following question: *Are there any basic contact forces involved in the ice-structure interaction process that exhibit a similar decrease with the rate as the global load?* An answer to this question is shown in Fig. 6. It can be seen that at a range of low sliding velocities the kinetic friction exhibits a similar decrease with the rate as the global load in ice indentation. This phenomenon was proposed originally by Bowden and Hughes (1939) and confirmed later by Barnes et al. (1971), Evans et al. (1976), Tusima and Tabata (1979), Oksanen (1983), Saeki et al. (1986), Gagnon and Molgaard (1989) as well as Jones et al. (1991). Thomson and Robbins (1990) analysed the slip-stick phenomenon in steady-state sliding and provided a plausible explanation for the negative rate effect.

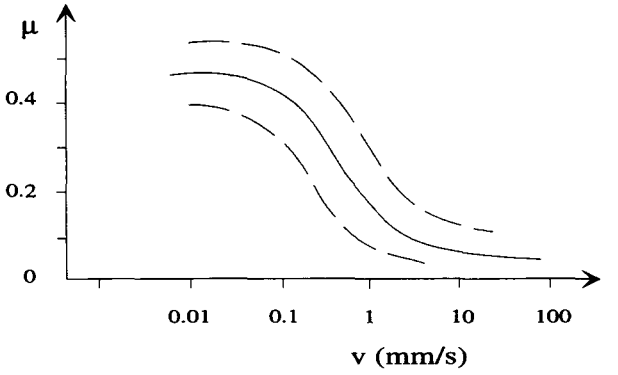

Figure 6. Kinetic friction as a function of sliding velocity v.

A tentative assumption is made here that the negative gradient seen in the kinetic friction (Fig. 6) provides a physical explanation to the negative gradient in the global load. This statement is supported by the indentation test data provided by Kato et al. (1986). Using sev-

eral flat and vertical structures with different coefficient of friction, they showed that the global ice force increases with increasing coefficient of friction.

In the present discussion we emphasise the importance of the compliance of the structure. Therefore, let us consider two different scenarios of the loading phase – one for low indentation rate and another for high rate (Fig. 7). Both laboratory experiments and field studies show (e.g. Jordaan & Singh 1994) that the ice extrusion process may involve compaction and sintering of the crushed ice into fused material in the central part of the ice edge. The vertical extent of this fused ice (S) is shown by L in Fig. 7/phase A3.

Fig. 4 illustrates that in the case of a compliant structure, the relative velocity v_r (du_I/dt) between the structure and the ice sheet varies in a wide range. After an ice failure, v_r and correspondingly the extrusion velocity v_e of the crushed ice are high. In the initial stages of a loading phase the velocity v_r may cross the zero level and become negative for a short period. Therefore, the extrusion velocity v_e of the crushed ice will also attain values close to zero. Referring to the velocity dependence of the kinetic friction we can see that substantial frictional forces T act on both sides of the layer of the crushed ice at the period of low velocities. By so doing the frictional forces will enhance the compaction of the fused material (S) and prevent the extrusion of crushed ice. This statement is supported by the data discussed in Sect. 2.1 (Muhonen et al. 1992; Kärnä et al. 1993). A layer of compated ice was always found at the ice edge after a test.

The porosity of the compacted and fused ice (S) may approach the porosity of the intact ice. Therefore, it can transmit significant forces between the structure and the edge of the intact ice. The contact pressures between the ice edge and the structure are distributed over the height L , which can amount to about 30 % of the ice thickness (Muhonen et al. 1992). The frictional force T extends over the same area and exerts a confining effect at the ice edge at low indentation rate.

In the case of high rate of interaction (Fig.7/scenario B), the velocity v_r and correspondingly the extrusion velocity v_e remain at a high level. Under this condition the frictional forces remain low and the extrusion process does not cease. Hence, the extent L of the fused material remains small or fused material does not exist at all. Joensuu & Riska (1989) as well as Fransson et al. (1992) report about such a condition in a series of tests where the contact forces were concentrated on a very narrow area (contact line) as depicted in the phases B3 to B4 of Fig. 7. Due to the concentration of the contact pressure and the low level of the frictional forces, the crushed ice does not provide any significant confining effect on the ice edge at the condition of high indentation rate.

The vertical expansive displacement v_i at the ice edge remain smaller in the case of low indentation rate due to the confinement provided by frictional force T and the compacted ice "S" (compare phases A3 and B3 in Fig. 5). Therefore, the ice edge is likely to resist a higher horizontal force at low rate. This prediction was confirmed in an analysis by Shkhinek et al. (1999, Fig. 7) who studied how the cross-sectional failure force depends on the extent L of the interfacial pressure.

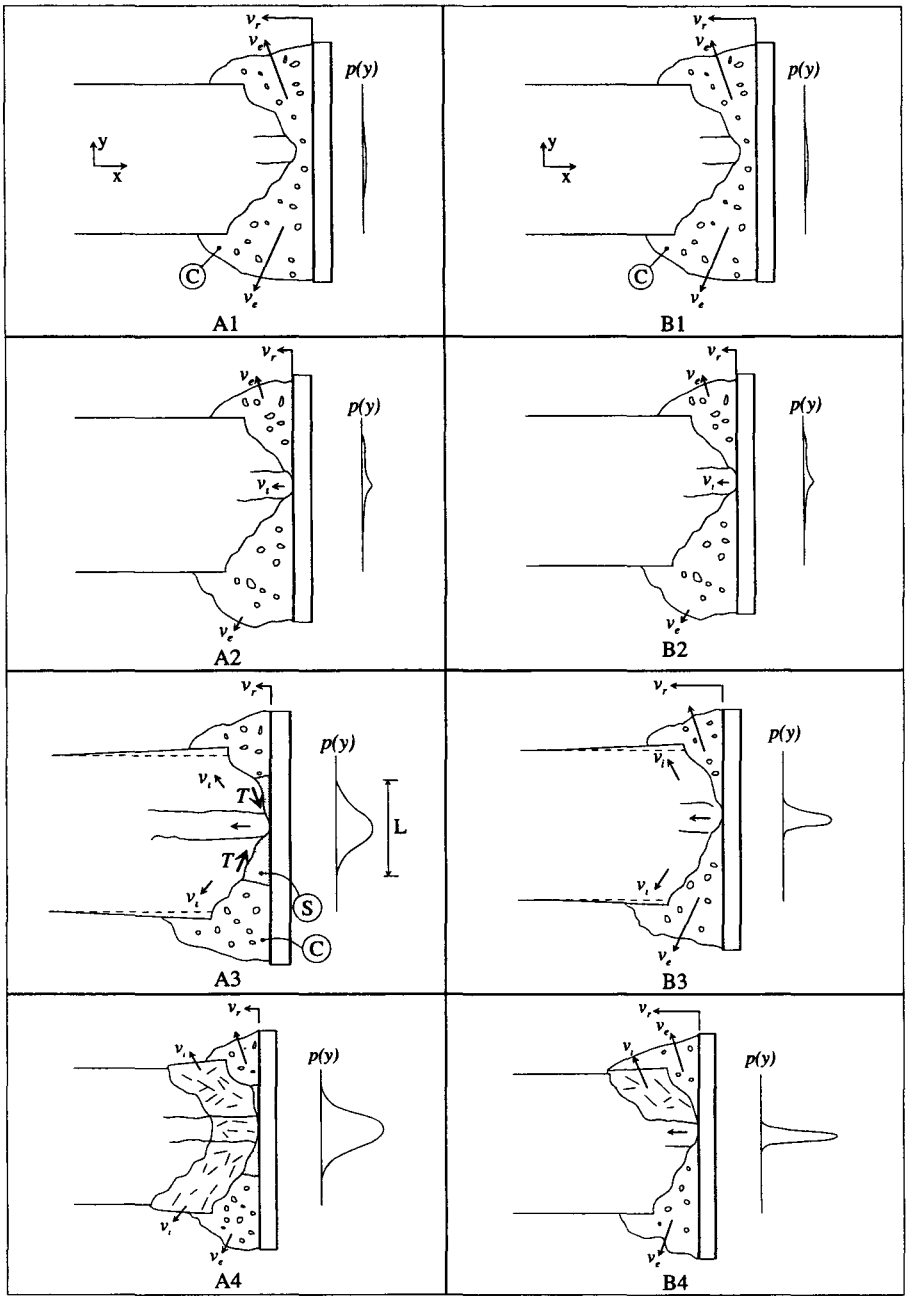

Figure 7. Scenario for the loading phase in low rate (A1 - A4) and in high rate of interaction (B1-B4).

Sodhi et al. (1998b) also found that the interfacial pressure is distributed over a large contact area if the rate of indentation was low, whereas a "line-like" contact was seen at higher rates (≥ 3 mm/s) of indentation. The spreading of the interfacial pressure over a large contact area was attributed to creep deformation within the ice. This explanation seems plausible because a servo-controlled hydraulic jack was used to provide a constant indentation velocity. However, a reference to ice creep is less credible in the case of a compliant structure where contact pressures are distributed over a large contact area. The loading phase of a compliant structure occurs at a very low rate but the loading time is probably not sufficiently long for any significant creep deformation to develop.

2.3 Rate dependent crack propagation

Figure 8 depicts the cross section of the damaged ice edge after a typical ice indentation test (Muhonen et al. 1992; Kärnä et al. 1997). Horizontal cracks depicted in Fig. 8 have been seen in almost all indentation tests. Hirayama et al. (1975) noted that these cracks are caused by vertical tensile stresses. They also postulated that the propagation of the horizontal cracks provides a primary driving mechanism for the ice failure. Numerical studies carried out by Shkhinek at al. (1999) suggest that the details of the ice failure mode discussed here depend substantially on the ratio between the tensile and compressive strength of the ice.

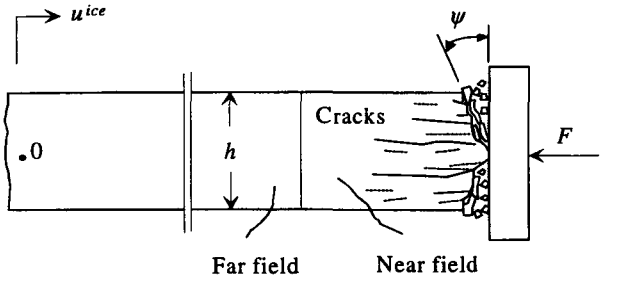

Figure 8. Near field zone with a wedge-shaped edge and horizontal cracks.

Thin sections taken from the ice edge after different indentation tests show (Kärnä et al. 1997) that the length of the horizontal cracks increases with a decrease in the average rate of indentation. This phenomenon was confirmed by Kamesaki et al. (1997). After each major event of ice failure, the ice edge gets a wedge shape. Tuhkuri et al. (1997) discribe a theoretical model that explains the formation of the wedge-shaped ice edge. The wedge angel ψ shown in Fig. 8 defines the overall geometry of the ice edge at a vertical cross section. Experimental data indicates that the wedge angel varies with the rate of indentation in the same way as the length of the horizontal cracks. In the horizontal plane the ice edge is irregular after a major failure event.

Let us now study the influence of the horizontal cracks and the wedge angel by considering compliant structures. Due to the structural compliance, each major loading phase occurs at a low rate. Accordingly, an increase in the structural compliance causes an increase in the wedge angel. Each major loading phase is followed by a transient rebound motion of the

structure against the ice edge. During this motion the structure may have new contacts with the intact but irregular ice edge. Due to the high velocity, these local contacts will lead to small cracks and secondary failures at the sharp ice edge. As discussed by Daley et al. (1998), this kind of failure can be characterised as "pulverisation due to a rapid cascade and coalescence of macrocracks". Due to the concurrent rebound motion, the sharp ice edge evolves into a blunt ice edge. The irregularity of the ice edge in the horizontal plane is reduced. Accordingly, the next major loading at a low rate will occur with a good contact between the structure and the ice edge. This mechanism has been used in numerical models to predict the difference in the global loads due to changes from non-simultaneous to almost simultaneous ice failure (Eranti 1992; Kärnä et al. 1992, 1997, 1999).

The discussion above pertained to the influence of the rate dependent horizontal cracks in one vertical cross section of the ice edge. It should be appreciated that these cracks are two dimensional. In the horizontal direction they are likely to have a direct influence on the correlation between the local forces. The present numerical models do not consider this phenomenon.

3. SUMMARY

This paper addressed the present knowledge on the contact phenomena in the interaction between ice sheets and vertical offshore structures. The main focus was on a phenomenon termed here as negative pressure gradient. At a transitional range of ice velocity, the global force degreases significantly as the velocity increases. As a consequence, structures may suffer from ice induced vibrations. Also, the global load on a compliant structure can be 50 % to 150 % higher than on a rigid structure.

The change from simultaneous into non-simultaneous failure at various cross sections of the ice edge provides a qualitative explanation for the negative pressure gradient. However, more fundamental concepts are needed in numerical models of the dynamic ice-structure interaction. This paper proposes that future models should pay attention to the propagation of the horizontal cracks, to the velocity dependent friction and also to the compaction/sintering process that influences the vertical pressure distribution at the ice edge.

ACKNOWLEDGMENT

This work has been undertaken within the LOLEIF-Project in the framework of the EU-sponsored Marine Science and Technology (MAST-III) Programme under contract no.MAS3-CT97-0078

REFERENCES

Barnes, M.A., Tabor, D, & Walker, J.C.F. (1971). The friction and creep of polycrystalline ice. *Proc. Roy. Soc. London, Series A*, 324(1557), pp. 127-155.

Bekker, A.T., Gomolski, S.G., Farafonov, A.E. & Truskov, P.A., Analysis of ice compressive tests of the Okhotsk sea ice samples. *Proc. 14th IAHR Ice Symp.* Vol. 1, pp. 583-587.

Blanchet, D. & DeFranco, S.J. (1996). Global first-year ice loads: Scale effects and non-simultaneous failure. *Proc. 13th IAHR Ice Symp.*, Beijing, 1996. pp. 203-213.

Bowden, F.P. & Hughes, T.P. (1939). The mechanism of sliding on ice and snow. *Proc. Roy. Soc. London, Series A*, 172(949), pp. 280-298.

Carter, D. & Michel, B. (1971). Lois et mécanismes de l´apparente fracture fragile de la glace de rivière et de lac. Ice Mechanics Lab., Univ. Laval, Report S-22.

Daley, C. (1992). Ice edge contact and failure. *Cold Reg. Sci. Techn.* 21, 1-23.

Daley, C., Tuhkuri, J. & Riska, K. (1998). The role of discrete failures in local ice loads. *Cold Reg. Sci. Techn.* 27 (1998) 197-211.

Eranti, E., (1992). Dynamic ice structure interaction - Theory and applications. *VTT Publications No. 90.* Espoo 1992. 81 p.

Evans, D.C.B., Nye, J.F. and Cheeseman, K.J. (1976). The kinetic friction of ice. *Proc. R. Soc. Lond. A.* 347, 493-512 (1976).

Fransson, L., Olosson, T. & Sandkvist, J., (1992). Observations of the failure process in ice blocks crushed by a flat indentor. *Proc. 11th Int. Conf. Port Ocean Eng. under Arctic Cond.* (POAC´91). St.John´s, Canada, Vol 1, pp. 501-514.

Gagnon, R.E. (1998). Analysis of visual data from medium scale indentation experiments at Hobson's Choice Ice Island. *Cold Reg. Sci. Techn.* 28(1998) 45-58.

Gagnon, R.E. & Molgaard, J. (1989). Crushing friction experiments on freshwater ice. *Proc. IUTAM/IAHR Symp. on Ice/Structure Interaction.* Memorial University of Newfoundland. St.John's, Newfoundland, Canada 14-17 August 1989.

Hirayama K., Schwarz, J. & Wu, H.C., (1975). Ice forces on vertical piles: indentation and penetration. *Proc. 3rd IAHR Ice Symp.*, Hanover NH, pp. 429-445.

Joensuu, A. & Riska, K. (1989). Contact between ice and structure. Helsinki University of Technology, Laboratory of Naval Architects and Marine Engineering, Report M-88, Otaniemi, Finland. (in Finnish).

Jones, D.E., Kennedy, F.E. & Schulson, E.M. (1991). The kinetic friction of saline ice against itself at low sliding velocity. *Annals of Glaciology*, Vol. 15, pp. 242-246.

Jordaan I.J. & Singh, S.K. (1994). Compressive ice failure: Critical zones of high pressure. *Proc. IAHR Ice Symp.*, Trondway, Norway, pp. 505-514.

Kamesaki, K., Yamauchi, Y. Horikawa, T., Kawasaki, T., Ishikawa, S. & Tozawa, S. (1995). Experimental study on independent failure zone of ice crushing. *Proc. 10th Int. Symp. Okhotsk Sea Ice.* Pp. 146-151.

Kamesaki, K., Yamauchi, Y and Kärnä, T. (1996). Ice force as a function of structural compliance. *Proc. 13th IAHR Ice Symp.* Beijing, 1996. Vol. I, pp. 395-402.

Kamesaki, K., Tsukuda, H. and Yamauchi,Y. (1997). Indentation tests with vertically placed ice sheet. *Proc. 14th Int. Conf. Port Ocean Eng. under Arctic Cond.* (POAC´97). Yokohama, Japan, Vol. IV. pp. 245-250.

Kato, K., Sodhi, D. and Haynes, D. (1986). Some effects of friction on ice forces against vertical structures. *Proc. 5th Int. Conf. Offshore Mech. Arctic Eng.* (OMAE´86). Vol. 4, pp. 528-533.

Kärnä, T. (1992). A procedure for dynamic soil-structure-ice interaction. *Proc. 2nd Int. Offshore and Polar Eng. Conf.* (ISOPE-92). San Francisco, Vol II, pp. 764 - 770

Kärnä T., Muhonen, A. and Sippola M. (1993). Rate effects in brittle ice crushing. *Proc. 12th Int. Conf. Port Ocean Eng. under Arctic Conditions.* (POAC´93). Hamburg, August 17-20. Vol. 1. pp. 59-71.

Kärnä, T. (1994a). Finite ice failure depth in penetration of vertical indentor into an ice edge. *Annals of Glaciology* 19, pp. 114-120.

Kärnä, T. (1994b). Mitigation of steady-state vibrations induced by ice. *Proc. 4th Int. Offshore and Polar Eng. Conf.* (ISOPE'94). Osaka, April 10.15, 1994.

Kärnä, T., Kamesaki, K. and Tsukuda, H. (1997). A Flaking Model of Dynamic Ice-Structure Interaction. VTT Building Technology, Internal Report RTE38-IR-7/1997.

Kärnä, T., Kamesaki, K. and Tsukuda, H. (1999). A numerical model for dynamic ice-structure interaction. *Computers and structures* 72(1999) 645-658.

Michel, B. & Toussaint, N. (1977). Mechanisms and theory of indentation of ice plates. *J. Glaciology* 19, No 81, pp. 285-301.

Michel, B. *Ice Mechanics* (1978). Les Presses de l'Université Laval. Québec. 499 p.

Muhonen, A., Kärnä, T., Eranti, E. Riska, K. Järvinen, E. & Lehmus, E. (1992). Laboratory indentation tests with thick freshwater ice. Vol I. *VTT Research Notes 1370.* Espoo, 92 p.

Määttänen, M. (1978). On conditions for the rise of self-excited ice-induced autonomous oscillations in slender marine pile structures. *Winter Nav. Board*, Finland, Res. Rep., 25.

Määttänen, M. (1981). Laboratory tests for dynamic ice-structure interaction. *Eng. Struct.*, Vol 4, April, pp. 111-116.

Nakazawa, N., Terashima, T., Saeki, H. and Ono, T. (1993). Factors influencing the coefficient of friction between sea ice and various materials. *Proc. 12th Int. Conf. Port Ocean Eng. under Arctic Cond.* (POAC'93). Hamburg, August 17-20, Vol I, pp. 97-105.

Oksanen, P. (1983). Friction and adhesion of ice. Technical Research Centre of Finland. *Publications 10.* Espoo 1983, 36 p.

Peyton, H.R., (1966). Sea ice strength. University of Alaska, Geophysical Institute. UAG R-182. Final report for Department of the Navy, Office of Naval Research, Contract Nonr-2601(01). December 1966. 153 p.

Saeki, H., Ono, T., Nakazawa, N., Sakai, M. & Tanaka, S. (1986). The coefficient of friction between sea ice and various materials used in offshore structures. *J. Energy Resources Technology*, Vol. 108, March 1986, pp. 65-71

Sanderson, T.J.O. (1983). *Ice Mechanics - Risk to offshore structures.* Graham&Trotman. London 1983. p. 156.

Schwarz, J. (1970). The pressure of floating ice fields on piles. *Proc. IAHR Ice Symp.*, Reykjavik, No. 6-3, 12 p.

Shkhinek, K, Kapustianksy, S. Jilenkov,A. & Kärnä, T. (1999). Numerical simulation of the ice failure process. *Proc. POAC'99.*

Singh, S.K. (1993). Mechanical behaviour of viscoelastic material with changing microstructure. Memorial University of Newfoundland. St.John' s. Canada. (Diss.). 195 p.

Sodhi, D. & Morris C.E. (1984). Ice forces on rigid, vertical, cylindrical structures. CRREL Report 84-33. 36 p.

Sodhi, D. (1988). Ice-induced vibrations of structures. *Proc. IAHR Ice Symp.* Sapporo, Japan.

Sodhi, D. (1991). Effective pressures measured during indentation tests in freshwater ice. *Proc. 6th Int. Cold Regions Specialty Conf.* Hanover NH, February 26-28, pp. 619-627.

Sodhi, D. (1997). Correlation of ice crushing forces in segments of an indentor. *Proc. 14th Int. Conf. Port Ocean Eng. Arctic Cond..* (POAC'97). Yokohama, Vol. IV. pp. 423-430.

Sodhi, D. (1998a). Nonsimultaneous crushing during edge indentation of freshwater ice sheets. *Cold Reg. Sci. Techn.* 27 (1998) 179-195.

Sodhi, D.S., Takeuchi, T., Nakazawa, N., Akagawa, S. & Saeki, H. (1998b). Medium-scale indentation tests on sea ice at various speeds. *Cold Reg. Sci. Techn.* 28(1998) 161-182.

Takeuchi, T., Kawamure, M. and Akagawa S. (1997). Ice-structure interactions in medium scale field indentation tests. *Shimizu Teh. Res. Bull.* No. 16 (March 1997), pp. 47-53.

Thomson, P.A. & Robbins, M. (1990), Origin of stick-slip motion in boundary lubrication. *Science,* Vol. 250, pp. 792-794.

Timco, G.W. & Frederking R.M.W. (1995). Experimental investigations of the behaviour of ice at the contact zone. In: *Mechanics of Geomaterial Interfaces*, A.P.S. Selvadurai, and M.J. Boulon, Eds, pp. 35-55. Elsevier Science B.V. 1995.

Tsuchiya, M., Kanie, S., Ikejiri, K. & Yoshida, A. (1985). An experimental study on ice-structure interaction. OTC 5055. *Proc. 17th Annual OTC* , Houston, TX, pp. 321-327.

Tusima, K. and Tabata, T. (1979). Friction measurements of sea ice on flat plates of metals, plastics and coatings. *Proc. 5th Int. Conf. Port Ocean Eng. under Arctic Cond.,* (POAC'79). Trondheim, Norway, Aug. 13-18 1979. Vol. I, pp. 741-754.

Tuhkuri, J. (1995). Experimental observations of the brittle failure process of ice and ice-structure contact. *Cold Reg. Sci. and Techn.* 23 (1995) 265-278.

Tuhkuri, J., Goldstein, R.V. and Osipenko, N.M. (1997). Modelling of the fracture surface of an ice block failing against a structure. *Proc. 14th Int. Conf. Port Ocean Eng. Arctic Cond., (POAC'97).* Yokohama, Japan, Vol. IV, pp. 263-269.

Wu, H.C., Chang, K.J. & Schwarz, J. (1976). Fracture in the compression of columnar grained ice. *Eng, Fracture Mech.*, 1976, Vol 8, pp. 365-372.

A MODEL FOR RIDGE FIELD STATISTICS

Mikko Lensu
Helsinki University of Technology, Espoo, Finland

ABSTRACT

Sea ice ridge fields are described by the size and arrangement of ridges. The usual surface description is by distributions for cross-sectional height and ridge spacing. An alternative description of ridge arrangement in terms of local ridge density is formulated. Local density is determined from data by counting the number of ridges in a segment of given length, or the occupation number. A model for the ridge occupation number statistics is constructed by considering the evolution as a simple ball-into-bin process. This combines a clustering process, where the creation rate of new ridges increases with local ridge density, with a Poisson process, where new ridges are created in random locations. A relationship between the suggested model and the usual lognormal hypothesis for ridge spacing distributions is given.

1. INTRODUCTION

A usual regional average description of ridging in sea ice fields is by ridge density d, or the number of ridges per km, and average cross-sectional sail height $\langle h \rangle$. These parameters are easily determined from surface profile data measured by a laser profilometer, for example. The regional variation in ridging characteristics is described by models for the ridge spacing distribution and for the sail height distribution. The mean value of the spacing distribution is then $1/d$.

However, another description is possible. This is done by dividing a surface profile with average ridge density d into smaller segments and determining the ridge densities d' for them. The ridge arrangement is then described by a distribution $f(d'|d)$ which can be interpreted as the probability to find local ridge density d' if the regional density is d. This is tantamount to the counting of the numbers n' ridge sails in the segments, called here occupation numbers. Thus the ridge arrangement is as well described by distributions $k(n'|n)$ which give the probability to find a segment containing n' ridges if there are altogether n ridges.

This approach is not fixed to any given length scales. Thus it can be generally defined for length scales L_i and L_j that

$$k(n_j|n_i) \tag{1}$$

is the probability to find n_j ridges in a segment of length L_j when this is contained in a longer segment with n_i ridges and of length L_i (Figure 1). Such probabilities are easily determined from surface profile data and the description in terms of local ridge densities is given by

$$d_i = n_i / L_i , \quad d_j = n_j / L_j \tag{2}$$

Description in terms of occupation numbers or local densities has several advantages. The scale of the description can be chosen to suit the application. The ridge spacing distribution gives only the relative frequencies of certain spacing length categories but no information on how the spacings are arranged in the field. It cannot answer questions like 'what is the probability for a ship of length 100 m to be in contact with more than 5 ridge sails at the same time? This, on the other hand, can be obtained from the probability $k(n_j|n_i)$ where L_j=100 m and L_i is the scale of the region across which the ship is traversing. Thus varying the scale the arrangement of ridges in different scales can be described.

Another feature is that the description, unlike ridge spacing distributions, can be formulated in two horizontal dimensions. Horizontal ridge density is defined as the length of ridge sail per square km. If the ridge field is isotropic, the horizontal density is $\pi/2$ times the linear density (Mock et al. 1972). Thus, instead of segments, squares with side lengths L_i and L_j is considered. This makes possible the comparison of the statistics with those of ridging measures defined for SAR images.

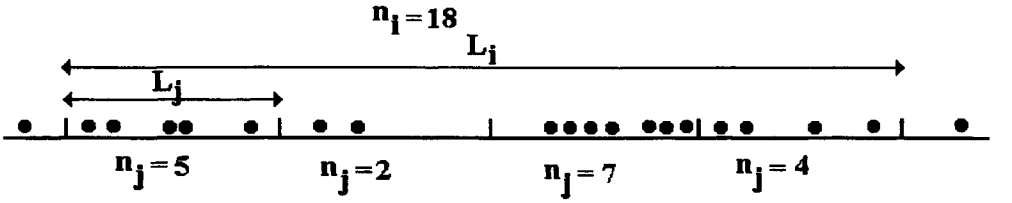

Figure 1. The description of ridge arrangement by occupation numbers. Ridge sails are idealised as balls in a bin. Local ridge densities are given as n_j/L_j.

2. A MODEL FOR THE OCCUPATION NUMBER STATISTICS

The segments L_j of a linear profile of length L_i are considered as bins and the ridge sails in the segments as balls in the bins. If the thickness increases in deformation, part of this manifests as creation of new ridge sails, that is, as the appearance of new balls into bins. The evolution is modelled as a process where new balls one at a time are deposited to the profile (which can be considered as the combined bin with length L_i). It is assumed that the probability for the ball to end into a certain bin may depend on the number of balls already in the bin together with the length of the bin. Given two bins the probability for the ball to end into either of them must equal the probability that it ends into a twice as large bin containing the balls of the two bins. This entails that the probability for the ball to end into a bin of length L_j and containing n_j balls must be proportional to

$$n_j + \phi(L_j) \tag{3}$$

where ϕ is some additive function. If there is a linear coordinate x along the profile, ϕ can be the integral of any function of x across the bins. Thus geographical gradients can be included into the model. However, it is assumed here that there is no geographical variation in which

case the probability for the ball to end the bin is proportional to $n_j + aL_j$ and is given as

$$\frac{n_j + aL_j}{n_i + aL_i} \tag{4}$$

The probabilities satisfy then the following recurrence relation

$$k(n_j|n_i) = k(n_j - 1|n_i - 1)\frac{n_j - 1 + aL_j}{n_i - 1 + aL_i} + k(n_j|n_i - 1)\left(1 - \frac{n_j - 1 + aL_j}{n_i - 1 + aL_i}\right), \quad n_j = 0,1,...,n_i \tag{5}$$

If n_j=0 or n_j=n_i either the last or first term on the right counts. Iterating from $k(0|0)$=1 the result is

$$k(n_j|n_i) = \frac{\binom{aL_j + n_j - 1}{n_j}\binom{aL_i - aL_j - 1 + n_i - n_j}{n_i - n_j}}{\binom{aL_i + n_i - 1}{n_i}} \tag{6}$$

which is recognised as a negative hypergeometric distribution (Johnson and Kotz 1969). The expectation is $E(k)=n_iL_j/L_i$ and the variance

$$Var(k) = \frac{L_j n_i}{L_i}\frac{(aL_i - n_i - 1)(aL_i - aL_j)}{aL_i(aL_i + 1)} \tag{7}$$

3. COMPARISON TO DATA

In spite of its appearance (6) is convenient to apply as it is a finite combinatorial entity and a program for the probabilities can be easily written if not found from statistical packages. There is only one varied parameter a. For ridge data the profile length L_i, segment length L_j, and the occupation numbers n_i and n_j are fed into (6) and the parameter a is varied for optimal fit. As this is done using several segment lengths L_i a range of values is found. It is desirable that the variation in a is small enough that it can be considered as a constant. It is however apparent that the probability of a ridge to form an empty segment is dependent on the occupation number of a longer embedding segment. To take this into account in an average it is allowed that the probability of a ridge to become created in a segment is proportional to

$$n_j + c + a'L_j = n_j + (c/L_j + a')L_j = n_j + aL_j \tag{8}$$

Thus $a=c/L_j + a'$. For short segments the component c/L_j is expected to dominate in a and for long segments the component a'. The latter is interpreted as a pure Poisson process component, that is, its strength measures the intensity with which ridges are created at randomly chosen locations. On the other hand, n_j+c can be called the clustering process component as it describes how the appearance of additional ridges depends on local ridge

density. If such dependence exists, ridges tend to become created into locations that are already ridged and thus tend to form clusters.

The model is applied to a set of laser profilometer data collected from the Bay of Bothnia in March 1997 during the ZIP-97 experiment which constituted the field phase of ICESTATE project (Haapala and Leppäranta 1997). The Bay of Bothnia is the only Baltic basin that has ice cover even during mild winters. The maximum thickness of thermally grown ice is about 1.2 m and typical ridges have 1-3 m high sails and 5-15 m deep keels. The highest measured ridges have been 3.5 m high while visual observations suggest that maximum heights are about 5 m. Four more extensive laser surveys from the Bay of Bothnia have been reported; these are summarised in Lensu (1998). The average ridge heights for all these surveys are within 8 cm which is about the same order as the inaccuracy due to snow cover. The basinwide average ridge height can be therefore assumed to be a constant, about 0.73 m for 0.5 cutoff. The average ridge densities, on the other hand, vary from 3/km to 18/km.

The March 1997 survey with the total profile length 270 km was from the Northeast quadrant of the basin and its basic statistics are described in Lensu (1998). Cutoff height was 0.5 m, average sail height was 0.76 m, sail height distribution obeyed the standard exponential model, and average density was 18/km. The winter was mild and the basin did not attain persistent thick ice cover. The ridged pack was very active dynamically. Its area was increased by a succession of ridging phases consuming the thermally grown level ice and creating large areas of open water that became covered by ice during the next cold period. Strong winds increased the ridge density to high values and the ridge joined into a continuous netlike pattern.

Ridges exceeding 0.5 m and passing the Rayleigh criterion were identified from the data and the statistics for the occupation number n_j were determined using segment lengths L_j ranging from 12.5 to 1600 m in binary succession. The average $\langle n_j \rangle$ is ridge density multiplied by L_j /1000. The coverage for $n_j > 0$ gives the relative length of profile that is ridged in the scale L_j. Thus, for example, a ship of length 100 m would be in contact with at least one ridge for 54 % of the track length, have then contact with 3.33 ridges in the average, and encounter maximally 17 ridges at one and the same time. It is also seen that the correlations between n_j and the average cross-sectional height h or the same segment are small. They increase gradually as regional variation begins to count. Thus local ridge density and local ridge height can be assumed to be independent.

L_j [m]	Mean $\langle n_j \rangle$	Max.of n_j	Mean for n_j >0	Coverage for n_j >0	Corr(n_j,h)
12.5	0.23	5	1.39	0.16	0.05
25	0.45	8	1.76	0.26	0.09
50	0.91	10	2.34	0.39	0.10
100	1.82	17	3.33	0.54	0.13
200	3.64	29	5.21	0.70	0.13
400	7.28	43	8.65	0.84	0.18
800	14.56	78	15.78	0.92	0.17
1600	29.12	123	29.77	0.97	0.21

Table 1. The parameters of occupation number distributions calculated for different segment lengths L_i.

The distribution (6) was fitted to the data by finding the value of a for each segment length and separating the linear dependence a' on segment length for c. The parameter c showed slight variation which does not improve the fit essentially from that obtained by using constant values c=0.5 and a'=2. The distribution model for these values is shown in Figure 2. It is seen that the model is a good description as far as the number of segments is enough to resolve the histogram properly.

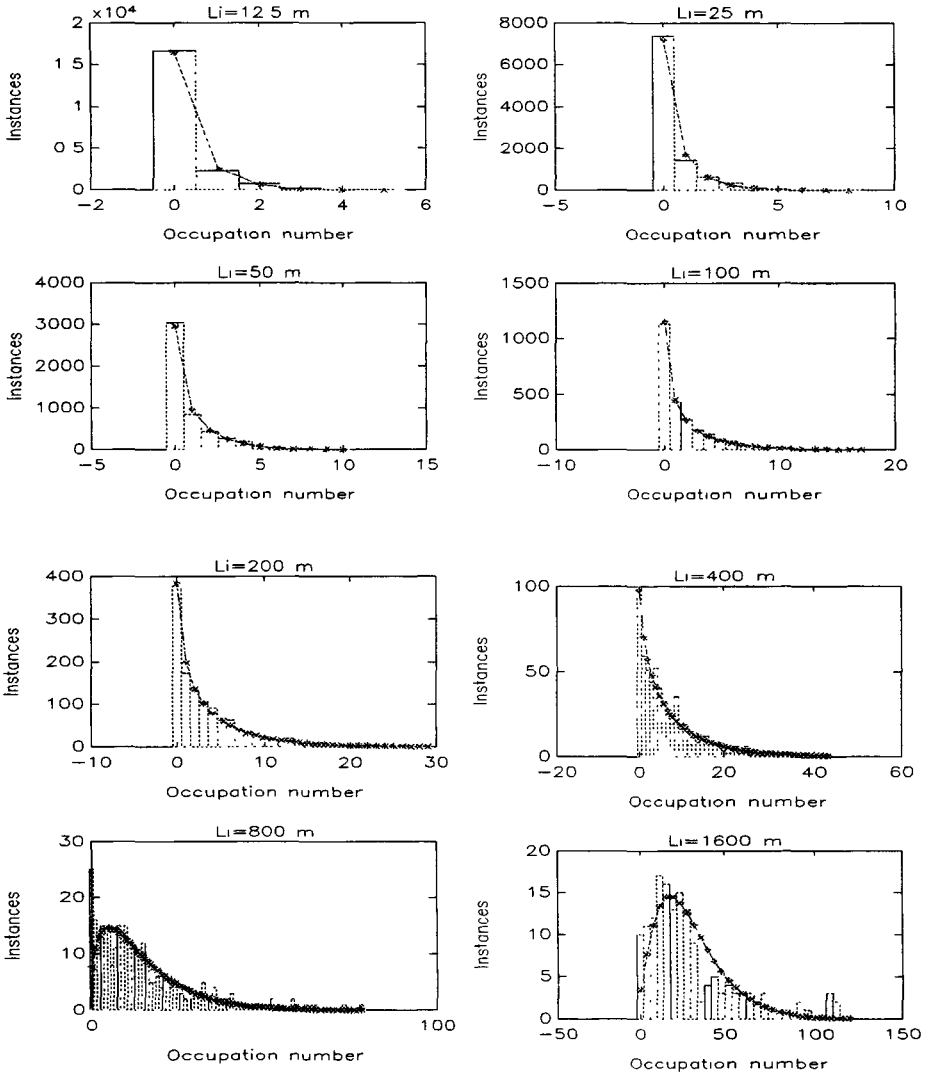

Figure 2. The distribution model (eq.6, the line) for the data of Table 1 (the histogram) using parameter values c=0.5 and a'=2 in (8).

4. APPROXIMATIVE DESCRIPTIONS DERIVABLE FROM THE MODEL

The model was interpreted as resulting from a process that contains both Poisson and clustering components. The parameter a' tunes the relative intensity of the Poisson process. If (8) is taken to be the rate with which new ridges are created, then a' is the Poisson intensity or Poisson rate per unit length. The strength of the clustering process, on the other hand, can be assumed to be proportional to the average occupation number $\langle n \rangle$. The average of the rate is

$$\langle n_i \rangle + c + a' L_j = (d + c / L_j + a') L_j \tag{9}$$

where d is ridge density. Thus for $d+c/L_j >> a'$ the clustering process dominates while for $d+c/L_j << a'$ the Poisson process dominates. For the present data as d=18.2 and a=2 the Poisson component is very weak.

The distribution (6) is applicable to data due to its finiteness that matches exactly to the number of segments and ridges in the data. After finding a model (6) asymptotic forms can be used to find a more customary distribution model. These are derived by three kinds of limits:

1. If $a/(d+c/L_j)$ is large or small, pure Poisson or clustering process is obtained respectively.
2. If the total number N of ridges is large, discrete distributions defined for all nonnegative values n are obtained. These are parameterised by the average occupation number $\langle n_j \rangle$ and are not dependent on the profile length L_i.
3. If $\langle n_j \rangle$ is large, continuous approximations may be used.

Thus, pure Poisson process gives first the binomial distribution, which is finite and discrete. It can be approximated then by a Poisson distribution, which is discrete but not finite, and finally by a normal distribution. For pure clustering process there is not a simple finite approximation. On the other hand, for large number of ridges the distribution is then a negative binomial

$$k(n_j) = \binom{c + n_j - 1}{n_j} p^c (1-p)^{n_j} \quad , \quad p = \frac{c}{c + \langle n_j \rangle} \tag{10}$$

(Johnson and Kotz 1969).This is generally the non-finite approximation of (6) when c is replaced by $c+aL_j$. The continuous approximation for large $\langle n_j \rangle$ is a gamma distribution

$$k(n_j) = \frac{1}{\Gamma(\alpha)} \beta^{\alpha} n_j^{\alpha-1} e^{-\beta n_j} \quad , \quad \alpha = c + aL_j, \beta = (c + aL_j) / \langle n_j \rangle \tag{11}$$

(Ochi 1990). A convenient approximation of clustering process is obtained by assuming c=1 and a'=0 in which case a very simple geometric distribution model is obtained ⟨⟩

$$k(n_j) = p(1-p)^{n_j} \quad , \quad p = 1/(1 + \langle n_j \rangle) \tag{12}$$

In the limit of large $\langle n_j \rangle$ this can be approximated by a negative exponential distribution with mean value $\langle n_j \rangle$. Geometric distribution can be used if the occupation number histogram shows a sufficiently linear slope in semilogarithmic scale. For the analysed data, as the Poisson component was weak and c=0.5 the geometric approximation is still a good model up to segment length 400 m (Figure 3). The discrepancy with the negative hypergeometric model concerns mostly the value n_j=0 which is larger than the value obtained by extending the rather good linear slope found for values n_j>0. Thus the geometric distribution model describes well the relative abundancies of ridges in occupied segments but the relative coverage of unoccupied segments, corresponding to the first histogram bin, becomes too small.

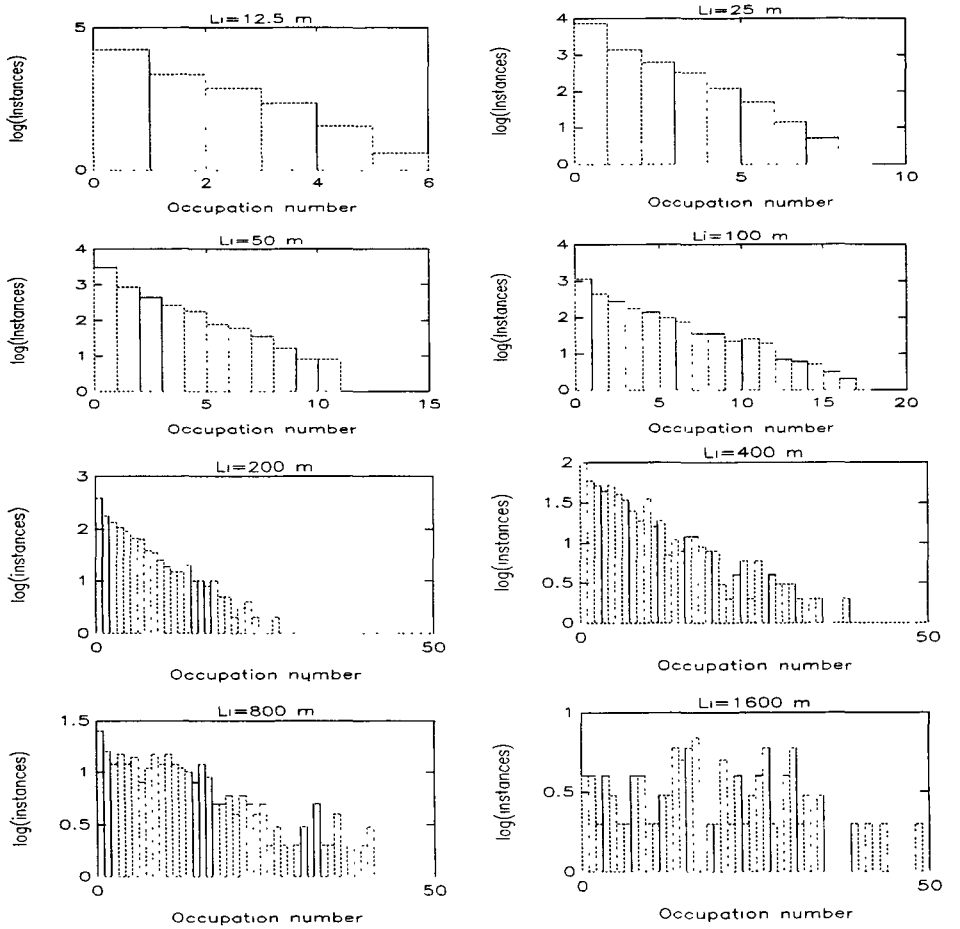

Figure 3. Histograms for the data of Table 1 in semilogarithmic scale. Geometric distribution model can be applied to linear sections of the slopes.

5. DISCUSSION

The negative hypergeometric model was found to be a good description of the analysed data. According to the model interpretation the Poisson process component in ridging is weak and ridging is thus predominantly a clustering process where ridges are attracted by already existing ridges. To compare the occupation number statistics with ridge spacing statistics the following process is considered.

1. Ridges are created in a sequential process.
2. The probability that a ridge is created into an existing spacing is proportional to x^{ρ} where x is spacing length.

If $\rho=1$ this probability is proportional to spacing length, the process is approximately a Poisson process, and the spacing length distribution is negative exponential. If $\rho=0$ the probability does not depend on spacing length. It is shown in Lensu (1997) that this process produces asymptotically lognormal spacing length distribution. Now if $\rho=0$ for any group of spacings the probability that the next ridge is created in the group is proportional to the number of spacings in the group. Thus if the ridge spacings at a certain time t_0 are taken to represent bins, and the ridges appearing in the spacings at later times as balls, the probability for the next ball to land into a bin with n_j balls is n_j+1. Thus the distribution for the numbers of balls in the bins is geometric. Lognormal and geometric distributions are thus two ways to describe the same process.

This is approximately similar to the occupation number description with fixed segment lengths, the better the higher ridge density is. A segment with n_j ridges contains n_j-1 complete spacings and two incomplete spacings if $n_j>0$, or only one incomplete spacing in case $n_j=0$. However, also in a pure clustering process there is nonzero probability that a ridge is created into an empty segment, this because it is embedded into some larger nonempty segment. This was included by assuming the constant c.

However, the process cannot be pure a clustering process as this cannot get off from the ground unless there are already some ridges. The Poisson component, even when weak, dominates when the ridge density is low. If the ridge density grows without limit the clustering process will always take over at a certain stage. Thus in general both negative exponential and lognormal features may be found in spacing distributions. What the mixed cases are is difficult to formulate for spacings but for occupation number distributions (6,10,11) they are given.

The negative exponential distribution for spacings was proposed by Hibler et al. (1972) and Mock et al (1972) found a good agreement for aerial image data. A good fit for keel spacings was found in Wadhams (1980), for the mid range of keel spacings in Wadhams and Horne (1980), for sail spacings exceeding 100 m in Wadhams and Horne (1980), and for sail spacings between 100 and 250 in Wadhams (1981). Wadhams and Davy (1986) found that the lognormal distribution was generally a better model over the whole range of keel spacings. The results were corroborated for the keels by Key and McLaren (1989) and for sails by Dierking (1995). For Baltic data Lewis and others (1993) found lognormal acceptable while the exponential was rejected. Lognormal distribution was also found to be an applicable but not very good model in Lensu (1995,1998). Thus it appears that both exponential and lognormal features may manifest in spacing distributions.

6. CONCLUSIONS

The motivation of the present work as a part of the ICESTATE project (Tuhkuri et al. 1998) has been to find descriptions of ice cover that have built-in unambiguous reference to scales. This was attained by describing ridging by local ridge density which is equivalent to the counting of ridge occupation numbers in profile segments. For occupation number distribution a model with the following properties was constructed:

1. The distribution is finite and matches the exact numbers of ridges and segments.
2. The distribution can be formulated for any profile and segment lengths.
3. The reference to scales is unambiguous as the distribution $k(n_j|n_i)$ is defined over scale L_i and has resolution L_j.
4. A two-dimensional description is possible.
5. There is only one parameter that measures the relative intensity of Poisson and clustering processes.
6. Pure Poisson and clustering processes are found as special cases and correspond to the negative exponential and lognormal hypotheses for spacing distribution.
7. Continuous approximations in terms of well known distributions are found.
8. For clustering process a simple geometric distribution model can be approximately used.

A very good fit was found using the proper model (6) and the geometric approximation was also acceptable for shorter segment lengths. The variation in ridge density in shorter scales may be described in a simple way using the geometric distribution which is directly parameterised by the ridge density. This is expected to apply when the spacing distribution is lognormal.

ACKNOWLEDGEMENTS

The work was supported by the European Commission, DG XII, through the Marine Science and Technology programme 1994-1998 (MAST III) under contract MAS3-CT95-0006. The participants in this joint project entitled ICESTATE are Helsinki University of Technology, Nansen Environmental and Remote Sensing Center, Scott Polar Research Institute, University of Helsinki, and University of Iceland.

REFERENCES

Dierking, W. 1995: Laser profiling of the ice surface topography during the Weddell Gyre Study 1992. J. Geophys. Res. 100 C3, 4807-4820.

Haapala, J. and Leppäranta, M. (editors) 1997 ZIP-97 Data Report. University of Helsinki, Department of Geophysics, Report No. 37.

Hibler, W.D. III, Weeks, W.F: and Mock, S.J. 1972. Statistical aspects of sea-ice ridge distributions. J. Geophys. Res. 77, 5954-5970.

Johnson, N.L. and Kotz, S. 1969 Distributions in statistics: Discrete distributions. Wiley, New York.

Key, J. and A.S.McLaren (1989) Periodicities and keel spacings in the under-ice draft distribution of the Canada Basin. Cold Reg. Sci. Technol. 16,1-10.

Lensu, M. 1995. The analysis of laser profilometer data: AEM flights in the Baltic, Winter 1994. Helsinki University of Technology, Ship Laboratory report series M-195

Lensu, M. 1997 Correlations between fragment sizes in sequential fragmentation. J. Phys.A: Math. Gen. 30, 7501-7507

Lensu, M. 1998 Laser profilometer measurements in the Bay of Bothnia during the ZIP-97 Experiment. Helsinki University of Technology, Ship Laboratory Report Series M-232.

Lensu 1999 A mesoscale downscaling structure for morphological density variables. Ice State synthesis report (to appear).

Lensu and Tuhkuri 1999 Ice State and scale structure. Ice State synthesis report (to appear).

Lewis, J.E., Leppäranta, M. and Granberg, H.B. 1993. Statistical properties of sea ice surface topography in the Baltic Sea. Tellus 45 A, 127-142.

Mock, S.J., Hartwell, A.D. and Hibler, W.D. III 1972 Spatial aspects of pressure ridge statistics. J. Geophys. Res. 77 (30), 5945-5953

Ochi, M.K. 1990 Applied probability and stochastic processes. John Wiley & Sons.

Tuhkuri, J., Lensu, M., Riska, K. Sandven, S., Thorkildsen, F., Haapala, J., Leppäranta, M., Doble, M., Aksenov, Y., Wadhams, P. and Erlingsson, B. 1998. Local ice cover deformation and mesoscale ice dynamics, "Ice State". Proc. 3rd European Marine Science and Technology Conference, Vol. 1, The European Commission, DG XII pp. 315-328.

Wadhams, P. 1980: A comparison of sonar and laser profiles along corresponding tracks in the Arctic Ocean. In R.S. Pritchard (ed.), Sea Ice Processes and Models, pp. 283-299. University of Washington Press, Seattle.

Wadhams P. 1981 Sea ice topography of the Arctic Ocean in the region 70 W to 25 E. Philosophical Transactions of the Royal Society of London, Ser. 1A, 302 (1464), 45-85

Wadhams, P. and Davy, T. 1986: On the spacing and draft distributions for pressure ridge keels. J. Geophys. Res. 91 C9, 10697-10708.

Wadhams, P. and Horne R.J. 1980 An analysis of ice profiles obtained by submarine sonar in the Beaufort Sea. J. Glac. 25 (93) 401-424.

ON THE CONSTRUCTION OF KINETIC THEORY OF ICE COVER TAKING INTO ACCOUNT THE EVOLUTION OF INTERNAL ICE STRUCTURE

A.Marchenko
General Physics Institute of Russian Academy of Sciences
Moscow, Russia

ABSTRACT

The kinetic approach for ice cover (IC) modeling is developed in the paper for the case, when internal structure of IC is characterized by two scalar parameters: the thickness and the damage. The functions of redistribution of IC on the thickness and the damage are constructed to describe some scenarios of ice melting and freezing, ice ridging, damage accumulation and damage healing. The conceptions of internal and free energy of IC are incorporated into the model. It is shown, that the choice of the redistribution function dictates the expression for energy dissipation and plasticity flow rule of the medium.

1. INTRODUCTION

Kinetic approach for the description of large scale dynamics of sea IC has been developed in the AIDJEX models (see, for example, Coon et al., 1974). The IC is considered as two dimensional continuum floating on sea surface. Let us assume that a part of sea surface of area S is related with material point of the model. The length $L = \sqrt{S}$ can be considered as the scale of the averaging of the model. In the case when L is equal to several tens kilometers the ice floes of various thickness float on sea surface of area S. The functions of thickness distribution $g(t,x,y,h)$ and cumulative thickness distribution $G(t,x,y,h)$ have been considered to describe internal structure of Lagrangian element of IC (Thorndike and Maykut, 1973). The definitions of these functions are given by following formulas

$$g(t,x,y,h)dh = \frac{S_h(h,h+dh)}{S},\ G(t,x,y,h) = \int_0^h g(t,x,y,\eta)d\eta, \qquad (1.1)$$

where $S_h(h,h+dh)$ is a part of sea surface with area S covered by the ice with dimensionless thickness $h_i \in (h,h+dh)$. It is assumed that this part is related to the material point of IC which has the coordinates (x,y) in the time moment t.

In other interpretation, which is based on stochastic theory approach, the function $g(t,x,y,h)$ is the function of density probability (Timokhov and Kheisin, 1987; Timokhov,1998). The integral

$$P(t,x,y,h_1,h_2) = \int_{h_1}^{h_2} g(t,x,y,h)dh$$

is equal to the probability of the finding ice floes with thickness $h_i \in (h_1,h_2)$ in the point (x,y) in the moment of time t.

In general case the function of thickness distribution satisfies to the kinetic equation

$$\frac{dg}{dt} = \Psi[t,x,y,h,\mathbf{e}^p;g], \quad \frac{d}{dt} = \frac{\partial}{\partial t} + \mathbf{v}\cdot\nabla, \quad \nabla = \left(\frac{\partial}{\partial x},\frac{\partial}{\partial y}\right), \tag{1.2}$$

where $\mathbf{v} = (v_x, v_y)$ is drift velocity of Lagrangian element of IC and Ψ is the redistribution function, which depends not only on time, spatial coordinates and ice thickness, but also on the tensor of plastic strain rate $\mathbf{e}^p$ of IC. The function Ψ depends on the function of thickness distribution g functionally.

The function Ψ describes the rate of changing of thickness distribution function under the influence of plastic deformations of Lagrangian element of IC. The construction of the redistribution function is important step of ice modeling, since this function defines the scenarios of the reconstruction of internal ice structure under the influence of plastic deformations. The function Ψ is analog of the integral of collisions in kinetic gas theories (Lifshitz and Pitaevskii, 1979). The function of density distribution of gas molecules on velocities is the analog of thickness distribution function.

The kinetic approach is transformed into continuum mechanics modeling, where internal structure of Largangian element of IC is described by two scalar parameters: ice thickness $h(t,x,y)$ and ice compactness $A(t,x,y)$, if we put

$$g(t,x,y,\eta) = A(t,x,y)\delta(\eta - h(t,x,y)) + (1 - A(t,x,y))\delta(\eta), \tag{1.3}$$

where $\delta(x)$ is Dirac delta - function.

Large scale model, where internal structure of IC is characterized by three scalar parameters: ice thickness h, ice compactness A and ice damage Σ, has been developed by Goldstein and Marchenko (1998) on the basis of continuum damage mechanics. In this approach ice damage is analog of the splinterity of IC. The present work is devoted to the construction of kinetic theory of the IC for the case, when the function of distribution g depends on two structural parameters: ice thickness h and ice damage Σ.

The paper is organized as follows. In § 2 scalar damage parameter is defined. In § 3 the kinetic equation for the function of thickness and damage distribution and normalization conditions for redistribution functions are formulated. In § 4 general methodology of the construction of redistribution functions is developed. In § 5 the redistribution functions describing two scenarios of ice ridging are constructed. In § 6 the redistribution functions describing damage accumulation and damage healing processes are constructed. In § 7 the energetic relations following from the first and the second thermodynamic laws are

considered. In § 8 the main results obtained in the paper are formulated, and peculiarities of ridging processes described by the model are discussed.

2. SCALAR DAMAGE PARAMETER

Let us define scalar damage parameter $\Sigma \in (0,\infty)$ by the formula $\Sigma = S_f / S_p - 2$, where S_f is total area of the surface of ice pieces composing the IC floating on ocean surface with area S, and S_p is the area of total projection of these pieces on the horizontal plate (x,y). One can see that $S \geq S_p$ and $S_f \geq 2S_p$.

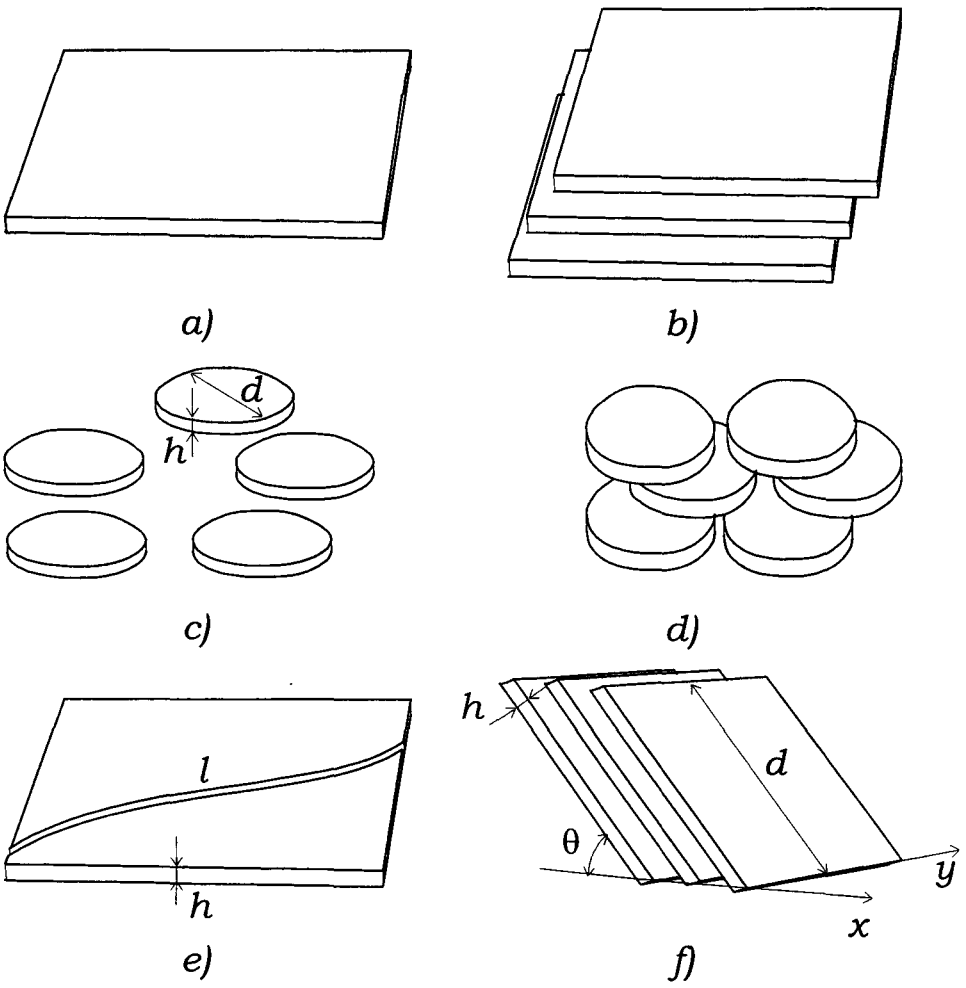

Figure 1. The examples of media with various values of damage parameter.

Let us consider some examples of specially constructed continuous media to demonstrate the calculation of damage parameter. If the medium is continuous infinite plate without internal faults (figure 1 *a*), then it has only two free surfaces – upper and lower and the value of damage parameter $\Sigma_a = 0$. If the medium consists of N infinite plates which are put on each other, then $\Sigma_b = 2(N-1)$. If $N = 3$, then $\Sigma_b = 4$ (figure 1 *b*). On the figure 1 *c*) the medium consists of identical disks with dimensional thickness h and diameter d. The value of damage parameter of the medium is equal to $\Sigma_c = 8hd^{-1}$. If the medium consists of N layers of the disks, which are put on each other, then $\Sigma = 2(N-1) + 8Nhd^{-1}$. If $N = 3$, then $\Sigma_d = 4 + 24hd^{-1}$ (figure 1 *d*). One can see that $\Sigma_c \to \Sigma_a$ and $\Sigma_d \to \Sigma_b$ by $d \to \infty$.

If the crack length l runs through the IC of the thickness h, and the crack penetrates completely throughout the whole ice thickness, then the damage parameter would be $\Sigma_e = 2lh/S$ (figure 1 *e*). On the figure 1 *f* the medium consists of a large number inclined bands, which are put on each other. Let us assume that the thickness and the width of each bend are equal to h and d respectively, the length of each bend is infinite in the direction y and the angle between the plane of each bend and the axis y is equal to θ. In this case the damage is equal to $\Sigma_f = 2(dh^{-1} + 1)\sin\theta - 2$, when $h < d\tan\theta$ and $h\sin^{-1}\theta << L$. Here L is the length of Largangian element of the medium. One can see that in the cases *a* – *d* the values of damage parameter do not depend on the scale of averaging of the model. In the cases *e* and *f* the value of damage parameter depends on this scale.

Thus it is shown that the values of damage parameters of the media with various internal structure can be equal. The scalar parameter Σ defined in the present paper does not give detailed description of internal structure of materials. From our point of view this parameter characterizes the degree of material splinterity only. Continuum damage mechanics models taking into account crack orientation and a degree of crack opening can be used for more detail description of material features (see, for example, Sjolind, 1987).

3. THE FUNCTION OF THICKNESS AND DAMAGE DISTRIBUTION

The space of the parameters, characterizing internal structure of IC is equivalent to one fourth of the plane Ω: $h > 0$, $\Sigma > 0$, where h is non-dimensional ice thickness. Let us consider the function of thickness and damage distribution $g(t, x, y, h, \Sigma)$. The integral

$$I[\omega] = \int_{\omega} g dh d\Sigma, \quad \omega \in \Omega \tag{3.1}$$

is equal to fractional area of sea surface covered by IC, structural parameters of which lie in the region ω of the plane Ω. The function g satisfies to the normalization $I(\Omega) = 1$. By analogy with (1.3) the function $g(t, x, y, h, \Sigma)$ is represented in the form

$$g(t,x,y,h,\Sigma) = (1 - A(t,x,y))\delta(h,\Sigma) + g_i(t,x,y,h,\Sigma), \tag{3.2}$$

where $\delta(h,\Sigma)$ is two-dimensional Dirac delta-function. From the formula (3.2) follow that the integral from the function $g(t,x,y,h,\Sigma)$ over a small vicinity of the origin in the plane (h,Σ) tends to $W = 1 - A(t,x,y)$, where $W \in (0,1)$ is equal to fractional area of open water.

Let us write the equations describing the variation of the function of thickness and damage distribution in the form

$$\begin{aligned} &\frac{dg_i}{dt} + g_i e_I^p = \psi_i[t,x,y,e_{\alpha\beta}^p; g_i], \\ &\frac{dW}{dt} - \theta(W,e_I^p) A e_I^p = \psi_w[t,x,y,e_{\alpha\beta}^p; g_i], \end{aligned} \tag{3.3}$$

where

$$e_I^p = \nabla \cdot \mathbf{v}, \quad \theta(W,e_I^p) = \begin{cases} 1, & W > 0 \\ 0, & W < 0 \end{cases}, \quad \theta(0,e_I^p) = \begin{cases} 1, & e_I^p \geq 0 \\ 0, & e_I^p < 0 \end{cases}$$

and $e_{\alpha\beta}^p$ is the tensor of the rate of plastic strains. It is assumed that the deformations responsible for the relative displacement of ice fragments in the area S are plastic.

The terms of the equations (3.3) proportional to e_I^p define the flows of ice concentration and the portion of open water area into Lagrangian element of IC. The function ψ_i is equal to the rate of ice redistribution by various fractions in the space of states Ω. The function ψ_w is equal to the rate of the variation of open water portion in Lagrangian element of IC and named open water production.

The form of redistribution function defines the set of physical phenomena, which are described by IC model. Further we consider the redistribution functions describing the scenarios of ice ridging, damage accumulation and damage healing, freezing and melting of the ice, which reflect some properties of real physical processes in sea IC.

Let us perform the redistribution function ψ_i by the following sum

$$\psi_i = \psi_{fm} + \psi_r + \psi_{+\Sigma} + \psi_{-\Sigma}, \tag{3.4}$$

where ψ_{fm} is related to ice thickness redistribution under freezing or melting process, ψ_r defines ice thickness and damage redistribution under the ridging, $\psi_{+\Sigma}$ defines ice damage accumulation due to plastic deformations not associated with the ridging, $\psi_{-\Sigma}$ defines ice damage healing under thermodynamic processes.

It is supported that there are plastic deformations, which are not accompanied by ice ridging. In the present model (see § 4) the ridging is possible under the influence of compression stresses on IC with compactness $A = 1$. Except the ridging there are following plastic deformations of IC in the model: pure shear, pure compression of IC with compactness $A < 1$ and pure tension. Any plastic deformations are accompanied by the reconstruction of internal structure of IC and damage accumulation. We have separated the redistribution functions relating to the ridging and damage accumulation to emphasize that these processes can proceed independently.

Let us formulate additional normalize conditions following from natural assumptions about physical properties of the processes under the consideration. It is assumed, that damage accumulation and damage healing processes don't produce the variation of the area of water surface covered by the ice of given thickness:

$$\int_0^\infty \psi_{\pm\Sigma} d\Sigma = 0. \tag{3.5}$$

Let integrate the first equation (3 3) over the Ω and sum ones with the second equation (3.3). Taking into account the condition $I(\Omega) = 1$ and the condition (3.5) one can find

$$\psi_w + \int_\Omega \psi_r dh d\Sigma + \int_{\Omega_0} \psi_{fm} dh d\Sigma = (1 - \theta(W, e_I^p)) e_I^p, \tag{3.6}$$

where Ω_0 is a small vicinity of the ray $h > 0$. The integral from φ_{fm} over Ω_0 describes the rate of the changing of open water fraction due to ice freezing or melting. Thus, open water production can take place due to the ice ridging, the melting of thin ice or the freezing of open water. In the last case the open water production is negative

It is assumed that the following condition has place by the ridging

$$\int_\Omega \psi_r dh d\Sigma < 0, \quad \psi_w \geq 0. \tag{3.7}$$

The condition $\psi_w > 0$ means that the rate of the covering open water by the ice due to the ridging is less than the rate of the covering open water by IC under pure compression. The rate of the covering open water surface by IC due to the compression without ridging is given by proportional to e_I^p term in the second equation (3.3). If ice ridging is possible under pure shear deformations when $e_I^p = 0$, then from the condition (3.7) follow $\psi_w > 0$. In this case from the second equation (3.3) follow that ice ridging produces the decreasing of ice compactness.Note, that this process is admissible in AIDJEX models (Thorndike et al., 1975).

It is assumed, that the mass of Lagrangian element of IC is conserved under any plastic deformations and under damage healing processes

$$\int_{\Omega} h\psi_{\pm\Sigma} dh d\Sigma = 0, \quad \int_{\Omega} h\psi_{r} dh d\Sigma = 0. \tag{3.8}$$

The variation of this mass is possible under the influence of ice freezing and melting only.

4. THE REDISTRIBUTION FUNCTION

Let us consider the redistribution function ψ_R, where the subscript R takes one from the values fm, r, $+\Sigma$, $-\Sigma$. The variation of the function of thickness and damage distribution g_i during the time dt equals to $\psi_R dt$. Denote this quantity by $\delta\Psi_R$ and represent ones in the form

$$\delta\Psi_R = \int_{\Omega} \Gamma_R[h, h', \Sigma, \Sigma'; g_i, \delta\varepsilon^p_{\alpha\beta}] g_i(h', \Sigma') dh' d\Sigma' - g_i(h, \Sigma). \tag{4.1}$$

Here and further the arguments t, x and y of the functions are omitted. The kernel Γ_R defines the scenario of the process and depends functionally on the function of density distribution g_i and the variation of the tensor of plastic deformations $\delta\varepsilon^p_{\alpha\beta} = e^p_{\alpha\beta} dt$.

Let us define the following expression of the kernel Γ_R

$$\Gamma_R(h, h', \Sigma, \Sigma'; g_i, \delta\varepsilon^p_{\alpha\beta}) = \delta(h - h')\delta(\Sigma - \Sigma') b_R + \tag{4.2}$$
$$+ \delta(h - h'(1 + \Delta^h_R))\delta(\Sigma - \Sigma'(1 + \Delta^\Sigma_R)) a_R.$$

Here $a_R g_i$ and $b_R g_i$ are the portions of water surface area covered by IC, which structure changes and does not change during the time dt respectively. The quantities Δ^h_R and Δ^Σ_R define the variations of IC parameters during this time.

Consider two particle cases, when the integrals in the formula (4.1) are simply calculated. In the first assume, that $\Delta^h_R << 1$ and $\Delta^\Sigma_R << 1$. Let us substitute the expression (4.2) into the formula (4.1) and calculate the integrals. Up to the high order terms we find

$$\delta\Psi_R = a_R g_i - \frac{\partial}{\partial h}\left(a_R g_i h \Delta^h_R\right) - \frac{\partial}{\partial h}\left(a_R g_i \Sigma \Delta^\Sigma_R\right) - (1 - b_R) g_i. \tag{4.3}$$

In the second case assume $\Delta^h_R = const$ and $\Delta^\Sigma_R = const$. After the calculation of the integrals we have

$$\delta\Psi_R = \frac{a_R\left(\frac{h}{1 + \Delta^h_R}, \frac{\Sigma}{1 + \Delta^\Sigma_R}\right) g_i\left(\frac{h}{1 + \Delta^h_R}, \frac{\Sigma}{1 + \Delta^\Sigma_R}\right)}{(1 + \Delta^h_R)(1 + \Delta^\Sigma_R)} - (1 - b_R(h, \Sigma)) g_i(h, \Sigma). \tag{4.4}$$

The redistribution functions like (4.3) are related to the process, when the variations of IC structural parameters are small during the time dt. In particular, ice freezing and melting can be associated with these processes. Assuming that all IC fractions take part in the process, we set $a_{fm} = 1$ and $b_{fm} = 0$. From this follow the simple formula for the redistribution function

$$\psi_{fm} = -\frac{\partial(v_{fm} g_i)}{\partial h}, \tag{4.5}$$

where v_{fm} is the rate of the variation of IC thickness.

5. PARAMETRIZATION OF ICE RIDGING

It is assumed, that the ice damage is accumulated under the ridging due to the piling up of ice pieces on each other without their fracture. Therefore, the total area of ice pieces is constant under the ridging

$$\int_{\Omega} \Sigma \psi_r dh d\Sigma = 0. \tag{5.1}$$

The normalize condition (5.1) is additional hypothesis. It is assumed that ice floes destruction has place under the influence of plastic deformations which are preceded to the ridging.

Let us consider ridging scenario, where IC has properties of granular material, surface density of which grows proportionally ice thickness (Hopkins et al.,1994). The growth of the thickness and the damage under the compression of homogeneous IC is described by the equations

$$\frac{dh}{dt} + he_I^p = 0, \quad \frac{d\Sigma}{dt} + \Sigma e_I^p = 0. \tag{5.2}$$

The function $a(h,\Sigma)$ redistributes the compression $e_I^p dt$ between ice fractions with various values of thickness and damage parameters. The variations of thickness and damage parameters of each fraction during the time dt are equal to $-a(h,\Sigma)he_I^p dt$ and $-a(h,\Sigma)\Sigma e_I^p dt$ respectively. Let us assume $a_r = 1 + ae_I^p dt$ and $b_r = 0$. From the formula (3.3) one find

$$\psi_r = \left[ag_i + \frac{\partial}{\partial h}(hag_i) + \frac{\partial}{\partial \Sigma}(\Sigma ag_i) \right] e_I^p (1 - \theta(W, e_I^p)), \quad A = 1. \tag{5.3}$$

The redistribution function (5.3) satisfies to the conditions (3.8) and (5.1), if the formula

$$\int_{\Omega} a g_i dh d\Sigma = 1 \tag{5.4}$$

has place. After the substituting of the formula (5.4) into the condition (3.6), we find, that the production of open water $\psi_w = 0$ in the scenario under the consideration.

In the second scenario of ice ridging, which are described by the formulas (4.4), the thickness and the damage are increased in finite number of times under the influence of small deformations. From this follow, that only a small portion of IC takes part in the ridging, and the area of this part is proportional to dt. Denote $k_h = 1 + \Delta_r^h$ and $k_\Sigma = 1 + \Delta_r^\Sigma$. Assuming $a_r = (1 - b_r)/k_h$, one can find, that the second formula (3.8) is satisfied. The function a_r can be chosen in any form satisfying to the conditions (3.7). One of possible variants is the following

$$a_r = \frac{\alpha(e_I^p, e_{II}^p) a_r^h g_i dt}{(k_h - 1)\int_{\Omega} a_r^h g_i dh d\Sigma}, \tag{5.5}$$

where $a_r^h = a_r^h(h, \Sigma)$, $e_{II}^p = e_1^p - e_2^p \geq 0$ and $e_{1,2}^p$ are principal values of the tensor of the rate of plastic deformations. Let us substitute the expression (5.5) into the formula (4.4) and then into the condition (3.6). One can find as a result

$$\psi_w = \alpha(e_I^p, e_{II}^p) + (1 - \theta(W, e_I^p))e_I^p. \tag{5.6}$$

The function $\alpha(e_I^p, e_{II}^p)$ must be chosen so that the condition $\psi_w > 0$ has place in accordance with the condition (3.7).

Consider the example, when the ridging has place under the compression of continuous IC with $A = 1$, $\alpha = -e_I^p$ and $\psi_w = 0$. Let us set $k_h = k_\Sigma = n$. The redistribution function is written in the form

$$\psi_r = e_I^p(\psi_r^1 + \psi_r^2)(1 - \theta(W, e_I^p)), \tag{5.7}$$

where

$$\psi_r^1 = n a_r^h(h, \Sigma) g_i(h, \Sigma) S_r^{-1}, \quad \psi_r^2 = -a_r^h\left(\frac{h}{n}, \frac{\Sigma}{n}\right) g_i\left(\frac{h}{n}, \frac{\Sigma}{n}\right)(nS_r)^{-1},$$

$$S_r = \int_{\Omega} a_r^h(h, \Sigma) g_i(h, \Sigma) dh d\Sigma,$$

One can check, that ψ_r satisfies to the conditions (3.8) and (5.4). The quantity $\psi_r^1 dhd\Sigma e_I^p dt$ defines the outflow of a portion of the IC with structural parameters h and Σ under the ridging, the quantity $\psi_r^2 dhd\Sigma e_I^p dt$ defines the influx of the area of this fraction due to the ridging of the IC with parameters h/n and Σ/n. This scenario can be interpreted as a multiple rafting.

The formulas (5.5) and (5.6) in the case, when $g_i = g_i(h)$ and $\alpha(e_I^p, e_{II}^p) = \sqrt{(e_I^p)^2 + (e_{II}^p)^2}\,\alpha_r(\chi)$, where $\chi = \arctan(e_{II}^p / e_I^p)$, define the redistribution function from the paper (Thorndike et al., 1975).

6. PARAMETRIZATION OF DAMAGE ACCUMULATION AND DAMAGE HEALING

The redistribution function $\psi_{-\Sigma}$ describing damage healing has the form analogous to the redistribution function of ice freezing – melting

$$\psi_{-\Sigma} = -\frac{\partial(v_{-\Sigma} g_i)}{\partial \Sigma}, \tag{6.1}$$

where $v_{-\Sigma} < 0$ is damage healing rate.

Let us consider the process of damage accumulation due to plastic deformations, which are not associated with ice ridging. It is assumed, that $a_{+\Sigma} + b_{+\Sigma} = 1$. The quantity $a_{+\Sigma} g_i$ is equal to fractional area of IC with parameters h and Σ, where the accumulation of ice damage has place. In the case when the rate of damage accumulation is proportional to $|e_I^p|$ and e_{II}^p one find

$$\psi_{+\Sigma} = -\frac{\partial}{\partial \Sigma}\left[\left(a_{+\Sigma}^I \mid e_I^p \mid \theta(W, e_I^p) + a_{+\Sigma}^{II} e_{II}^p\right) g_i\right], \tag{6.2}$$

where $a_{+\Sigma}^I \geq 0$ and $a_{+\Sigma}^{II} \geq 0$.

We can assume that ice damage accumulation under the influence of plastic deformations has place in the cases when the value of damage parameter is less than some critical value Σ_*. If $\Sigma > \Sigma_*$, then plastic deformations don't destroy ice pieces and are realized due to relative displacements of them only. The accumulation of the damage up to the values $\Sigma > \Sigma_*$ is possible due to ridging processes.

7. ENERGETIC RELATIONS

Let us define the surface density of internal energy U of IC by the formulas

$$U = \rho_i \int_\Omega hug_i dhd\Sigma + \Pi, \quad \Pi = \frac{\rho_i g \Delta_\rho}{2} \int_\Omega h^2 g_i dhd\Sigma, \tag{7.1}$$

where $\Delta_\rho = (\rho_w - \rho_i)/\rho_w$, ρ_i and ρ_w are ice and water densities, g is gravity acceleration, u is volumetric density of ice internal energy. The potential energy of IC, which is considered as hydrostatic equilibrium floating body, have been defined in the paper (Rothrock, 1975). The term Π is distinguished in the expression for internal energy U, since physical sense of this term is not associated with classical representations about internal energy of a medium. Nevertheless the energy Π is internal with respect to kinetic energy of ice drift.

The first and second thermodynamic laws, which are written for Lagrangian IC element, have the following form (Goldstein & Marchenko, 1998)

$$\rho_i \int_\Omega h\delta(ug_i)dhd\Sigma + \delta\Pi = \sigma^{\alpha\beta}\delta\varepsilon_{\alpha\beta} + \delta Q^e - U\delta\varepsilon_I^p + \tag{7.2}$$
$$+ \rho_i \int_\Omega (u + g\Delta_\rho h)v_{fm} dtdhd\Sigma,$$

$$\rho_i \int_\Omega hT\delta(sg_i)dhd\Sigma = \delta Q^e + \tau_d^{\alpha\beta}\delta\varepsilon_{\alpha\beta}^p + \delta Q' - \tag{7.3}$$
$$- \rho_i \int_\Omega hTs\delta\varepsilon_I^p dhd\Sigma + \rho_i \int_\Omega Tsv_{fm} dtdhd\Sigma,$$

where s is volumetric density of ice entropy, T is the temperature, δQ^e is heat flux into the element of IC from atmosphere and ocean, $\delta Q' \geq 0$ is noncompensated heat, which is extracted by damage healing (Sedov,1984), $\tau_d^{\alpha\beta}\delta\varepsilon_{\alpha\beta}^p$ is energy dissipation due to the friction between ice pieces.

It is supported, that the tensor of full deformations is equal to the sum of the tensors of elastic and plastic deformations $\varepsilon_{\alpha\beta} = \varepsilon_{\alpha\beta}^e + \varepsilon_{\alpha\beta}^p$. Plastic deformations of compacted IC induce the growth of potential energy Π under the ridging, the accumulation of ice damage and energy dissipation. Therefore the work of internal stresses on the plastic deformations can be represented in the form

$$\sigma^{\alpha\beta}\delta\varepsilon_{\alpha\beta}^p = (\tau_{+\Sigma}^{\alpha\beta} + \tau_d^{\alpha\beta} + \tau_r^{\alpha\beta})\delta\varepsilon_{\alpha\beta}^p, \tag{7.4}$$

where $\tau_{+\Sigma}^{\alpha\beta}\delta\varepsilon_{\alpha\beta}^p$ is equal to the work for damage accumulation, $\tau_r^{\alpha\beta}\delta\varepsilon_{\alpha\beta}^p$ is the work for the increasing of potential energy under the ridging.

Volumetric density of free energy is defined by the formula $F = u - Ts$ and is the function from the temperature T, the tensor of elastic deformations $\varepsilon_{\alpha\beta}^e$ and ice damage

parameter Σ. The dependence of the free energy from Σ is stipulated by the changing of internal structure of the material under the plastic deformations. In this case one portion of the work of internal stresses goes on the changing of internal structure of the material, while the other part goes into the dissipation (Sedov, 1984).

From the equations (7.2) and (7.3) with using of the normalize conditions (3.5)-(3.8) one can find

$$\frac{\partial F}{\partial T} = -s, \quad \rho_i \int_\Omega h \frac{\partial F}{\partial \varepsilon^e_{\alpha\beta}} g_i dh d\Sigma = \sigma^{\alpha\beta}, \quad \rho_i \int_\Omega hF\psi_{-\Sigma} g_i dh d\Sigma = -\frac{dQ'}{dt}, \quad (7.5)$$

$$\rho_i \int_\Omega (hF + \tfrac{1}{2}\Delta_\rho g h^2)\psi_r dh d\Sigma = \tau_r^{\alpha\beta} e^p_{\alpha\beta}, \quad \rho_i \int_\Omega hF\psi_{+\Sigma} dh d\Sigma = \tau_{+\Sigma}^{\alpha\beta} e^p_{\alpha\beta}. \quad (7.6)$$

From (7.4) – (7.6) follow that the representation of free energy function F and the functions v_{fm}, ψ_r and $\psi_{\pm\Sigma}$ fully defines the dissipation in the medium if elastic and plastic strains are known. These functions must satisfy to the conditions of the positiveness of the dissipation and noncompensated heat. The formulas (7.6) can be used for the definition of the critical stresses $\tau_r^{\alpha\beta}$ and $\tau_{+\Sigma}^{\alpha\beta}$, which are needed for the ridging or for damage accumulation, if the functions ψ_r and $\psi_{\pm\Sigma}$ are given. On this way the conditions of the realization of plasticity deformations can be found. The inverse approach, when the redistribution functions are found from (7.6) with using given plasticity conditions and dissipation function, have been realized in the paper (Rothrock, 1975).

8. CONCLUSIONS

In the present paper the kinetic approach for the description of IC deformations is developed for the cases, when internal structure of IC is defined by two structural parameters: the thickness and the damage. The kinetic equation describing the evolution of the function of thickness and damage distribution is formulated. General normalization conditions for the redistribution function describing the changing of the function of thickness and damage due to plastic deformations of IC are formulated. The examples of redistribution functions relating to ice ridging, damage accumulation and damage healing are constructed. On the basis of the kinetic approach the energetic relations following from the first and the second thermodynamic laws are formulated. It is shown that the representation of the function of free energy and redistribution function defines the dissipation in the system and the conditions of the realization of plastic deformations. The full system of the equations describing IC dynamics consists of the equations of mass, impulse and energy balance and rheology equations, which describe the relations between internal stresses in IC and plastic strain tensor.

In AIDJEX modeling the main chain of the processes, the realization of which results in ice ridging of pack ice, consists in the following. On the first step the production of open water (lead formation) under plastic shear and extension has place. On the second step young thin ice forms in the leads. Then the ridging of the young ice realizes under the compression

and shear deformations. In our approach open water production due to shear deformations is absent, and the chain of the processes causing ice ridging, can consist in the following. On the first step the accumulation of ice damage has place under the influence of plastic shear deformations. Then thin ice and high damaged ice form pressure ridges. The open water production can be realized under the influence of plastic extension only. The scenario of young ice ridging can realize also due to the production of open water by the extension.

ACKNOWLEDGMENTS

This work has been supported by the Russian Foundation for Basic Research under Project Code 99-01-00925.

REFERENCES

Coon,M.D., Maykut,G.A.,Pritchard,R.S.,Rothrock,D.A. and Thorndike,A.S. 1974. Modeling the pack ice as an elastic-plastic material. Aidjex Bull., No. 24:1-105.

Goldstein,R.V. and Marchenko, A.V.1998. On large scale modeling of sea ice cover taking into account accumulation of cracks and cracklike faults. Ice in surface waters. Proceedings of the 14th Int. Symp. On Ice, A.A.Balkema, Rotterdam, Brookfield, Vol.1: 637-642.

Hopkins, M.A., Hibler, W.D. III and Flato, G.M. 1991. On the numerical simulation of sea ice ridging process. J. Geoph. Res., Vol. 96, NC 3: 4809-4820.

Lifshitz, E.M., Pitaevskii, L.P. 1979. Physical kinetics, Moscow: Nauka. (in Russian)

Rothrock, D.A. 1975. The energetic of the plastic deformation of pack ice by ridging. J. Geoph. Res., Vol. 80, No. 33: 4514-4519.

Sedov, L.I. 1984. Continuum mechanics. II., Moscow: Nauka, 528 p. (in Russian)

Sjolind, S.G. 1990, Continuum damage modeling of polycrystalline ice. Ptoc. IAHR Ice Symp., Espoo, Finland: 449-463.

Timokhov, L.A. and Kheisin, D.E., 1987. Dynamics of sea ice. Mathematical models. Leningrad· Gidrometeoizdat , 272 p. (in Russian)

Timokhov, L.A. 1998. Ice dynamics model. In Lepparanta, M. (editor), Physics of Ice-Covered seas. University of Helsinki.

Thorndike,A.S. and Maykut,G.A. 1973. On the thickness distribution of sea ice. Aidjex Bull., No. 21:31-48.

Thorndike,A.S., Rothrock,D.A., Maykut,G.A. and Colony, R. 1975. The thickness distribution of sea ice. J. Geoph. Res., Vol. 80, No. 33: 4501-4513.

ICE RIDGE FORMATION DUE TO THE INTERACTION OF DRIFTING AND STATIONARY ICE FIELDS

A.V. Marchenko
General Physics Institute of Russian Academy of Sciences
Moscow, Russia

ABSTRACT

The model of ice ridge formation is constructed on the basis of integral equations following from the equations of mass, impulse and energy balance. The numerical calculations of two scenarios of ice ridge formation due to the collision of drifting and stationary ice fields are carried out. It is assumed that the main external force producing ice drift and ridging is the wind drag force. It is shown that ice ridging process can be accompanied by self-oscillations of the drifting ice field.

INTRODUCTION

The stationary fast ice is formed in the shelf zone of Arctic seas in a cold seasons of year. The process of fast ice formation starts in a shallow water regions, which are closed from the wind, and finishes at the beginning of January as a rule. Thus this process takes three month duration. During this time the ice cover, which has been formed near the coast line, is broken and passed away in the sea repeatedly. The inverse process, when drifting ice come to the coast, do also take place. Ice ridges oriented along coast line or isobates are the typical structural futures of fast ice. Sometimes the keels of ice ridges being in sea regions with the depth from 10 to 20 mets are grounded. Stamukhas and ice islands are settled in these regions also. Grounded ice ridges and stamukhas are anchoring points for the fast ice as well as islands and an uneven coastline (Kovacs and Sodi, 1980, Wadhams, 1980).

The internal structure of an ice ridge is different from the structure of level ice. The ice ridge consists of separate ice pieces, which can displace with respect to each other. Therefore one may consider a ridge as a granular material. The ice pieces are frozen together and the consolidated kernel is formed in the central part of the ice ridge over time. Usually it is assumed that the submerged and above-water parts of ice ridges are in hydrostatic equilibrium and have isosceles triangle shape. The bases of these triangles lay on the level of sea surface (Zubov, 1944, Kovacs and Sodi, 1980). The slope angles are defined by typical sizes of ice pieces in the ridge and drag coefficient between them. In the cases where ice ridge keel is grounded the shape of the keel and the sail will be other. The balance between buoyancy and gravity forces acting on the ridge is broken in that case.

Theoretical works on the modeling of ice ridge formation can be separated in two sets conventionally. The work of the first type (Coon et al., 1974, Rothrock,1975, Shinohara, 1990, Gray and Killworth, 1996) are related to the development of the methodology of the accounting of ice ridging in the models describing large scale dynamics of ice cover. Ice ridging is considered as the mechanism of a redistribution of the ice on the thickness under the influence of plastic deformations. The main result of these works is the construction of

various types of the redistribution function. The works of the second type are related to the investigation of patterns of the formation of a single ice ridge in a continuous ice cover. In this approach ice ridge can be considered as a specific line on the horizontal plane, which is characterized by some parameters defining the structure of the ice ridge. From our point of view this approach is more interesting for the description of fast ice dynamics. In the first time it is motivated by bounded width of the fast ice zone which is not normally less then tens kilomets. Moreover there are several bands of continuous and hummocked ice in the fast ice zone as a rule (Odisharia and Tcvecinskii, 1997).

One of the first models of the formation of a single ice ridge has been developed in the paper of Parmeter and Coon (1972). It is assumed that there are two stages of ridge formation: the piling-up of ice pieces on each other and the formation of new ice pieces under the interaction of the edge of continuous ice plate with the ridge. The ice pieces are pushed up under the water and on the ice surface in equal amounts during the first stage, so that the balance between buoyancy and gravity forces is broken. The edge of continuous ice plate is bend due to the process. The edge is broken as only bending stresses will rich some critical value. The height of ice ridge can be defined from the condition. Coon (1974) has investigated the critical stresses needing to start ridging of continuous ice consisting of separate ice floes of given sizes.

The other approach has been developed in the works of Hopkins with co-authors (Hopkins et al.,1991, Hopkins and Hibler, 1991, Hopkins, 1994,1996). The problem under the investigation is ice ridge formation by the compression of two ice plates. The ice ridge is considered as a pile of ice pieces of given shape, which can interact with each other in a viscous – elastic way. The motion of each ice piece is described by separate equations. The formation of new ice pieces due to the fracture of the edge of ice plates is taken into account also. The use of modern computer gives the possibility to calculate the motion of a large number of ice pieces and find realistic pictures of the ridging. Moreover it is possible to define the relations between energy inputs stipulating the increasing of potential energy of the ice, the displacement of ice pieces inside the hummock and the dissipation due to the friction between ice pieces.

The main goal of present work consists in the construction of ice ridging model and numerical calculations of ice ridge formation due to the interaction of drifting and stationary ice fields. Our approach is based on the using of integral relations between parameters characterizing the state of ice cover element, and on the investigation of the relations between the values of these parameters on the various sides of the discontinuity lines (Sedov, 1983, Doronin and Kheisin, 1975). We try to take into account energetic relations, which have been found in the papers of Hopkins with co-authors.

The paper is organized as following. In the § 1 the integral relations and the relations on a discontinuity line are deduced. The equations describing the formation of single ice ridge under the compression are constructed in the § 2. Numerical calculations of ice ridge formation in the place of contact of two ice fields under the influence of constant wind are carried out in § 3 and § 4 for various initial conditions of the problem. There are the comparison of the results of numerical calculations with experimental data and the discussion in the conclusion.

1. BASIC EQUATIONS

The laws of mass, impulse and energy balance of ice cover have following form

$$\frac{\partial m}{\partial t} + \nabla \cdot (m\mathbf{v}) = 0, \quad \nabla = \left(\frac{\partial}{\partial x}, \frac{\partial}{\partial y} \right), \tag{1.1}$$

$$\frac{\partial (m\mathbf{v})}{\partial t} + \nabla \cdot (\mathbf{v} m\mathbf{v}) = \nabla \cdot \boldsymbol{\sigma} + \mathbf{F}, \tag{1.2}$$

$$\frac{\partial \mathcal{E}}{\partial t} + \nabla \cdot (\mathcal{E}\mathbf{v}) = \nabla \cdot (\boldsymbol{\sigma} \cdot \mathbf{v}) + \mathbf{F} \cdot \mathbf{v}, \tag{1.3}$$

where m is the mass of ice cover, floating on sea surface with unity area, $\mathbf{v} = (v_x, v_y)$ is the vector of ice drift velocity, $\boldsymbol{\sigma}$ is the tensor of internal stresses in the ice cover, $\mathbf{F}$ is the vector of surface density of external forces acting on the ice cover from the atmosphere and ocean, $\mathcal{E}$ is the surface density of full energy of the ice, t is the time, x and y are the horizontal coordinates.

The surface density of full energy $\mathcal{E}$ is defined by the formula

$$\mathcal{E} = m(u + k) + \mathcal{P}, \quad u = u(\boldsymbol{\varepsilon}^e, T, \Sigma), \quad k = |\mathbf{v}|^2 / 2, \tag{1.4}$$

where u is internal energy of unity mass of the ice, k is kinetic energy of unity mass of the ice, $\mathcal{P}$ is surface density of potential energy of the ice cover. It is assumed, that u depends on the tensor of elastic strains $\boldsymbol{\varepsilon}^e$, the temperature T of the ice and, possibly, on other parameters, which are denoted by the letter Σ and characterize internal structure of the ice cover.

The potential energy of ice cover floating on the ocean surface with area S is defined by the formula

$$\mathcal{P}_S = \int_S \mathcal{P} dx dy, \quad \mathcal{P} = A(\rho_i g \int_{z_b}^{z_s} z dz - \rho_w g \int_{z_b}^{0} z dz), \tag{1.5}$$

where A is ice compactness, ρ_i and ρ_w are the densities of the ice and the water, g is acceleration due to gravity, $z_b(x)$ and $z_s(x)$ are the values of vertical coordinate z relating to top and bottom surfaces of the ice cover, water surface level coincides with the plane $z = 0$.

Let us assume, that all parameters characterizing the state of ice cover depend on the time t and space coordinate x only. Consider a part of the ice bounded by the straight lines

$x = x^-$ and $x = x^+$, which moves along x - direction with the velocities V^- and V^+, respectively. After the integration of the equations (1.1) – (1.3) from x^- until x^+ one find (Makshtas and Marchenko, 1994)

$$\frac{dM_r}{dt} = [m(V - v_x)], \tag{1.6}$$

$$\frac{d\mathbf{I}_r}{dt} = [\boldsymbol{\sigma}_n + m\mathbf{v}(V - v_x)] + \mathbf{F}_r, \tag{1.7}$$

$$\frac{d\mathcal{E}_r}{dt} = [\boldsymbol{\sigma}_n \cdot \mathbf{v} + \mathcal{E}(V - v_x)] + A_r, \tag{1.8}$$

where M_r, $\mathbf{I}_r = (I_{x,r}, I_{y,r})$ and $\mathcal{E}_r$ are the linear densities of the mass, impulse and energy of the ice lying in the region $x \in (x^-, x^+)$, $\boldsymbol{\sigma}_n = \boldsymbol{\sigma} \cdot \mathbf{n}$ is the vector of internal ice stresses, $\mathbf{n} = (1,0)$ is unity normal. The notation $[\lambda]$ means the difference of the values of the quantities λ by $x = x^+$ and $x = x^-$: $[\lambda] = \lambda^+ - \lambda^-$. The linear densities of external force $\mathbf{F}_r$ and the work of this force A_r are defined by the formulas

$$\mathbf{F}_r = \int_{x^-}^{x^+} \mathbf{F} dx, \quad A_r = \int_{x^-}^{x^+} \mathbf{F} \cdot \mathbf{v} dx. \tag{1.9}$$

The equations (1.1) - (1.3) assume the existence of discontinuous solutions in which the characteristics of the state and the motion of ice cover are discontinuous functions of space variables. The discontinuous solutions can simulate the motions by which typical space scales of the changing of ice cover parameters much less than the scale of space averaging of ice cover model. Typical example is the edge of ice cover, where ice compactness and ice thickness change by a jump from zero to some values.

Let us assume, that discontinuity line coincides with the axis y. For the finding of the relations between ice parameters on various sides of the discontinuity one set $x^- = x^+$, $V^+ = V^- = \mathcal{V}$, $M_r = 0$, $\mathbf{I}_r = 0$ and $\mathcal{E}_r = 0$ in (1.6) – (1.8). As a result we have (Marchenko, 1992)

$$[m(\mathcal{V} - v_x)] = 0, \tag{1.10}$$

$$[\boldsymbol{\sigma}_n + m\mathbf{v}(\mathcal{V} - v_x)] = 0, \tag{1.11}$$

$$[\boldsymbol{\sigma}_n \cdot \mathbf{v} + m(\mathcal{V} - v_x)\mathcal{E}] = 0, \tag{1.12}$$

where $\mathcal{V}$ is the velocity of the motion of the discontinuity.

2. THE MODEL OF ICE RIDGE FORMATION

Consider the plane problem on the formation ice ridge in the place of contact of two ice floes with thickness h^- and $h^+ > h^-$ (see Figure 1). The ice ridge is formed under the compression due to the influence of wind drag force $\mathbf{F} = (F_a, 0)$ on the upper ice surface by $x \in (x_0, x^-)$. It is assumed that ice floe of the thickness h^- is failed under the compression and the pieces of ones are pushed up on the ice cover and under the water. Due to the process the ice ridge is formed in the region $x \in (x^-, x^+)$. The ice floe of the thickness h^+ has not strong destruction and displacements in the x direction.

The velocity of ice motion does not depend on x in the region $x \in (x_0, x^-)$ and equals to $v = dx_0 / dt$. Therefore the first relation (1.7) for the ice from the region $x \in (x_0, x^-)$ is written in the form

$$\rho_i h^- L \frac{dv}{dt} = F_a + F_w + \sigma_{xx}^-, \quad \frac{dL}{dt} = V^- - v. \tag{2.1}$$

Wind and water drag forces on the top and bottom surfaces of the ice cover are defined by the formulas

$$F_a = \rho_a C_a V_a^2 L, \quad F_w = -\rho_w C_w v^2 L, \tag{2.2}$$

where $\rho_a = 1 kg \cdot m^{-3}$ is air density, $C_a = 0.003$ and $C_w = 0.01$ are drag coefficients on the interfaces air – ice and water – ice, $V_a > 0$ is the wind velocity.

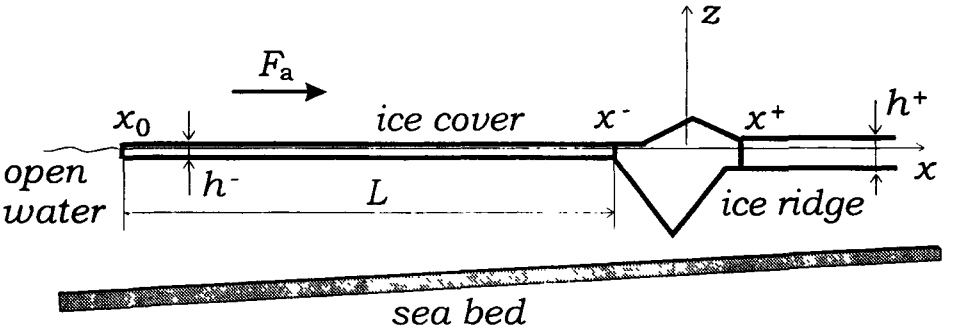

Figure 1. The scheme of ice ridge formation due to the influence of wind action on the ice field of the length L.

Let us use the law of mass balance (1.6) for the ice being in the region $x \in (x^-, x^+)$. If we suppose that the ice velocity is equal to zero in the point $x = x^+$ one can find

$$\frac{dU_r}{dt} = h^+V^+ - h^-(V^- - v), \tag{2.3}$$

where U_r is the linear volume of the ice ridge.

The power of the work A_r, which is accomplished by the wind in the region $x \in (x^-, x^+)$, is much less than the power of the work accomplishing by the wind in the region $x \in (x_0, x^-)$, since $L >> x^+ - x^-$. Therefore we will neglect the quantity A_r in a comparison with the value of $-\sigma_{xx}v$. Supposing $A_r = 0$ from the law of energy balance (1.8) for ridged ice one find

$$\frac{d\mathcal{E}_r}{dt} = -\sigma_{xx}^- v + \mathcal{E}^+V^+ - \mathcal{E}^-(V^- - v), \tag{2.4}$$

The system of four equations (2.1), (2.3) and (2.4) contains seven unknown quantities v, L, V^+, V^-, σ_{xx}^-, U_r, $\mathcal{E}_r$ and is unclosed. It is assumed, that the quantities $h^\pm$, $\mathcal{E}^\pm$, ρ_i, ρ_a, C_a and V_a are given. Let consider two additional half-empiric hypotheses about the shape of ice ridge and on energy dissipation during the ridging, which give possibility to close the system.

Let us assume, that the shape of ice ridge is characterized by the parameters l_j having the dimension of the length and by the non-dimensional parameters θ_i, which define the slope angles of the ridge. Assume that the parameters $l_1 = h_s$ and $l_2 = h_k$ define the height of ridge sail and ridge keel, respectively. Space disposition of ice ridge is defined by the coordinates of gravity center and by the angles defining the space orientation of the ridge for given values of l_j and θ_i. If the ridge is in the state of hydrostatic equilibrium, then the balance between buoyancy and gravity forces has place

$$\rho_w U_w = \rho_i U_r, \tag{2.5}$$

where U_w is linear volume of submerged part of the ridge.

Let us assume that the orientation, the shape and relative disposition of the keel and sail of the ridge do not change during the ridging. Therefore one set $\theta_i = const$ $(i = 1-4)$ and $l_j = const$ $(j > 2)$. In this case from the condition (2.5) it follows that

$$h_k = h_k(h_s), \quad x^\pm = x^\pm(h_s), \quad U_r = U_r(h_s). \tag{2.6}$$

The formulas (2.6) can be named as hypothesis of self – similarity of ice ridge shape. With accordance to the hypothesis the shape of ice ridge can be characterized by one parameter only. In the given case this parameter is the height h_s of ridge sail.

The hypothesis on the dissipation consists in the following. It is assumed that the energy input for the increasing of potential energy of ice during the ridging takes determined part from full energy input

$$d\mathcal{E}_r = \alpha d\mathcal{P}_r, \tag{2.7}$$

where α is a proportionality factor. If we neglect by energy input on the change of kinetic energy of ice pieces inside the ridge, then the rate of energy dissipation during the ridging is equal to $(\alpha - 1)d\mathcal{P}_r / dt$. It was shown in the works of Hopkins and Hibler (1991), Hopkins, Hibler and Flato (1991) and Hopkins (1994), that the coefficient α can take values from 2 to 16.8.

From (1.5) follows that the linear density of potential energy of an ice ridge is equal to

$$\mathcal{P}_r = \int_{x^-}^{x^+} \mathcal{P} dx. \tag{2.8}$$

From (2.6) and (2.8) it follows that

$$\mathcal{P}_r = \mathcal{P}_r(h_s). \tag{2.9}$$

From (2.3) and (2.4) with regard of (2.6), (2.7) and (2.9) we get the expression for linear load, which is necessary for the ridging,

$$\sigma_{xx}^- = \mathcal{E}^- - \frac{h^-}{Z}\left(\alpha \frac{d\mathcal{P}_r}{dh_s} - \mathcal{E}^+ \frac{dx^+}{dh_s} + \mathcal{E}^- \frac{dx^-}{dh_s}\right), \tag{2.10}$$

$$Z = \frac{dU_r}{dh_s} - h^+ \frac{dx^+}{dh_s} + h^- \frac{dx^-}{dh_s}.$$

From the law of mass balance (2.3) and the condition $v \geq 0$ follow the inequality $Z \geq 0$.

A closed system of the equations describing the evolution of v, L and h_s is found from (2.1), (2.2) and (2.3) and has the following form

$$\rho_i h^- L \frac{dv}{dt} = \rho_a C_a V_a^2 L - \rho_w C_w v^2 L + \sigma_{xx}^-, \tag{2.11}$$

$$\frac{dL}{dt} = \frac{dx^-}{dh_s}\frac{dh_s}{dt} - v, \quad Z\frac{dh_s}{dt} = h^- v.$$

3. THE RESULTS OF NUMERICAL CALCULATIONS

Let us assume that the submerged and above-water parts of ice ridges are in hydrostatic equilibrium and have isosceles triangle shape (see Figure 2) (Zubov, 1944). Let the coefficient of a filling of the ridge by ice pieces be equal to one and the slope angles of submerged and above-water parts of the ridge are equal. From the equation (2.5) follows

$$h_k = \sqrt{\frac{1-\delta}{\delta}} h_s, \quad \delta = \frac{\rho_w - \rho_i}{\rho_w}. \tag{3.1}$$

The linear density of potential energy of the ridge is equal to

$$\mathcal{P}_r = \frac{\rho_i g}{3\tan\theta}\left(1 + \sqrt{\frac{1-\delta}{\delta}}\right) h_s^3. \tag{3.2}$$

The boundaries and linear volume of the ridge are defined by the formulas

$$x^+ = \sqrt{\frac{1-\delta}{\delta}} \frac{h_s}{\tan\theta}, \quad x^- = -x^+, \quad U_r = \frac{h_s^2}{\delta \tan\theta}. \tag{3.3}$$

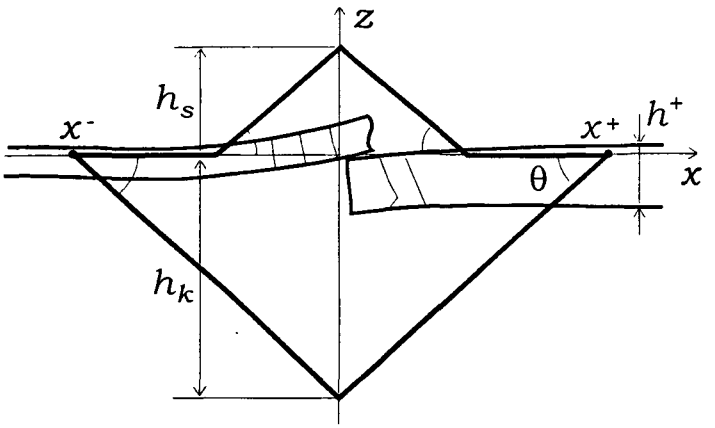

Figure 2. The scheme of ice ridge structure.

From the condition $Z > 0$ it follows that

$$h_s > h_{cr} = \tfrac{1}{2}\sqrt{\delta(1-\delta)}(h^- + h^+). \tag{3.4}$$

In accordance to the definitions (1.4) and (1.5) the ratio of surface densities of kinetic and potential energy is equal to $r = v^2/(\delta g h)$ for level ice with thickness h. Assume that

$v \approx 0.3 m \cdot s^{-1}$, $\rho_w = 1000 kg \cdot m^{-3}$, $\rho_i = 930 kg \cdot m^{-3}$ and $h \geq 0.3 m$. We find $r \approx 0.004$. Let the thermodynamic and stress states of the ice cover in the vicinity of the points $x = x^+$ and $x = x^-$ be approximately equivalent. Consider this energy level as zero level. In this case we can set

$$\mathcal{E}^{\pm} = \delta \rho_i g (h^{\pm})^2 / 2. \tag{3.5}$$

Further we will support that $h^- = 0.3 m$ and $h^+ = 0.5 m$ in the numerical calculations.

The system of equations (2.11) has stationary solutions, where $v = 0$, $L = const$, $h_s = const$ and the balance between wind drag force and stresses inside the ridge has place

$$\sigma_{xx}^- = -\rho_a C_a V_a^2 L. \tag{3.6}$$

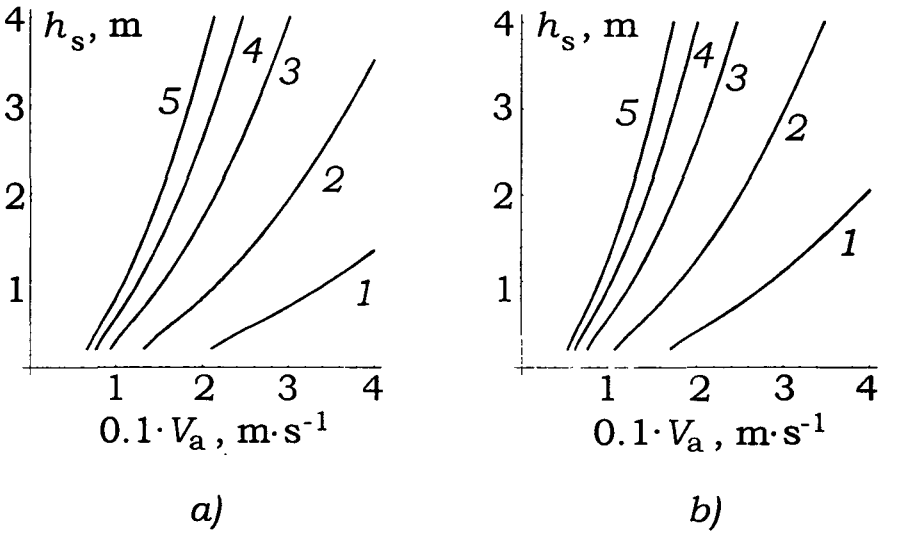

Figure. 3. The curves of the dependence of the height of ridge sail h_s on wind velocity $_a$, which are found from the condition of the balance between wind drag force acting on the ice field with length L and the force of ice ridge resistance: $L = 2 km$ (*1*), $5 km$ (*2*), $0 km$ (*3*), $5 km$ (*4*), $20 km$ (*5*). The coefficient $\alpha = 10$ (*a*), 5 (*b*).

The dependencies of the height h_s of ridge sail on wind velocity V_a for different values of the parameter α and the length of ice field L are shown in Figure 3. These dependencies

are described by the equation (3.6). From (3.1) it follows that the height of ridge keel is defined by the formula $h_k \approx 3.64 \cdot h_s$.

The results of numerical calculations of the changing of the height h_s and the velocity of the motion of ice field v in the time are shown in Figure 4 for non-stationary ridging. It is assumed that the ridging is caused by wind influence, and the wind velocity is equal to $V_a = 15 m \cdot s^{-1}$. In the initial time moment $t = 0$ ice cover stay in a rest and $v(0) = 0$. The initial height of ridge sail is equal to $h(0) = \sqrt{\delta}(h^- + h^+) \approx 0.2 m$, the parameter $\alpha = 10$. The initial values of the length $L(0)$ are equal to $5\,km$ (*1*), $0\,km$ (*2*) or $5\,km$ (*3*) (see Figure 4).

One can see, that the time of the duration of the ridging depends on the length $L(0)$, the time increases if the length $L(0)$ grows. The ridging process is sufficiently slow and can take one hour when $L(0) > 15\,km$. The velocity v of ice field motion is not more than $0.2 m \cdot s^{-1}$. The final height of ridge sail approximately equals to the height following from the condition of force balance (3.5). The value of total displacement of moving ice field during the ridging is equal to $40 m$ in the case (*1*), $200 m$ in the case (*2*) and $400 m$ in the case (*3*)) (see Figure 4).

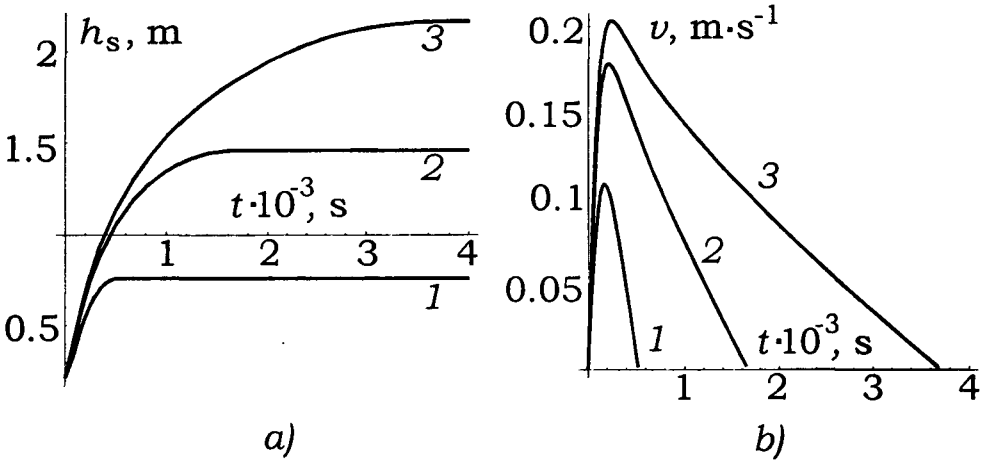

Figure 4. The dependencies of the height of ridge sail h_s and the velocity of the motion of ice field v on the time during non-stationary ridging process. The initial values of ice field length are equal to $L(0) = 5\,km$ (*1*), $0\,km$ (*2*) and $5\,km$ (*3*).

From the calculations we have that the formation of ice ridges with keel height $10 - 15\,\mathrm{m}$ is possible under the influence of the wind on level ice field in the cases, when wind velocity has order $20\,\mathrm{m} \cdot \mathrm{s}^{-1}$ and the length of ice field is not less $20\,\mathrm{km}$.

3. COMPRESSION AND RIDGING OF DRIFTING ICE COVER UNDER ITS INTERACTION WITH STATIONARY ICE FIELDS

Consider the problem of the compression of a dispersed ice field by the collision with stationary ice. Let us assume that in the initial time moment $t = 0$ the ice cover in the region $x < 0$ has the compactness $A < 1$, and stationary thick ice is in the region $x > 0$. Let dispersed ice cover has a constant drift velocity $v_1 > 0$, which induced by wind influence:

$$v_1 = \sqrt{\frac{\rho_a C_a}{\rho_w C_w}} V_a, \tag{4.1}$$

It is assumed that the collision of dispersed ice field with stationary ice has place by $t = 0$. In the moment the compactness of the dispersed ice field changes by jump from A to 1 in the vicinity of the line of contact $x = 0$ due to the collision (see Figure 5). The velocity of the dispersed ice changes from v_1 to 0 also in this moment. This "shock wave" propagates in the region $x < 0$ with the velocity $\mathcal{V}$, which is found from the law of mass balance (1.10), where we set $m^- = \rho_i h^- A v_1$ and $m^+ = \rho_i h^- v$. One find

$$\mathcal{V} = \frac{v - A v_1}{1 - A}, \tag{4.2}$$

where v is the velocity of compacted ice cover, which is in the region $x \in (x_0, x^-)$ and $x^- = 0$ by $t = 0$.

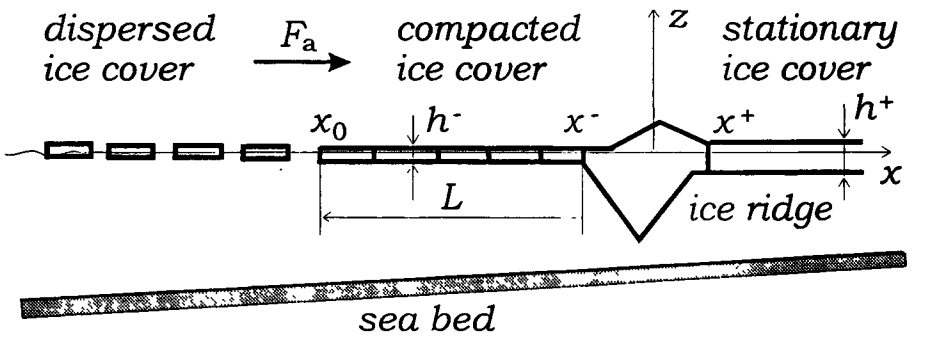

Figure 5. The scheme of the compression of dispersed ice cover and the formation of ice ridge under wind influence on the compacted ice field.

The line of the "shock" separates the dispersed ice cover and compacted ice cover. Let the length of the compacted ice field be equal to $L = -x_0$. We set that $v = 0$ and $L = 0$ by

$t = 0$. The motion of compacted ice field will begin in the point $x = 0$, when the length L equals to the value for which the balance condition (3.6) has place. The initial value of $\sigma_{xx}^{-} = \sigma_{xx}^{0}$ which is necessary to start ridging must be given. Further we define σ_{xx}^{0} from the formula (2.10) in which we substitute some small initial value of ridge sail $h_s^0 > h_{cr}$.

The closed system of equations describing the considered process has the form

$$\rho_i h^{-} L \frac{dv}{dt} = \rho_a C_a V_a^2 L - \rho_w C_w v^2 L + \sigma_{xx}^{-},$$

$$\frac{dL}{dt} = \frac{dx^{-}}{dh_s}\frac{dh_s}{dt} - v - \mathcal{V}, \quad Z\frac{dh_s}{dt} = h^{-} v. \tag{4.3}$$

In the calculations it is assumed that the thickness of dispersed and compacted ice fields is equal to $h^{-} = 0.3\,\mathrm{m}$. The results of numerical calculations are displayed in Figure 6 for wind velocity $V_a = 15\,\mathrm{m}\cdot\mathrm{s}^{-1}$, the parameter $\alpha = 10$. The compactness of dispersed ice field is equal to $A = 0.8$ (*a*) and $A = 0.7$ (*b*). From (4.1) follow, that the velocity of free drift of dispersed ice field is equal to $v_1 = 0.25\,\mathrm{m}\cdot\mathrm{s}^{-1}$. The physical time is equal $8\,\mathrm{h}$ in the numerical calculations.

One can see, that the ridging starts after $0.7\,\mathrm{h}$ and $1.1\,\mathrm{h}$ after the collision by $A = 0.8$ and $A = 0.7$, respectively. In both cases the ridging starts when $L \approx 2.5\,\mathrm{km}$. Before the start of the ridging the velocity of "shock" between dispersed ice field and compacted ice field is equal to $\mathcal{V} = -1\,\mathrm{m}\cdot\mathrm{s}^{-1}$ by $A = 0.8$ and $\mathcal{V} = -0.6\,\mathrm{m}\cdot\mathrm{s}^{-1}$ by $A = 0.7$.

After the beginning of the ridging the velocity of compacted ice field v has several oscillations during finite time interval τ. The amplitude of the oscillations decreases in time. After some time interval the oscillations come to an end and the increasing of the velocity v stands monotonic. The typical value of v is equal to several centimeters per second. The time of the oscillations are equal to $\tau = 2.2\,\mathrm{h}$ when $A = 0.8$ and $\tau = 4.4\,\mathrm{h}$ when $A = 0.7$. From Figure 6 one can see that the number of oscillations decreases with the decreasing of the value A.

The height of ridge sail riches $3.5\,\mathrm{m}$ by $A = 0.8$ and $2.5\,\mathrm{m}$ by $A = 0.7$ after eight hours after the beginning of the motion. The heights of ridge keels are equal to $12.7\,\mathrm{m}$ and $9.1\,\mathrm{m}$, respectively. In the first case the law of ridge sail increasing is approximated by the formula $h_s \approx V_s(t-2)+1$, where $V_s = 0.4\,\mathrm{m}\cdot\mathrm{h}^{-1}$ and $t \geq 2\,\mathrm{h}$. In the second case an analogous dependence has the form $h_s \approx V_s(t-3.4)+1$, where $V_s = 0.3\,\mathrm{m}\cdot\mathrm{h}^{-1}$

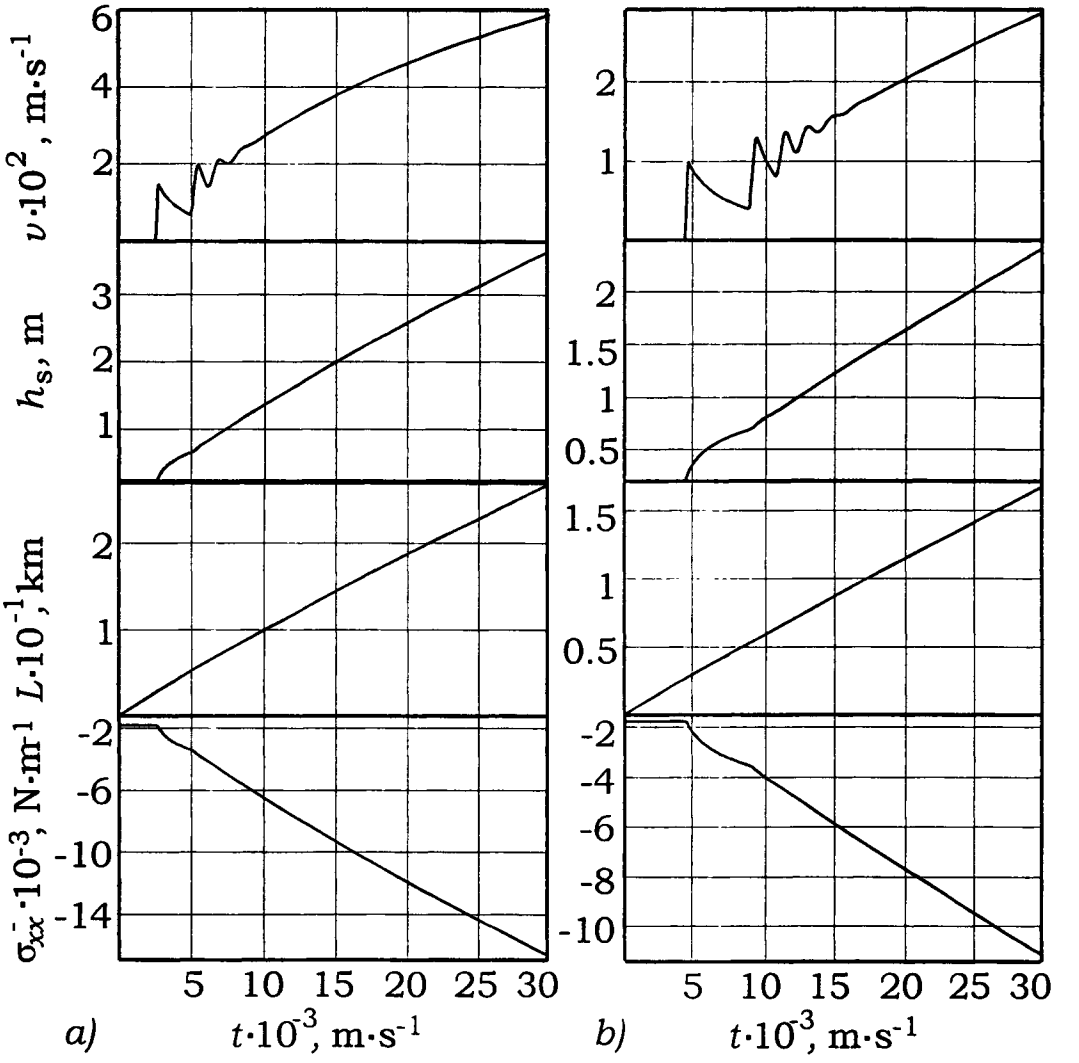

Figure 6. The results of numerical calculations of the compression of dispersed ice cover and the ridging of compacted ice field under the influence of wind stresses acting on the compacted ice field with length L. The compactness of the dispersed ice is equal to $A = 0.8$ (*a*) and $A = 0.7$ (*b*).

The linear load of the compression has order $10\,\mathrm{kPa} \cdot \mathrm{m}^{-1}$ when the height of ridge sail is $1 - 2\,\mathrm{m}$. Since ice thickness $h^- = 0.3\,\mathrm{m}$, then internal stresses in ridged ice are equal to $33\,\mathrm{kPa} \cdot \mathrm{m}^{-2}$. The linear load of the compression increases indefinitely by the increasing of the height of ridge sail

CONCLUSIONS

The model of ice ridging is developed and numerical calculations of two scenarios of single ice ridge formation are carried out in the work. In the limits of the model it is shown that the formation of ice ridge with the height of ridge sail $3-4\,\mathrm{m}$ is possible due to the influence of wind with the velocity $15-20\,\mathrm{m\cdot s^{-1}}$ on the ice field of the length $15-20\,\mathrm{km}$. Internal ice stresses arising in the ice during the ridging have the order $10\,\mathrm{kPa\cdot m^{-2}}$ and much less than the strength of the ice under the compression, which has the order $10^3\,\mathrm{kPa\cdot m^{-2}}$. Therefore ice ridging starts in the places where the strength of the ice is failed.

The duration of ice ridging depends on the scenarios of ones. In the case, when ice ridging is induced by wind influence on single ice floes compressed to the edge of stationary ice, the time of the ridging is proportional to the length of the floe. If floe length is less $20\,\mathrm{km}$ and wind velocity is less $15\,\mathrm{m\cdot s^{-1}}$, then the time of the ridging is not more one hour. Maximal velocity of the pushing of the ice on ice ridge can reach tens centimeters per second. The height of ridge sail can reach $2\,\mathrm{m}$.

Ice ridging can continue a long time when there is the influx of drifting ice on sea edge of compacted ice. The heights of ridge sail and keel can reach a large values in the case. The ridging process can have self-induced oscillations at the beginning of the ridging. The period of the oscillations depends on the velocity of the influx of drifting ice on sea edge of compacted ice. In the above considered examples this period has order of one hour and the velocity of compacted ice field is not more $6\,\mathrm{cm\cdot s^{-1}}$ during first eight hours of the ridging. The acceleration of compacted ice field can be sufficiently large during the oscillations. Probably these oscillations will accompany by intensive acoustic radiation. Self-induced oscillations of ice cover during the ridging can explain the structure of observed acoustic noises in Polar seas.

From the calculations follow that the height of ridge sail can reach $3\,\mathrm{m}$ under the ridging during eight hours. In the considered approach the height of ridge keel will reach $11\,\mathrm{m}$. The ridges with such keel can impact into sea bed on shallow water and turn into stamukhas later.

ACKNOWLEDGMENTS

This work has been supported by the Norwegian Polar Institute (Physical mechanisms of formation and destruction of fast ice in the western Arctic basin) and the Russian Foundation for Basic Research under Project Codes 97-05-62926 and 99-02-17005.

REFERENCES

Doronin, Yu. P. and Kheisin, D.E., 1975. Sea ice. Leningrad: Gidrometeoizdat, 320 p. (in Russian)

Coon, M.D., 1974. Mechanical behavior of compacted Arctic ice floes. J. Petrol. Tech.,

Vol. 26: 466-470.
Coon, M.D., Maykut, G.A., Pritchard, R.S., Rothrock, D.A., Thorndike, A.S., 1974. Modeling the pack ice as an elastic-plastic material. AIDJEX Bull. 24: 1-105.
Gray, J.M.N.T. and Killworth, P.D., 1996. Sea ice ridging schemes. J. Phys.Oceanogr., Vol. 26: 2420-2428.
Hopkins, M.A. and Hibler, W.D.III., 1991. On modeling the energetic of the ridging process. J. Offshore Mech. and Arctic Eng., Vol. 113: 105-108.
Hopkins, M.A., 1996. On the mesoscale interaction of lead ice and floes. J. Geoph. Res., Vol. 101, No. C8: 18,315-18,326.
Hopkins, M.A., 1994. On the ridging of intact lead ice. J. Geoph. Res., Vol. 99, No. C8: 16,351-16,360.
Hopkins, M.A., Hibler, W.D.III and Flato, G.M., 1991. On the numerical Simulation of the sea ice ridging process. J. Geoph. Res., Vol. 96, No. C3: 4809-4820.
Kovacs, A. and Sodi, S., 1980. Shore ice pile-up and ride-up: field observations, models, theoretical analyses. Cold Region and Technology, No. 2: 209-288.
Makshtas, A.P. and Marchenko, A.V., 1994. On the modeling of the structure of ice cover in marginal ice zones of sea drifting ice. In the book "The regularities of large scale processes in Norwegian energy active zone and adjacent regions". St.-Petersburg: Gidgometeoizdat· 150-163. (in Russian)
Marchenko, A.V, 1992. On the propagation of discontinuities in a drifting ice cover. J. Applied Mathematics and Mechanics (PMM), Vol. 56, No. 3: 346-358.
Odisharia G.E., Tcvecinskii A.S., Remisov V.V. and al. 1997. Baydaraskaya Bay Environmental Conditions. The basic Results for the Pipeline "Yamal-Center" Underwater Crossing Design. Moscow: GEOS, 432 p (in Russian)
Parmeter, R.R. and Coon,M.D., 1972. Model of pressure ridge formation in sea ice. . J. Geoph. Res., Vol. 77· 6565-6575.
Pritchard, R.S., 1990. Sea ice noise-generating processes. J. Acoust. Soc. Am., Vol. 88, No. 6: 2830-2842.
Rothrock, D.A., 1975. The energetics of the plastic deformation of pack ice by ridging. J. Geoph. Res., Vol. 80, No. 33: 4515-4519.
Sedov, L.I., 1983. Mechanics of continuous medium. Vol. I.. Moscow: Nauka, 528 p. (in Russian)
Shinohara, Y., 1990. A redistribution function applicable to a dynamic model of sea ice. J. Geoph. Res. Vol. 95, No C8: 13,423-13,431.
Wadhams, P. 1980. Ice characteristics in the seasonal sea ice zone. Cold Region and Technology, 2: 37-87.
Zubov, N.N., 1944. Arctic ice. Moscow: Izdatel'stvo Glavsevmorputi, 360 p. (in Russian)

EXPERIMENTAL VOYAGE OF TANKER *UIKKU* – DEMONSTRATION OF THE RELIABILITY OF THE YEAR ROUND NAVIGATION IN THE WESTERN AREA OF THE ARCTIC WITH THE HELP OF RUSSIAN ICEBREAKERS

V. Mikhailichenko[1], V. Peresypkin[2] and L. Tsoy[2]
[1] NSRA, Moscow, Russia
[2] CNIIMF, Saint-Petersburg, Russia

ABSTRACT

In an effort to test the possibility of the year round seaborne transportation of the hydrocarbon raw material from the Western area of the Arctic to Europe, the European Commission countries concerned put forward the international Arctic Demonstration and Exploratory Voyage (ARCDEV) Project for which the participation of icebreakers and specialized scientific institutions of Russia was required. Finnish and Russian ice tankers took part in the implementation of the Project. In April-May 1998 Finnish tanker *Uikku* made an experimental voyage to the Ob Gulf, to Sabeta, from which it carried 10660 t of gas condensate to Rotterdam. Russian tanker *Vilyuysk*, after having supplied arctic ports Dickson and Dudinka with oil products, on May 29 1998, called at Kharasavey (Western Yamal), took cargo of gas condensate amounting to 9290 t and on June 12 delivered it to Rotterdam. Icebreaker support of the tanker in the Arctic was provided by nuclear icebreakers *Taimyr* and *Rossiya*.

To perform scientific investigations, Russian icebreaker *Kapitan Dranitsyn* was selected. The icebreaker accommodated 60 scientists and specialists of six European countries and Russia. Along the route of tanker *Uikku* six scientific ice stations were set up enabling important information to be obtained on the environmental conditions as well as on physical and mechanical properties of the ice cover during the period of early spring navigation in arctic seas and in the Ob Gulf. The resulting data are of special interest taking into account the fact that ice conditions in winter 1998 in the Western Arctic were heavy, not more frequent than once in 8-10 years. Therefore the experimental voyage, having been made under extreme conditions of the navigation along the Northern Sea Route (NSR), was not only of scientific interest, but also of practical significance in that it was an opportunity to prove the feasibility of the year round navigation to the Ob Gulf under the assistance of Russian nuclear icebreakers.

The present paper contains the results of the voyage of tanker *Uikku* to the Ob Gulf. It brings out the importance of the correct choice of route through ice and assesses needs in icebreaker support considering special features of icebreaker escorting and gives recommendations on the admissible ice class to provide safe navigation in the Western Arctic.

1. BRIEF DESCRIPTION OF THE VOYAGE OF TANKER *UIKKU* TO THE OB GULF

For the execution of the exploratory voyage to the Ob Gulf in accordance with the European Union Project ARCDEV, use was made of tanker *Uikku* of the Finnish Shipping Company NEMARC. This tanker has the highest ice class as to the Finnish-Swedish Rules - 1A Super, and the propeller propulsive turning *Azipod* system for the first time used on ice ships.

Principal characteristics of tanker *Uikku* and of the icebreakers which participated in the ARCDEV Project are presented in Table 1. Russian diesel-electric icebreaker *Kapitan Dranitsyn* was selected as a scientific basis to carry out investigations during the voyage. Escorting of tanker *Uikku* through ice of the Kara Sea was envisaged by nuclear icebreaker *Rossiya* which happened to be on the NSR at that time. Shallow draft nuclear icebreaker *Vaigach,* escorting ships on the Murmansk-Dudinka route section, had to make a channel in the fast ice of the Ob Gulf to the point of destination - Sabeta.

Table 1

Characteristics of tanker and icebreakers taking part in the experimental voyage

Characteristics	Tankers		Icebreakers		
	Uikku	*Vilyuysk*	*Rossiya*	*Vaigach*	*Kapitan Dranitsyn*
Ice category	1A super	UL	LL1	LL2	LL3
Year of construction	1977	1977	1985	1990	1980
Length, m	151.5	151.5	136.0	140.6	121.3
Breadth, m	22.2	23.0	30.0	29.2	26.5
Draft, m	9.5	9.2	11.0	8.1	8.5
Displacement, t	22600	24570	23460	19600	14900
Deadweight, t	16150	17200	-	-	-
Capacity, m^3	16890	17580	-	-	-
Type of engine	Diesel-electric	Low speed	Nuclear	Nuclear	Diesel-electric
Shaft power, kW	11 400	8 280	49 000	25 000	16 200
Number of propellers	1×FPP* *Azipod*	1×FPP	3×FPP	3×FPP	3×FPP
Speed, kn	17.0	15.7	20.8	20.2	19.0
Icebreaking capability, m	1.0	0.5	2.5	1.9	1.4

* FPP - fixed pitch propeller

On April 25 at 19.00[1] tanker *Uikku,* after having been inspected for its compliance with requirements of the Rules of the navigation on seaways of the NSR, took aboard a Russian pilot and a radio operator, weighed the anchor at the roadstead of the port of Murmansk, and independently moved towards the ice edge of the Barents Sea. The Headquarters of Marine Operations of the western part of the Arctic, taking into consideration the severe ice situation in the Kara Strait as well as recommendations of Arctic and Antarctic Research Institute on the selection of the easiest way to the Ob Gulf, decided to escort tanker *Uikku* around the cape Zhelania of the Novaya Zemlya. Accordingly recommendations were given to tanker in regard to the place of its approach to the ice edge. On April 26 at 23.00 tanker *Uikku* reached the ice edge at point 72°42'N, 46°20'E and awaited there the arrival of icebreaker *Kapitan Dranitsyn.*

Icebreaker *Kapitan Dranitsyn* completed its preparations for the voyage on April 26 and, after taking aboard an international testing team, on April 27 at 01.40, cleared the berth of the port of Murmansk and sailed off after tanker *Uikku.* Forty-two specialists of European companies and scientific institutions (Neste, Kvaerner Masa-Yards, Hamburgische Schiffbau-Versuchsanstalt, Shell, MTW Schiffswerft, Technomare, Lloyds' Register, Institute of Ship Operation, Maritime Transport and Simulation, Nansen Environmental and Remote Sensing

[1] Here and further on Moscow time

Center, Hydromod) and 27 scientists of Russian organizations (Arctic and Antarctic Research Institute, Central Marine Research Institute, Krylov Institute, State Hydrographic Enterprise) were aboard the icebreaker.

Sailing in open water took place under conditions of the slight sea (2-3 numbers). However on opposite course angles the wind became stronger such that some splashing and icing of the bow portion of the upper deck occurred.

On April 28 at 00.00 icebreaker *Kapitan Dranitsyn* approached the ice edge and began penetrating the close floating ice cake where tanker *Uikku* was drifting. At 01.35, at point 72°40'3N, 46°05'2E, the icebreaker came up to the tanker and started escorting by leading. Having information about the presence of vast fractures near the western coast of Novaya Zemlya, the convoy laid east to find the shortest way to the coastal zone with a polynya. Route of the tanker escorted by icebreaker *Kapitan Dranitsyn* along Novaya Zemlya northwards is shown in Figure 1 (section 1-2).

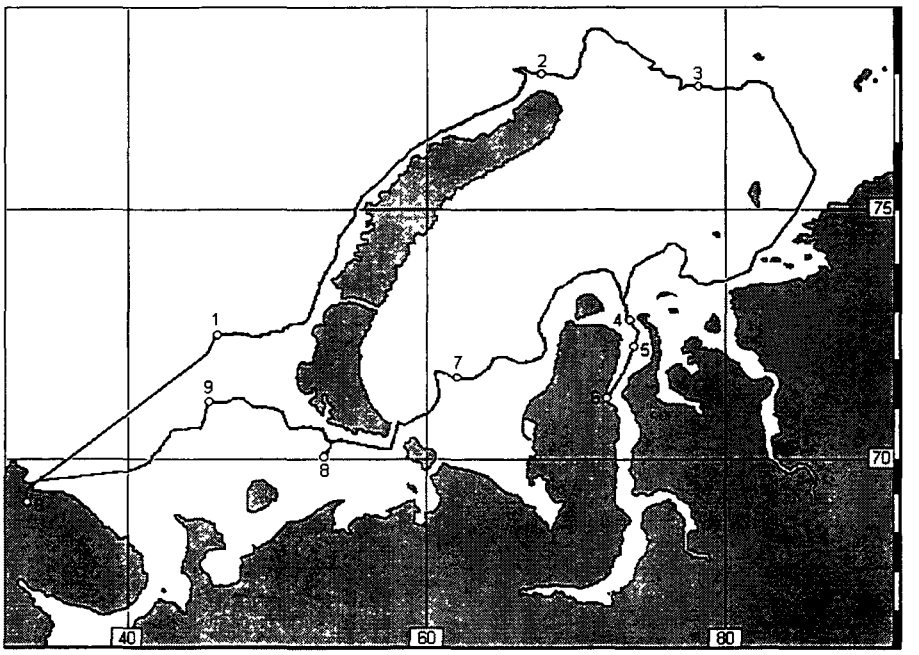

Figure 1. Route of tanker *Uikku* and icebreaker *Kapitan Dranitsyn* during the exploratory voyage to the Ob Gulf: 0 – port of Murmansk; 6 – site of loading of the gas condensate Sabeta; 2, 3, 5, 6, 7, 8 – scientific ice stations; 1, 9 – ice edge in the Barents Sea; (4 – 6) – channel in the fast ice of the Ob Gulf broken through by *Vaigach*. Sailing of *Uikku*: independently (0 – 1, 8 – 0); under the support of *Kapitan Dranitsyn* (1 – 2, 4 – 6, 6 – 4); under the support of *Rossiya* (2 – 4, 4 – 8).

Proceeding through fractures in young ice (nilas, grey ice) and crossing separate patches of open water at a speed of 14-15 kn the convoy reached the northern extremity of Novaya Zemlya. On April 29 at 09.15 at point 77°16'N, 66°10'E the convoy came across vast fields of

the concentrated first year ice and stopped to perform helicopter ice reconnaissance. After such reconnaissance and having received recommendations on proceeding through the ice, icebreaker *Kapitan Dranitsyn,* at 10.50, resumed escort of tanker *Uikku.* Movement of the convoy was made mainly by changing courses along cracks and fracture systems and forcing the in-between ice isthmuses. The ice consisted of fields of first-year ice with a medium thickness of 70-120 cm and hummocking being 2/5-3/5. Under these conditions, average speed of the convoy was maintained at 6-8 kn. By 19.00 on April 29, after the passage of the meridian of cape Zhelania and transitioning from the Barents Sea to the Kara Sea (at point 77°11'N, 68°54'E), the convoy came up to vast fields of first-year thick ice with a thickness of about 1.5 m and hummocking 3/5-4/5. Movement sharply slowed down. The icebreaker had to change over to ramming. During the last watch from 20.00 to 24.00 icebreaker *Kapitan Dranitsyn* made 22 rammings and the convoy moved ahead only by 5.1 miles at an average speed of 1.3 kn.

On April 30 up to 02.30, the icebreaker continued to break the channel by ramming. However, while realizing that icebreaker *Kapitan Dranitsyn* is not capable of escorting *Uikku* in the Kara Sea, the Headquarters of Marine Operations of the Murmansk Shipping Company sent the nuclear icebreaker *Rossiya* which was near the Arkticheskogo Instituta Islands and escorted ships to the Yenisei Gulf to meet the convoy. Pending the arrival of nuclear icebreaker *Rossiya* the first scientific ice station on the route was set up. The programme of scientific investigations included measurement of the physical and mechanical properties of ice, tests for the study of dynamic strength of ice (Drop Ball Tests), and constructing profiles of outer and underside surface of the ice cover. At 13.50 on April 30 nuclear icebreaker *Rossiya* approached the site of tanker *Uikku* with *Kapitan Dranitsyn* (77°13'8N, 69°18'4E) and at 14.35 took them in escort through ice of the Kara Sea. Order of the convoy: nuclear icebreaker *Rossiya*, icebreaker *Kapitan Dranitsyn*, tanker *Uikku.* Movement under escort of the nuclear-powered vessel was carried out mainly through fractures and the channel made earlier by icebreakers *Rossiya* and *Sovyetskiy Soyuz* in compacted fields of the first-year medium and thick ice with hummocking on the average of about 2/5. The most northern point, with co-ordinates 77°54'6N, 71°22'4E, was passed on April 30 at 19.05.

On the 1-st of May at 07.20 tanker *Uikku* needed to stop for 3 hours to repair the hydraulic system. During the repair, the second scientific ice station (77°04'N, 78°43'E) was deployed. At 09.40 the convoy resumed movement and headed east around the ice massif, Izvestiy TsIK and Arcticheskogo Instituta Islands coming out to open floating ice and the Taimyr polynya. Throughout the day, escorting was carried out mainly through the succession of fractures and young ice and by forcing individual isthmuses. At 23.00 the most eastern point (75°35'8N, 85°52'6E) en route of the convoy to the Ob Gulf was passed and here the course changed from east to west. Average speed of escorting for the day amounted to 12-13 knots.

On the 2-nd of May up to noon the convoy moving along the Taimyr polynya developed speed of 15-16 knots. At 10.20, at point 73°39'N, 78°33'E, nuclear icebreaker *Rossiya* left the convoy and sailed to support another convoy moving to the Yenisei Gulf and escorted by nuclear icebreaker *Sovyetskiy Soyuz.* However, at 12.30, icebreaker *Kapitan Dranitsyn,* which was leading tanker *Uikku,* when forcing the barrier in the field of hummocking ice by ramming, got stuck. As the result of wind becoming stronger, compression up to numbers 2-3 at the ice field joints was brought about. The Administration of the Headquarters of Marine

Operations made a decision to bring again the nuclear icebreaker *Rossiya* to the escorting of icebreaker *Kapitan Dranitsyn* and tanker *Uikku*. It lead them to fast ice of the Ob Gulf, to where the channel to Sabeta, which was made by nuclear shallow draft icebreaker *Vaigach* on April 28-29, begins. At 12.50, the *Rossiya* arrived and started to break ice near the immovable tanker *Uikku*. The inefficient escorting by leading with such breakage of ice lasted up to 14.50. At 15.30, after delivery of towing ropes, the nuclear icebreaker *Rossiya* began to lead the tanker at close tow. During the rest of the day the convoy was moving under compacting ice and the speed dropped to 3-4 knots. At 21.20 the towing rope broke and nuclear icebreaker *Rossiya* continued escorting *Uikku* by leading. Icebreaker *Kapitan Dranitsyn* fell behind the convoy and was breaking through compressed ice independently, practically all the time working by ramming.

On the 3-rd of May at 01.24 due to the poor advance movement under conditions of compression and the continuous breaking of ice near the *Rossiya* again took the tanker in tow. By the morning the compression diminished, the convoy entered grey and thin ice and the speed of towing reached 11-12 knots. At 11.40 nuclear icebreaker *Rossiya* reached point 72°56'N, 73°38'E at the entrance to the Ob Gulf and completed the escort of tanker *Uikku*. In 3.5 hours icebreaker *Kapitan Dranitsyn* arrived and took the tanker under escort along the channel in the Ob Gulf made earlier by icebreaker *Vaigach*. Nuclear icebreaker *Rossiya,* while drifting in the vicinity of the Shokalskogo Island, initiated the preventive maintenance. At 15.08, the convoy, consisting of icebreaker *Kapitan Dranitsyn* and tanker *Uikku,* started moving along the channel. The channel made 4 days earlier was in a good state; it was filled with the small ice cake having a concentration of 10/10. The fast-ice thickness at the entrance to the Ob Gulf was about 1 m and in the area of the Tambei Gulf and Sabeta, the level ice thickness was about 1.5-1.8 m. Average speed of the convoy in the channel amounted to 11-12 knots. At 16.20, at point 72°48'5N, 74°04'9E, the convoy stopped to accept the delegation arrived by helicopter *Mi-8* from Sabeta. Icebreaker and tanker were visited by leaders of the Directorate on Transport of the European Commission , representative of the Finnish Ministry of Foreign Affairs, heads of Neste and Kvaerner Masa-Yards companies, chief of the Northern Sea Route Administration, of the Ministry of Transport of the Russian Federation, Assistant vice-president of the State Duma, General Director of the Murmansk Shipping Company, Vice-Governor of the Yamalo-Nenetskiy District et al. At 17.32 the traffic along the channel resumed. At 18.45 the convoy stopped to perform investigations on the fast ice of the Ob Gulf. Scientific ice station No.3 (72°34'5N, 73°56'6E) was set up. At 23.15, after the completion of scientific work, the convoy proceeded to Sabeta.

On May 4 at 10.37, at point 71°18'1N, 72°08'6E, the convoy reached the end of the channel and came to the site of loading of gas condensate at Sabeta. Average speed of escort of tanker *Uikku* on this day was about 10 knots. At 10.45, icebreaker *Kapitan Dranitsyn* started preparing the ice berth for the tanker. After that, at 16.52, tanker *Uikku* was moored to the berth and icebreaker *Kapitan Dranitsyn* assumed the watch in the immediate vicinity of the tanker. It took 3.6 days for the reception of cargo with all auxiliary operations (connection and disconnection of hoses). During the berthing and the loading of the tanker the investigations on ice (scientific ice station No. 4) were made.

On May 8 at 08.35 tanker *Uikku* finished taking cargo and at 09.30 icebreaker *Kapitan Dranitsyn* began breaking ice near the tanker for enabling it to leave the berth. At 12.10, the convoy started from Sabeta heading north along the channel. During berthing, the channel

regelated and was blocked with snow. This resulted in slower movement on the way back. On separate stretches covered with snow, icebreaker *Kapitan Dranitsyn* had to resort to ramming. Movement was also slowed due to forced stops when the *Kapitan Dranitsyn* cooling systems failed in shallow water.

On May 9 at 08.00, icebreaker *Kapitan Dranitsyn* and tanker *Uikku* approached the point (73°00'N, 73°25'2E) of meeting with nuclear icebreaker *Rossiya,* which was waiting for the convoy at the outlet of the Ob Gulf. Taking into consideration the improvement of ice situation in the south-western part of the Kara Sea, it was decided to perform the escorting of tanker *Uikku* through the Kara Strait. During the day, the *Rossiya,* moving along fractures and areas of thin ice, had brought the icebreaker *Kapitan Dranitsyn* and tanker *Uikku* to the Yamal flaw polynya. Average speed of the convoy along the western coast of the Yamal Peninsula to the south was 12-13 knots.

On May 10, during the watch from 00.00 to 04.00, nuclear icebreaker *Rossiya* turned to the west in accordance with the recommendations of the Headquarters of Marine Operations to cross the ice massif in the direction of the Kara Strait. Movement of the convoy was carried out through a succession of fractures alternating with fields of the first year medium and thick ice with a hummocking of 2/5-3/5. On some heavy stretches the nuclear icebreaker had to work by ramming and break ice near the stuck icebreaker *Kapitan Dranitsyn* and tanker *Uikku.* However, the average speed of escorting during the whole day was 8-9 knots. At 17.00, at point 71°49'N, 61°30'E, situated approximately halfway between the Yamal Peninsula and the Kara Strait, the convoy stopped to perform scientific investigations. Scientific ice station No. 5 was set up.

On May 11, at 01.05, nuclear icebreaker *Rossiya* resumed leading of icebreaker *Kapitan Dranitsyn* and tanker *Uikku.* Until noon, movement of the convoy was carried out, with the help of the helicopter reconnaissance, through a succession of fractures, crossing partially and slightly compressed fields of first-year hummocked ice. Average speed of escorting was always 8-9 knots. At the approaches to the Kara Strait the ice situation became considerably more complicated, hummocking increased up to 3/5-4/5, at places of contact between ice fields the compacting of numbers 1-2 was observed. Icebreaking operations became operations more frequent. At 14.45, at point 71°03'N, 59°10'E, the convoy order was changed: tanker *Uikku* was put behind *Russia* and icebreaker *Kapitan Dranitsyn* was now the last in the chain. At 21.30 (70°15'5N, 57°28'5E) the convoy passed the Kara Strait and entered a vast fracture near Novaya Zemlya.

On May 12, at 02.20, at point 70°24'2N, 54°16'5E, the nuclear icebreaker having completed the escorting of tanker *Uikku* and icebreaker *Kapitan Dranitsyn,* left the convoy and proceeded east. At 03.40 (70°16'N, 53°39'5E) the icebreaker *Kapitan Dranitsyn* and tanker *Uikku* deviated from their route, searching for an ice field to carry out scientific investigations. At 05.00 (70°08'5N, 53°17'E) icebreaker *Kapitan Dranitsyn* penetrated into a field of first- year medium ice with a hummocking of 3/5-4/5 where the scientific station No. 6 was set up. Before the completion of the research work on the ice floe, tanker *Uikku* received recommendations on the route to the ice edge and at 06.45 began independent movement towards the west. The tanker arrived in Murmansk and dropped anchor at the roadstead at 20.15 on May 13 1998. At 15.40 icebreaker *Kapitan Dranitsyn,* on the completion of research, headed for Murmansk. At 08.15, at point 70°45'3N, 45°19'E, it

crossed the ice edge and entered open water. Sailing in open water took place under rather rough seas where the maximum amplitude of rolling of the icebreaker was 20-23°.

On May 14 at 09.00 icebreaker *Kapitan Dranitsyn* arrived in the port of Murmansk and at 9.30 moored at the berth. On the same day at 12.30 tanker *Uikku* left the roadstead of the port of Murmansk and continued its voyage with the load of gas condensate arriving in Rotterdam on May 19. Round-trip voyage of the tanker from Europe to Sabeta lasted for about a month despite the extremely heavy ice conditions in the western Arctic, which indicates good organization of the voyage and excellent icebreaker servicing. Resulting data for ship and convoy average speeds and power consumption of icebreakers and tanker are shown in Figure 2.

2. SELECTION OF THE ROUTE OF THE CONVOY NAVIGATING IN ICE

Figure 1 represents the route of tanker *Uikku* and of accompanying icebreaker *Kapitan Dranitsyn* realized during the experimental voyage on the Project ARCDEV. Due to the heavy ice situation in the Kara Sea, the route from Murmansk to Sabeta turned out to be approximately 1.5 times longer in comparison with the average statistics. On the way back the route also increased 1.2 times as against the usual one. However the selected route of the convoy was optimized and was the shortest one from the viewpoint of time consumption for the passage through the ice seaway. Thick and heavily hummocked ice of the Novozemelskiy massif having blocked the way to the Ob Gulf turned out to be practically insuperable even for nuclear icebreakers. Thorough investigation of the ice situation to find the shortest way to the Ob Gulf was required. Use was made of photos and radar satellite images in providing for the strategic ice reconnaissance. Visual survey of ice in front of the convoy using a helicopter helped in the tactical ice reconnaissance. The latter permitted to substantially improve the manoeuvrability of ships in ice.

Figure 3, showing the image of the Kara Sea from Russian satellite *Meteor* made on May 5, 1998, presents variants of the route from the Ob Gulf recommended by specialists of Arctic and Antarctic Research Institute on the basis of the results of the analysis of the image data. However, as one can see from Figure 1, the actual convoy route differed noticeably from the satellite image planned versions.

Final route was selected by the Headquarters of Marine Operations and the experienced shipboard hydrologist V.Losev[1] while being on the helicopter barraged ahead of icebreaker *Rossiya* provided for the optimum escorting of ships along cracks and fractures. Figure 4 shows a fragment of the ice chart made by V.Losev and the recommended path of the convoy through the Novozemelskiy massif. In Figure 5 one can see cracks in the ice massif used for the escorting of ships.

So, the correct choice of route, especially under heavy ice conditions, depends a lot on the tactical (helicopter) ice reconnaissance. It is difficult to overestimate the importance of a helicopter-guide in the fulfilment of ice operations. Use of the ice reconnaissance in such conditions allows to double or treble the speed of ship escorts. This was clearly demonstrated during the experimental voyage of tanker *Uikku* to the Ob Gulf in the extremely heavy ice in April-May 1998.

---

[1] V.Losev perished on March 8 1999 during the ice reconnaissance flight over the Kara Sea after having worked in the Arctic for more than 40 years

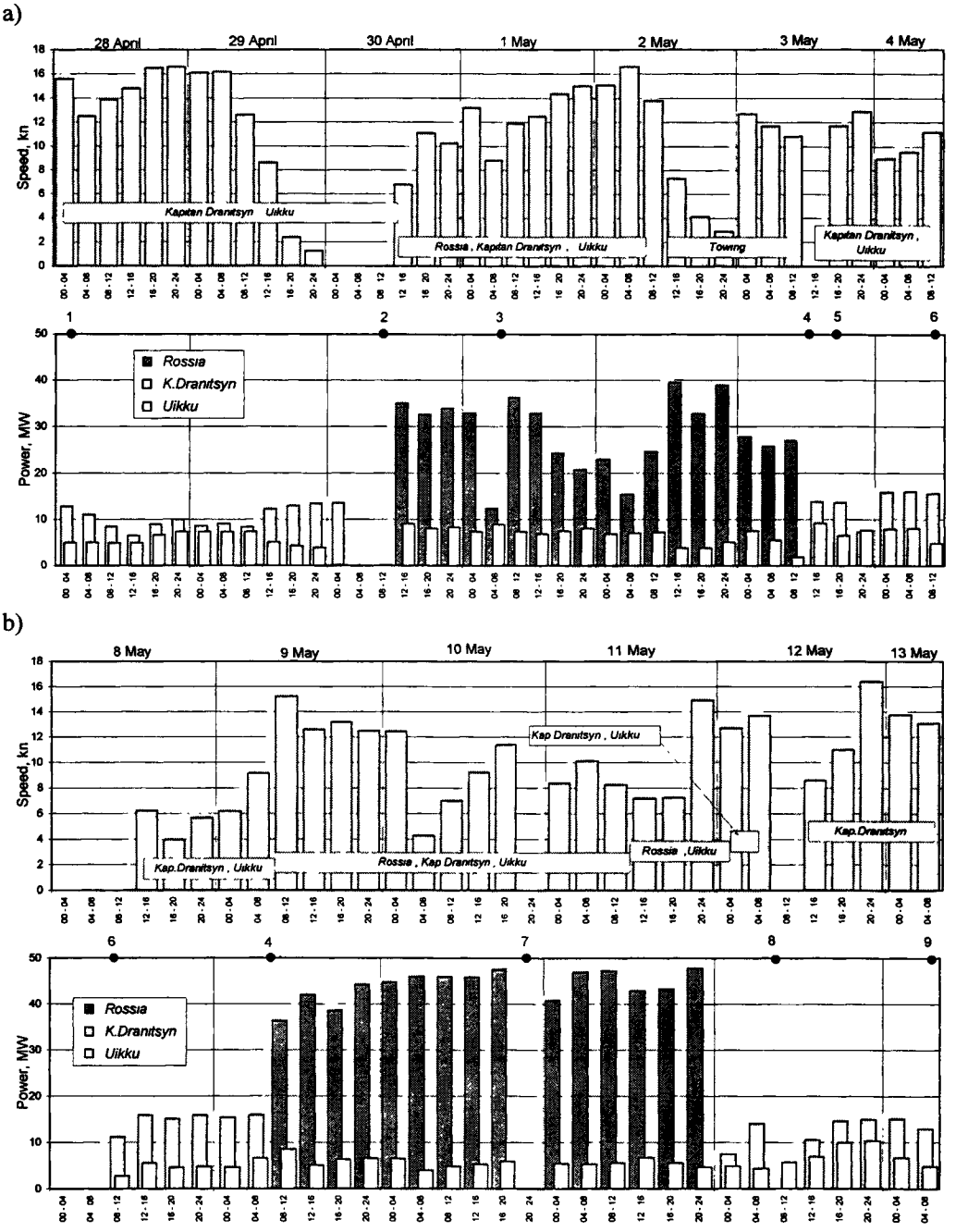

Figure 2. Average speeds and power levels for tanker *Uikku* and icebreakers *Kapitan Dranitsyn* and *Rossiya* during each watch period on their way from Murmansk to Sabeta (a) and back (b) ; • typical points of the route corresponding to numbered locations shown in Figure 1).

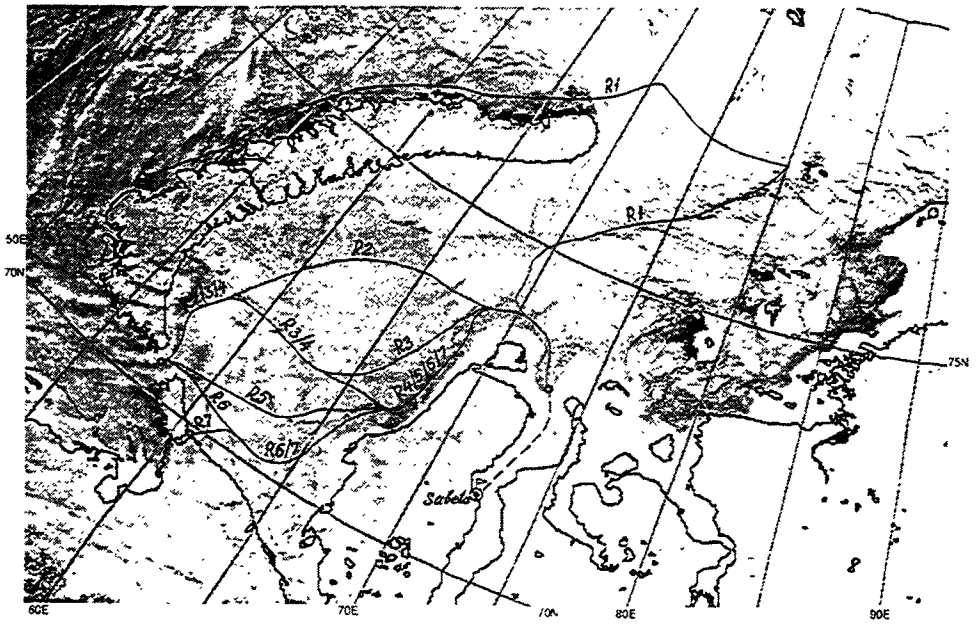

Figure 3. Photo of the ice cover of the Kara Sea from satellite *Meteor*. Preliminary choice of the route of the convoy out of the Ob Gulf.

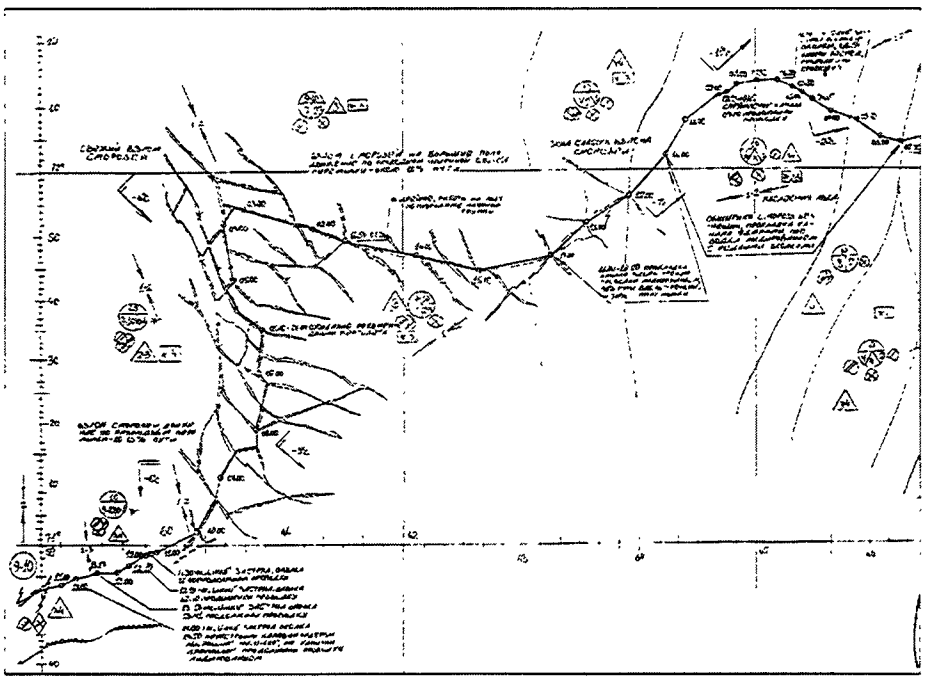

Figure 4. Scheme for the escorting of tanker *Uikku* through the Novozemelskiy massif on May 10-11, 1998 made from helicopter ice reconnaissance

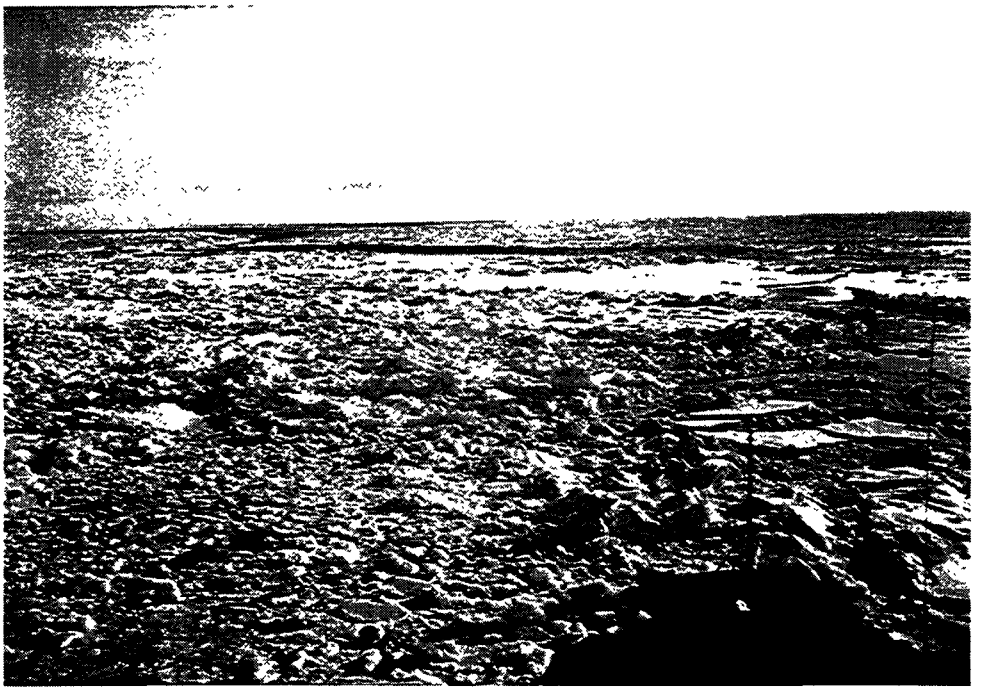

Figure 5. Kara Sea, Novozemelskiy massif. Choice of the route along cracks and fractures.

3. ICEBREAKER SUPPORT

The voyage of tanker *Uikku* on Project ARCDEV made in early spring does not favour the possibility of year-round operation of transport ships in the Arctic without icebreaker support. On the contrary, the need for icebreakers has been proved by long-standing Russian experience of navigation on the NSR. Safe, year-round navigation in the western part of the Kara Sea may only be ensured by ships with an icebreaking capability[1] of not less than 2.5-2.6 m (Figure 6). To achieve such capability a large icebreaking cargo ship should possess a propulsion plant with power of about 60 MW consuming about 400 t of fuel daily. For a 30-day voyage then, such ship should have a 12 000-t fuel capacity, which, in effect makes the cargo ship a carrier of only its own fuel. Besides, it should be noted that an icebreaking transport ship, as compared with a specialized icebreaker, has considerably less propulsion, manoeuvrability and capability of getting released from sticking. This is due to its greater relative length and parallel middlebody. To compensate for the above factors, the icebreaking capability of a cargo ship should be increased by at least 10 %, which corresponds

[1] The ability to maintain a continuous speed of 1.5-2.0 kn through level , compact ice of a specified maximum thickness (about 1 m/s).

to an increase of power by approximately 30 %. However, such a power increase would compromise the cargo ship's economic efficiency because, most of the time, it operates in open water, as opposed to icebreakers that specialize in ice operations.

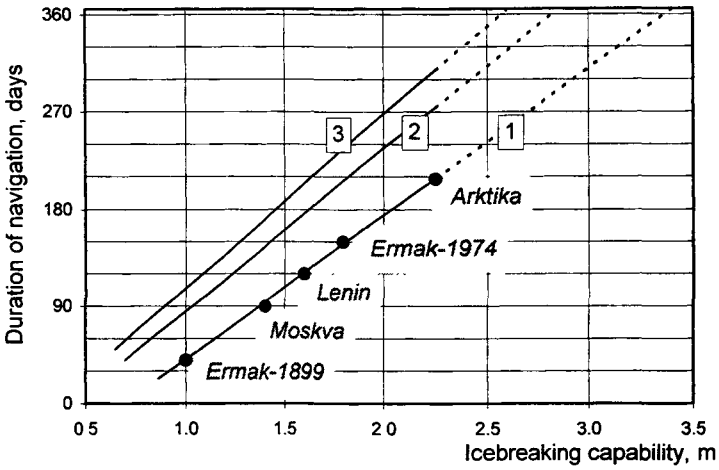

Figure 6. Relationship between the duration of navigational period in the Arctic and the icebreaking capability of icebreakers: 1 - transit navigation along the NSR and in the eastern area of the Arctic, 2 - western area of the Arctic, 3 - western part of the Kara Sea

The experimental voyage realized in accordance with the ARCDEV Project, in support of graph in Figure 6, has shown that diesel-electric icebreakers of the *Kapitan Sorokin* type, the icebreaking capability of which does not exceed 1.4 m, are not capable of assuring winter navigation in the Kara Sea. Efficient escorts of ships under these conditions may be provided only by nuclear icebreakers of the *Rossiya* type. It can be seen from Figure 2 that even this icebreaker, while escorting tanker *Uikku* and icebreaker *Kapitan Dranitsyn,* most of the time used power close to the maximum. The escort was carried out under the heaviest conditions which made it necessary for the *Rossiya* to tow the tanker, despite the presence of the auxiliary icebreaker *Kapitan Dranitsyn.* At the same time, the rather high average convoy speed achieved during the voyage is indicative of the reliability of escort in the western part of the Arctic year round, a tribute to the ice navigational tactics and skills gained in Russia on the basis of the long-standing experience.

4. ICE CLASS OF SHIPS ADMITTED FOR THE OPERATION IN THE KARA SEA

Results of this experimental voyage of tanker *Uikku* to the Ob Gulf, the analysis of operational experience of the Russian icebreaking cargo fleet in the Kara Sea, and statistics of ship damages allow recommendations on the required ice class needed for safe navigation in the western Russian Arctic to be formulated. During traditional periods of summer navigation in open floating and broken close floating ice between Murmansk (Arkhangelsk)

and the Ob Gulf (Yenisei Gulf) cargo ships with ice class L1 of the Russian Marine Register of Shipping (MRS) may sail under the assistance of icebreakers. Admittance of ships with lower ice classes is excluded. Ice class L1 corresponds to class 1A of the Finnish-Swedish Rules and to PC7, which is the lowest ice classification being developed for the unified requirements of IACS and the IMO Code on the safety of ships navigating in polar waters.

During extended periods of the arctic navigation (up to December - January) in the Kara Sea, Ob and Yenisei Gulfs the UL MRS class ships may navigate with a fair degree of safety under the escort of icebreakers. This class roughly corresponds to class 1A Super of the Finnish-Swedish Rules and to class PC6 of the new unified code. During the winter-spring period, reliable, safe, and efficient navigation in the Kara Sea may be provided only by ULA MRS class ships under the escort of powerful nuclear icebreakers. Ice class ULA may be identified as the international class PC5 of the future IACS Rules and the Polar Code.

5. CONCLUSIONS

While summing up the results of the successful demonstration voyage of tanker *Uikku* to the Ob Gulf in early spring 1998 under extremely heavy ice conditions, one can come to the following principal conclusions:

1. Long-standing Russian experience in the exploration of the NSR and construction of arctic ships provide grounds to the claim that icebreaker escort of cargo ships in the Arctic is the most efficient and economically justified method of navigation.
2. The availability of powerful nuclear icebreakers with the use of the satellite and air-ice reconnaissance ensures with a fairly high degree of reliability efficient year-round navigation in the western part of the Arctic.
3. Prospective tankers for year-round navigation in the Kara Sea under the assistance of powerful icebreakers should be not lower than ULA-class of the Russian MRS and have high manoeuvrability. Tanker *Uikku* has ice class *1A Super,* and, as to the hull shape, power level, and especially manoeuvrability, (thanks to the *Azipod* propulsion steering system) is advantageous compared with other ships of this class and of class UL MRS. At the same time, a drawback of its propulsion unit was brought to light in the process of the exploratory voyage (about 10 short failures in the electrical circuit were detected). This indicates the necessity to continue study of the reliability and efficiency of this system in the Arctic.

DETERMINATION OF THE ICE LOADS ON OFFSHORE STRUCTURES FROM FIRST YEAR RIDGES

Dr. B.D. Noskov and Dr. S.I. Rogachko
Moscow State University of Civil Engineering, Moscow, Russia

ABSTRACT

Drifting first year hummock formations (ridges or hummock fields) in the process of interaction with offshore structures will cause maximum internal ice loads. According to the recommendations current codes in Russia hummock force action is to be determined with the help of hummock coefficient which increases ice load from level ice field of design thickness.

The value of this coefficient depends on geographical position of the constriction site and, actually, is not scientifically grounded, because it does not take into account the main characteristics of hummock formations. Due to this reason the application of this coefficient in the design practice will lead to certain inaccuracy in the calculation of ice load, which, as a result, may cause either a breakdown of a design structure or unjustified investments.

The main hummock characteristics to be taken into consideration in calculations are their metrical and strength parameters. The determination of design characteristics of hummock formations may be carried out with the help of corresponding engineer survey in the region of future construction during a certain period recommended by the codes.

Such survey and research are rather expensive arrangements which require very experienced and high-skilled personnel and researches as well as special technical means including research ships.

This paper will present the method of determination of ice loads from hummocks and estimated performance determined in a more simple way without high expenses. This method may be applied at a preliminary deign stage.

1. INTRODUCTION

The most significant ice load on offshore structures in freezing seas will come from first-year ridges and hummock fields. According to the current Russian codes (SNiP 2. 06.04-82*, 1986 and VSN 41.88, 1988.) the factor of force action of hummock formations is to be taken into account by means of the hummocking coefficient which increases ice load from ice level field with a design thickness.

The design values of this coefficient recommended by the codes are not scientifically grounded. Due to this reason the application of this approach in the design practice is likely to lead to quite certain inaccuracy. As a result a design structure may either meet with an accident with grave consequences or the realisation of such project will require unreasonable investment.

The drawback of this method of determining force action of hummock formations on offshore structures lies in the fact that in the process of its

application the main parameters of hummocks are not taken into account. This parameters include first of all metric and strength characteristics of hummock parts. In order to determine the above properties it is necessary to perform the corresponding complex engineering survey for a number of years. As the world practice shows, these surveys require to organise expensive expeditions using sea vessels of ice class as well as aviation.

Nevertheless, considerable expenses can be avoided while applying the method of determination of force action of hummocks which is described in this paper.

2. BACKGROUND AND RESULTS

In the 1980s during the large-scale studies experimental values of hummocking coefficients were investigated. The results of these investigations were published in a number of papers (Belov, Kopaeigorodskiy et al., 1986; Rogachko et al., 1994; Vardanian, Belov et al., 1986). Besides this, there were conducted the tests investigating the contribution of each part of a hummock field to the global ice load.

Many researchers, are known, to look at a hummock as a body consisting of three parts (sail, refrozen layer and keel ones). Each of the named parts interacting with a structure and being destroyed takes part in the forming of the global ice load. To estimate the ice load from each part of a hummock the experiments were carried out. According to the developed methods (Noskov, Vardanian et al., 1985) the ice tanks were made in the fast level ice field where a large-scale model of a hummock field consisting of fragments of level ice field with the thickness h_d was simulated. Soon after the creation of such a hummock field, when the ice fragments composing the hummock through all its height were not refrozen, these fragments were cut through by a rigid cylinder model of a support part of a structure with the help of the experimental installation and the ice load was registered. This load after the calculation correction corresponds to the load from unconsolidated keel part. After the ice fragments composing a hummock field were refrozen in the sail part of a hummock and after the formation of the middle consolidated layer with thickness $h_m = 1{,}5h_d$ a repeated cutting of a field was conducted by a cylinder model of an obstacle of the same diameter with registration of the global load from the three parts of a hummock. And, finally, at the last stage of the experiments out of the undistorted hummock part there was removed only a sail part and the experiment in which the support part was cut through with the help of a cylinder model was repeated and the registration of the ice load from middle and keel parts was provided.

The analysis of the experimental results revealed that the main contribution to the global ice load from a hummock field produces the refrozen layer of a hummock formation. If the level of porosity of this refrozen layer is about zero, the value of ice load ranges from 66% to 80% . The contribution to the global load produced by keel and sail parts constitutes on average 2.5% and 19.2% correspondingly.

The results of the experimental research allowed to establish a new approach in determining ice load from hummock formations which is based taking into

account the thickness and strength characteristics only of the middle part of a hummock.

On the basis of the analysis of natural observation data in the area of the future construction the average thickness of ice fragments from sail part of a design hummock h_b is determined. This parameter allows to determine the time of the hummock formation according to the hydrometeorological station nearest to the construction site. In order to do this, the sum of the average negative daily air temperature during the period from the beginning of the process of ice formation till the time of the appearance of the design hummock - Δt.

$$\Delta t = 0{,}25h^2_b. \tag{1}$$

Then the sum of the average daily negative air temperature during the period from the appearance of the design hummock till the end of the period of ice formation.

$$\Delta t_1 = \Sigma t - \Delta t, \tag{2}$$

where Σt - the sum of the daily average of negative air temperature during the period of ice formation (average annual during the period of observation).

As the results of our and anther investigations showed (Timco and Goodrich, 1988; Vardanian, Belov et al., 1986) the thickness of the middle refrozen layer of a hummock is about twice as thick as that of level ice surrounding a hummock formation, which is formed during the same period in the same temperature conditions. Then the thickness of the refrozen middle layer:

$h_m = 2h$, where $h = 2\sqrt{\Delta t_1}$.

The strength of the middle part of a hummock R_m may equal the strength of a level ice field R_c, which may be determined according the recommendations based on the results of the great number of studies ice strength properties in the frozen seas and presented in the code (AMENDMENT No 2 SNiP 2. 06.04-82*, 1995).

As a result, the global ice load from a hummock may be defined by means of Korzhavin's classical dependence (Korzhavin, 1962), taking into account the shape and strength parameters of the middle layer of a design hummock and the coefficient which takes into account the contribution of keel and sail parts.

$$F_r = 1.3mkR_cbh_m, \tag{3}$$

where m - coefficient of obstacle shape; k - indentation factor; R_c - ice uniaxial compression strength; b - obstacle width; h_m - thickness of the refrozen middle layer of a hummock formation; 1,3 - numerical coefficient which takes into account the increase of the ice load from the hummock caused by the cutting of sail and unconsolidated keel parts by a structure.

Thus, the ice load determined by means of the proposed methods my by made more on the basis of the additional data on a design hummock.

3. CONCLUSIONS

Thus, the paper suggests the method which allows to determine ice load from first year hummock formations depending on the period of their existence.

4. REFERENCES

AMENDMENT No 2 SNiP 2. 06.04-82*. 1995. Loads and action on offshore structures (from waves, ice and vessels). Bulletin of Construction technology, No 9, 24 p., No 10, pp. 19-21, No 11, pp. 23-24.

Belov, A.B., Kopaeigorodskiy, E.M., Vardanian, S.S., Noskov, B.D., Rogachko, S.I. 1986. The interaction between hummock formations and an cylinder support part. Proceedings Soyuzmorniiproekt, Port engineering and survey in the offshore region, Transport, Moscow.

Korzhavin, K.N. 1962. The effect of ice action on offshore structures. USSR Academy of Science, Novosibirsk, 224 p.

Noskov, B.D., Vardanian, S.S., Kopaeigorodskiy, E.M., Rogachko, S.I. Belov, A.B., et al. The method of hummock formation modelling. Copyright No 1219708 from 22.11.1985.

Rogachko, S.I., Evdokimov, G.N. and Burdyug, T.P. 1994. The action of sea ice on offshore construction. Proc. of the Int. Conf. on Offshore Mechanics and Arctic Engineering. Vol. IV, , pp. 93-97.

SNiP 2. 06.04-82*. 1986. Loads and action on offshore structures (from waves, ice and vessels). Gosstroy USSR, Moscow, 38 p.

Timco, G.W. and Goodrich, L.E. 1988. Ice ruble consolidadtion IAHR, Proceeding of The 9th International Simposium on ice, Vol 2, Japan, Sapporo.

Vardanian, S.S., Belov, A.B., Noskov, B.D., Rogachko, S.I. 1986. The research of the effects of hummock formatioms on offshore structures on the continental shelf. Mezhvuz, The effects of external factors on offshore structures, Moscow.

VSN 41.88. 1988. Departmental construction norms (experimental). The design of ice-resistant stationary platforms. Minnefteprom, USSR, Moscow., 137 p.

ICE PERFORMANCE MEASUREMENTS ONBOARD MS PIONIER

T. Nyman[1], J. Kokkonen[2]
[1]VTT Manufacturing Technology, Finland
[2]Finnish Maritime Administration, Finland

ABSTRACT

An automatic measuring system was installed in December 1997 onboard MS *Pionier*, a typical vessel operating in the winter traffic of the Saimaa Canal, acquiring data about the performance of the ship until the end of the winter. The data consists of the propulsion quantities, the propeller shaft torque, the rotation speed of the propeller, and the propeller pitch. The data also includes the rudder angle recorded every two seconds on the hard disc of the measuring PC, and the ship's position data obtained from the DGPS unit. This data was used to analyse the power consumption, delays caused by ice conditions, and the total resistance of the ship.

1. INTRODUCTION

Saimaa is a wide lake system (Figure 1, top left) in south-eastern Finland with a waterway system of 1,895 km the passage depths of which exceed 2.4 m. A total of 775 km of these waterways are so-called deep fairways with passage depths of 4.2 – 4.35 m. The Saimaa waterway system is connected to the Gulf of Finland via the Saimaa Canal (Figure 1, top-right).

The length of the Saimaa Canal is 42.9 km and the elevation difference between the water levels of the southern Saimaa region and the Gulf of Finland is about 76 m. The eight locks of Saimaa Canal (Figure 1 bottom) are 85 m long, 13.2 m wide, and have a water depth of 5.2 m. In the locks, the lower gates are cheek gates while the upper gates are vertical lift gates.

Originally, the Saimaa Canal was designed for an eight-month traffic season but, as the use of the canal increased, the traffic season was prolonged to 9.5 – 10 months, from April to January. Further, the Finnish Maritime Administration started a project in co-operation with VTT Manufacturing technology to study the possibilities of prolonging ship-borne traffic along the Saimaa Canal to year-round use. Also, the proposed Kymi Canal plan has been studied as an alternative solution for arranging winter inland navigation in Finland. This work, i.e., the long-term measurements onboard MS *Pionier*, is part of this project. The objective of this measurement has been to collect data about *Pionier's* performance during winter on her route from the sea area to the inland harbours of Saimaa via the Saimaa Canal. This data can be utilised to verify the calculation models that will be used when estimating the possibilities of the year-round traffic.

The long-term measurements were started at the beginning of December 1997 and ended at the end of April 1998. The measurements were continued during the winter of 1998/99, but the analysis of those measurements will not be completed until in the autumn of 1999.

The favourable attitude of the ship's owner, Interscan Schiffahrts GmbH, as well as the co-operation with the Finnish Maritime Administration and Finncarriers Ltd made the measuring onboard MS *Pionier* possible.

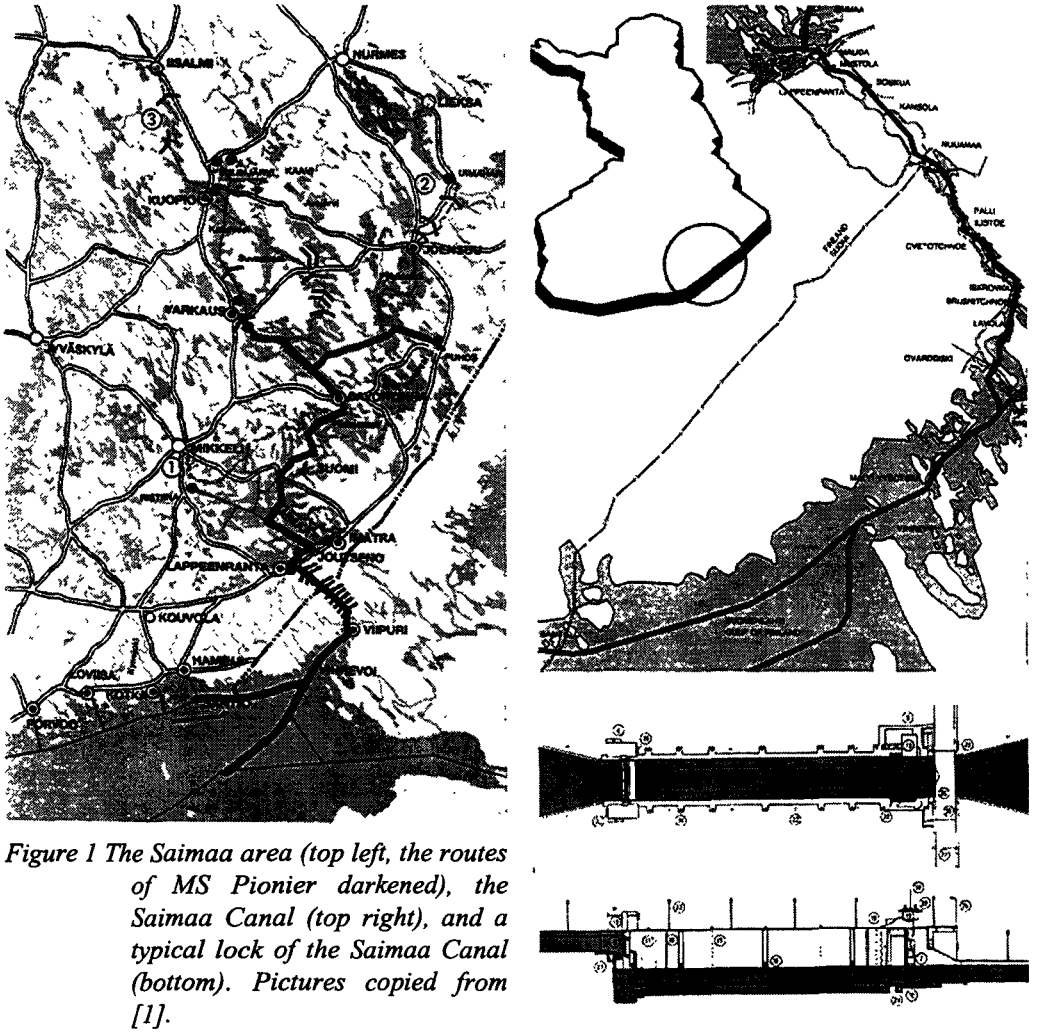

Figure 1 The Saimaa area (top left, the routes of MS Pionier darkened), the Saimaa Canal (top right), and a typical lock of the Saimaa Canal (bottom). Pictures copied from [1].

2. THE SHIP AND THE ONBOARD MEASURING EQUIPMENT

2.1 The Ship

When selecting the ship for the long-term measurements, the selection criteria were that the ship should be a typical vessel for winter traffic in the Saimaa Canal and the main dimensions of the ship should correspond to the maximum values allowed in the canal.

The selected ship, MS *Pionier* (Figure 2), is owned by Interscan Shiffahrts GmbH. She is a multipurpose cargo vessel with a double hull and a cargo capacity of 4,418.7 cubic metres for bulk and 93 TEU in cargo hold and 44 TEU on deck for containers. As can be seen from the main dimensions (Table 1), the width and the length of the ship exceed the maximum

allowable dimensions so the ship needs a dispensation for passing through the Saimaa Canal and for sailing along the deep fairway in the Saimaa area. The draught, too, exceeds the limit, which means that the ship cannot use her full cargo capacity in Saimaa.

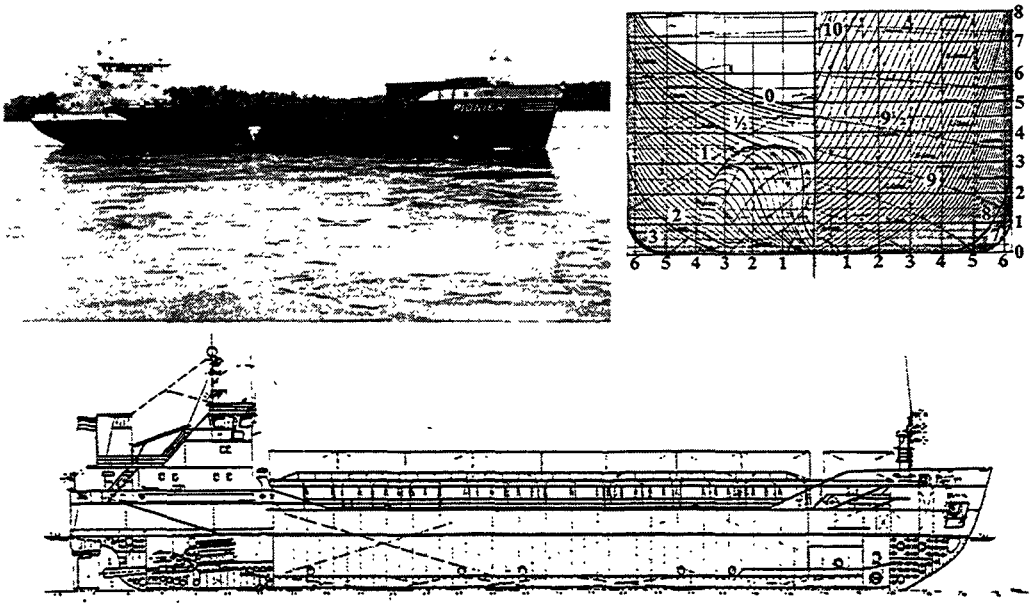

Figure 2 MS Pionier photographed in Saimaa (top left), body plan (top right) and general arrangement (bottom).

Table 1 Principal dimensions of MS Pionier.

	MS Pionier	Max. allowable dimension
Length, overall	82.30 m	82,00 m
Length, perpendicular	78.90 m	
Breadth	12.50 m	12,20 m
Draught	4.884 m	4,35 m
Draught in ballast aft/fore	3.75/2.75 m	
Trial speed, full cargo, full power	11.0 kn	
Power	1200 kW (600 1/min)	
Propeller type	4-bladed CP	
Propeller diameter	2.8 m	
Rudder	Becker-rudder, A_r=6.15m^2	
Dead-weight	2850 ton	
Finnish Swedish ice class	IB	

2.2 The Onboard Measuring System

The measuring system onboard MS *Pionier* was designed to function automatically and register signals as a function of the ship's position. The measured signals were the rotation speed of the propeller, the torque of the propeller shaft, the propeller pitch, and the rudder angle. The propulsion power was calculated from the torque and the rotation speed. The ship's position was obtained from the DGPS-unit. All measured and calculated signals were recorded at the intervals of two seconds on the hard disc of the measuring computer.

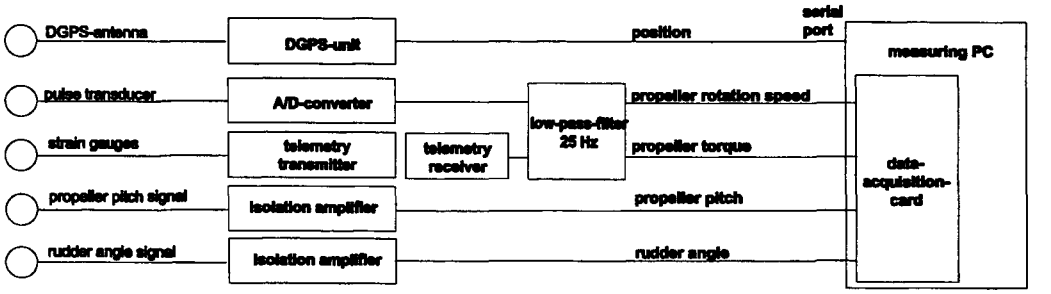

Figure 3 Schematic diagram of the measuring system onboard MS Pionier.

3. THE ROUTE AND THE CLIMATIC AND ICE CONDITIONS

The measuring system was activated 5 December 1997 at the harbour of Puhos, the easternmost harbour of the deep fairway (Figure 1 top left). From Puhos MS Pionier sailed via Savonlinna to the northernmost end of the Saimaa Canal in Lappeenranta and via the Saimaa Canal to the Gulf of Wyborg on the Gulf of Finland the port of destination being somewhere in Western Europe. In addition to this trip the measuring system of MS Pionier was active during two round-trips performed in ice conditions from the Gulf of Finland to the harbour of Varkaus on Saimaa. The first of them was 23.-31.12 1997, at the end of the traffic season of the Saimaa Canal and the second, 17.-23.4.1998, in the beginning of the new traffic season. The environmental and load conditions of the different voyages are presented in Table 2.

Table 2 The environmental and load conditions of the different trips performed by MS Pionier in the winter of 1997/98 (Gulf of Finland=GoF).

Route	Puhos-GoF	GoF-Varkaus	Varkaus-GoF	GoF-Varkaus	Varkaus-GoF
Date	5-6.12.-97	23-25.12.-97	30-31.12.-97	17-18.4.-98	21-23.4.-98
Air temperature [°C]	-7	-5	-7	0	0
Frost sum [°Cd]	100-147	179-257	222-303	890-1015	890-1015
Level ice thickn. [cm]:					
– Gulf of Finland	10-15	15-20	20-30	40-55	40-55
– Saimaa Canal	0-5	5-26	0-28	43-60	43-60
– Southern Saimaa	7-14	14	19	42	42
– Northern Saimaa	16	22	18-26	68	68
Load condition	loaded	loaded	loaded	ballast	loaded

The winter was quite mild untill the end of January 1998 as can be seen from the frost sum curves for the winter of 1997/98 in Figure 4. The period when the Saimaa Canal was closed was quite cold the air temperatures being on the southern Saimaa on the average of -6,5°C and in Varkaus on the average of -8,3°C. The frost sum reached its maximum by the middle of April being about 900°Cd in Lappeenranta and about 1000°Cd in Varkaus. The long time averages are 1000°Cd for Lappeenranta and 1100°Cd for Varkaus. The level ice thicknesses increased over the long time averages as can be seen from Figure 5 (right) in which the ice thickness curve measured in Oravi is compared with the minimum and maximum values measured in the winters of 1986-91. Oravi locates on Iso Haukivesi, one of the biggest lakes of the Saimaa water system. The climatic conditions in Oravi correspond those of Varkaus as can be seen from the ice thickness values measured outside Akonniemi, one of the harbours of Varkaus. The level ice thicknesses on the southern Saimaa were about 5 cm thinner than those measured in Varkaus. The ice thickness values in Table 2 given for Saimaa area were measured on the open lakes where the ice cover is thickest whereas in the straits the ice cover is thinner due to current. Some of the straits can be totally icefree. The ice thicknesses on the Saimaa Canal in the winter of 1997/98 were measured by the Finnish Maritime Administration. The results are presented in Figure 5 (left).

Often the ice conditions on the Gulf of Finland outside the Gulf of Vyborg are the most difficult barrier for the traffic from the Gulf of Finland to the Saimaa Canal because the ice cover on the area can be heavily ridged due to winds. The level ice thicknesses during the passages of MS Pionier on the Gulf of Vyborg correspond the long time averages measured outside the Finnish harbour Kotka on the eastern Gulf of Finland as can be seen from the ice maps and ice thickness curves in Figure 6. On the voyages performed in December MS Pionier used the southern fairway on the Gulf of Finland (Figure 1 left) whereas on the voyages performed in April MS Pionier used the northern fairway along the Finnish south coast. During the voyages the ice conditions were quite light so no icebreaker assistance was needed.

In general the fairway channels on the routes of MS Pionier were quite light although the winter of 1997/98 can be categorized almost as a normal winter when using the level ice thicknesses and the frost sums as measures. The main reason for this is that during the frost period in the winter of 1997/98 the Saimaa Canal was closed and the ship traffic on the waterways of Saimaa was not very busy.

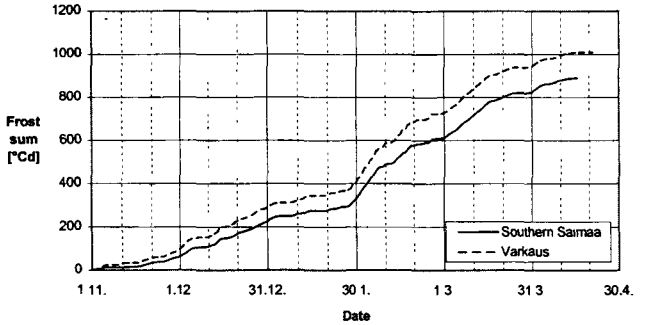

Figure 4 The frost sums measured in the winter of 1997/98 in Varkaus and in the southern Saimaa by the Finnish Meteorological Institute.

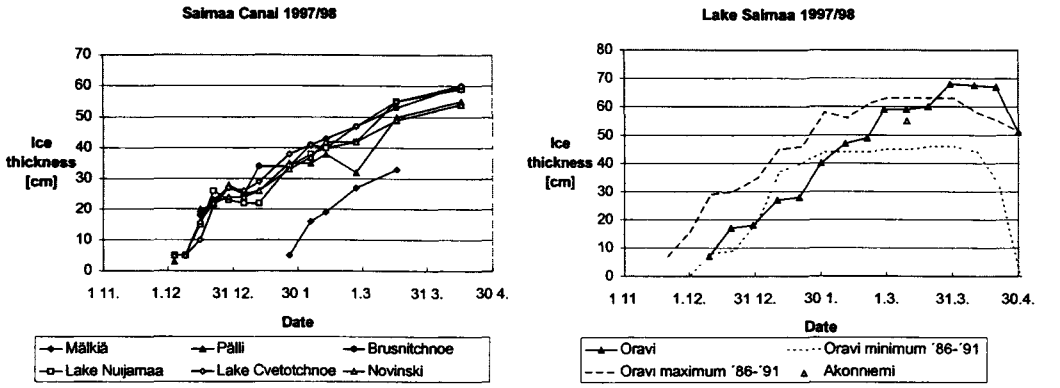

Figure 5 The level ice thicknesses measured on the Saimaa Canal in the winter of 1997/98 by the Finnish Maritime Administration (left) and in Oravi on the Lake Saimaa measured by the Finnish Environment Institute(right). The corresponding minimum and maximum curves measured in the years 1986-1991 [4] in Oravi as well as the thicknesses measured outside the Akonniemi harbour in Varkaus in 1998 are also presented.

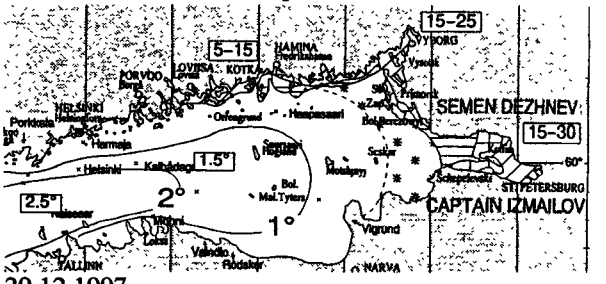

29.12.1997

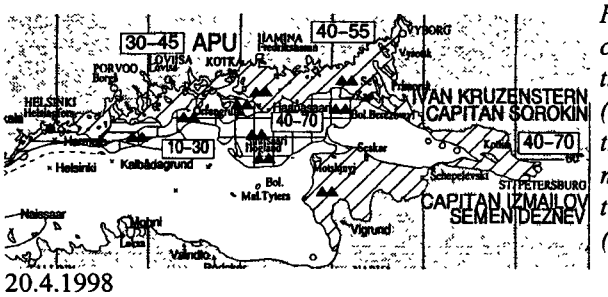

20.4.1998

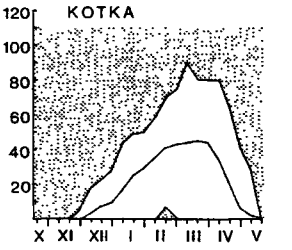

Figure 6 The ice maps published by the Finnish institute of Marine Research corresponding the ice conditions during the first (top left) and the second (bottom left) round-trip of MS Pionier in the winter of 1997/98. The maximum, minimum and average level ice thicknesses outside Kotka harbour (1937-1985)(right) [5].

4. RESULTS

4.1 Energy consumption and power distribution along the route

Because the operations of he ship in canal differ significantly from those on the lake area the power consumption in canal is studied first separately in the following. In Figure 7 the speed, the power and the propeller pitch signals from two different canal voyages are presented as a function of the distance travelled downstream from the lock of Mälkiä. The first of the voyages took place in early December and the second in late April. From the figure it can be seen, that the signals are quite similar during the first 10 kilometers. After that, in Kansola (distance 10-12 km) the ice conditions on the latter voyage were at their heaviest and remained some heavier than on the first voyage untill the end of the canal. The speed limit for the excavated areas is 6,5 kn whereas on the canal lakes higher speeds can be used as can be seen from the speed signals (Lake Nuijamaa, distance 19-22 km, lake Cvetotchnoe, distance 30-34 km). The data in numerical form of the canal transits can be seen in Table 3 and the speed and power distributions in Figure 8. The high columns of the latter voyage in the lowest speed and power groups are due to the longer locking times.

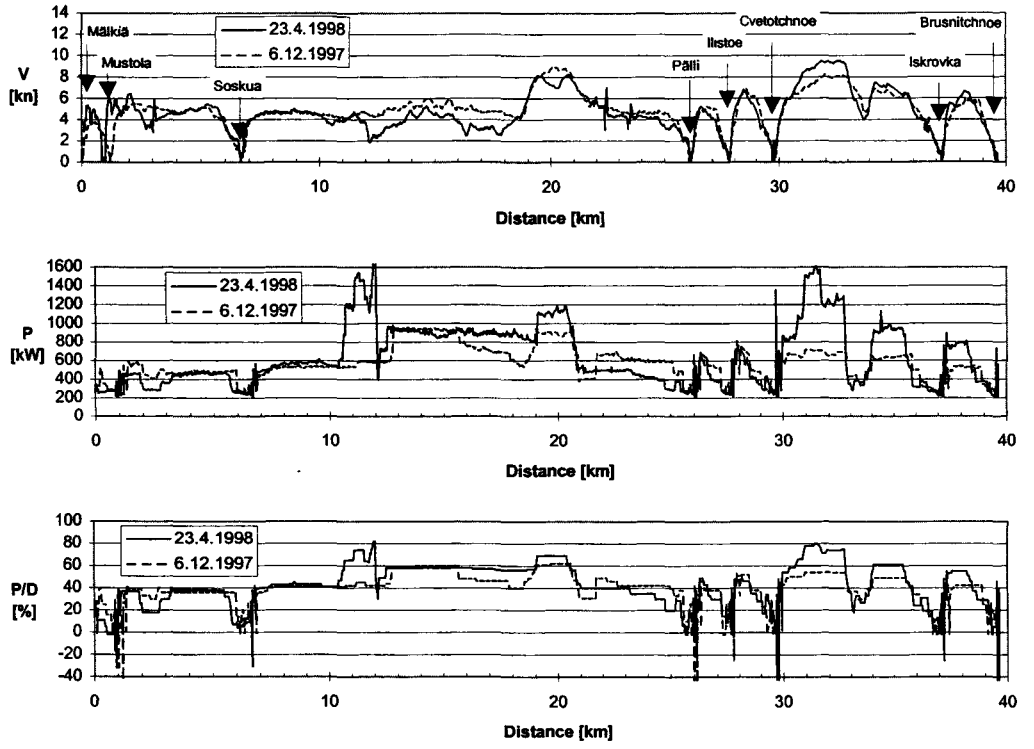

Figure 7 The speed, power and propeller pitch signals measured onboard MS Pionier as a function of the distance travelled downstream from the lock of Mälkiä.

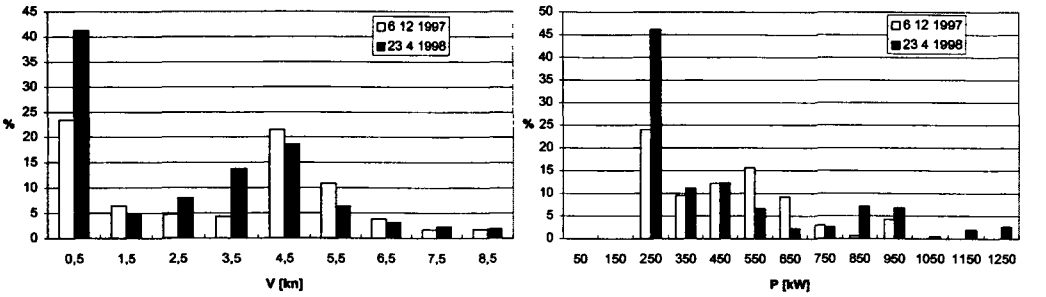

Figure 8 Speed and power distributions on the voyages performed 6.12.-97 and 23.4.-98.

Table 3 Data from the Saimaa Canal passages downstream of MS Pionier in the winter of 1997/98.

	6.12.1997	23.4.1998
Average speed	3,2 kn	2,5 kn
Average power	463 kW	471 kW
Average pitch	30%	28%
Average RPM	211 1/min	212 1/min
Total time	6,7 h	8,5 h
Total distance	39,6 km	39,6 km
Air temperature	-6°C	0°C
Frost sum	100°Cd	890°Cd
Level ice thickness (canal edges)	0-5 cm	52 cm

For four voyages performed on the lake area between the lock of Mälkiä and Varkaus the cumulative energy was calculated from the power signal and presented in Figure 9 as a function of the travelled distance. The first and the third of the voyages started from Mälkiä, the others started from Varkaus. The voyage of 17 April was performed in ballast condition, the others in loaded condition. The data for the performed voyages is also presented in numerical form in table beside the curves. From the figure it can be seen, that the total energy was smaller on the voyages performed in April. One reason for this is the lower speed of the ship on the April voyages. The other reason is the better efficiency of the propeller on smaller pitch values on the the used speed range. In spite of some heavier legs on the voyages performed in April the average ice conditions were quite light during all the four voyages. Significant part of each voyage was performed in straits where the current kept the ice cover very thin or they were totally icefree.

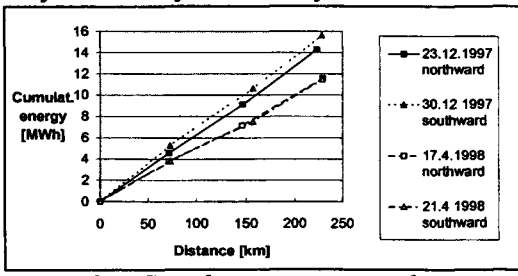

Date	V [kn]	P/D [%]	E [MWh]	Time [h]
23.12.	9,0	67	14,3	13,3
30.12.	8,8	66	15,6	14,1
17.4.	8,4	57	11,6	14,7
21.4.	8,5	54	11,5	14,5

Figure 9 Cumulative energy as a function of the travelled distance on four voyages.

4.2 Delays due to winter

The sources for delays due to winter for the traffic in the Saimaa Canal and Saimaa area can be categorized into four classes: delays due to waiting for icebreaker assistance, delays due to ice in canal locks, delays due to the ice in harbours, delays due to additional resistance. Because the ice conditions during the trips of MS Pionier were quite easy only one category, ice problems in locks, is dealed with in the following.

In severe winters various problems due to ice in the locks can exist. The ice is adhering to the lock walls decreasing the effective breadth of the lock causing problems for the ships of maximum breadth. The ice is also accumulating on the area downstream from the lock especially in the shallow locks where the flow-off is weak. This causes problems for the ships coming into the lock or out from the lock. Also, the accumulated ice prevents removing of ice from the lock. Third type of ice problems are the ice floes coming with the ship into the lock. In the worst case there is not enough space for the ship in the lock, so two lockings are needed; first one for the ice and then other for the ship. Also single iceblocks drifting to the gate recesses may prevent the opening of the lower gates when going downstream. The delays in the lockings of MS Pionier were of the latter type. In Figure 10 the sum of the locking times on each trip is presented as a function of the frost sum. Locking time was defined to start when the ship bow passed the first gate and end when the ship stern passed the second gate. From the figure it can be seen that when going upstream no delays were observed whereas when going downstream the locking times increased. However, the phenomenon was quite occasional.

Figure 10
Total locking times of MS Pionier as a function of the frost sum.

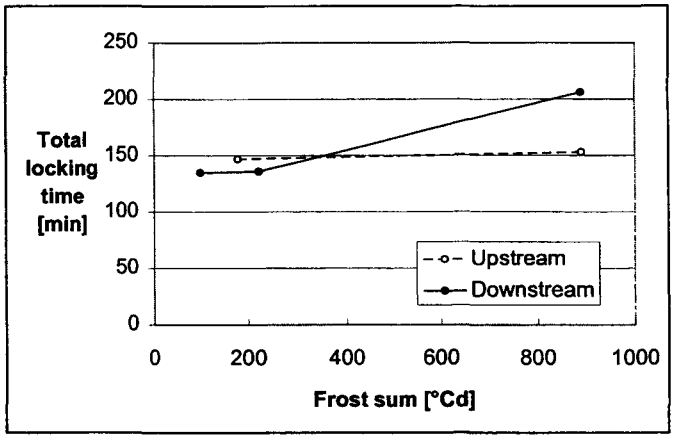

4.3 Resistance

The total resistance of MS Pionier was determined using the measured values of the speed of the ship (V), the rotation speed of the propeller (n) and the propeller pitch (P/D). The wake (w) and the thrust deduction (t) -fractions were estimated using the formulas presented in [2]. The estimated value for w was 0.33 and for t 0.20. The value of w was verified by calculating first the K_Q-value from the values of the propeller torque (Q) and n measured in icefree conditions. Then, from the open water K_Q-curve of the propeller of MS Pionier having the same pitch value as the measured one the advance coefficient J corresponding the calculated

K_Q-value was determined. When this J-value was compared with the J-value based on the measured V and n-values and estimated w-value a good identity was noticed. The estimated value of t was verified by calculating first J using the estimated w-value and the V and n-values measured in icefree conditions. Then, from the propeller open water curve corresponding the measured P/D -value the K_T-value was determined and the propeller thrust (T) calculated. Then, by multiplying the T with $(1-t)$ the total resistance (R_{tot}) was obtained. The R_{tot} values based on the measurements in icefree conditions correlated well with those estimated with the Holtrop method [3]. In the following, the assumption was made that the estimated w and t-values were valid also in ice conditions.

In Figure 11 the total resistance and the ship speed are presented as a function the travelled distance being based on the measurements performed onboard MS Pionier passing the deep fairway from Savonlinna to Varkaus. In Figure, too, the open water resistance of MS Pionier calculated with the Holtrop method is presented. Simultaneously, the thickness of the ice rubble was determined in four different transverse sections of the fairway channel. The positions of the profiled sections were labeled with letters A-D in Figure 12. The measured profiles can be seen in Figure 12. However, due to the prevailing conditions the rubble thickness in the centre of the channel could not be measured but it was assumed that it was the same as the thickness of the loose rubble near the solid channel edge. The resistances and the speeds at the moment when the ship passes the profiled sections as well as the thickness values of the ice rubble in the centre of the channel profile are presented in Table 4.

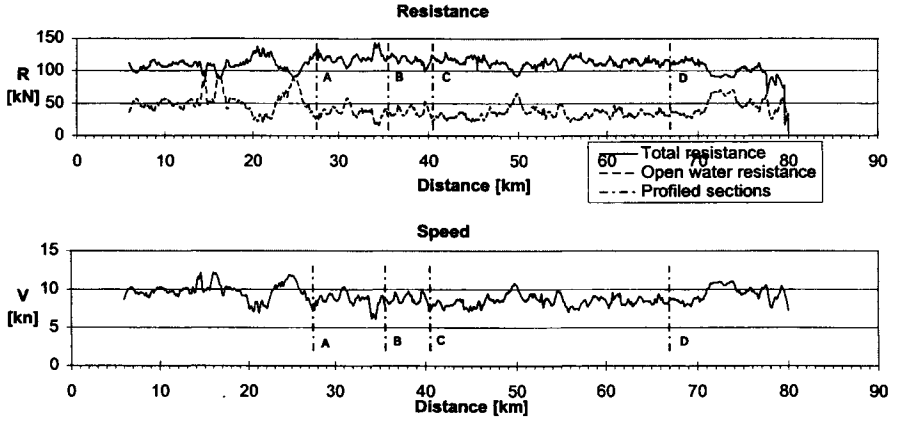

Figure 11 The total and open water resistances as well as the speed of MS Pionier presented as a function of the distance travelled from Savonlinna towards Varkaus. The letters A-D denote the positions of the measured channel profiles.

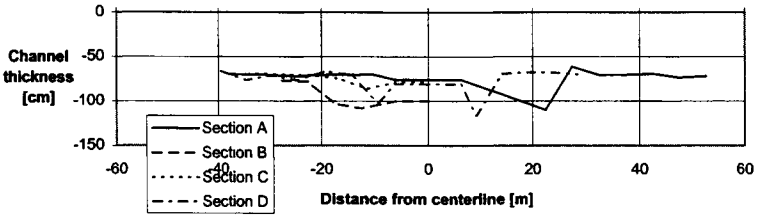

Figure 12 The measured channel profiles A-D.

Table 4 *The values of the ship speed, the rotation speed of the propeller, the propeller pitch, the propulsion power, the total resistance and the open water resistance as well as the thickness of the ice rubble in the centre of the channel at he moment when MS Pionier passed the measured channel sections A-D.*

Section	V [kn]	n [1/min]	P/D [%]	P [kW]	R_{tot} [kN]	R_{ow} [kN]	H_{ch} [cm]
A	7,7	212	65	1135	124	27	76
B	8,4	212	65	1023	122	34	100
C	9,2	212	62	894	107	42	79
D	8,6	212	62	954	112	35	81

5. CONCLUSIONS

The function of the measuring system onboard MS Pionier was reliable and data from five voyages in the winter of 1997/98 were collected, three of them were performed from the Saimaa area via the Saimaa Canal to the Gulf of Finland, two in opposite direction. From the data the power consumption, delays due to ice and total resistance in different areas of the Saimaa Canal and deep fairways of the lake Saimaa were analyzed. The ice conditions met by MS Pionier on the five voyages were quite light on the average, so no significant delays due to ice were observed except some increase in the locking times when going downstream the canal. In the power consumption on the total route from the Saimaa Canal to the harbour of Varkaus no clear increase due to ice conditions was observed between the voyages performed in late December and late April. However, in some parts of the route during the voyages performed in April the ice resistance in broken channel was about 60-80% of the total resistance. The channel thicknesses were about 70-100 cm in the middle of the channel. The measurements onboard MS Pionier were continued in the winter of 1998/99, the analysis of the results will be completed in the autumn of 1999.

6. REFERENCES

1. Finnish Maritime Administration, Inland Waterways District. The Waterway to Europe, The waterways of Saimaa and the Saimaa Canal. (in Finnish)
2. Levis, E.,V. Principles of Naval Architecture, Second Revision, Vol 2. The Society of Naval Architects and Marine Engineers, Jersey City NJ 1989.
3. Holtrop, J. A statistical re-analysis of resistance and propulsion data. International Shipbuilding Progress, No. 335, July 1982
4. Seinä, A. Duration of the ice season and statistics of fast ice thickness along lake Saimaa 1986-1991. Finnish Marine Research No. 259. Finnish Institute of Marine Research Helsinki 1991.
5. Leppäranta, M. et al Phases of the ice seasons in the Baltic area. Finnish Marine Research No. 254 Supplement 2. Finnish Institute of Marine Research Helsinki 1988.

EXPERIMENTS ON THE STRENGTH OF REFROZEN LAYERS OF FIRST-YEAR ICE RIDGES

S.I. Rogachko[1] and Tuomo Kärnä[2]
[1]Moscow University of Civil Engineering, Moscow, Russia
[2]VTT Building Technology, Espoo, Finland

ABSTRACT

Medium scale indentation tests were conducted on a freshwater lake to study the strength characteristics of refrozen layers of first-year ice ridges. Test were done first on level ice and then on accumulations of broken ice that were built and frozen in holes in the level ice. Some of these hummock models contained voids that simulated the defects on the natural ice ridges. The results indicate that the strength of a fully refrozen ice accumulation is slightly lower than the strength of natural level ice. Furthermore, the strength is reduced significantly if the ice accumulation contains voids. Additionally, uniaxial compression tests were done on test specimens that were prepared from the level ice and the hummock models.

1. INTRODUCTION

First year ice ridges pose in many Russian Arctic seas the most significant hazard for offshore platforms. The present methods to evaluate global loads due to ice ridges give very scattered results. One reason for this is that the internal strength characteristics of ice ridges are not well known. The consolidated (refrozen) and rafted layers of ice ridges are inhomogenous due to large variations in ice quality, macroscale voids, bending cracks and other kind of defects. These defects reduce the global ice strength, but quantitative data on this effect is missing. Therefore, the main objective of this fieldwork was to clarify how the ice strength depends on the amount of macro-scale voids that exist within a refrozen ice accumulation.

First-year ice ridge are often areal ice features with a linear sail and keel and an aerial consolidated layer. The consolidated layer consists of a central area with refrozen ice accumulation under the sail and an area of rafted ice. This paper deals with the refrozen ice accumulation, which is assumed to contain voids.

Square holes were made on the natural cover of the lake and the models of consolidated layer of hummock fields of different levels of porosity were built there. After the complete freezing of the ice, a stiff indenter was pushed into the hummock fields using a hydraulic actuator. Subsequently, prismatic specimens taken from the ice accumulations were subjected to uniaxial compression tests.

The experimental data were compared with the results of the laboratory study completed in 1995 at the Technical Center of Finland, with the similar test results of 1996 and also with those of the other authors.

2. TEST METHODS

2.1. Preparation of the hummock model

Models of the consolidated part of ice ridges were constructed on a small freshwater lake. First, a square hole with the dimension 1.3 m x 1.3 m was sawn in the level ice sheet (Fig. 1). This piece of level ice was broken into smaller ice blocks which were then extracted to the surface of the ice cover and split further into smaller fragments of variable size. The characteristic width of these fragments varied in the range of 20 cm to 30 cm. Subsequently, the hole in the level ice was filled with these ice fragments at random. Then refreezing of the ice fragments and the surrounding water occurred under natural winter conditions.

Figure 1. Hole in the level ice sheet for the preparation of a hummock model.

While preparing porous hummock models the square hole was not sawn to the full level ice. Instead, a square hole with a solid ice bottom was prepared. The hole was kept dry while broken ice fragments were placed on it. Besides the ice blocks, some waterproof sealed packets of size 7cm x 7cm x 10cm were put in layers on the hole. After the ice fragments and packets were put into the form they were flooded with supercooled water to achieve complete freezing of ice with the packets. Then, a hole was made in the bottom of the ice sheet and water filled the voids between the ice fragments and packets. The target porosity of the refrozen ice accumulations was 10 %. The hummock models of this type were prepared in the end of January 1997, when the thickness h of ice cover amounted to 0.5 m. The freezing period lasted for about 1.5 month until the beginning of the experiments.

The ice accumulations prepared are believed to represent the refrozen ice accumulations within the consoliated layer of a first-year ridge. The size of the ice fragments and the voids were selected such that a single fragment of a void would not dictate the strenght of the ice accumulation.

2.2. Experimental setup

Figure 2 shows the experimental setup used in the tests. A mobile steel frame built on metal skis and equipped with a chain hoist was used to support hydraulic cylinder. The hydraulic cylinder was connected with an electro-hydraulic station on the shore through a system of flexible hoses of high pressure. The hydro-drive was powered through a mobile electro-power station. A stiff indenter with a cross section of 0.4 m x 0.4 m was fixed on the rod of the hydraulic cylinder. The ratio between the indenter widht and the blocksize is in the range of 1.3 to 2.0. The effect of changes in this ratio was not studied. A thrust plate was fixed in the rear end of the cylinder. The area of this plate was 2.5 times as large as the indenter area.

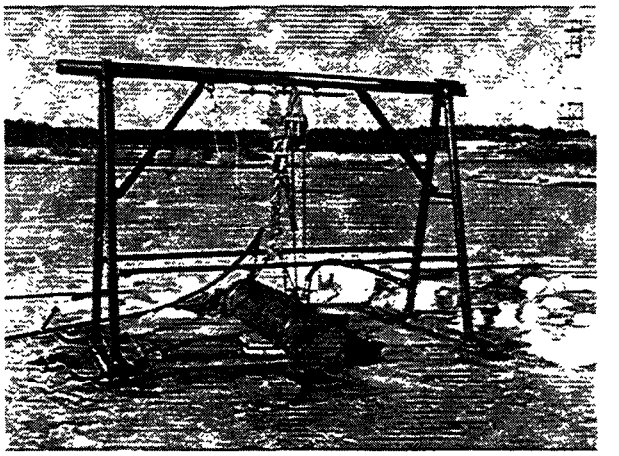

Figure 2. General view of the experimental setup.

2.3. Indentation tests

The tests were made when the ice accumulations were fully frozen. A rectangular hole was cut through the ice in front of the hummock model. The hydraulic cylinder with the indenter was installed at an appropriate level on the hole using the hoist. After that, preliminary thrust of the cylinder was done in such a way that the front part of the stiff indenter touched the hummock model directly and the rear thrust plate contacted the butt-end of the hole in the level ice field. After fixing the displacement transducer and preliminary switching on measuring instrumentation the hydro- system was launched and the stiff indenter on the rod of the hydraulic cylinder was indented into the hummock model. In the course of each test the pressure changes in the hydro- system were registered with the pressure transducer on the oscillogram of the light-beam oscillograph as well as the displacement of the stiff indenter in time.

The pressure in the hydro-system was recalculated into the global ice load with the help of a calibration diagram. The calibration diagram was defined experimentally before the beginning of the tests using a force transducer with a capacity of 500 kN. The process of the experiments was recorded also by video- and photocameras.

2.4. Uniaxial compression tests

After the indentation tests on the hummock models and on the natural ice cover, a series of uniaxial tests were made on ice specimens. For this purpose, prismatic ice blocks were taken out of the consolidated layer of the hummock with different levels of porosity. The ice blocks were sawn into ice samples oriented parallel to the freezing plane. The methods used in specimen preparation and testing were based on the recommendations given in /1/. The tests were carried out on a hydraulic machine with the capacity of 1000 kN. Specimen deformation was registered by displacement transducer. The time signals of these transducers were registered on an oscillogram.

3. EXPERIMENTAL RESULTS

3.1. Indentation tests

After the formation of the ice cover in December 1996, regular cleaning of snow was made in the test site to enhance the ice growth. In January 1997 the thickness of the natural level ice was about 0.4 m. At this time, five hummock models with the porosity p of 0 % were prepared. In addition, five hummock models with the target porosity of about 10 % were prepared. Experimental research started on 11 March and lasted 14 days. At the time of the tests the air temperature was around 0 °C and the temperature of ice changed from –2 °C to 0 °C. The first series of tests were done on the natural ice cover. The actual contact area was 0.4 m x 0.345 m. The results of these experiments are presented in Table 1.

Table 1. The results of indentation tests.

Type of ice	Contact area (cm x cm)	Ice thickness (cm)	Porosity (%)	Ice temperature (°C)	R_I (Mpa)	Mean strenght (Mpa)
Natural level ice	40x34.5	56	1.2	-1	3.86	3.82
	40x34.5	56	1.2	-1	4.61	
	40x34.5	56	1.2	-1	3.00	
	40x34.5	56	1.2	-1	3.75	
	40x34.5	56	1.2	-1	3.86	
Hummock 1	40x33.5	53	1.9	0	3.00	3.10
Hummock 2	40x30	53	1.9	0	4.26	
Hummock 3	40x37	53	1.9	0	2.46	
Hummock 4	40x34	53	1.9	0	2.67	
Hummock 5	40x40	52	16	-1.5	2.27	2.22
Hummock 6	40x40	53	16	-1.5	2.18	

The mean value of the failure pressures R_{max} on level ice tests was 3.82 MPa. The maximum failure pressure R_{max} averaged on the indenter area did not exceed 4.61 Mpa in different tests. The minimum value was 3.00 MPa. The depth of the indenter penetration into the level ice was equal to 0.36 m, the average indentation velocity was 5.4 mm/s. The ice failure was brittle. At a maximum load the ice edge experienced a spalling failure where the ice surface near the upper and the lower edges of the indenter were extruded up and down. This type of ice failure is presented in Figs. 3-4.

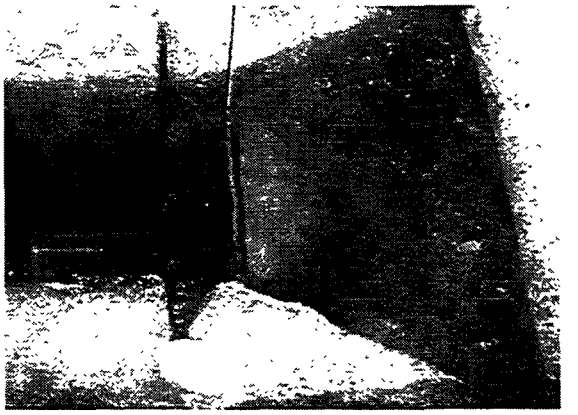

Figure 3. Failure of level ice in front of the indenter.

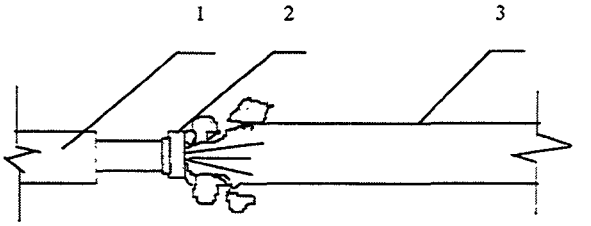

Figure 4. Sketch of the ice failure mode in the indentation tests.
1 – Hydraulic cylinder; 2 – Indenter; 3 – icesheet.

The indentation tests on the hummock models with different levels of porosity were carried out in the similar way. The mean value of the failure pressures on these tests was 3.10 MPa. This value is 81% of the corresponding value for level ice tests. The difference in the ice temperature may explain this difference (Table 1). In uniaxial tests the mean strengths of the natural level ice and hummock model with no voids showd the same strentgth. The maximum ice failure pressure reached 4.26 MPa (Table 1), and the minimum was recorded as 2.46 MPa. The average indentation velocity was 5.7 mm/s. The character of the ice failure was similar to the spalling failure with horizontal splits as observed in the tests on level ice. As a result, wedge-shaped ice edges were developed in front of the indenter (Fig. 4). It should be noted that similar type of failure has been observed on freshwater level ice in laboratory conditions /3, 4/.

Due to technical problems, only two tests on porous hummock model were made. The average level of porosity p was 16 %. Due to presence of voids within the ice accumulation, the failure character of these experiments differed a little from the previous tests. The cracks developed along the voids and ice blocks bulged out. Nevertheless, when the indenter stopped, the ice edge exhibited a similar wedge-shape as in the previous tests. The indentation velocity in these tests was on average 10.8 mm/s. The mean value of the failure pressures on these tests was 2.22 MPa (Table 1). This value is 58% of the corresponding value for level ice tests. The maximum value of the ice failure pressure area did not exceed 2.36 MPa, and the minimum was 2.18 Mpa.

The results of the present tests (1997) and the corresponding results of the tests made in winter 1995/96 /2/ are in a good agreement with the data compiled by Sanderson /5, 6/, as shown in Fig. 5.

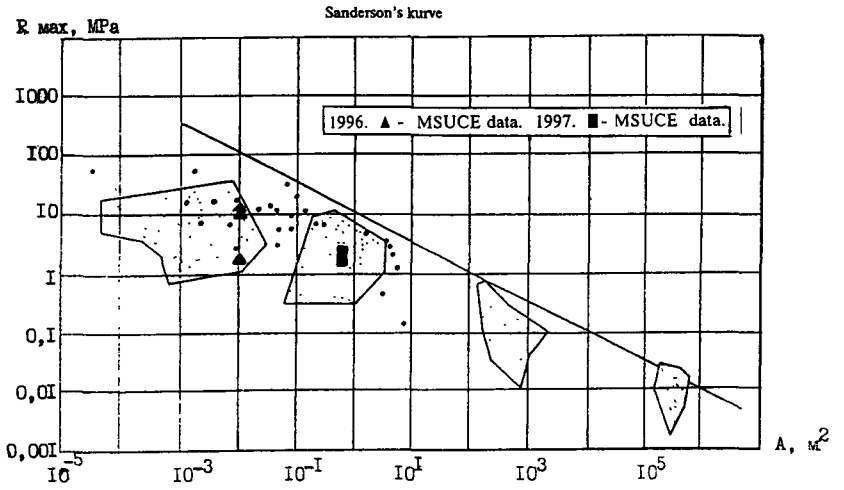

Figure 5. Sanderson's pressure-area curve with experimental data of MSUCE (Moscow University of Civil Engineering).

3.2. Uniaxial compression tests

Altogether, 11 specimens out of the level ice field, 8 specimens out of the hummock models with a 0 % level of porosity, and 19 specimens out of the hummock models with 10 % porosity were subjected to uniaxial compression tests. All the specimens were loaded in the direction parallel to the plane of the ice cover. The target size of the specimens was 15x15x30 cm^3. It should be noted that the temperature of the tested specimens ranged from -2°C to -0.5°C. Tests were carried out at a target strain rate of 10^{-3} s^{-1}. The failure mode of the specimen was splitting along a plane parallel to the loading direction. The experimental results for the three types of specimens are tabulated accordingly in Table 2.

Table 2. The results of uniaxial compression tests.

Type of ice	Specimen size			ρ,	p, (%)	R_c,	Mean strenght
	a (cm)	b (cm)	l (cm)	(kg/m^3)		(Mpa)	(Mpa)
Natural level ice	18.3	15.9	32.0	905.3	1.6	1.73	1.16
	11.7	18.3	34.6	912.0	0.9	1.95	
	12.0	19.4	32.6	918.5	0.2	1.22	
	12.6	18.1	33.0	911.3	1.0	0.72	
	12.1	17.7	34.2	910.7	1.0	0.64	
	11.2	19.2	34.7	912.0	0.9	0.77	
	12.2	17.1	27.0	905.5	1.6	1.37	
	12.3	17.2	27.4	905.5	1.6	1.46	
	15.1	15.4	26.4	900.9	2.1	0.64	
	13.6	14.9	35.2	917.5	0.3	1.49	
	12.5	14.4	29.9	899.3	2.3	0.76	
Hummock with no added porosity	17.6	16.0	31.4	917.8	2.4	0.88	1.17
	18.8	13.6	31.4	893.0	2.9	1.54	
	16.7	15.2	34.0	894.3	2.8	1.45	
	17.4	15.2	31.5	919.1	0.1	0.92	
	17.2	16.3	33.5	906.1	1.5	1.36	
	18.2	17.2	32.7	890.0	3.3	0.99	
	17.4	16.4	36.3	919.9	0.0	1.18	
	18.7	17.4	37.0	894.6	2.8	1.05	
Hummock with 16% target porosity	19.5	23.8	44.3	792.3	13.8	0.46	0.46
	26.3	22.5	43.5	733.0	20.2	0.36	
	24.5	23.9	41.0	743.0	19.2	0.26	
	20.5	23.3	44.4	785.5	14.5	0.36	
	15.3	17.0	36.5	776.7	15.5	0.28	
	16.7	16.8	33.4	781.4	15.0	0.21	
	15.2	16.8	32.8	773.9	15.8	0.53	
	15.1	16.8	34.3	715.3	22.2	0.36	
	16.0	16.5	33.0	728.9	20.7	0.74	
	14.2	17.7	35.5	750.0	18.4	0.50	
	17.2	17.2	36.0	796.7	13.3	0.44	
	13.6	19.2	31.0	831.1	9.6	0.77	
	14.1	16.4	31.0	775.8	15.6	0.53	
	15.4	17.5	28.5	789.9	14.0	0.64	
	13.6	17.8	31.0	754.3	17.9	0.38	
	18.3	14.0	30.0	796.3	13.4	0.60	
	13.8	21.3	30.5	812.4	11.6	0.35	
	14.9	17.2	30.1	730.0	20.6	0.60	
	14.1	18.9	36.4	773.7	15.8	0.39	

Figure 6 shows a compilation of the results of the uniaxial compression test from the winters 1995/96 /2/ and 1996/97. The sample size was the same in these two test series. Figure 6 shows also the data on uniaxial compression tests performed in laboratory conditions at VTT, Finland in 1995 /7/.

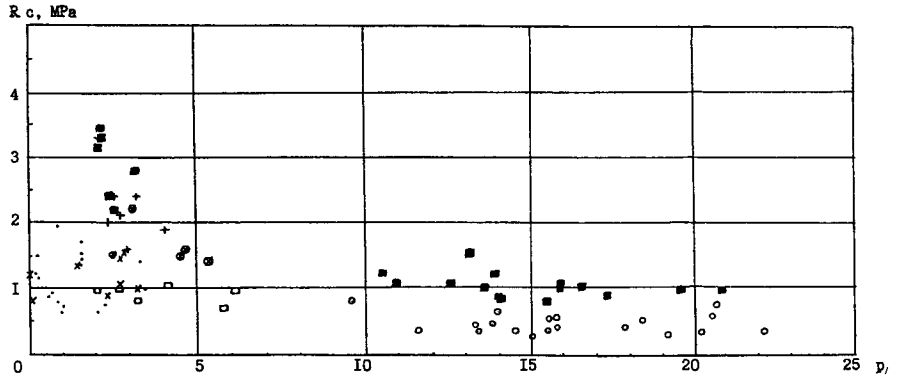

Figure 6. Uniaxial compression strength R_c [Mpa] as a function of the porosity p (%).

1997: ● - level ice at –2 °C; × - hummock model with no voids at –2 °C;
❡ - hummock model with 10% porosity at –0.5 °C
1996: ♣ - level ice at –8 °C; + - hummock model at –10 °C
1995 /7/: ■ - freshwater ice at –5 °C; ⊗ - hummock model at –11.5 °C

Finally, Fig. 7 presents the ratio between the indentation strength R_{max} and the uniaxial compression strength R_c as a function of the contact area A. In this figure, the indentation strength R_{max} is normalized with the uniaxial compression strength R_c at the same porosity.

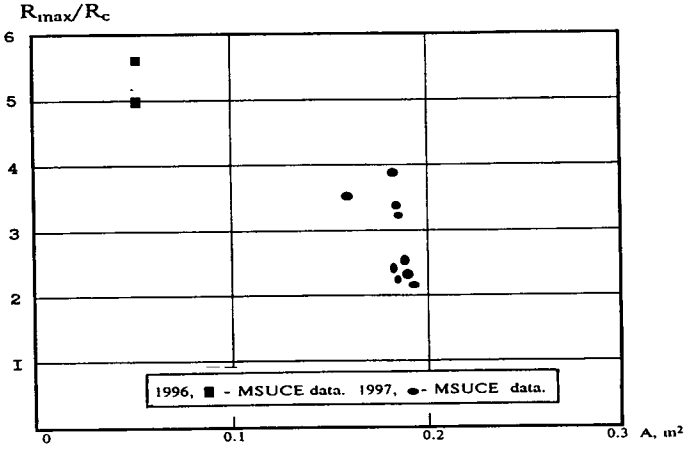

Figure 7. The ratio R_{max}/R_c as a function of the contact area.

4. CONCLUSIONS

This report complements earlier laboratory and field data on the strength of porous ice accumulations that are met in the refrozen layers of first-year ice ridges. In the medium scale indentation tests, the strength of the hummock models with zero porosity was 81% of the corresponding strength on level ice. The difference in the ice temperature may explain this difference. In uniaxial tests the mean strengths of the natural level ice and hummock model with no voids showed the same strength. For hummock models with 16% porosity the strength in the indentation tests was reduced to 58% of the level ice strength.

A sufficient amount of data points is now available to make preliminary evaluations of the integral strength of these refrozen layers. This data can also be used to develop analytical and numerical models for determining global ice loads caused by drifting first-year ice ridges.

ACKNOWLEDGMENT

This work has been undertaken within the COSAR project (INTAS-94-463) funded by the International Association for the promotion of co-operation with scientists from the independent states of the former Soviet Union. The work was also supported by the LOLEIF-Project in the framework of the EU-sponsored Marine Science and Technology (MAST-III) Programme under contract no.MAS3-CT97-0078"

5. REFERENCES

1. Schwarz J., et. al. Standardized methods for measuring mechanical properties of ice. -Cold Reg. Sci. Technol., ¹4, 1981, pp. 245-253.

2. Choice of Offshore Structures for Arctic Regions (Final report of the COSAR project). VTT Building Technology, Internal report RTE38-IR-4/1997. Ed. T, Kärnä. pp. 39-50.

3. Muhonen A., Kärnä T., Eranti E., Riska K., Järvinen E. and Lehmus E. Laboratory indentation tests with thick freshwater ice. Vol 1. Technical Research Centre of Finland. Espoo, 1992, 198 p.

4. Timco G.W. Indentation and penetration of edge-loaded freshwater ice sheets in the brittle range. Proc. fifth (1986) OMAE Symp., Vol. V, ASME, pp. 444-452.

5. Iyer S.H. A state of the art review of local ice loads for the design of offshore structures. Proc. IAHR Ice Symp. 1988, Sapporo, Japan, pp. 509-566.

6. Sanderson T.J. A Pressure Area Curve for Ice. IAHR Working Group on Ice Forces. 3rd State-of-the-Art Report. U.S. Army Cold Regions Research and Engineering Laboratory, Special Report 87-17. pp. 75-98.

7. Rogachko, S.I., Evdokimov, G.N., Melnikov, M.V., Kärnä, T. and Lehmus, E. The Influence of Porosity on Mechanical Strength of Hummocks. 37. Proc. 16 th Int. Conf. Offshore Mechanics and Arctic Engineering (OMAE'97&POAC'97). Yokohama, April 13-18, 1997. Vol IV, pp. 151-157.

NOTATIONS

h	thickness of ice, cm;
R_c	uniaxial compression strength of ice specimens, MPa;
R_{max}	ice failure pressure in an indentation test, MPa;
ρ	density of ice, kg/m^3;
p	porosity of ice, %;
A	cross-section area of specimens, cm^2;
a	width of specimens, cm;
b	thickness of specimens, cm;
l	length of specimens, cm;
t_i	air temperature, °C

OIL RECOVERY METHODS IN BALTIC SEA AND SUB ARCTIC CONDITIONS

J.E.Rytkönen VTT Manufacturing Technology, Espoo, Finland

ABSTRACT

Arctic and Sub-Arctic conditions form a special task for oil recovery operations due to the special environmental features and the cold climate. Ice is often the most problematic element in oil recovery operation in sea areas. Ice floes and drifting ice will decrease significantly the use of conventional oil recovery methods, or even stop the oil combating operations completely. Even the monitoring of oil among the ice is difficult. This is infact one of the task to be developed in the future.

This paper givs a brief overview of the basic oil combating methods in sea areas, especially in the Baltic Sea conditions. Furthermore, discussion on their usefulness in cold climates, in the presence of ice, is carried out, too. Some novel oil recovery systems developed and tested in Finland are presented.

1 INTRODUCTION

The threat of a marine oil spill in both open and ice covered sea is growing in regions close to both Finland and Russia. Russia has plans to build up new oil terminals in the Gulf of Finland, a 400 km long shallow Bay surrounded by Finland, Estonia and Russia. The total freight rate of the planned new Russian terminals will increase the maritime traffic in the Gulf of Finland to twice the size of the current figures (Rytkönen, 1999). The increase of the oil transportation will be even higher, and even three times higher oil transportation figures are expected after the Russian oil terminals have been constructed. Oil transportation in the Gulf of Finland has already increased due to the increased transit traffic through Estonian ports.

The increased threat of marine oil spill in ice is also expected in the near future in Arctic seas. The interest and activities aimed at exploiting the hydrocarbon resources will grown in spite of the current 'stagnation period' due to the low market price of the crude oil. There are already increasing signs of oil production activities in the Norway's side of the Barents Sea. A great deal of speculation has also been made on the hydrocarbon resources of the North-Western part of Russia, and when those resources will be exploited.

This papers summarizes the state of the art survey conducted on the oil spill combatting methods in Arctic and Sub-Arctic conditions, and especially in the presence of ice. First the oil combatting methods available for icy conditions are discussed. The selection of the suitable response techniques follows here the division presented by (Evans, 1988) for the Arctic conditions: the containment, recovery, disposal and logistics. Then the efficiency of the methods is evaluated on the basis of the published test results etc. In addition the Finnish experiences on combatting oil in ice are discussed.

2 CONTAINMENT

The booms in general use today are: fence booms, curtain-type booms (which can further be divided in to the following categories due to their flotation: internal foam, external foam, self-inflatable, pressure-inflatable), external tension booms, fire containment booms and tidal seal booms (Schulze, 1995). Among these types there are also many special oil booms such as absorbent booms or the use of ice formation as oil barriers. Important design parameters for booms are the buoyancy, roll & heaving response and freeboard of the boom.

The conventional oil booms all have their limitations due to growing wave height, current speed or the critical speed of the recovery vessel when booms are mounted onboard. But neither of them is capable of working properly among ice. Theoretically, one could surround a small ice & oil area, but when there exists wind or strong current with increased drifting force the boom system will fail. The oil can escape before any damage to the boom occurs. The hinges between the boom modules, anchor points etc have not been designed to withstand moving ice forces. Even if the boom were allowed to move with the ice, the behaviour will be unpredictable. However, due to the number of case studies with failed booms in ice, booms are normally left out of the oil-in-ice-cases.

Oil booms can be used, if the ice floe field is so sparse that the ice floes can be avoided by steering the boom and recovery vessel between the floes. Another application, where the conventional oil boom in ice may be used as in open water, is in the free track behind an icebreaking marine structure in moving ice. The booms used for ice management in drifting ice or in rivers can also be used for oil combatting purposes.

In solid ice the convential booms can be used for limiting the oil spreading under the ice. Firstly a slot of sufficient size must be made in the ice cover with a motorized saw, see Figure 1. In finland, such an ice saw, installed in an amphibious vehicle, exists (HELCOM, 1994). The ice saw is able to saw a 19 cm wide channel in an ice sheet of 1.3 m in maximum thickness at a maximum speed of 1.3 km/h. After the slot has been sawn in the ice sheet, the boom can be deployd in the slot. Figure 2 illustrates some possible applications of the conventional booms in solid ice.

Special barriers can also be used for containment, Fire containment booms are usually stronger and heavier and could also be used with ice with the limitations described before. Other special booms are bubble and water jet barriers. Bubble barriers have been tested in Arctic conditions, and they have their excellent application for example in oil terminals, where oil spill during the loading or unloading process can be isolated to the harbour by switching the compressor to lead pneumatic air to the underwater bubble lines. Air bubbling lines are generally used in harbours or marinas to keep certain areas of the pier free of ice.

Another special boom type is a pneumatic underwater boom, which has been mounted on the seabottom, surrounding the loading/unloading terminal or offshore platform, If an oil spill occurs, the booms will be filled by air, thus they will rise to the surface and restrict the oil spreading from the site.

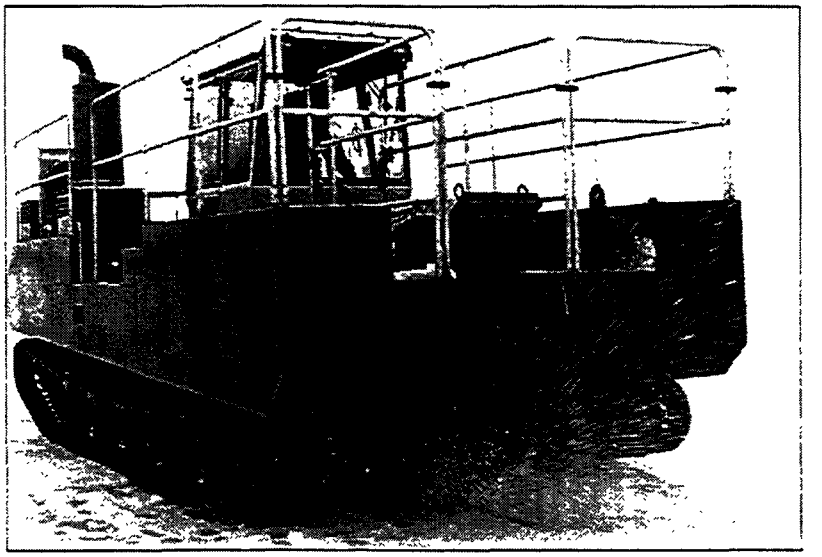

Figure 1. The ice saw in operation.

3 MECHANICAL RECOVERY METHODS

From the environmental point of view, mechanical recovery is usually considered as the most favourable marine oil spill combatting method. For this purpose, there exists several technical innovations and equipments. Most of the mechanical recovery devices, i.e. skimmers, have been designed for open water operations, but some equipments are especially designed for use in ice conditions. In addition, several proposals for using different open water devices in ice have been presented.

Skimmers can be stationary, advancing, self-propelled or modified stationary/advancing applications. A good collection of the various skimmers is presented in (Schulze, 1995). In the following, the mechanical recovery equipments proposed to work in ice has been dealt with in two categories: the recovery vessels and the larger recovery units that are usually installed in a vessel as an elementary part. The second category consists of the smaller, portable skimmers operated . from onboard ships and boats.

The largest oil recovery unit for ice conditions in Finland is the LORI Ice Cleaner (Fig. 3) unit installed as a separate bow section in front of an assisting ice-breaking or tug-boat. The recovery system of LORI consists of two sets of brushes, water spraying nozzles to loosen the oil from ice and lift the oil away from water. A prototype of this device was tested by VTT in 1991 in heavy ice conditions (Rytkönen, 1992). A more detailed description of the system is also given in (Lampela, 1992).

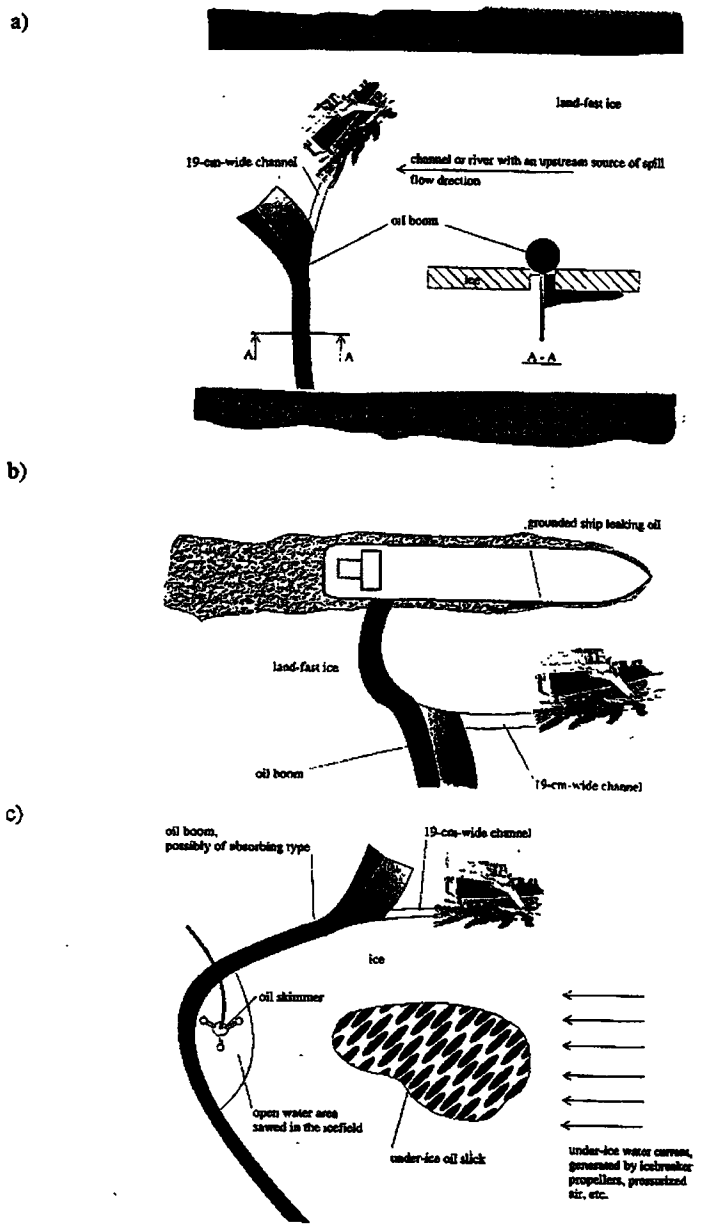

Figure 2. Examples of different uses of conventional oil booms in ice.
a.) ice saw cutting a slot into the ice. Thus an oil boom can be assembled to the slot.
b.) oil boom assembly with an aid of ice saw.
c.) forming a slot downstream for oil collection and recovery activities.

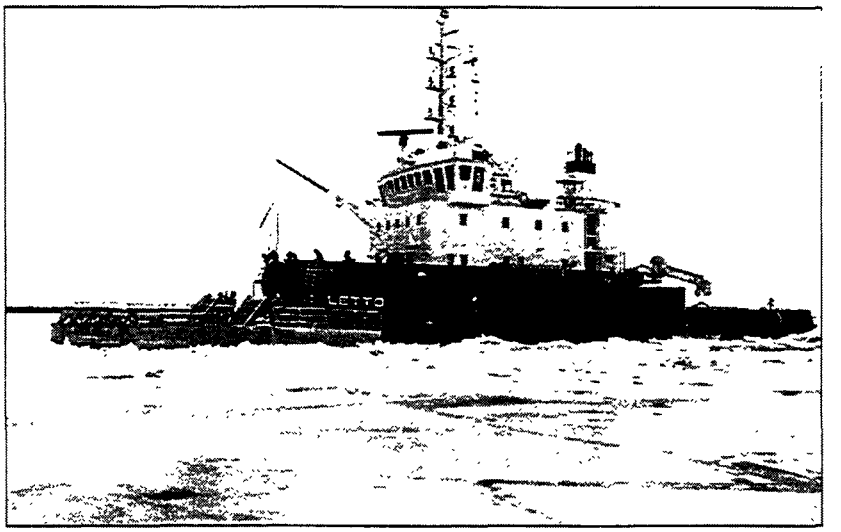

Figure 3. LORI Ice Cleaner.

There are also some other commercial efforts which have been reported to work in ice conditions, such as ARCAT, ARCTICSKIM (Liukkonen, 1997). However, due to the very limited data on the ice trials the author is not aware of any other large-scale skimmer capable of working in ice other than LORI's prototype. Icebreakers and escort barges, however, can be used for combating oil during the winter as a base for operation. Equipped with oil recovery devices they can also be used for oil collection. Modern azimuthing type propulsion systems can also be used to form water jets under the ice level, or push the ice and oil in a certain direction.

The most often used portable type skimmers in ice conditions are weir and suction skimmers which assembed in a slot can be used effectively. A weir skimmer might be working also in sparse floe ice in calm water, if the ice thickness is essentially bigger than the oil fill thickness between the ice floes. By precise ballasting it should be possible to adjust the vertical position of the skimmer so that only oil from between the ice floes goes into the skimmer, whereas the ice remains out, see Figure 4.

Another suitable device in ice conditions is a rope-mop skimmer. Its function, however, will be difficult to maintain due to the freezing of the bristles of the rope. It has been tested for example in the case of oil under ice.

Brush skimmers are widely used in Finland and Sweden. Their recovery efficiency is dependant on the adhesion between oil and the brush shaped recovery elements of the skimmer. The brushes may have the form of endless chains or drums. They are effective in open water, especially with high viscosity oils. In ice conditions their use has been limited with rather insignificant recovery results.

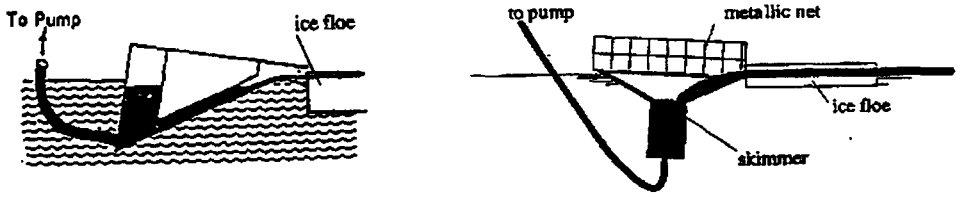

Figure 4. Weir skimmers prevented from entering the ice.

4 ON-SITE DISPOSAL

The most widely known methods in this category are; chemical treatment of oil, in-situ burning and bio-remediation. Dispersants are the most common among the use of the chemical treatments. Other additives such as demulsifiers, sinking and gelling agents have been used, but to a far lesser extent.

The working principle of dispersants, which are usually liquids, and contain surfactants. When spread on the oil slick, they disperse the oil into small droplets. The small oil droplets mix into the water column and are carried away and spread in the water mass of the open ocean by waves and sea currents.

The presence of ice usually considerably decreases the effect of dispersants . In the first place, ice is a mechanical barrier that in some cases may prevent the dispersant from reaching the oil. No data on the efficiency of dispersants applied on an under-ice oil slick were found from the literature. However, if the location of the oil slick is known, it should be easy to drill a hole in the ice cover above the slick and treat the oil with a dispersant through the hole. Dispersants in broken ice have been used, and the pumping action of the waves in broken ice pieces or floating slush ice can increase the dispersant efficiency.

The dispersants have, in spite of their rather wide use, two main disadvantages. The first one is the fact, that dispersants do not remove the oil from the sea. The other is the possible toxicity of the dispersants themselves or the compounds they may form with the oil. In Finland the use of dispersants is not prohibited by the law, but Finland has signed an international agreement to prefer mechanical clean-up methods for oil spills in Finnish territorial waters. In some extreme situations, however, the Finnish Environment Institute may also consider other means, such as the in-situ burning or use of dispersants. The use of dispersants should be approved beforehand. Principally the same policy is followed in the Netherlands, Denmark and Norway. In Sweden the dispersants are not used under any circumstances (Liukkonen, 1997).

The in-situ burning as an oil spill countermeasure has been studied for over 30 years. Especially in North-America the method is today considered as one of the best countermeasures of oil spills in the sea, including cold and ice regions. The difficulties with

this technology have been the control of burning, ignition, efficiency of burning, smoke formation and the fate and possible toxicity of the residues. However, in-situ burning is an effective tool to reduce the amount of a large oil spill at the beginning of the recovery work.

5 LOGISTICS

From the environmental point of view, the mechanical recovery of oil out of the sea is the most favourable clean-up method, but from the logistic point of view it is the most difficult and laborious one. The mechanical clean-up firstly requires the transportation of the personnel and equipment to the spill site. In the case of an Arctic spill this may be rather time consuming and expensive. Aircraft, helicopters and hovercraft may be used for quick response. The recovery equipment, if not always present and on stand-by on an offshore platform or tanker, may need the ship-borne transportation that may be rather time consuming. It is also a fact that any really effective mechanical recovery system for ice conditions does not exist. Thus, the mechanical recovery of oil out of an ice-covered sea is laborious, time consuming and ineffective, thus also expensive. In addition, from the logistic point of view, additional difficulties are storing, transporting and the final disposal or treatment of the recovered oil.

6 NEW FINNISH EXPERIENCES

The novel beach cleaner developed by Mr E. Mykkänen of the Finnish Environment Institute is basically designed for shore-line clean-up activities, but it can also be used for oil recovery operations in ice. The beach cleaner unit, shown in Figure 5, is designed to be assembled on the top of the boom of the amphibious type pumping bucket dredger, normal excavator or onboard a normal recovery vessel. The system consists of a special oil collecting bucket equipped with rotating brush and pump.

The device was tested in 1997 in full-scale conditions, and results showed more than a 50 % recovery rate in broken ice conditions. The shore-line recovery rate was even better, in some tests as high as 80 %. The device was also used in 1999 when oil was spilled from burning tank wagons in Vainikkala, Finland. The devise will be again tested in full-scale in late August 1999 in connection the joint oil combating exercise on the Lithuanian coastline.

An idea to use vibrations to separate oil from ice is a novel method to separate oil from oil: the recovery unit submerges the ice blocks and oil under the water surface. A vibrating plate or grid makes the ice blocks vibrate and rotate. Due to the fact that usually the bottom and side surfaces of ice blocks are more oily than their top surfaces, the rotation of the ice blocks is important. The vibration separates the oil from the ice blocks. The oil thus separated from ice forms loose particles in water, which will rise due to their buoyancy to the space inside the recovery unit. To allow the oil drops to rise but to prevent the ice blocks from entering the recovery unit, the vibrating plate as well as the outer shell of the recovery unit is perforated with sufficiently small holes or made of a grid with sufficient mesh size. Inside the recovery unit, the oil drops enrich on the water surface, from which the oil is recovered with a sufficient skimmer or pump. The principle is shown in Figure 6.

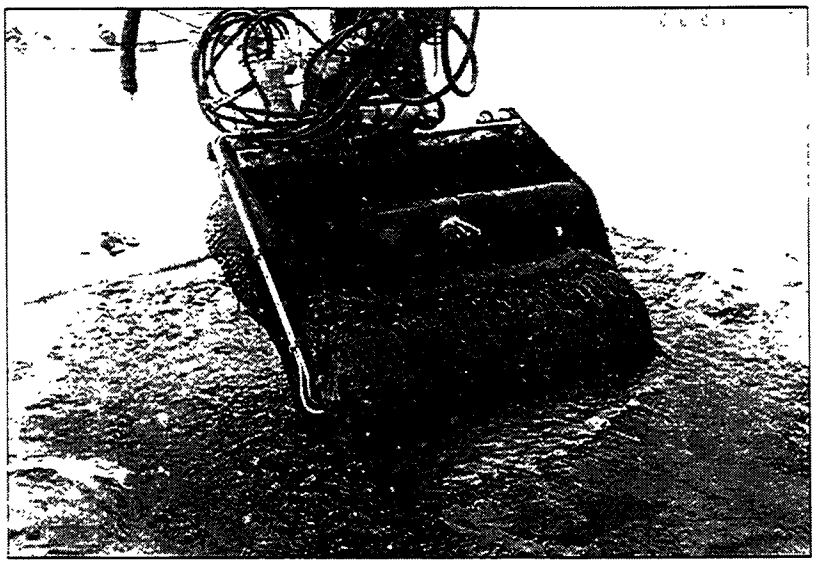

Figure 5. The beach-cleaner unit suitable also for ice conditions.

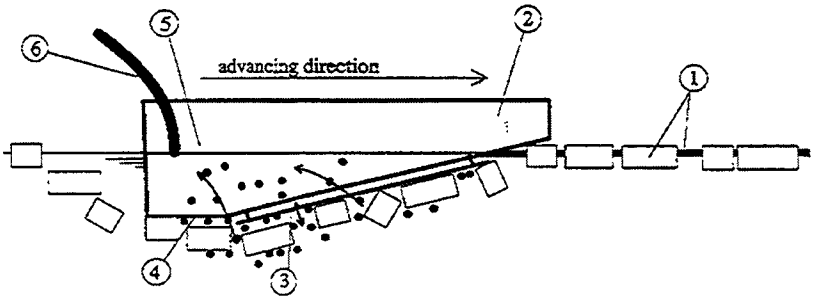

1: oil between ice blocks
2: recovery unit
3: vibrating perforated plate or grid to make the ice blocks to vibrate and rotate
4: perforated outer shell of the recovery unit
5: space inside the recovery unit, where the oil enriches on the water surface
6: skimming the oil out of the water surface inside the recovery unit

Figure 6. Oil recovery system employing a vibrating plate for oil-ice separation.

The system was tested by VTT in 1998 in the laboratory scale with good results. The prototype device is under construction in the scale 1:2 and will be mounted in the existing oil recovery boat to be tested in the winter 1999/2000.

A vacuum pump installed in a truck has been tested in oil recovery operations among broken ice in a port alongside a pier. Figure 7 shows the recovery action schematically.

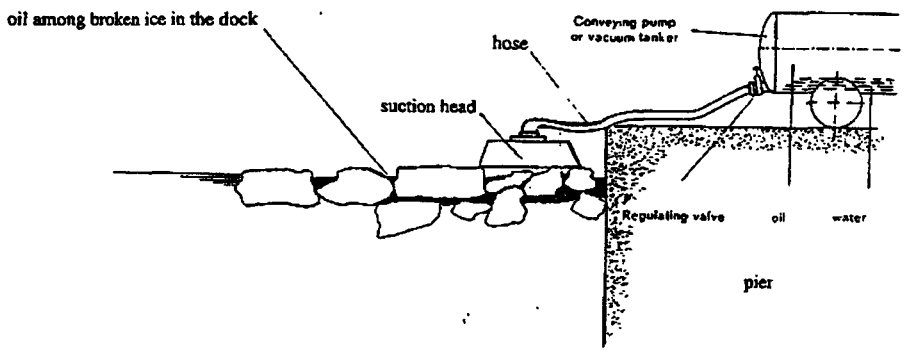

Figure 7. Use of vacuum pump to recover oil among broken ice.

When applying the vacuum pump for oil recovery from the ice-covered sea, the pump itself can be expected to work. The important detail, and thus the main objective for product development is the suction head design to prevent ice entering the system and simultaneously allowing the oil to go in. The idea of a vacuum pump for oil recovery is attractive, because it may be possible to connect it to existing suction dredgers.

7 CONCLUSIONS

According to the well-justified common opinion, the mechanical clean-up is the most preferable oil spill countermeasures from the environmental point of view. On the other hand, however, the experience and the literature survey have shown that no really effective mechanical oil spill clean-up method for ice conditions exists. The field trial in 1994 in the Northern part of Oulu (Oulu 1994), latest small oil spills reported in the oil terminals and experiences in (Johannessen, 1997) have showed, that a small or medium size of oil spill among ice could be handled rather well with modern technology. The larger oil spill, however, is still difficult or almost impossible to cope with.

Finnish oil combating authorities have, for several years, worked to develop new oil recovery technology for ice-infested waters. Numerous novel equipments or recovery ideas have been tested. Similar activities could be recorded world-wide. But more research should be done for the more accurate monitoring of oil with ice, better recovery devices and the development of logistics.

Maritime traffic is increasing every year, and in spite of the more sophisticated vessel traffic systems (VTS) and other means to improve the maritime safety, there will always exist spills of different sizes. The known hydrocarbon resources also form a significant new potential for oil transportation in Arctic areas. Thus, when the oil price again increases, greater pressure to fasten the production activities in the Northern hemisphere will exist. The technology then

required should be suitable to the ice conditions and severe Arctic or Sub-Arctic environmental conditions.

8 ACKNOWLEDGEMENT

The author expresses his grattitude to Mr. Seppo Liukkonen of Germanischer Lloyds by his efforts on the oil recovery research during his long career at VTT. Some of the ideas presented in this paper are based on the mutual discussions with him and the author during the long evenings with intensive reporting and research. Special thanks belong also to Mr. Erkki Mykkänen of the Finnish Environment Institute who is actually the father and the inventor of most of the new oil recovery devices tested and developed in recent years in Finland.

9 REFERENCES

Evans, D. D. 1988. In Situ Burning of Oil Spills. Alaska Arctic Offshore Oil Spill Response Technology Workshop Proceedings, NIST Special Publication 762, Washington DC, USA, pp. 47 - 95.

HELCOM, 1994. HELCOM Oil Combatting Excercise, Oulu-94. Video recording, English narration, Duration 11 min.

Johannessen, B.O., Jensen, H., Solsberg, L. & Lorenzo, T.1997. Program for Mechanical Oil Recovery in Ice Infested Waters (MORICE). Workshop on Safe and Clean Industrial Development - in cold climate and in ice conditions. 11-13 August 1997, Rosersberg, Sweden.

Lampela, K.1992. Mechanical oil combatting methods in ice and cold conditions and experiences obtained from them. Proceedings of the Seminar on Combatting Oil Spills in Ice and Cold Conditions. Baltic Marine Environmental Commission (HELCOM), 1-3 December 1992. P. 193 - 201.

Liukkonen, S.1997. Oil Spill combatting methods for ice-covered waters. Technical Report. VTT Manufacturing Technology. January 1997.

Liukkonen, S. & Rytkönen, J., Beach Cleaner Tests in Kokkola 26.3.1997. VTT Manufacturing Technology. Report VALB-251. 31 p + 1 app.

Rytkönen, J. 1992. Experiences of coping with oil spills in broken ice. Petro Piscis II, Bergen Norway. Paper H-4. 11p.

Rytkönen, J. 1999. The marine transportation and harbour activities in the Gulf of Finland now and in the future (in Finnish). Research Report VALB-400. VTT Manufacturing Technology. 92 p + 14 app.

Schultze, R (editor). 1995. World Catalog of Oil Spill Response Products. Fifth Edition. Baltimore, USA.

Simpson, W., Hillman, S., Dragnich, R., Easley, R. & Florida, M.1984. Oil Spill Response in Arctic, Part 3, Technical Documentation. Anchorage, Alaska, USA. 76 p + appendices.

THE IMPROVEMENT PLANS FOR FINNISH INLAND WINTER NAVIGATION

J.E.Rytkönen [1] and K. Kostiainen [2]
[1] VTT Manufacturing Technology, Espoo, Finland
[2] Finnish Maritime Administration, Helsinki, Finland

ABSTRACT

The Finnish Maritime Administration started a research project with VTT Manufacturing Technology to study the possibilities of improving inland transportation. during the winter. The studies were started in 1996 with an analysis of the experiences and lockage procedures of the year-round base waterways constructed elsewhere. Later, the project widened to contain the following sub-tasks: ship traffic studies, studies related to channel and ship lock operations during the winter and ice conditions studies.

This paper describes the basic sub-projects of the research programme and their main findings and results. The main objective of the study has been to describe the technical measures developed for handling ice problems during the winter and to evaluate their suitability for both the Saimaa and proposed Kymi-Mäntyharju Canal. Each alternative has different environmental design conditions, even if the climatic conditions are quite similar: For Saimaa Canal the main problems related to winter navigation are based on the shallow waterways, small lock dimensions and pack ice formation in the Gulf of Finland. For the Kymi-Mäntyharju alternative, however, the main problems are assumed to be caused by flowing water, frazil ice formation and the existing hydro-electric power production of the waterway in the Kymi-river. The problems of the Mäntyharju Canal are related more to the inadequacy of water in shallow and narrow lakes, especially when crossing the watershed between the main lake reservoirs.

1. INTRODUCTION

The sea area of Finland freezes every year. In moderate winters only the coastal areas freeze, but in severe winters almost all of the Baltic Sea freezes. In the sea areas, nine ice-breakers help to maintain a smooth traffic flow to and from the 23 coastal ports, even in the most difficult ice conditions, thus securing the foreign trade vital to us.

Inland navigation in Finland during the winter is concentrated in the Saimaa region where there are internal transports year-round. The Saimaa Canal traffic season ends in January and begins in April. In the beginning and at the end of the season, the conditions may occasionally be very challenging. At the moment, there is no traffic in ice conditions on any of the other inland waterways in Finland.

The problems related to winter inland navigation are mainly caused by the severe environmental conditions which dominate in the Northern hemisphere. The main parameters for describing the conditions are the long-term air temperatures, heat storage of the water, discharges and current velocities. Other important parameters affecting winter navigation are

the channel depth, cross-sectional form, bathymetric changes, channel width and bends. The average sum of freezing days of the Saimaa Canal area is about 1 000 - 1 200 d°C. The corresponding figures for the proposed Kymi Canal are slightly higher than in the Saimaa area.

In effective ice thickness, one third of the thickness of the snow cover is added to the thickness of solid ice and it is usually used in calculations for ship performance in level ice. Figure 1 shows the minimum values of the effective ice thickness measured in four stations along the Lake Saimaa's waterways which were 4.20 - 4.35 metres in permissable draught, during the years 1986 - 1991.

On average, freezing starts in the middle of November in the northern parts of Saimaa and at the end of November in the southern parts of Saimaa. The breaking up of the ice starts before the middle of May, on average. The effective ice thickness reaches its maximum in the middle of March. The average maximum thickness of the solid ice varies on Lake Saimaa from 50 cm to 60 cm.

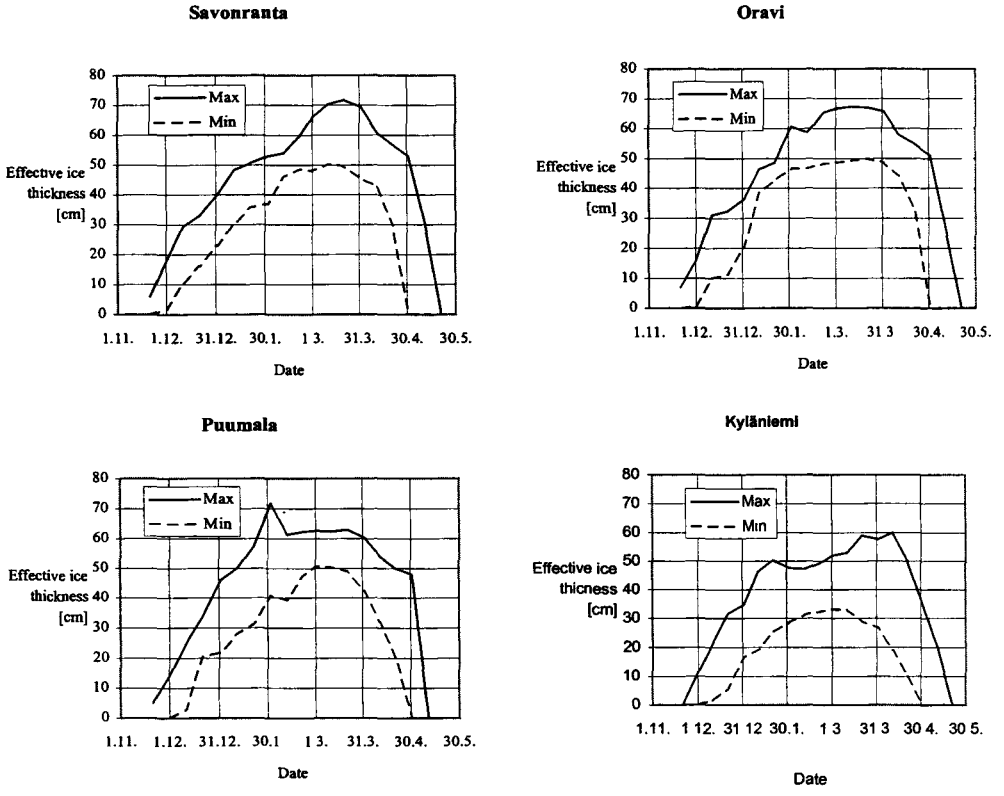

Figure. 1. The minimum and maximum values of the effective ice thickness measured in four stations along the deep fairway (4.2-4.35 metres) in the Saimaa area during the years 1986-1991.

In the effective ice thickness, one third of the thickness of the snow cover is added to the thickness of solid ice.

Winter traffic has a considerable effect on the forming of the ice cover. Towards the end of the traffic season, the temperature of the water body in the channel is close to 0 °C. This means that in difficult conditions, the thickness of the ice cover increases fast due to the constant traffic that breaks the forming ice cover. In average winters, the thickness of the ice cover is about one metre at its maximum.

The Saimaa Canal meets the Baltic Sea on the Bay of Vyborg, where the ice conditions may be very severe, especially in the early spring. When the ice cover weakens in spring, the winds often cause pack ice on the Bay of Vyborg several metres thick, which aggravates the traffic conditions in the channel even though the ice conditions on the channel itself are not that difficult. Rapid changes in ice conditions make the problem even worse, turning a seemingly harmless situation into a very difficult one in a few days.

The task of this paper is to describe the general observations and results of various sub-projects to improve r- traffic. during the winter. The objective of the work has been to study the possibilities of prolonging the ship- borne traffic along the Saimaa Canal from a 10-month season to a year-round activity. The proposed Kymi-Mäntyharju Canal plan has also been studied as an alternative solution for arranging winter navigation in Finland.

2. INLAND WATERWAYS IN FINLAND

The total length of the inland waterways in Finland is about 8 000 km. The state owned ship locks of the inland waterways are presented in Fig. 2. Of these waterways, 800 km are part of the Saimaa waterways with passage depths of 4.2 to 4.35 m connected to the Baltic Sea by the Saimaa Canal. Most of the freight transport in the Saimaa region is carried through these waterways.

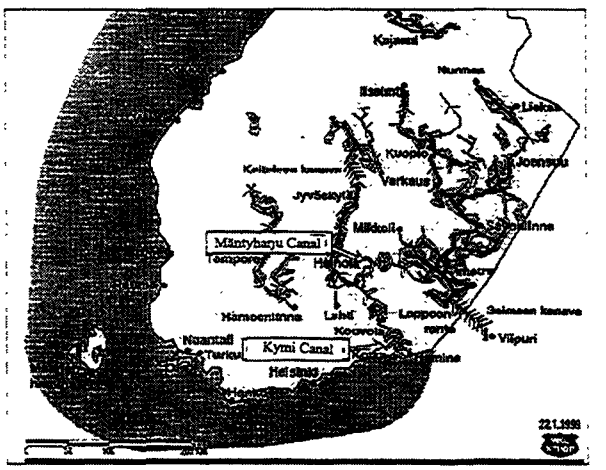

Figure. 2. The waterway network in Finland.

The total length of waterways with a permissable draught of less than 4.0 m is abt. 5 400 km. Where freight traffic is concerned, the most important of these waterways are the ones with passage depths of 2.4 - 3.4 m in the Saimaa and Päijänne regions. The length of such waterways in the Saimaa region is about 1 120 km. They are used for floating timber in bundles and transporting both timber and minerals by barges. In the Päijänne region the length of the waterways is about 1 400 km, and they are used for floating timber in bundles.

The waterways of Saimaa, of the Päijänne region and of the other waterway systems with passage depths of less than 2.4 m are used mainly for boating and passenger traffic. They have little importance to the national economy, though locally they may be very important.

The inland waterways consist of eight locks in the Saimaa Canal and 24 other locks. At the end of the summer in 1993, when the Keitele Canal was completed, its five locks were added, bringing the total to 37. The transportation figures for the Saimaa Canal indicated about 1.62 million tons of cargo in 1998. Figure 3 shows the transportation through the Saimaa Canal in 1989-99. The transporation figure through the other state owned (excluding Saimaa Canal) channels has annually been about 3 million tonnes.

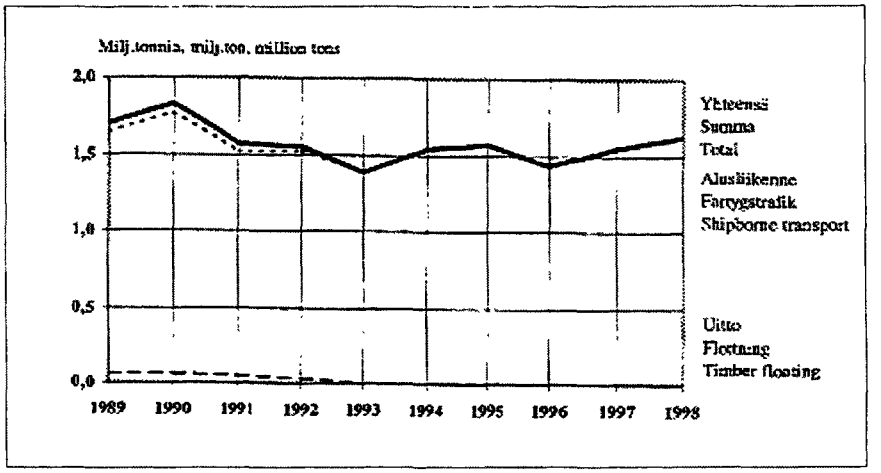

Figure. 3. Goods carried through the Saimaa Canal 1989-1998.

On inland waterways, there is traffic in ice conditions but only in the Saimaa region. The Saimaa Canal and its passageways with depths of 4.2 - 4.35 m are open for part of the winter. And, since 1990 there has been year-round transports in the Saimaa Lake region.

In the Saimaa region, internal transport volume during the winter is about 60 - 70 000 tons per month. Goods are carried by a buffer and barge. Transported goods are mainly timber and minerals. Most wintertime traffic is concentrated in the central and Southern parts of the Saimaa region, where there are no railway connections. Both the 4.2 - 4.35 and 2.4 - 3.4 m waterways are used.

In 1994 an agreement between Finland and Russia determined the traffic season for the 4.2 - 4.35 m deep channel: the season starts on April 10th at the latest, and ends on January 15th at the earliest. According to this agreement, the Inland Waterways District of Finland and the Russians from the Bay of Vyborg are responsible for the assistance of traffic up to the entrance of the channel From there onwards, the Finnish Maritime District is solely responsible. A Finnish-Russian channel delegation determines the length of the traffic season each year on the basis of the prevailing ice conditions.

Other channels under the supervision of the Finnish Maritime Administration are kept open from May 15th till October 31st, ice conditions allowing. There is no actual wintertraffic on these locks. The opening and closing of the channels must be announced in the local newspapers, or by some other appropriate media.

The Saimaa Channel locks are 85 m long, 13.2 m wide, and the water depth in them is 5.2 m. In the locks, the lower gates are mitre gates and the upper gates vertical lift gates. A layout of the locks is presented in Figure 4. The bottom width of the excavated parts of the channel is 28 m, and the passage width on the channel lakes 45 m. Navigation in the channel is allowed without a special permit for vessels with a length of less than 82.0 m, a breadth less than 12.2 m, a draught of less than 4.35 m, and a mast height of less than 24.5 m.

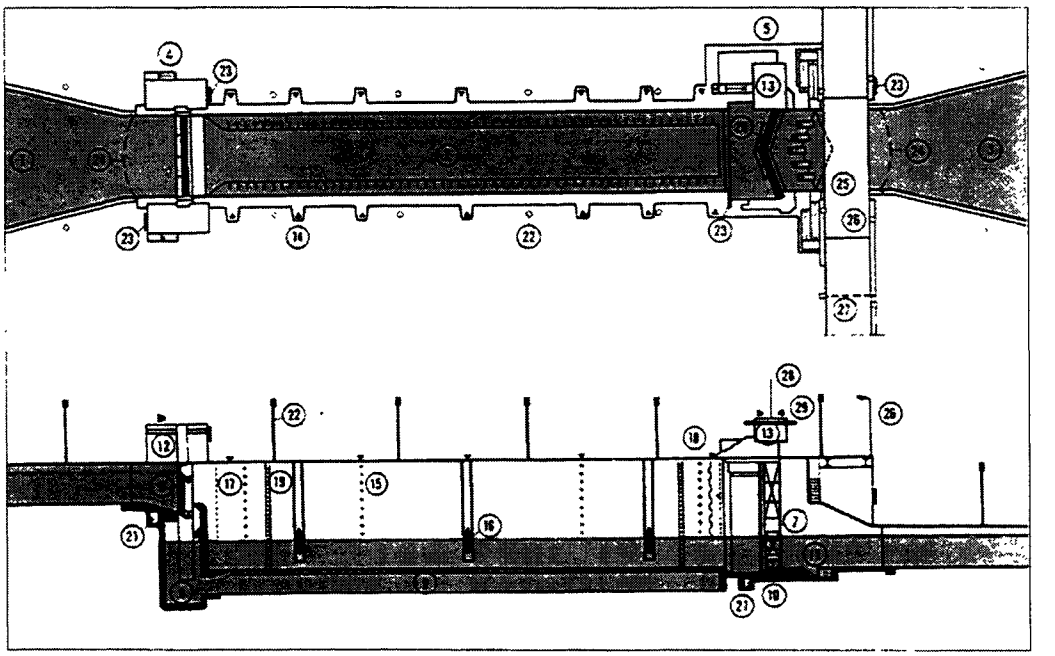

Figure. 4. A layout of the Saimaa Channel lock.

The typical heads of the Saimaa ship locks vary from 5...6 m up to 12...13 m. The total head between Lake Saimaa and the Gulf of Finland is 76 m.

The heads of the proposed Kymi ship locks vary from 6...7 m up to 12....13 m, and the total head is about 81 m, see Table 1.

Table 1. The ship locks of Kymi Channel and their heads.

Tavastila Line	Ship Lock	Note	Head (m)
	Kimola		11.5
	Voikkaa		9.9
	Kuusankoski		8.9
	Keltti		6.5
	Myllykoski		8.0
	Anjala	2 power plants	11.1
	Juurikorpi		7.9
	Ylänummi		12.5
			Total head 81.1 m

3. WINTER PROBLEMS AND TRADITIONAL ICE HANDLING METHODS

The basic problems for the winter traffic are the accumulation and freezing of ice in the ship locks and navigational channels. Ice and snow will freeze on the walls of the ship locks, thus reducing the effective width of the lock. The formation of ice will also cause problems in using the gates over an increased locking period, creating extra maintenance costs due to the continuous ice removal operation and repairs. The problems will continuously develop, becoming more severe as the winter progresses, until finally the locks should be closed totally and reopened again in the spring. The main problems with the Saimaa Canal are the long and shallow channels with bends, which easily lead to the accumulation of ice.

Generally, the difficult sections of the lake areas between the harbours are abrupt turnings and the meeting points of shallow and deep waters. In these points the water can freeze below the zero point with a heavy formation of frazil ice leading to heavy freezing. The wind drift-ice problems, such as pack ice formations at Lake Saimaa, are very scarce.

A proposed channel in the Kymi River would connect Lake Päijänne to the Baltic Sea. The total length of the eight-lock channel from the city of Heinola to the sea would be about 90 km. The type of locks in this channel corresponds to those in the Saimaa Canal. The channel is dimensioned for vessels whose length is 120 - 140 m, width 15 - 16 m and permissable draught 4.5 m. Its planned vertical clearance is 10 m and it is designed for year-around traffic. The same dimensioning has naturally been used as a basis for the Mäntyharju Canal plan, which will connect the lake Päijänne to the Lake Saimaa. The Mäntyharju canal plan consists of 6 ship locks.

The Kymi Canal differs considerably from the Saimaa Canal. Most of the Kymi Canal follows the Kymi River, with flowing water, that stays clear of ice for most of the winter. Only about 25 kilometres of the channel's total length is excavated.

When comparing the technical ice control methods abroad and in Finland, there are no significant differences. The technical equipment to diminish and remove ice from locks and channels are e.g. heating elements, air bubble curtains, surface current generators, hot water jets and special gates for the passage of ice floes. The major problem of the fairways abroad is the rafting of ice which does not occur in Finnish inland waterways. Trollhättan Canal in Sweden is working year-round. This is possible due to the smooth climate and the short winter period with minor ice problems. Furthermore, the strong discharge from Lake Vänern to the River Göta with the relatively high thermal content will improve the maintenance of the channel.

4. IMPROVEMENT PLANS AND RESEARCH ACTIVITIES

In the studies in order to extend then navigation period in Saimaa Canal and planned Kymijoki and Mäntyharju Canals (Holm, 1998), hydrological and metereological data were collected and analysed, long-term measurements by ships and ice reconnaissence flights were made. Difficult streches for navigation in the planned canals were determined by studying the plans and by making field studies.

First ice measurements at the ship were carried out during the winter 1996/97 later continued by measurements in 1997/98 and 1998/99. Two vessels typically operating via the Saimaa Canal, the MS Pionier and MS Premiere, were equipped for long-term measurement. Ice conditions as well as the position and speed of the vessel, shaft torque, the speed of rotation of the propeller and its pitch were observed during the voyage on board the vessel. The measured signal of the speed and the capacity of the shaft were presented as a function of the dinstance travelled, the signal of the speed also as a function of time, and the lentgh of the voyage is divided into the streches of pilot (Figure 5). The measured results were compared with the estimations of resistance to ship motion. Principally the calculated resistances to ship motion were considerably bigger than the measured ones.

During the winter 1996/97 the capacities of vessels were also analyzed on the basis of the average speed calculated from the time spent in the different legs of the route and the length of the said leg. The highest drop in speed was found to be in the route from Vuokala to Joensuu. The reach between the locks of Soskua and Lake Nuijamaa was found to have the most severe ice conditions in the Saimaa Canal. More profound discussion of the results is given in (Nyman & Kokkonen, 1999).

There is a need to develop the ice-breaker assistance further and the ice-breaking properties of the vessels. The preliminary studies have shown, that the ice-breaking assistance should be maintained with at least two vessels.

The hummocking of the sea ice in the Bay of Vyborg and the Eastern part of the Gulf of Finland can cause difficulties in maintaining year-round navigation, especially during the spring The thickness of the largest ice hummocks in the pack ice-zone was 4 - 6 m, which

was detected during the full-scale trials of this research programme.The speed of the vessel dropped to the less than half compared to the speed at sea, and almost three rammings were required per one kilometer. Furthermore the shipping channel entering both Vyborg and the canal is shallow leading to unwanted waiting periods when the sea level of the Bay of Vyborg is low. The plans to deepen the problematic part of the fairway have been made and work will be completed before the year end 1999.

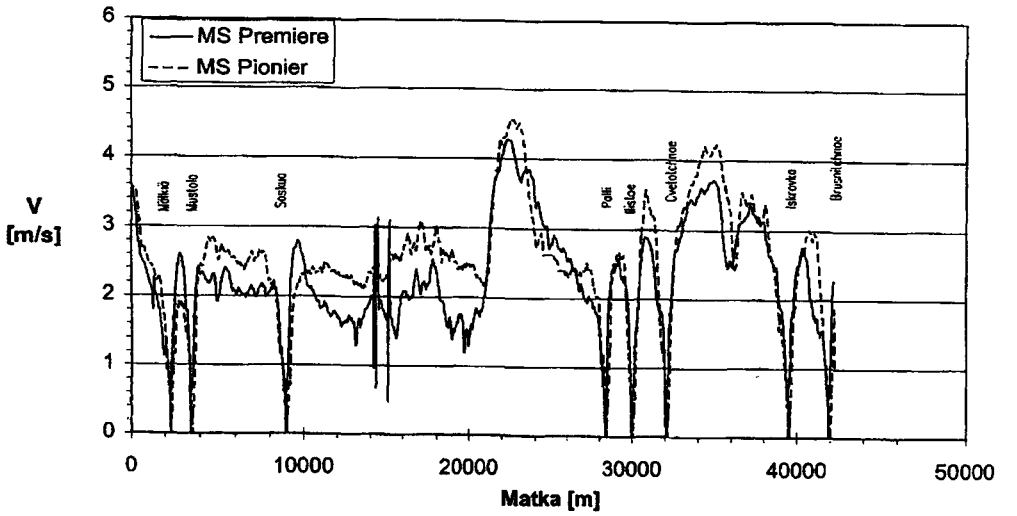

Figure 5. An example of the measured velocities of MS Premiere and MS Pionier, winter 1997/98.

Preliminary heat transfer and ice formation calculations have been made in order to estimate the utilisation of surface current generators in the ports of Lake Saimaa. It may be advantageous, however, to maintain ice cover in the port area. with a smaller heat transferr to the atmosphere from water. Acceptable ice thickness should be specified according to ship manoeuvring operations in the port that it would be not difficult to carry out. In this respect the ice formation in a vessel track has been evaluated in more detail. On the basis of some of the engineering methodologies found from the literature (e.g. Ettema, R. & Huang, L. 1990; Eranti, et al. 1983) the number of passages increases ice formation significantly and it seems that keeping the fairway open in the canal year round is fairly difficult, except during very mild winters. Principally the calculated ice growth values were considerably higher than the measured ones. This led to the additional ice measurements in the Kymijoki and Mäntyharju Canal site in 1998/99. Furthermore ice model series was conducted with the Kvaerner Masa-Yards Arctic Research Center to optimize the required canal cross-section on the basis of the manoevring cabability of the ship and the proposed ice conditions.

The present ice problems of the River Kymijoki were also studied. Some hydro-electric power stations have problems with the accumulation of ice in the trashracks and with the ice breakup as a result of water level fluctuations. The ice problems in the free flowing sections of the

River Kymijoki will linger also after the proposed canal has been constructed.. Due to the fact that there is a possibility of ice jam formations and problems for ship manoeuvres more detailed numerical modeling is required for the estimation of the drifting ice and the formation of potential ice jams. The shiphandling simulator of VTT has already been modified to be used for the simulations of river conditions. Thus ship manoeuvres have already been conducted in open water conditions in selected difficult sections such as river bendings, openings of the excavated canal in the river etc. A more detailed description of the River Kymijoki studies is given in (Laasonen & Holm, 1999).

On the basis of these studies, however, it can be concluded that the cross-section of the excavated canal should be made large enough for a vessel to run among ice floes. The additional discharge in the canal would become unprofitable.

Some studies were also conducted to evaluate the possibility of using the proposed Mäntyharju canal year-round. Mäntyharju Canal runs mainly through shallow lakes, and the canal sections are relatively short. The ice formation will correspond to the conditions of the lake and canal cuts in Lake Saimaa. Therefore the ice problems will be concentrated in places where the canals are built in connection with locks constructed through excavated open cuts, by small radii of curvature in the canal and the short entrance routings to locks. It was found during the study that the construction of the canal will cause some local adverse environmental effects and the prerequisities for the implementation of the lay-out should be investigated carefully with respect to the environment.

5. CONCLUSIONS

The experiences with the Saimaa Canal have shown that the wintertime traffic will not be effective or economical without new technical solutions or innovations. The industry of the lake area has pointed out the necessity of the year-round inland navigation. There have also been a lot of debate on the economical use of the existing Canal, canal fee-policy of the Russian authorities in Vyborg and the future of the canal due to the fact the contract between Finland and Russia to use Russian territory for canal traffic will end in 2013. The industry has also pointed out, that the existing dimensions of the Saimaa Canal are already now too small for economical shipping activities, even in the open water season.

In connection with the improvement plans of the Saimaa Canal a new inland canal route has been proposed from the city of Kotka up to the town of Heinola, as a Kymi Canal. This route requires another new canal from Lake Päijänne (Heinola) to Lake Saimaa, thus the proposed Mäntyharju Canal would be the missing link between these two main lakes. The preliminary fairway and ship lock design is based on a totally new ship design concept with a design breadth and length of the ship of 16.0 m and 130...140 m, respectively. The preliminary design permissable draught of the ship is 4.5 m.

The main issue now is to optimize the required channel cross-section and the find out the minimum channel bending radius in order the new lay-out of the Saimaa Canal, or the proposed Kymi-Mäntyharju Canal can be drawn on the map. The proposed Kymi-Mäntyharju Canal has also been a topic of public debate, several times. Another issue that has risen is whether or not a new waterway route for maritime traffic is needed. Nevertheless, the proposed Kymi-

Mäntyharju Canal offers a good alternative for verification of the possible improvement to the totally new consept, and to the developing the Finnish inland waterway network. Thus, it has been only natural to realize that the proposed canal alternatives also must be based on the year-around traffic system.

6. ACKNOWLEDGEMENTS

The authors will express their best grattitudes to the numerous experts participating the research programme for the inland waterway improvement. Special thanks belong to Messieurs Reijo Brunou and Kosti Holopainen for their assistance on the ice measurements in the winter 1998/99. Professor Mauri Määttänen should also be mentioned here as a skillful pilot of the airborne surveys on the ice fields of the River Kymijoki and Lake Saimaa. Thanks belong also to the Regional Environmental Institutes in Tampere and Kouvola for the important assistance in flow velocity and ice measurements.

7. REFERENCES

Eranti, E., Penttinen, M. & Rekonen, T. 1983. Extending the ice navigation season in the Saimaa Canal. 7th International Conference on Port and Ocean Engineering under Arctic Conditions (POAC). Espoo.

Ettema, R. & Huang, T. Ice Formation in Frequently Transited Navigation Channel. CCREL, Special Report 90-40. December, 1990.

Holm, O, Nyman, T., Piironen, S., Riipi, T. & Rytkönen J. 1998. Winter Navigation in Inland Waterways - Finnish Experiences and Improvement Plans. 29th PIANC International Navigation Congress. 6-11 September 1998, The Hague. Section I/Subject 3. ISBN 2-87223-095-5. P. 17 - 32.

Laasonen, J. & Holm, O. 1999. The Impacts of the Proposed Kymijoki Navigational Channel on the Hydro-Power Plants. Proc. of the 15th International Conference on Port and Ocean Engineering under Arctic Conditions. Helsinki, August 23-27, 1999.

Nyman, T. & Kokkonen, J. 1999. Ice Performance Measurements onboard MS Pionier. Proc. of the 15th International Conference on Port and Ocean Engineering under Arctic Conditions. Helsinki, August 23-27, 1999.

Rytkönen, J. 1999. Sisävesiliikenteen talvitehostamistutkimuksia jatkettiin kuluneen talven aikana. Research activities to improve inland waterways were carried out during the past winter (in Finnish). Vesitiet 1/1999.

VTT, 1999. Facilitating Winter Traffic in Lake Saimaa and Proposed Kymijoki and Mäntyharju Canals. Summary Report (Confidential)1996-1998. VTT Manufacturing Technology, February 1999. 26 P.

FORECASTING OF SPEEDS OF THE MOVEMENT OF SHIPS ON WATERWAYS OF THE NSR BY THE MATHEMATICAL SIMULATION

L. Tsoy and Yu. Glebko
CNIIMF, Saint-Petersburg, Russia

ABSTRACT

On the basis of statistic materials on the operation of the Russian fleet in the Arctic as well as of full-scale experimental data and systematic model tests, an algorithm of the calculation of speeds of icebreakers and cargo ships of traditional type and a mathematical model of their movement on waterways of the Northern Sea Route (NSR) in the independent mode of sailing and as a part of convoys were developed. This model being a combination of analytical relationships and logical links describes the ship/icebreaker interaction and takes into account particular features of the ice propulsion of ships and icebreaker forming a convoy. Ice conditions over the NSR used in the model are based on results of the statistical processing of numerous voyages in particular directions taking down ice parameters immediately en route. Out of individual features of ship upon which its passability in ice mostly depends, the model takes into account principal dimensions, displacement, form and state of the hull shell plating, propulsion plant power, type of the power transfer and characteristics of the propeller system. By the mathematical model developed, the forecast estimation was made of speeds and return trip duration of tanker *Uikku*[1] under the escort of icebreakers *Kapitan Dranitsyn* and *Rossiya* as applied to the experimental voyage in April-May 1998 of the tanker to the Ob Gulf envisaged by the programme of investigations of the European Commission (Project ARCDEV). In turn, the experimental voyage permitted obtaining more accurate information on the conditions of winter navigation on line Murmansk - Ob Gulf and on elements of the tactics of the icebreaker escorting of tanker under these conditions as well as making appropriate calibration of the movement of the model in question in ice.

1. DESCRIPTION OF THE MATHEMATICAL MODEL

The developed mathematical model of the movement of ship after the icebreaker takes into account individual distinctive features of ship and icebreaker affecting their ice performance (Tsoy, 1983). The model is a set of analytical dependencies and their logical connectives describing concerted movement of a ship and an icebreaker. On the basis of this model an algorithm was produced and a program consisting of four independent subprograms prepared:

1. Calculation of the ship's speed and time consumption when moving through open water taking into account seasonal variations of speed, direction and frequency of wind, height, direction and frequency of seaways.

---

1 Main characteristics of ships participating in the voyage (length, m × breadth, m × draft, m × displacement, t × shaft power, kW × ice category × icebreaking capability, m): *Uikku* - 151.1 × 22.2 × 9.5 × 22600 × 11400 × 1A Super × 1.0; *Kapitan Dranitsyn* - 121.3 × 26.5 × 8.5 × 14900 × 16200 × LL3 × 1.4; *Taimyr* and *Vaigach* - 140.6 × 29.2 × 8.1 × 19600 × 25000 × LL2 × 1.9; *Rossiya* - 136.0 × 30.0 × 11.0 × 23460 × 49000 × LL1 × 2.5.

2. Calculation of ice propulsion characteristics of an icebreaker and of a ship in the independent movement on separate ice stretches of the route with invariable ice conditions. Making of the channel by icebreaker and movement of cargo ships through this channel are considered separately.
3. Calculation of time consumption for the icebreaker's and ship's joint (in a convoy) breaking through the route.
4. Calculation of the duration of voyage taking into consideration cargo handling operations and unproductive idleness; determination of a number of voyages, mass of the transported cargo; calculation of economical factors taking account of operating costs or leasing rates for ship and icebreaker.

The main programme inputing the initial data forms versions of calculation, prepares the work of sub-programmes, produces files of results, draws up output tables.

1.1. Simulation of movement in open water

Sailing in open rough sea brings about the reduction of the ship's speed. In the model, rate of the speed reduction is determined in dependence on loading (under loaded conditions, in ballast), speed of movement in calm water V_0, length of ship L and season of its operation. One can judge the speed losses in the south-eastern part of the Barents Sea of tanker *Uikku* calculated by the method of G.Aertssen (Aertssen, 1957) by bar graph of Figure 1. Considerable speed losses under loaded conditions can be attributed to the fact that ship has to sail mainly against wind and waves the direction of which are predominant in this region.

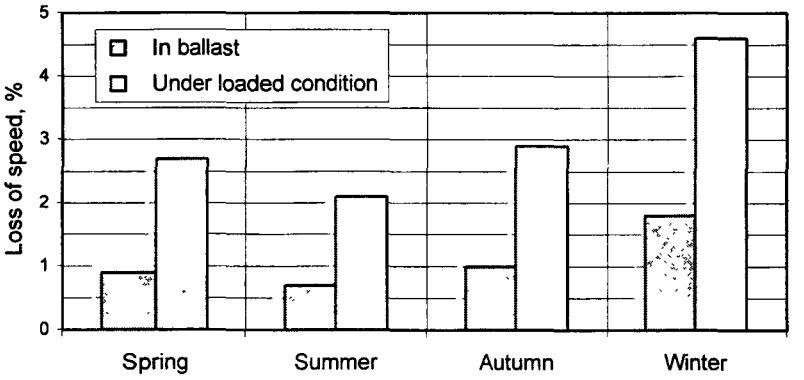

Figure 1. Speed losses of tanker *Uikku* in the Barents Sea

If there is no reference information on speed V_0, the model permits getting it by calculation with the use of the empiric formula (Tsoy, 1995):

$$V_0 = 2.55 N_p^{0.137} \left(\frac{L}{T\delta} \right)^{0.2}, \text{ kn.} \qquad (1)$$

In the initial data set, along with the length of ship L [m] there should be information on shaft power N_p [kW], draft T [m] and block coefficient δ.

1.2. Simulation of the movement in ice

When a ship moves through ice, the main criterion characterizing the ship's propulsion is the icebreaking capability h_i, that is maximum thickness of the level compact ice broken through in continuous motion, ice bending strength and steady speed being specified. The latter is taken equal to 1.5-2.0 kn and the ice bending strength – not less than 500 kPa. Ice has natural snow cower about 20-25 cm deep.

The icebreaking capability while being a principal criterion for the comparison of icebreaking qualities does not characterize the ice propulsion within the whole range of ice thicknesses: from zero (in open water) to a maximum value when ship or icebreaker has to force its way through ice by ramming. Assuming the relationship $V=f(h)$ to be linear, the ice propulsion of ship can be judged from two values: icebreaking capability h_i and speed in open water V_0 (Figure 2).

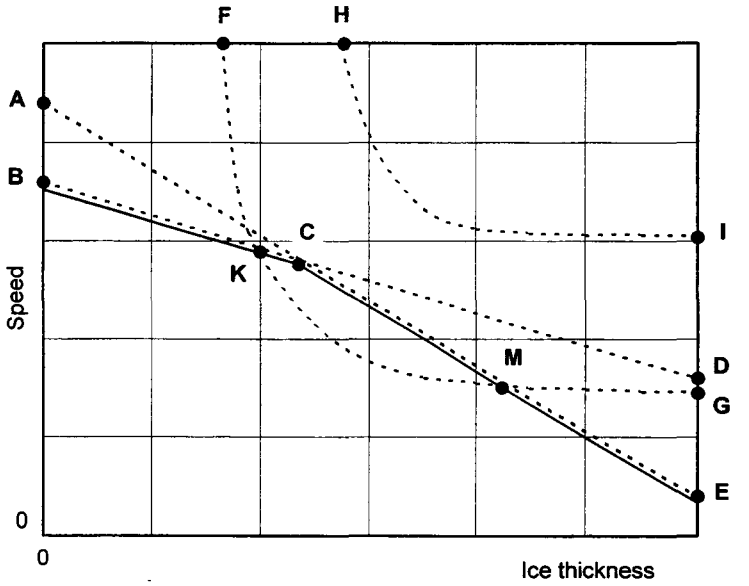

Figure 2. Diagram of the ice propulsion of ship escorted by icebreaker: *AE* - movement of icebreaker through the compact ice, *BD* - independent movement of ship in the channel, *BCE* - movement of the icebreaker-ship convoy, *FG* and *HI* - restrictions for ship of a low or high category of ice strengthenings

During the movement of a cargo ship it is supposed that the icebreaker carries out the escorting from one ice edge to the other. In the process of the escorting the speed of the convoy movement on each stretch is defined either by a speed of icebreaker making a channel (*CE*), if ship has a sufficient power not to lag behind, or restricted by the ship's speed in the channel (*BC*), if this speed is lower than that of the icebreaker due to a lower power of ship. This circumstance is graphically shown in Figure 2.

To ensure the safe escorting of ship, its speed may be additionally restricted in case of the insufficient extent of hull strengthenings the level of which depends on the ice category. The last figure shows restricting lines of safe speeds for ship with a high (*HI*) and low (*FG*) categories of ice strengthenings. In the first case, strength properties of ship provide for the possibility of its operation at maximum achievable speeds, in the second case there is the ice thickness range (*KM*) within which the operational speeds have to be reduced down to safe ones. A special block in the model calculates safe speeds of movement and introduces corrections into the diagram of the ship's ice propulsion (*BKME* line). If the initial data do not contain value h_i, in the model it is calculated by the following regression equation (Tsoy, 1995):

$$h_i = \frac{0.07\sqrt{\frac{P_e}{B}}\sqrt[6]{D}}{\sqrt[5]{\frac{L}{B}}\sqrt[26]{f_d}} \frac{\cos^{\frac{3}{2}}\varphi \sin^{\frac{1}{2}}\frac{\alpha_0+\beta_0+\beta_2}{3}}{\sin^{\frac{3}{2}}\left(90^0-\beta_{10}\right)}, \text{ m} \qquad (2)$$

where

φ - stem angle, deg
α_0 - entrance angle of design water line, deg
β_0 - flare angle of frame line No.0, that is at the fore perpendicular, deg
β_2 - flare angle of frame line No.2, deg
β_{10} - flare angle amidships, deg
B - breadth, m
P_e - propeller bollard thrust, t
D - displacement, t
f_d - coefficient of the dynamic ice/ship's hull friction.

Total propeller thrust needed for the calculation of icebreaking capability is determined by the AARI formula based on the experience of the design of domestic icebreakers:

$$P_e = k_p (d\ N_p)^{2/3}, \text{ kN} \qquad (3)$$

where

d - diameter of screw propeller, m
k_p - coefficient accounting for the geometry of screw propellers, their number and interaction with the ship's hull.

Number of screw shafts of ship is determined in accordance with requirements to the manoeuvrability and the efficient power handling. Critical power N_c which may be handled by one propeller without aeration and cavitation (at a relative propeller diameter of about 0.6 from draft) is determined by the formula of CNIIMF:

$$N_c = 213\, d^{2.5}, \text{ kW}. \qquad (4)$$

Out of other ship's individual particulars characterizing its icebreaking capability the model takes account of the following:

- type of steel and presence of protective ice resistant coatings,
- state of the ship's hull shell plating (age of ship),
- availability of means to increase the icebreaking capability (air- bubbling system, hydraulic washing system, heating etc.),
- power of the propulsion plant,
- type of power transfer.

The ice route specified by the model is made up of separate lengths of different ice age. Equivalent thickness of ice h_e was assumed as its main characteristic which includes ice thickness h_0 as well as allowances for hummocking Δh_H and snow cover Δh_s:

$$h_e = h_0 + \Delta h_H + \Delta h_s . \tag{5}$$

Components due to the hummocking of ice t [in numbers] and the snow depth h_s [m] are determined by the formula of G.Sergeev (Sergeev and Khromov, 1980) and by formula use by CNIIMF and Hamburgische Schiffbauversuchsanstalt:

$$\Delta h_H = 0.25\, t\, h_0 \tag{6}$$

$$\Delta h_s = k_s\,(h_s - 0.25\,) \tag{7}$$

$$k_s = 0.50 \text{ at } h_s \geq 0.25 \text{ m and } k_s = 0.33 \text{ at } h_s < 0.25 \text{ m}. \tag{8}$$

Other environmental factors are type of ice conditions (light, medium, heavy), seasonal variations in the strength of ice, location of ice edge and duration of ice period. To build up the ice route, appropriate statistic data are used. The results of observations during the last 45 years were used for determination of average values.

For the calculation of speeds V_i of movement of a transport ship through the channel made by icebreaker in ice of different thickness h_e a dimensionless diagram (Tsoy, 1982) was used which analytically may be represented in the following way:

$$V_i = V_0 \left(1 - k_c \frac{V_0 - 2}{V_0} \frac{h_e}{h_i} \right), \text{ kn.} \tag{9}$$

Coefficient k_c takes account of a relative width of the channel which depends on the ship's breadth and breadth of icebreaker.

Speed of the independent movement of icebreaker or cargo ship through drifting ice of different concentration is determined by the statistic relationship between the propulsion in compact and drifting ice. At a concentration of ice up to 5/10-6/10 a ship or an icebreaker due to its selective capability proceeds practically in the ice-free water. In ice with a concentration exceeding 7/10-8/10 icebreaker makes a channel and ship moves through it after the icebreaker.

When the speed of the continuous movement of icebreaker or ship becomes unsteady (less than 2 kn), the tactics of escorting changes. With this object in view there is a block in the model describing the process of surmounting a heavy ice section by ramming.

As in real conditions the ice is subject to drift, the model makes allowance also for the influence of concentration on the ice propulsion of ships within a convoy. The experience shows that the concentration of ice is not a less substantial factor than thickness and concentration of the ice cover. Under conditions of vigorous growth and formation of young ice the concentration in many cases altogether defines the possibility of ship to sail through ice and its safety. Account is taken as well of the impact of seasonal changes in the ice cover on the icebreaking capability of ships. In summer, in decayed ice, the icebreaking capability increases while in winter, in more compact ice with snow cover, it diminishes.

The speeds of the escorting of ships calculated by the above algorithm are net technical speeds. For the determination of gross speeds while making calculations of economical indices of the operation of ships the time needed for the breaking up of ice around stuck ships in convoy, for the preliminary making of a channel in heavy ice (reconnaissance by hull), expectation of the weather improvement (fogs, compacting etc.) is added to the net time needed for covering the route. Additional time consumption depends on season and area of navigation and is determined on the basis of processing of the statistic data.

Besides the calculation of speeds the model permits to determine the ship's and icebreaker's power consumption during the movement in convoy. Knowledge of coefficients of the utilization of power of icebreakers and cargo ships intended for the operation under specific conditions, along with the assessment of their economical efficiency, is also of importance for the design of power plants permitting to correctly select main modes of their operation and the needed power splitting by units.

The database for the formulas used for calculation was formed on the basis of information on Russian cargo ships and icebreakers of conventional type with a displacement of 2000 - 50000 t and power of 3 - 49 MW.

2. PREDICTIVE CALCULATIONS OF MOVEMENT SPEEDS

Initial information for the performance of calculations in accordance with the above procedure includes: direction of transportation, ice conditions on the route, main characteristics of ships and icebreakers, number of ships in the convoy and the amount of cargo aboard.

Ultimate destination points of the route of navigation in the Russian Arctic have been defined by objectives and tasks of the ARCDEV Programme: departure from Murmansk, passage to the point of loading in the Ob Gulf and return to Murmansk. The choice of route was made directly prior to the voyage in accordance with ice conditions in the Barents Sea. As the calculations were of the forecasting character they have been performed for two alternative versions of navigation: through the Kara Strait (Murmansk - ice edge - Kara Strait - Bely Island - Sabeta) and around the Cape of Zhelania (Murmansk - ice edge - Cape Zhelania - Bely Island - Sabeta).

For each of sections the initial information on length and ice conditions in April and May has been prepared. In doing so, it was assumed that the first (eastbound) half of the voyage would be made in ballast and the second (westbound) half - under loaded conditions. Figure 3, as an example, shows distributions of thickness and concentration of drifting ice on section ice edge - Kara Strait in April.

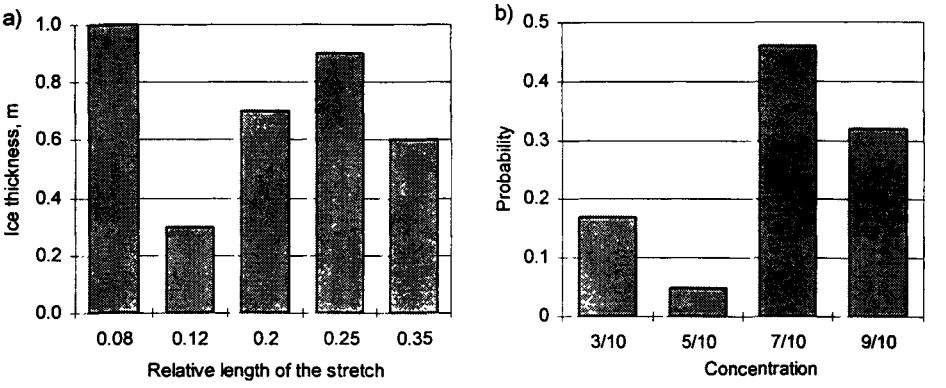

Figure 3. Distribution of ice thickness (a) and concentration (b) in April along the route section: ice edge - Kara Strait

In addition to thickness and concentration of ice the initial information includes data on hummocking, snow cover, compacting as well as on type of ice conditions. The latter was evaluated by the Headquarters of Marine Operations as heavy one.

A set of calculations made with the use of the above initial data permitted to obtain forecasting speeds and steaming time of tanker *Uikku* on separate route sections and for the voyage as a whole (Table 1).

Table 1

Speeds and time consumption by tanker *Uikku* at different versions of sailing and icebreaker assistance

Route sections	Icebreaker assistance	Speed, kn	Steaming time, h
Murmansk - Bely Island - Murmansk (through Kara Strait)			
Murmansk - ice edge	independently	16.0	10.7
Ice edge - Kara Strait	*Rossiya*	7.7	48.2
Kara Strait - Bely Island	*Rossiya*	9.3	47.4
Bely Island - Kara Strait	*Rossiya*	9.3	47.4
Kara Strait - ice edge	*Rossiya*	9.5	32.0
Murmansk - Bely Island - Murmansk (around the Cape Zhelania)			
Murmansk - ice edge	independently	16.0	24.4
Ice edge - Bely Island	*Rossiya*	9.7	65.8
Bely Island - ice edge	*Rossiya*	9.1	80.9
Ice edge - Murmansk	independently	14.7	19.7
Bely Island - Sabeta - Bely Island			
Bely Island - Sabeta	*Taimyr*	2.0	60.0
Sabeta - Bely Island	*Taimyr*	8.1	14.8

On the completion of the voyage, there presented a possibility to compare forecasting estimates with full-scale measurements. Results of such comparison as applied to voyage Sabeta - Murmansk are presented in Table 2.

Table 2

Comparison of the calculated and actual net time consumption of tanker *Uikku* in making voyage Sabeta – Murmansk

Route sections	Duration, h	
	calculated	actual
Sabeta – Murmansk	128.4	114.3
Sabeta – edge of fast ice of the Ob Gulf	20.8	19.8
Fast ice of the Ob Gulf – Kara Strait	56.0	51.9
Kara Strait – ice edge	37.8	21.7
Ice edge – Murmansk	13.8	25.0

Analysis of the results points to an acceptable compliance between calculated and actual data. Disparity for certain route sections is due to deviations of the specific synoptical and ice situation from the average statistics as well as to the organization of work of icebreakers escorting the tanker. Selection of the easiest route resulted in the fact that its length had increased approximately by 20 %. However, thanks to higher speeds of the escorting of ship these losses were compensated.

The model realized the condition based on the experience of the arctic navigation according to which over the stretch of the route amounting approximately to 20 % of its whole length ships are subject to compacting of an average force (1-2). During the experimental voyage this value turned out to be lower than the average statistical figure. Appreciable compactings were observed only in the Kara Sea on the passage from the Cape Zhelania to the fast ice of the Ob Gulf (about 13 % of the route) and from the fast ice to the Kara Strait (about 17 %).

3. CORRECTION OF THE MATHEMATICAL MODEL BY THE RESULTS OF THE EXPERIMENTAL VOYAGE

On the completion of the voyage, to check up the reliability of forecasting estimates, additional calculations were performed. New ice way was formed on the basis of the routine information on ice conditions along the route of the convoy. Deviations of average speeds on separate sections of the route did not exceed 6 %. Such fairly high degree of coincidence of calculated and actual speeds accounts for the corrections introduced into the model as to the structure of initial data and some functional blocks. In consequence of alterations, two additional parameters were inserted into the scheme, the influence of these parameters having been taken into account earlier by statistical coefficients.

At the preliminary stage of predictive calculations the operational speed of tanker in open water was 16 knots in ballast and 14.7 knots in loaded conditions. In accordance with the initial data the power level was supposed to be about 75 %. Actual tanker power consumption, however, was about 40 % on the one-way voyage and about 70 % on the return voyage. Additional calculations made for these power levels allowed to achieve the comparability of results and to assess errors. Calculated tanker speeds in open water were 12.5 knots in ballast and 14.3 knots under loaded conditions relative errors not exceeding 3 %.

Other factor, the consideration of which contributed to the increase of reliability of the calculated algorithm, is *the channel age*. As period of the existence of the channel becomes

longer the sailing through it grows increasingly difficult. The model takes into account the effect of age of the channel (time elapsed since its making) by the relationship obtained in 1978 in the course of tests of icebreaker *Kapitan Sorokin,* sister ship of *Kapitan Dranitsyn,* in the Yenisei Gulf in ice about 1.5 m thick (Figure 4). During the experimental voyage the channel in the Ob Gulf was made by icebreaker *Vaigach* (of the *Taimyr* type), but the convoy entered it after 4 days. By the moment of the convoy leaving the Ob Gulf the age of the channel was about 10 days. One can get an idea of the degree of compliance between calculated and actual speeds of movement from Figure 4, if two additional points recorded during the voyage are plotted.

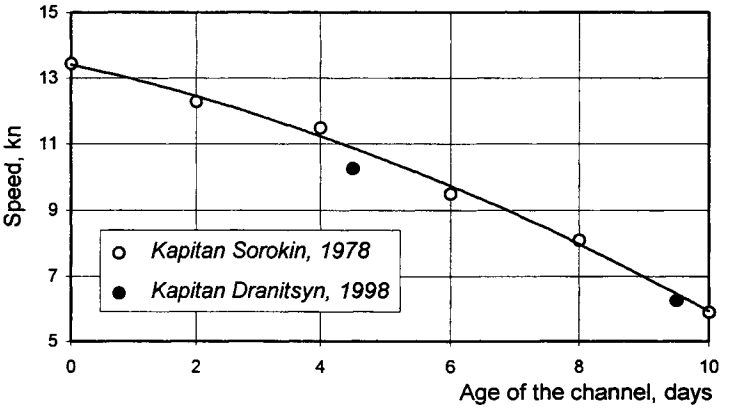

Figure 4. Effect of age of the channel in the fast ice on the speed of icebreakers of the *Kapitan Sorokin* type from the results of voyages in 1978 and 1998

Corrections introduced into the model by the results of the experimental voyage permitted to more accurately define the calculation scheme and to improve the reliability of the results thus obtained.

Bearing in mind the interest shown in the use of the NSR for transit transportation between Europe and Eastern Asia an example is given below of the calculation of speeds of icebreaking cargo ship with a deadweight of 30000 t. From Figure 5 one can judge the dynamics of the change of speeds throughout the year of the ship under the assistance of the existing *Rossiya* type icebreaker and of a prospective icebreaker having a power of 60 MW.

During a part of navigational period the ship in question with the ULA category of ice strengthenings and icebreaking capability of 1.6 m operates independently, but as navigational conditions become more severe it resorts to icebreaker services.

For the assessment of limits of probable errors the calculation of speeds was made for easy, medium and heavy types of ice conditions being of a cyclic character. The first and the third types recur once in four years and the second one – twice. Use of the apparatus of the theory of errors makes it possible to determine mathematical expectation and mean square deviation of a probable error within the four year cycle. For the curves presented in Figure 5 the value of the mean square deviation does not exceed 0.7-0.8 kn.

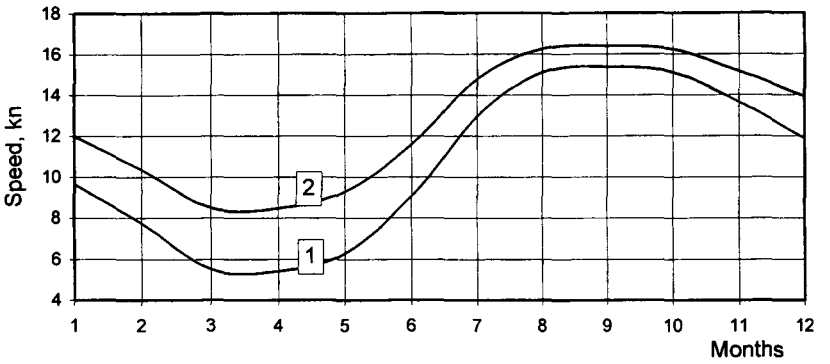

Figure 5. Average speeds of ship with a deadweight of 30000 t in the transit navigation along the NSR under the assistance of icebreaker of the *Rossiya* type (1) and of a prospective icebreaker with a power of 60 MW (2)

4. CONCLUSION

During the period of the preparation to the expedition within the framework of the ARCDEV Project and in the course of its pursuance a package of works was carried out directed towards the improvement of methodical approaches and methods of calculation used for the simulation of the movement of ships in ice, in particular:

- calculation model of the taking out of hydrocarbon raw materials from the Ob Gulf was developed;
- forecasting calculations and the results of the actual realization were compared the degree of compliance being estimated;
- efficiency of the calculation scheme in the mathematical simulation of the movement of ships independently and under icebreaker support both in the drifting and fast ice was corroborated;
- corrections are introduced into the structure of initial data and algorithm of the model permitting to improve the accuracy of forecasting estimates.

5. REFERENCES

Aertssen G. The effect of weather on the performance of cargo ships. Proceedings. Symposium on the behaviour of ships in a seaway. Wageningen. September, 1957.

Sergeev G., Khromov Yu. Hummocking and ice resistance to the moving ship. Meteorology and hydrology, No.10, 1980, pp. 100-104.

Tsoy L. Diagram for the determination of speeds of the movement of ships in ice channels. Proceedings of CNIIMF "Prospective types of sea ships", issue 275, 1982.

Tsoy L. Modelling of vessels movement in a channel broken up by icebreaker. *The 7th International Conference on POAC 83*. Proceedings. Vol.2. Espoo, April 1983.

Tsoy L. Assessment of ships' icebreaking capability at early stages of design. *Abstracts of papers. Conference on Shipbuilding, Shipping and Offshore Technology NEVA'95.* St.Petersburg, 1995, p. 53-54.

ON THE REQUIREMENTS TO POWER OF POLAR SHIPS

L. Tsoy and Yu. Glebko
CNIIMF, Saint-Petersburg, Russia

ABSTRACT

Consideration was given to current requirements to the power of icebreakers and cargo ice ships regulated by the Russian Marine Register of Shipping (MRS) and other classification societies. It was shown that formulas used by these societies for the determination of power do not adequately take into account the effect of the hull shape and of other ships' elements on the ice propulsion. Rules Recommendations not always comply with the modern practice of the construction of arctic ships frequently not having time to keep up with the experience of the operation of fleet in the Arctic. On the basis of the common approach to the ice classification of polar ships the analysis made has permitted preparing proposals as to the requirements to their ice propulsion depending on class and operational conditions.

1. REQUIREMENTS OF THE MRS TO THE POWER OF ICEBREAKERS

According to the Rules of the MRS in force all the icebreakers are divided into 4 categories. Requirements to each of the above categories depend on thickness of the compact floating ice or fast ice through which an icebreaker can move and on the total shaft power. Recommended values of the ice thickness and icebreaker power are shown in Table 1.

Table 1

Requirements of the MRS to the power and thickness of ice broken through by icebreakers of different categories

Category of icebreaker	Thickness of compact ice field, m	Shaft power, kW
LL1	> 2.0	≥ 47 807
LL2	< 2.0	22 065 - 47 808
LL3	≤ 1.5	11 032 - 22 065
LL4	≤ 1.0	< 11 032

As one can see, Rules unambiguously relate thickness of the ice broken by icebreaker with power of the latter. There is no accurate definition of the icebreaking capability, no indication is given of the speed of movement through ice and it is not clear whether this ice is level one, covered with snow and what is its strength.

In practice of the domestic icebreaker building there exists a universally recognized ship ice propulsion criterion – icebreaking capability h_i under which we understand thickness of the compact level ice broken up by ship moving at a speed of about 2 knots (1 m/s). It is assumed that the ice flexural strength is at least 500 kPa and ice has natural ice cover 20-25 cm deep. The indicated value depends on several ship's parameters principal ones being the following: power, forebody shape, draft and special means increasing the icebreaking capability.

Simultaneous assignment of the icebreaking capability and power of icebreaker adopted in the MRS Rules does not seem successful. Advanced achievements in the field of the development of a traditional forebody shape of icebreakers show that at the same icebreaking capability the power of icebreaker with the improved traditional bow shape (not to mention non-traditional hull lines which is the subject of special consideration of the Register) may be reduced by up to 50 % . Conversely, at the unchanged power it is possible to raise considerably the icebreaking capability of icebreakers of different categories, for instance, from 2.0 to 2.6 m with LL2, from 1.5 to 1.9 m with LL3 and from 1.0 to 1.3 m with LL4. A nuclear icebreaker of the *Arktika* type may be considered as ship with conventional forebody lines. Effect in the modification of shape is achieved through the reduction of stem angle φ by 20-25 % as well as through the increase of two angles: entrance angle α_0 by 20-25 % and flare angle β_0 of frame line No.0 – by 50-60 %. Figure 1 shows the anticipated dependence of the shaft power upon the icebreaking capability of icebreakers with improved hull lines.

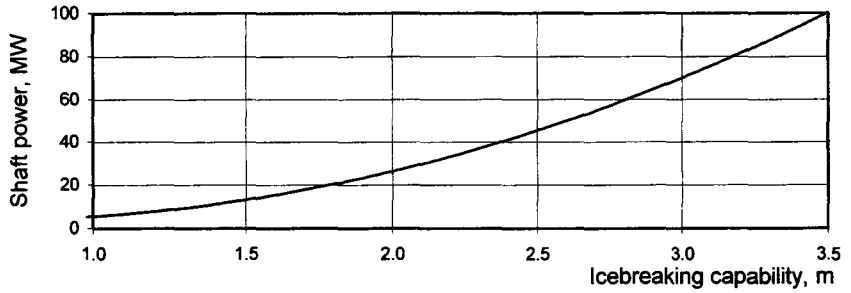

Figure1. Dependence of the shaft power on the icebreaking capability of icebreakers with improved lines

The inexpediency of regulating simultaneously icebreaking capability and power of icebreakers is also proved by the fact that, for instance, at a set icebreaking capability two icebreakers with the same hull shape but different drafts may have different values of power owing to the change of diameter of propellers and of their thrust.

For the tentative assessment of the needed shaft power N_p of icebreakers with a triple-shaft propulsion plant, depending on their icebreaking capability h_i [in metres] and draft T [in metres], the following empirical formula put forward by L.Tsoy may be used:

$$N_p = \frac{51 h_i^3}{T^{12}}, \text{MW}. \tag{1}$$

However, it is more correct to impose requirements not for the power of icebreakers, but for the icebreaking capability taking into account that the latter is a more informative characteristic of icebreaking possibilities of the ship. Accordingly the classification of icebreakers should be based on the criterion of icebreaking capability depending on the purpose and anticipated operational conditions which in turn depend on the period of navigation and area of the Arctic.

2. REQUIREMENTS OF THE RUSSIAN MRS TO THE MINIMUM POWER OF CARGO SHIPS

The MRS requirements now in force to a minimum power of ice ships (except ULA category ships) are based on the requirements to ships of baltic classes of the Finnish-Swedish Rules (FSR) which determine a minimum shaft power by the formula:

$$P_{min} = f_1 f_2 f_3 (f_4 D + P_0), \text{ kW}. \quad (2)$$

The same formula is used in the Rules of the Germanischer Lloyd (GL) and in somewhat changed form in the Rules of the American Bureau of Shipping (ABS).

Besides four coefficients it contains in an obvious way only one parameter – displacement D. Coefficients, in their turn, depend on the stem angle φ, breadth of ship B, its ice category and type of propulsion device. Parameter P_0 being a function of displacement and ice category is given in a tabulated form. Of some interest is the qualitative and quantitative influence of these parameters upon the minimum acceptable power.

Coefficients f_1 and f_2 should be considered jointly because the MRS imposes restrictions on their product. One can judge the influence of principal parameters upon these coefficients from Figure 2 obtained taking into account all the requirements and restrictions.

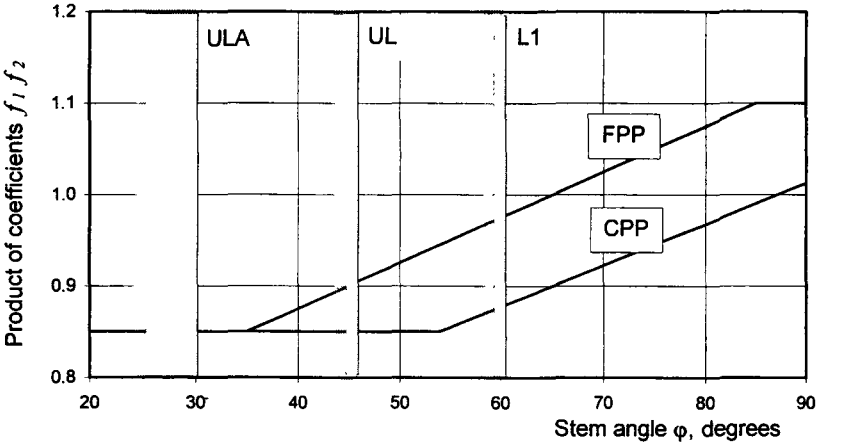

Figure 2. Influence of the stem angle on the product of coefficients $f_1 f_2$ with due account of the type of propulsion plant

The analysis shows that the influence of stem angle φ starts having an effect at values exceeding 35° for ships with fixed pitch propellers (FPP) and 54° for ships with controllable pitch propellers (CPP) which are outside the zone of recommended values. The reduction of stem angle by each degree for ships with FPP results in the decrease of minimum power only by 0.5 %; so, for example, the reduction of angle φ from 45° down to 35° will result in the decrease of minimum power by 5 %. The result obtained is inconsistent with experimental data and the experience of designing ice ships. The above reduction of stem angle under other equal conditions will lead to the increase of icebreaking capability at least by 20 % (Tsoy,

1989). This corresponds to the win of power approximately by 50 % and not by 5 % as it was obtained by the MRS recommendations.

From the point of view of the improvement of ice performance of ships the advantage of CPP against FPP does not seem apparent. It is not clear, why in the presence of CPP the reduction of minimum admissible power by 10 % is allowed. At the interaction with ice irrespective of type of the propulsion plant the thrust of propellers is reduced. In one case (CPP) it occurs through the automatic decrease of pitch, in the second (FPP) – at the expense of the reduction of the number of rpm. The CPP has a lower efficiency as well as lower thrust while moving astern. Astern / ahead movement thrust ratio with the CPP does not exceed 54-55 %, with the FPP it is 70-75 %. These disadvantages deteriorate operational capabilities of ship in ice. Therefore the reduction of power on ships fitted with propulsion plants of this type seems unjustified. Besides, in accordance with the MRS Rules only ships with UL and L1 category of ice strengthenings (Figure 2) have dependence of power upon the type of propulsion plant. However the advisability to use CPP on ships of these categories seems to be questionable both from the economical and operational points of view. The lower is the ice category of ship the shorter is its service life in ice and the less significant are advantages of CPP against FPP.

Coefficient f_3 depends on breadth B and displacement D of ship the degree of this influence being regulated by conditions:

$$1 \le f_3 = \frac{1.2\,B}{D^{1/3}}. \tag{3}$$

From relations (3), the inequality (4) presented graphically in Figure 3 may be obtained. On the same figure, values of breadth for 40 ice ships built in different years according to the MRS Rules are plotted.

$$B \ge 0.833\,D^{1/3}. \tag{4}$$

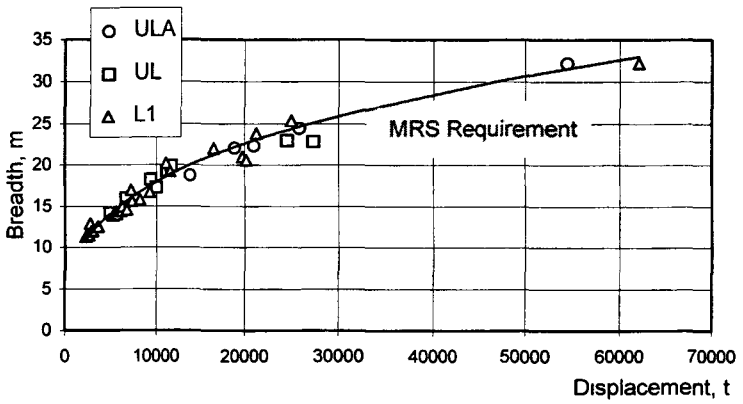

Figure 3. Ship's breadth / displacement and ice category relationship

Practically full coincidence of the MRS curve with actual values points to the fact that coefficient f_3 for ships of traditional types is always close to unity and hence its dependence on breadth and displacement does not exist.

Coefficient f_4 is more convenient to consider not separately, but as a component of multiplier $(f_4 D + P_0)$ being a part of the formula (2). This multiplier is a basic power which after correction by coefficients f_1, f_2 and f_3 becomes the investigated value P_{min}. The basic power depends on the displacement, ice category, coefficients f_4 and P_0. One can see the character of this relationship in Figure 4. The increase of displacement is accompanied by the smooth rise of the basic power: with the increase of the displacement by 1 % the basic power level increases approximately by 0.5 %.

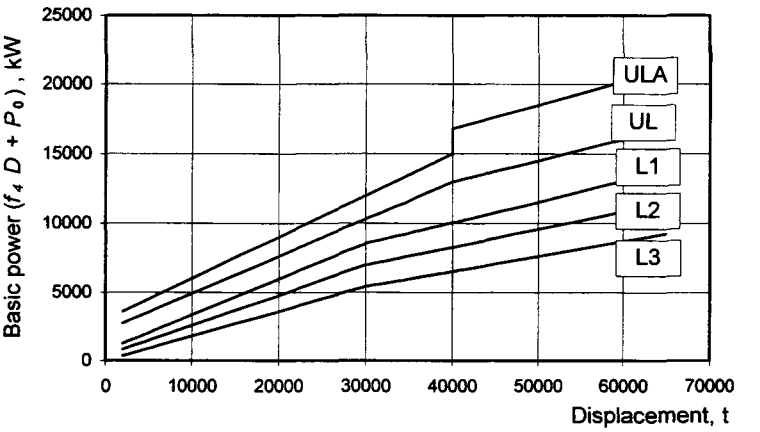

Figure 4. Dependence of the basic power of ships of different ice categories upon the displacement

Exception is the stepwise change of the basic power for ULA category ships with a displacement of 40000 t. At this point there is a break in power equal to 1800 kW. The nature of the break is not clear and it is scarcely possible to physically explain this event.

Taking into account all the components entering in the formula (2) the values of P_{min} for ULA (Figure 5) and UL (Figure 6) category ships were calculated, not only displacement, but also breadth of ship being varied. Relationships presented in the last figure have been obtained for ships with FPP and stem angle 45°. If ship is fitted with CPP the level of minimum power is reduced approximately by 6 % due to the reduction of product of coefficients $f_1 f_2$ from 0.9 down to 0.85. The attention is focused on the obtained minimum of power corresponding to a displacement of about 5000 t. Starting with this level, further reduction of the displacement contained in the formula (3) denominator is accompanied with a considerable increase of coefficient f_3.There are no restrictions in the Rules for a maximum value of this coefficient, even at D tending to zero.

Comparison of power values of domestic ULA category ships with design values obtained in accordance with the MRS requirements is shown in Figure 7. As one can see, in practice, the power of ULA category ships exceeds 1.5-2.0 times that regulated by the Rules being a result of customers imposing requirements for the icebreaking capability.

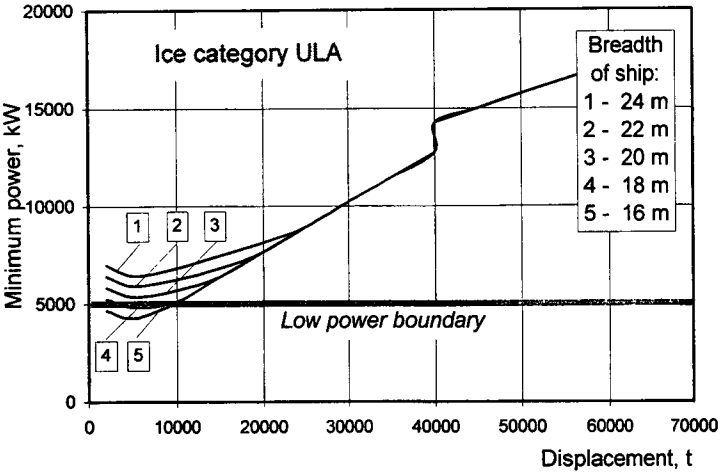

Figure 5. Minimum admissible shaft power of ships of ULA category depending on the displacement and breadth

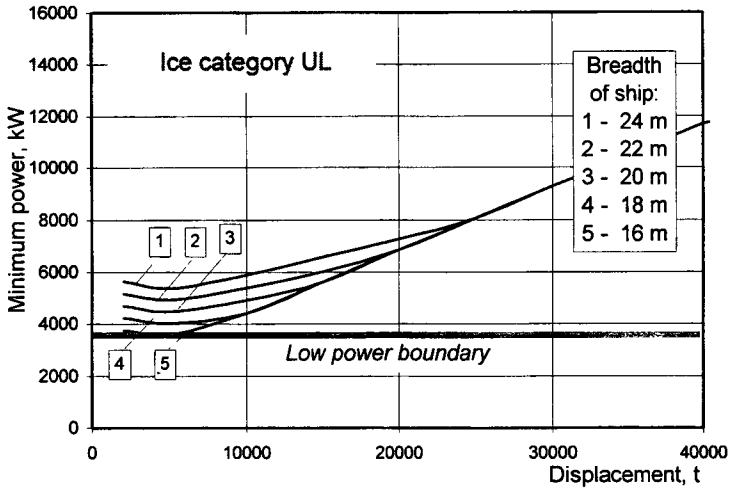

Figure 6. Minimum admissible shaft power of ships of UL category (with FPP) depending on the displacement and breadth

Really, in the domestic practice, while ordering ships of the ULA category and lately also of the UL category the request for proposal specifies the required icebreaking capability of ship. This permits for a customer to have clear ideas as to the operational possibilities of ship. Therefore the power of ships of the active ice navigation is a derivative value of the required ice propulsion depending on the assumed operational conditions in the Arctic.

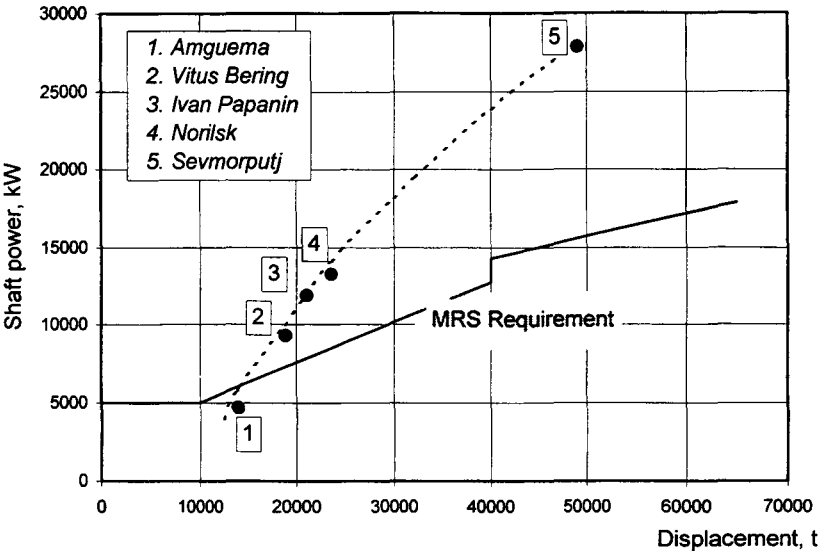

Figure 7. Comparison of the shaft power of existing ULA category ships with the level of the MRS requirements

As the experience of designing UL category ships has shown, power of these ships is mainly selected proceeding from the condition to provide for a set speed of motion in open water. Therefore in the Arctic they work exclusively escorted by icebreakers. As the practice shows, it is advisable while giving out a request for proposal for ships of this category to specify also a minimum value of the icebreaking capability assuring admissible propulsion in a channel behind the icebreaker during extended periods of the arctic navigation. On the basis of the experience this value should be at least 0.5-0.6 m.

Operation of the L1 category ships in the Arctic is allowed only in summer. As this takes place, they should possess minimum necessary ice strengthenings and have the hull shape facilitating motion through ice. The experience of the construction and operation of ships of this category shows that at the forebody characteristics recommended by the MRS Rules the icebreaking capability is 0.3-0.4 m. This permits them to satisfactorily navigate under the escort of icebreakers in freezing non-arctic seas and in easy summer ice conditions in the Arctic.

As a whole, the analysis made permits stating that the above formula for the determination of a minimum shaft power practically does not permit to take into account particular features of the ship's hull shape and accordingly does not encourage to use advanced lines reducing the required power at a given icebreaking capability.

Comparison of the MRS requirements with approaches of other classification societies, in articular, of FSR, GL and ABS, is of no interest, because power there is determined from similar formulas. Approximate correspondence of ice categories in Rules of the above societies is shown in Table 2. Ice category ULA is the exception as it has no matching foreign analogue.

Table 2

Correspondence between ice categories of different classification societies

Classification society	Ice categories			
MRS	UL	L1	L2	L3
FSR	IA Super	IA	IB	IC
GL	E4	E3	E2	E1
ABS	A1	A0	B0	C0

In the nearest future, starting in 2001, it is intended to introduce certain changes into requirements to the power of ships of 1A and 1A Super categories in the FSR. New formulas are more cumbersome, with a number of coefficients and intermediary condition:

$$20 \geq \left(\frac{L/B}{B/T}\right)^3 \geq 5. \tag{5}$$

Checking calculations by new formulas were made for 40 Russian ships of two ice categories – L1 and UL which correspond to IA and IA Super categories (Table 2). Half of these ships have a power level lower than the required one and another one-third do not comply with condition (5). The results obtained may be attributed to the fact that Russian experience was not taken into consideration in the renewal of requirements and while deducing new empirical formulas.

3. REQUIREMENTS OF DNV FOR THE POWER OF THE PROPULSION PLANT OF ICE SHIPS

Requirement of the Det Norske Veritas (DNV) Rules for power P of ice ships, contrary to the Rules considered, is based on the evaluation of the ship's ice propulsion by the overcome thickness t of the level ice at a speed of 4 knots and this seems to be logic. The power required by the DNV Rules depends also on breadth B, draft T and several coefficients:

$$P = 15\ C_x\ C_p\ C_n\ t\ B\left(1 + 1.6\ T + 27\sqrt{\frac{t}{\sqrt[4]{T}}}\right), \text{kW}. \tag{6}$$

Ice thickness t is determined as a product of factor 0.1 by a number of ice class IN (number in the class symbol). The first of coefficients accounts for the stem angle φ, the second – for type of the propulsion plant (CPP, FPP), the third – for the effect of nozzle on the thrust of propeller. When calculating coefficient C_x, the conditions (7) should be met which structurally correspond to conditions (8) for the determination of coefficient f_2 in formula (2):

$$C_x = 0.9 + \frac{\varphi}{200}, \quad \text{but} \quad 1.0 \leq C_x \leq 1.2; \tag{7}$$

$$f_2 = 0.675 + \frac{\varphi}{200}, \quad \text{but} \quad f_2 \leq 1.1. \tag{8}$$

Table 3 shows the comparison of power calculated by formula (6) with the actual shaft power of existing and future Russian icebreakers as well as of an icebreaking cargo ship of the *Norilsk* type, category ULA, moving through the level compact ice at a speed of 4 knots (coefficients C_p and C_n are equal to 1.0).

Table 3

Verification of DNV requirements to a minimum power

Name	t, m	B, m	T, m	Shaft power P, kW		Relative error, %
				calculated	actual	
Lenin	1.3	26.8	10.4	22 290	28 800	-23
Moskva	1.15	23.5	9.5	15 890	16 200	-2
Ermak	1.5	25.6	11.0	25 580	26 500	-3
Arktika	1.9	28.0	11.0	38 140	49 000	-22
Kapitan Sorokin	1.1	25.6	8.5	15 550	16 200	-4
Mudyug	0.7	20.0	6.0	6 170	9 300	-34
LK-60Ya (design)	2.4	33.0	11.0	58 920	62 000	-5
LK-110Ya (design)	3.0	40.0	13.0	100 330	100 000	0
Norilsk	0.8	24.0	9.0	10 210	13 300	-23

The tabulated figures allow to reveal not sufficiently adequate compliance of calculated values of power with actual ones and lack of any regularity in the effect of ship's hull characteristics. For instance, practically full coincidence of values for existing icebreakers *Moskva, Ermak, Kapitan Sorokin.* and prospective icebreakers has been obtained. However, the formers are of traditional and the latters of improved hull lines shape. Apparently the main reason lays in the fact that the ship's draft was not appropriately taken into account. According to calculations by formula (6), an increase of draft results in the increase of the required power. It is known, at the same time, that the increase of ship's draft allows to proportionally increase diameter of the propeller and its thrust at the invariable power. Positive influence of the increased diameter of propeller is prevailing and therefore in the evaluation of the icebreaking capability the required ship's power should decrease with the increase of draft, as it follows from formula (1). The ambiguity of the effect of draft T is due to the fact that it is present both in the numerator and in the denominator of formula (6). Direct dependence of power on the ice thickness, which can conventionally be taken as icebreaking capability, is logical. The analysis of the existing requirements to the power of ice ships has shown that these requirements are not sufficiently perfect and need in substantial corrections. From a position of the experience of navigation under ice conditions it is more correct to impose requirements not to power, but to the icebreaking capability of icebreakers and cargo ships in the fullest way reflecting their operational capabilities. This is the basis of the conclusion about the advisability to insert requirements to the icebreaking capability into international Rules on the safety of ships navigating in polar waters (Unified IACS requirements, Polar Code of IMO) being developed at present.

4. PROPOSAL TO IMPOSE REQUIREMENTS FOR A MINIMUM LEVEL OF THE ICEBREAKING CAPABILITY OF POLAR SHIPS

Subdivision of ships into polar classes presented in the Draft Code of IMO gives only some idea about the admissible safe (in respect to the ice strength) operational conditions of ships.

Long-standing experience of arctic navigations shows that ice class should characterize not only strength, but also operational capabilities of ships. While ordering a new ship, shipowner is first of all guided by operational criteria. These criteria allow him to assess the efficiency to use a future ship under the intended sailing conditions. Main criterion characterizing operational potentials of ships is the icebreaking capability. Imposing requirements to this parameter is advisable from the viewpoint of not only satisfactory operation, but also of the necessary safety under conditions specified for each class. It seems obvious that not only the efficiency, but also the safety of navigation in ice depends on the level of the ship's icebreaking capability. The corroboration of the above stated are emergency situations with ships having insufficient power levels, when the ships were driven astrand and onto rocks by ice drifting or were falling foul of each other, frozen into ice and became icebound, received dents and holes and even crushed under the ice compression. The history of polar navigation knows a lot of such cases (Smirnov, Mainagashev, Golokhvastov and Sokolov, 1993). Consequently, the ice classification of ships should make provision for the icebreaking capability determined for each class and conditions of the safe work in ice for hull structures.

The experience gained for many years in Russia of the design, construction and operation of arctic ships permits drawing up requirements to the icebreaking capability of ships depending on the polar class. Suggested values of the minimum acceptable icebreaking capability and examples of corresponding ships and icebreakers designed and built in accordance with the Rules of the MRS are presented in Table 4.

Table 4

Suggested division of ships by the minimum level of icebreaking capability depending on the polar class

Polar class	Minimum level of the icebreaking capability, m	Examples of Russian arctic ships	
		name	MRS category
PC1	3.0	• Design of the *icebreaker-leader* with a power of 110 MW	LL1
PC2	2.4	• Nuclear icebreaker *Arktika,* • Design of the nuclear icebreaker with a power of 60 MW	LL1 LL1
PC3	1.8	• Icebreaker *Ermak,* • Nuclear icebreaker *Taimyr*	LL2 LL2
PC4	1.2	• Icebreaker *Moskva,* • Icebreaker *Kapitan Sorokin,* • Barge carrier *Sevmorputj*	LL3 LL3 ULA
PC5	0.9	• Icebreaker *Mudyug,* • M/s *Norilsk,* • Electrically driven m/s *Vitus Bering,* • M/s *Ivan Papanin*	LL4 ULA ULA ULA
PC6	0.6	• M/s *Dmitry Donskoy,* • Tanker *Samotlor,* • Tanker *Ventspils*	UL UL UL
PC7	0.3	• M/s *Pioner,* • M/s *Volgoles,* • M/s *Bryanskles*	L1 L1 L1

As one can see from the table, the classification of ice ships adopted in the Draft Polar Code of IMO is in fairly good agreement with the Russian experience. It is suggested therefore to describe polar classes of ships in the Code as follows (Table 5):

Table 5

Class descriptions

Polar class	Minimum level of the icebreaking capability, m	Navigational conditions
PC1	3.0	Year-round in all polar areas of the world ocean
PC2	2.4	Year-round in moderate multi-year ice
PC3	1.8	Year-round predominantly in second-year ice
PC4	1.2	Year-round predominantly in first-year thick ice
PC5	0.9	Year-round predominantly in first-year medium ice
PC6	0.6	Summer/autumn operation in open floating ice
PC7	0.3	Summer operation in open floating ice cake

At early stages of design (prior to model tests), icebreaking capability h_i of ships with icebreaking hull lines of the traditional type (with a wedge-like forebody) may to a first approximation be determined by the following experimental and empirical formula of L.Tsoy (Tsoy, 1990):

$$h_i = \frac{0.07\sqrt{\frac{P_e}{B}}\sqrt[6]{D}\,\cos^{\frac{3}{2}}\varphi\,\sin^{\frac{1}{2}}\frac{\alpha_0+\beta_0+\beta_2}{3}}{\sqrt[5]{\frac{L}{B}}\sqrt[26]{f_d}\,\sin^{\frac{3}{2}}\left(90^0-\beta_{10}\right)}, \text{ m} \qquad (9)$$

where

φ - stem angle, deg

α_0 - entrance angle of design water line, deg

β_0 - flare angle of frame line No.0 (in the Russian practice the frame line No.0 is assumed to be at the fore perpendicular and not at the after one as it is the case abroad), deg

β_2 - flare angle of frame line No.2, deg

β_{10} - flare angle amidships, deg

L - vessel's length on DWL, m

B - vessel's breadth on DWL, m

P_e - total propeller bollard thrust, t

D - vessel's designed displacement, t

f_d - coefficient of the dynamic ice/ship's hull friction.

As the verification calculations made in their application to icebreakers and icebreaking cargo ships of the domestic and foreign construction show the suggested formula ensures fairly good agreement between calculated values of the icebreaking capability and actual ones. Relative deviations of the icebreaking capability for icebreakers *Arktika, Ermak, Kapitan Nikolaev* and of the supply vessel *Ivan Papanin* do not exceed 1 %, for icebreakers *Moskva, Kapitan Sorokin*, and *Kapitan Izmailov* - 2 %, for icebreakers *Lenin, Taimyr, Mudyug* and multi-purpose ship *Norilsk* - 3 % (Tsoy, Grechin, Karavanov, Glebko and Mikhailichenko, 1999).

5. REFERENCES

Smirnov A., Mainagashev B., Golokhvastov V., Sokolov B. Safety of navigation in ice. Moscow, Transport, 1993. 335 pages

Tsoy L. Investigations of the Effect of the Principal Dimensions Ratios and Hull Form on the Ship's Passability in Ice. *POAC 89. The 10th International Conference on Port and Ocean Engineering under Arctic Conditions*. Lulea, Sweden, June 1989. Proceedings. Vol.3. pp.1486-1492.

Tsoy L. Formula for the determination of the icebreaking capability and recommendations for the choice of hull lines of icebreakers and cargo ice ships. Collected proceedings of CNIIMF "Prospective types of sea cargo ships, their seaworthiness and ice performance". Leningrad, "Transport", 1990, pp. 141-144.

Tsoy L., Grechin M., Karavanov S., Glebko Yu., Mikhailichenko V. Arctic Environmental Law. Harmonization of Polar Ship Rules. International and National Provisions. *INSROP Working Paper* No.151-1999, IV.3.4, ISBN 82-7613-336-7, 1999, 55 pp.

LABORATORY AND FIELD STUDIES ON THE MECHANICS OF ICE RIDGE FORMATION

J. Tuhkuri, M. Lensu, S. Saarinen
Helsinki University of Technology, Ship Laboratory, Espoo, Finland

ABSTRACT

Ridges have been created in an ice basin by pushing two model ice sheets of non-uniform thickness together. All the ridging cases initiated as rafting during which the pushing force increased linearly with displacement. After the rafting phase, the ridge keel and sail started to form. During this stage the force continued to increase, but at a slower rate. The experiments also suggest that the ridging force may have a maximum value set by the horizontal strength of the ice sheet. The ridging force - ice thickness relationship has also been analysed. Field studies performed at the Northern Baltic revealed that the upper keel layer of three small ridges consisted of several layers of rafted ice and thus the field observations support the observations made during the laboratory tests.

1. INTRODUCTION

The mechanical deformation of the ice cover in northern seas takes place through ridging and rafting. The study of these processes is important because the energy expended in deformation determines the large-scale strength of the ice pack and because the horizontal stresses in the ice cover and the strength and thickness of ridges are important in the design and operation of Arctic vessels and offshore structures.

In this paper, ridging is understood as a process which occurs when two ice sheets move towards each other, ice blocks break off from the sheets and accumulate to form a pile. Rafting is here defined as a process where two ice sheets override and no piling up or down occurs. The case where several roughly horizontal layers of ice sheet lay on top of each other is also termed rafting in this work. The work reported here concentrated on formation of pressure ridges between two ice sheets of similar thickness. Such ridges are common in the Baltic Sea.

The ridging process and the related forces are not fully known, and several models have been proposed. Parmerter and Coon (1972, 1973) considered a process where two ice sheets move toward each other closing a lead filled with broken ice pieces. Kovacs and Sodhi (1980) suggested that when a moving ice sheet hits an obstacle (a pre-existing ridge or a thicker sheet) the ice sheet will first buckle and thus form ice blocks which then pile up to form a ridge. Sayed and Frederking (1984, 1986, 1988) modelled ridges as two-dimensional wedges and assumed that a critical state of the wedge simulates an actively forming ridge. Ridge formation has been studied also by using simulations. Hopkins (1994, 1998) used a two-dimensional discrete element method to study ridge formation when thin lead ice was driven against a thick floe. Recently, Hopkins et al. (1999) extended those studies by considering ridging between two sheets of equal thickness.

Ridging has also been studied in model ice tanks. In the earlier tests the ice sheet was either forced to break and accumulate against a plate or ice rubble was compressed between two ice sheets (Abdelnour and Croasdale, 1986; Timco and Sayed, 1986; Lensu and Green, 1995). Tuhkuri and Lensu (1998) were the first to report on successful laboratory tests of ridge building between two model ice sheets moving in opposite directions.

This paper will first review the ridging experiments performed and then discuss the ridging process and forces in detail. A special emphasis is on the analysis of the ridging force - ice thickness relationship. Also results from a field campaign conducted to verify the laboratory test will be introduced.

2. LABORATORY TESTS

2.1 Ice tank and model ice

The ice tank of the Ship Laboratory at the Helsinki University of Technology was used in the tests. The tank is a 40 m x 40 m water basin equipped with a cooling system and an xy-carriage. Water depth in the basin is 2.8 m. The x-carriage has a span of 40 m and is mounted on rails along the two sides of the basin. A smaller y-carriage hangs under the x-carriage and is mounted on round steel rails. The model ice currently used is granular fine grained ice (Jalonen and Ilves 1990). The model ice is produced by spraying a mixture of ethanol (~ 0.4 %) and water into air from nozzles mounted on the x-carriage while the carriage is moving at a constant velocity back and forth across the basin. The flexural and crushing strengths and the Young's modulus of each ice sheet used in the tests were measured. The flexural strength was determined from cantilever beam tests. Also the crushing (or compressive) strength was determined by using cantilever beams. The crushing strength was therefore measured only in-plane. The Young's modulus was determined by the plate deflection method.

2.2 Experimental set-up

The key element of the experiments was the use of model ice sheets with non-uniform thickness. Such ice sheets were produced in two stages. First an ice sheet was produced and broken into approximately square shaped floes which were randomly distributed across the tank. In the tests analysed here, the size of the floes was 500 mm x 500 mm. No ice was removed, but as some of the floes were pushed on top of the others, areas of open water were created. Then another ice sheet was produced on top of the floes. In the resulting ice sheet floes of thickness t_1 were embedded into a matrix with thickness t_2.

Figure 1 shows a sketch of the experimental set-up. A 6.0 m wide area of non-uniform ice was cut loose from the surrounding ice sheet by cutting parallel slots, leaving the far end uncut. Then the strip was divided into two parts by making a transverse cut. A 5.3 m wide pusher plate was placed against the free end. During an experiment the strip was compressed at a constant velocity with the pusher plate and the ridge formation was monitored. The ridge initiated at the transverse cut. The load on the pusher plate and its displacement were measured. Detailed description of the test method is given by Tuhkuri and Lensu (1998).

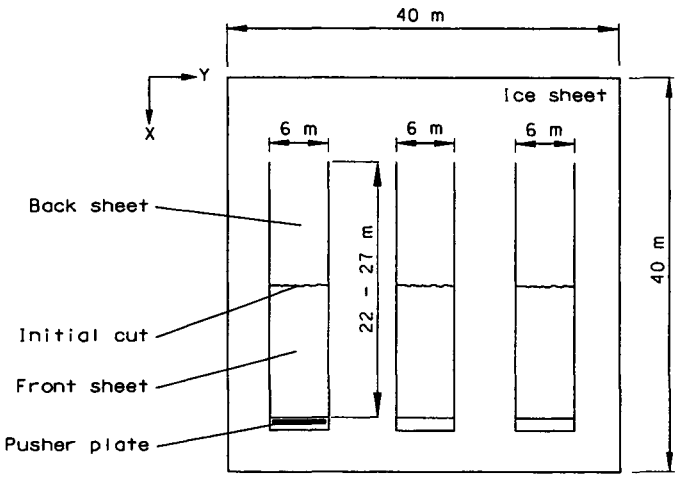

Figure 1. Experimental set-up. During a test the front sheet is pushed against the back sheet by the pusher plate.

2.3 Test results

Altogether 44 ridging or rafting tests have been conducted in three sets. Results from the two first sets have been reported by Tuhkuri and Lensu (1998) and Tuhkuri et al. (1998). Results from the third set are reported here. In this last group of tests, the ice thickness was systematically varied in order to find the ridging force - ice thickness relationship.

The main result of the whole test series is that for the first time ridges were created in an ice tank by pushing two ice sheets together. This was achieved by introducing a novel test parameter, the thickness ratio t_2/t_1. Ice sheets with uniform thickness ($t_2/t_1 = 1$) only rafted, but when t_2/t_1 was less than one, also ridges formed. A common feature for all the tests was initial rafting. In the beginning of each experiment the two ice sheets always rafted at the initial transverse cut. In some cases this rafting was finger rafting and in other cases simple rafting. When t_2/t_1 was large, this rafting continued for the whole test duration, but when t_2/t_1 was small, the initial rafting transformed into a ridging process. Figure 2 shows sketches of the observed four deformation types which can be described as follows:

A: After initial finger rafting, a ridge with both keel and sail formed. Type A ridges had a more or less sinusoidal shape, which means that both pressure and shear zones formed.
B1: After initial finger rafting the lower ice sheets failed and gradually formed rubble piles under each finger. No clear sail formed.
B2: Similar to B1 except that the deformation started as simple rafting and no fingers formed.
C: Only simple rafting and no rubble formation.

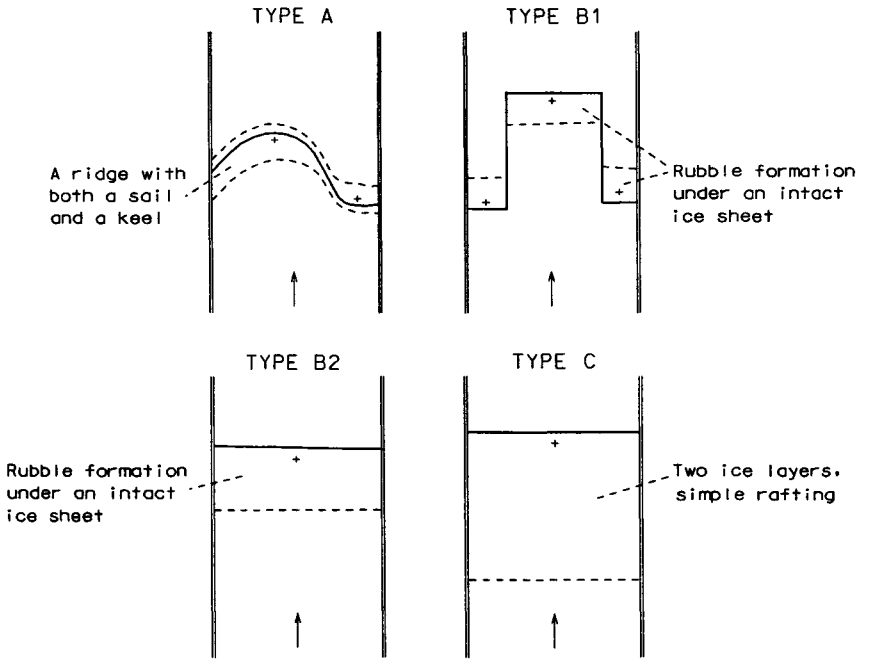

Figure 2. Sketces of the observed deformation types. Top views of the 6 m wide ice strips are shown. The dashed lines show extent of keel of overlap. + refers to an ice sheet on top and arrows to direction of movement.

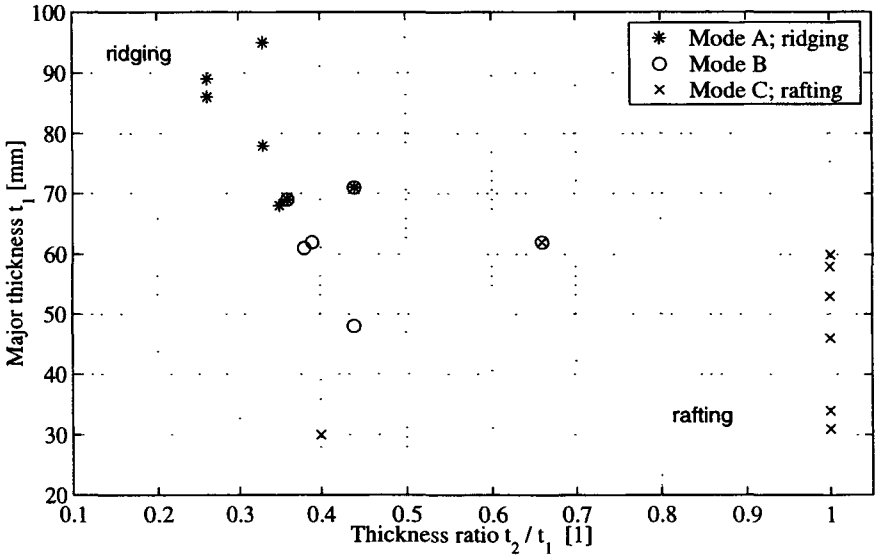

Figure 3. The observed ice cover deformation modes (Figure 2) as a function of the thickness ratio t_1/t_2 and the major thickness t_1.

Table 1. Test variables. The ice sheet consisted of ice floes with thickness t_1 embedded in matrix with thickness t_2. $\sigma_{f\downarrow}$ and $\sigma_{f\uparrow}$ are flexural strengths downwards and upwards, respectively, and E is Young's modulus. $\sigma_{f\downarrow}$, $\sigma_{f\uparrow}$ and E were measured from the surrounding ice sheet with thickness t_2. Type is the deformation type illustrated in Figure 2.

t_2/t_1 [mm]	Tests	t_2/t_1 [1]	v [mm/s]	$\sigma_{f\downarrow}$ / $\sigma_{f\uparrow}$ [kPa]	E [MPa]	Type
31/95	28, 29	0.33	12.3	10.0/21.5	27.4	A
26/78	36, 38	0.33	11.8	12.3/11.4	63.7	A
31/71	18, 20	0.44	10.1	22.1/31.1	130	A, B2
21/48	31, 32	0.44	10.9	37.4/47.7	368	B2
12/30	34, 35	0.40	10.8	51.0/42.2	243	C

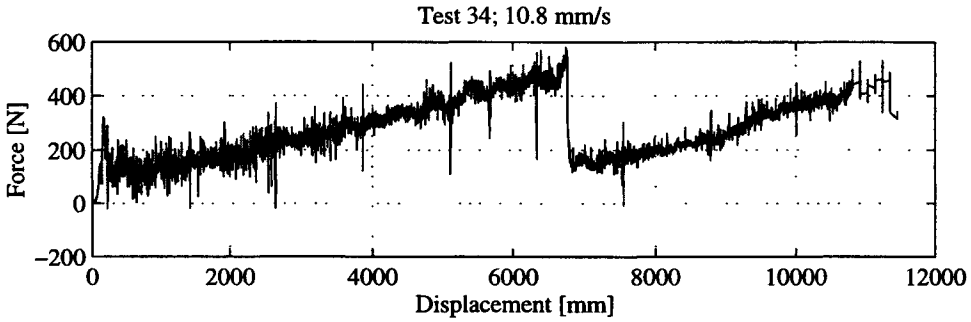

Figure 4. The force-displacement record of Test 34. The ice sheets rafted into three layers.

Only Type A ridges had a clear sail. From above, as in Figure 2, Type B formations look just like rafting even though there are large keels under the ice sheets on top.

Figure 3 shows that in addition to the thickness ratio t_2/t_1 also the major thickness t_1 effects the deformation mode. When $t_2/t_1 = 1$ or when the ice was thin, rafting only occurred. Analogously, low value of t_2/t_1 and thick ice favoured Mode A deformation. Type B ridges were obtained in the intermediate cases. Hopkins et al. (1999) have obtained the same result earlier by using the discrete element method.

As examples of the rafting and ridging processes, two tests are described here. Some test variables are listed in Table 1. The force-displacement record of Test 34 is shown in Figure 4. Test 34 started as Type C rafting when the front sheet went under the back sheet at the initial cut. This rafting continued until displacement x of the pusher plate was about 6.8 m. Then the front sheet failed under the back sheet and started to raft a third layer under the second layer. This interpretation of the rafting process was verified after the test with an underwater camera and is also indicated by the force-displacement record (Figure 4). The rafting force F increased linearly with displacement until the ice sheet failed and the load dropped abruptly. With continued rafting, the force again increased linearly. The extreme force drop at $x \approx 6.8$ m is linked with the front sheet failure over the whole width of the sheet. In other tests where the ice sheet failures were more local, such extreme force fluctuations were not observed. In other words, this Test 34 was kind of two-dimensional.

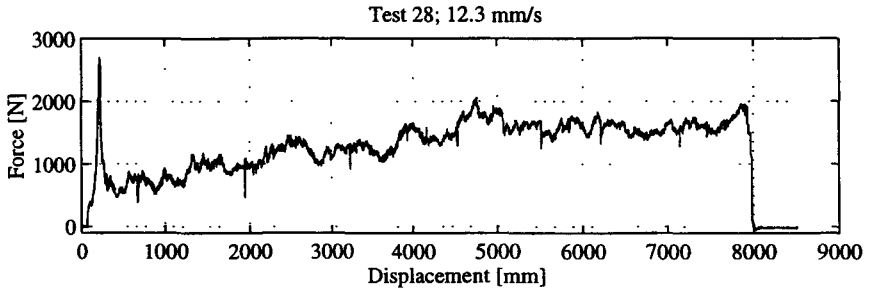

Figure 5. The force-displacement record of Test 28. A Type A ridge formed.

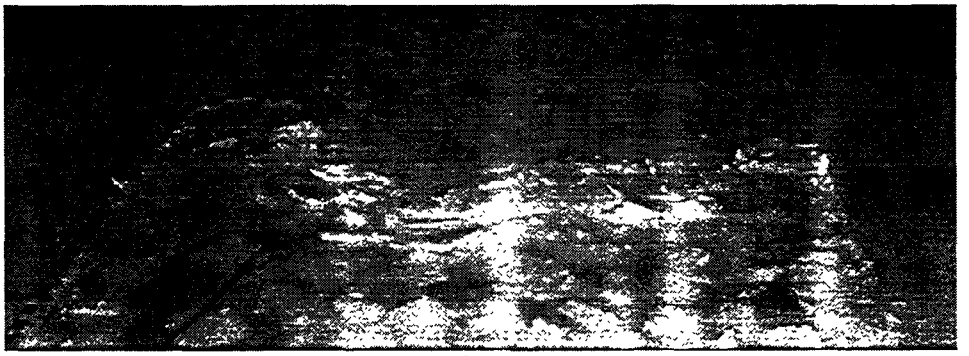
Figure 6. Photograph of the Type A ridge formed during Test 28.

A force-displacement record of a Type A ridging process is shown in Figure 5 (Test 28). Similarly with the rafting case shown in Figure 4, there is an initial force peak followed by a linearly increasing force. It is also typical to these tests that some force level is needed to start the process. The experiments suggest that the linear F-x record in the beginning of a test is due to an initial rafting phase. The rafting phase ends when usually a lower ice sheet starts to pile down to form a keel. During this phase the force continues to grow, albeit at a lower rate than during the rafting phase. In the later stages of a ridging process also a sail can grow and the order of overlapping can alternate. Finally, Figure 5 suggests that the ridging force reaches a maximum level towards the end of the test and then maintains that level. There is some visual evidence, that this force level is related to the horizontal strength of the ice sheet. A photo taken after Test 28 is shown in Figure 6. The test was stopped when the longitudinal crack formed in the front sheet.

Figure 7 shows the effect of ice thickness on the ridging/rafting force. The data for t_1 = 30 mm is from Test 35, but the data for the thicker sheets are each average values of two tests as listed in Table 1. Both the force needed to initiate a ridging process and the ridging force are increasing with ice thickness. The same data is also shown in Figure 8 where the data points are average forces during a displacement of 100 mm. The lower and upper groups of points are the average forces for the displacement ranges 1000 mm $< x <$ 2000 mm and 6000 mm $< x <$ 7500 mm, respectively. Also shown are a first order polynomial fitted to the lower group and a second order polynomial fitted to the upper group. Both curves show a rather good fit. The data suggest thus that, during the initial stages of the ridging processes, the

force-thickness relationship is linear. This is in line with the observation that ridging processes always start as rafting. The data give also some support to an assumption that during the later stages of ridging the force-thickness relationship is non-linear.

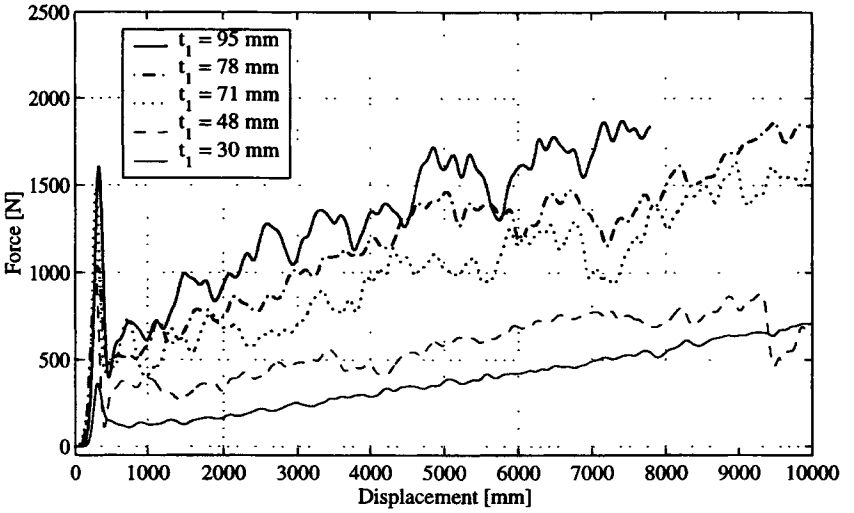

Figure 7. The force-displacement records from tests with different ice thicknesses t_1. The signals are low pass filtered at $0.02f_N$, where f_N is the Nyquist frequency.

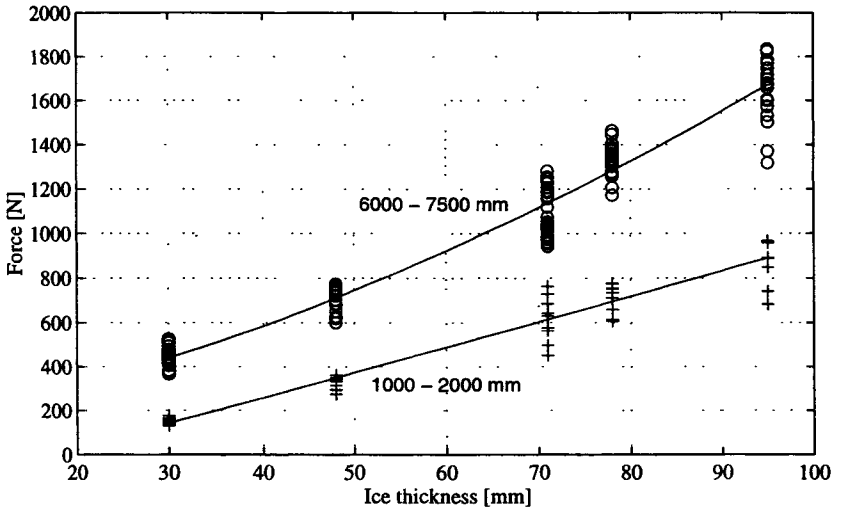

Figure 8. The ridging force shown in Figure 6 as function ice thickness. The data points are average forces during a displacement of 100 mm. Two ranges of displacement x are shown. A first order polynomial is fitted to the lower group of data and a second order polynomial to the upper group.

3. FIELD STUDIES

One of the novel observations of the laboratory tests was that rafting is an important part of all the ridging events. If ridges in nature form the same way, a part of a ridge cross-section should have rafted layers of the parent sheet. There is evidence that in some ridges this in fact is the case. Kankaanpää (1997) studied thin sections made from samples taken from two Baltic ridges. The thin sections showed that in one ridge there were two and in the other four to five rafted layers.

In order to further study this hypothesis, a field campaign was arranged in the Northern Baltic in March 1999. The site was located a few NM west from the Marjaniemi lighthouse at Hailuoto island. Strong northerly winds made a wide lead to the site earlier in the season and initiated growth of a new ice sheet. When this sheet was about 80 mm thick, strong southerly winds caused ridge formation. At the time of the field studies, the level ice was about 300 mm thick.

The goal of the field program was to study the internal structure of the ridges. Three ridges were studied. First a cross-section was measured by drilling holes with 51 mm ice auger along linear transsects crossing the sail and keel and extending to the level ice on both sides of the ridge. The surface elevation was measured with a rotating beam laser levelling device. After these measurements a trench was excavated through the ridge sail and the sail structure was visually observed. The third step of the work was to cut with a chain saw two parallel slots crossing the consolidated layer and keel. In this way a "thick section" through the ridge was obtained. This thick section, which was about 200 mm thick, was further cut into about 500 mm long pieces which were lifted up from the water and the thick section was reconstructed on the level ice. The blade length of the chain saw was 1.2 m which was enough to cut through the consolidated layer. Where clearly visible, the block structure of the consolidated layer was enhanced by a marker. The sections were then photographed and figures of the block structure were drawn based on the photos.

Figure 9 shows two ridge cross-sections measured. The figure shows clearly that the ridge formations have included a large amount of rafting. At least five rafted ice layers are visible on the left side of the ridges. Both the cross-sections are clearly non-symmetric. While the left sides contain continuous (long) rafted ice sheets, the right sides contain smaller ice blocks which are not that clearly organised. The shore is on the right side of these ridges and thus it is apparent that the left hand sheet has been the underthrusting one.

Apart from the internal structure of the ridges it is interesting *per se* that the ridges were formed from ice which was only 80 mm thick. The classical model by Parmerter (1975) states that there is a crossover ice thickness between ridging and rafting. Ice sheets which are thinner than the crossover thickness will raft and ice sheets thicker than the crossover thickness will ridge. Parmerter suggested that the crossover thickness is about 170 mm.

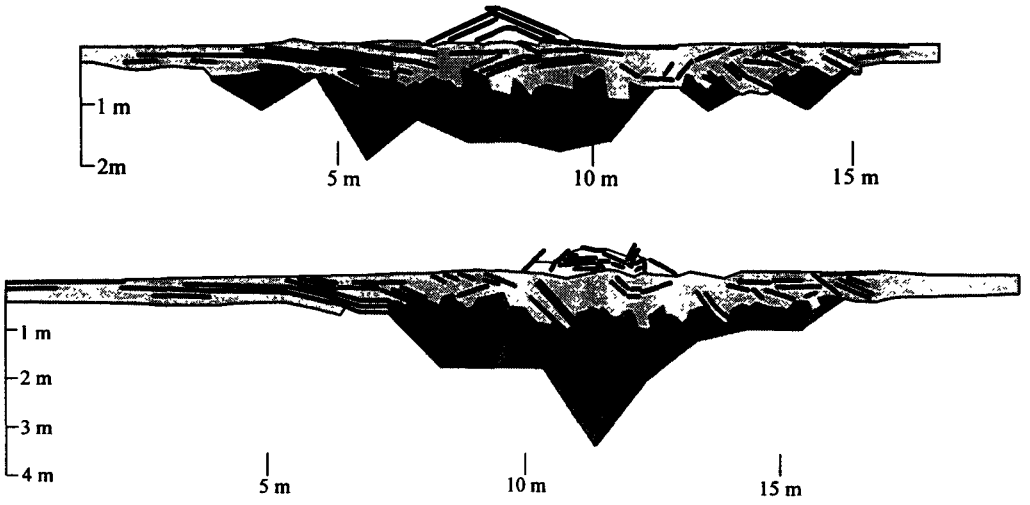

Figure 9. Cross sectional profiles of two ridges. The ridges were formed from the 80 mm thick ice shown with the thick black lines. This parent ice has been marked only clearly discernible within the consolidated layer. The light gray area is the consolidated layer cut loose and lifted up from water. Other dimensions were measured by drilling and levelling.

4. DISCUSSION

Based on the laboratory ridging tests, Tuhkuri and Lensu (1998) have formulated a simple ridging model sketched in Figure 10. After a threshold force value F_0 is reached, the initial rafting starts and continues as long as the sheets sustain the pushing force, which increases linearly with displacement. It is assumed that after displacement of l_R the lower ice sheet starts to fail and pile down. Due to the curvature needed to raft the two sheets, the lower sheet may be pre-broken. When the block piling starts, a rafting process transforms into a ridging process. The exact pile down process is not known, but it may include rafting of additional layers and sheet ride down along the keel slope (Figure 9). Some ice blocks will also ride up to form a sail. It can be assumed that with increasing depth of the rubble, higher force is needed to add blocks into the keel. At some stage this piling force may become high enough to break the ice sheet at another location and initiate ridging there, or alternatively the keel may start growing laterally. This stage defines the maximum force F_{MAX}.

In this model, the ridging force is assumed to be below the line defined by F_0, $\partial F/\partial x$, and F_{MAX}. The key elements of this model are that $\partial F/\partial x$ is set by rafting, that a maximum ridging force F_{MAX} exists, and that F_{MAX} is set by properties and failure process of the ice sheet surrounding the ridge and not by deformation of the ridge itself.

What are then the parameters that determine whether initial rafting transforms into ridging? In the laboratory test the key parameter was the non-uniform thickness. However, it is not claimed that ridges form only from ice sheets with non-uniform thickness, but rather that some sort of inhomogeneity of ice is an important factor. Thus the non-uniform thickness should be seen as a test method to model real inhomogenous ice sheets. Inhomogenous ice

may have rough surfaces, weak zones, and discontinuities in stress distribution, all contributing to short length of overlap before keel formation. In the experiments, one obvious effect of the non-uniform thickness was that the areas of thinner ice acted as weak zones in the ice sheets.

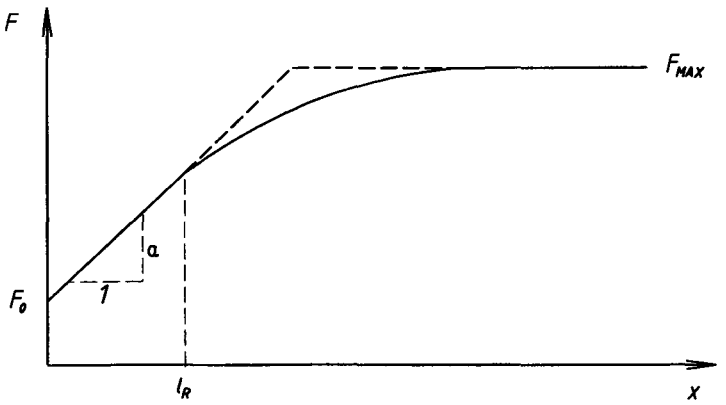

Figure 10. Schematic presentation of the force-displacement relation $F(x)$ according to the proposed ridging model.

5. CONCLUSIONS

The objective of the experimental work reported here was to study the ridge formation process. During each test a 6 m wide sheet of model ice was pushed against another similar ice sheet and both rafting and ridging were observed. Model ice sheets with non-uniform thickness were used in the tests.

All the tests initiated as rafting during which the pushing force increased linearly with displacement. After the rafting phase, the ridge keel and sail started to form. During this stage the force continued to increase, but at a slower rate. The transition from rafting to ridging (onset of ridging), was a function of both the ice thickness and the thickness ratio. The thicker the ice and the lower the thickness ratio were, the higher was the probability to obtain ridges. The experiments suggested that during the early stages of ridging, the ridging force - ice thickness relationship is close to linear. The data gave further some support to an assumption that during the later stages of ridging the force-thickness relationship is non-linear. There is also evidence that the ridging force may have a maximum value set by the horizontal strength of the ice sheet.

One of the key results from the laboratory experiments was that rafting is a central part of ridge formation. In order to verify this result, field studies were performed at the Northern Baltic. The field work revealed that consolidated layer of the three ridges studied consisted of several layers of rafted ice and thus the field observations support the observations made during the laboratory tests.

ACKNOWLEDGEMENTS

This work described here is part of the project "Local Ice Cover Deformation and Mesoscale Ice Dynamics" supported by the European Commission, DG XII, through the MAST III programme. The partners in the project were the Ship Laboratory, Helsinki University of Technology, Finland; Nansen Environmental and Remote Sensing Center, Norway; Scott Polar Research Institute, University of Cambridge, UK; Department of Geophysics, University of Helsinki, Finland; and Engineering Research Institute, University of Iceland, Iceland.

REFERENCES

Abdelnour, R. and K. Croasdale 1986. Ice forces associated with ridge building: Model tests and results compared with theoretical models. Proc. of *IAHR Ice Symp.* Iowa City, Vol. 3, pp. 227-245.

Hopkins, M.A. 1994. On the ridging of intact lead ice. *Journal of Geophysical Research*, 99, C8, 16351-16360.

Hopkins, M.A. 1998. Four stages of pressure ridging. *Journal of Geophysical Research*, 103, C10, 21883-21891.

Hopkins, M.A., Tuhkuri J. and Lensu, M. 1999. Rafting and ridging of thin ice sheets. *Journal of Geophysical Research*, (in press).

Jalonen, R. and L. Ilves 1990. Experience with a chemically-doped fine-grained model ice. Proc. of *IAHR Ice Symp.* Espoo, Vol. 2, pp. 639-651.

Kankaanpää, P. 1997. Distribution, morphology and structure of sea ice pressure ridges in the Baltic Sea. *Fennia*, 175:2, pp. 139-240.

Kovacs, A. and Sodhi, D.S. 1980. Shore ice pile-up and ride-up: Field observations, models, theoretical analyses. *Cold Regions Science and Technology*, 2, 209-288.

Lensu M. and Green J. 1995. Ice tank tests on pressure ridge formation. Espoo, *Helsinki University of Technology, Ship Laboratory*, Report M-202. 83 p.

Parmerter, R.R. 1975. A model of simple rafting in sea ice. *Journal of Geophysical Research*, 80, 15, 1948-1952.

Parmerter, R.R. and Coon, M.D. 1972. Model of pressure ridge formation in sea ice. *Journal of Geophysical Research*, 77, 33, 6565-6575.

Parmerter, R.R. and Coon, M.D. 1973. Mechanical models of ridging in the Arctic sea ice cover. *AIDJEX Bulletin* 19. 112 p.

Sayed, M. and Frederking, R.M.W. 1984. Stresses in first-year ice pressure ridges. In: Proc. of the 3rd *OMAE* Symp., New Orleans, USA, Vol. III, pp. 173-177.

Sayed, M. and Frederking, R.M.W. 1986. On modelling of ice ridge formation. In: Proc. of *IAHR Ice Symp.* 1986, Iowa City, USA, Vol. 1, pp. 603-614.

Sayed, M. and Frederking, R.M.W. 1988. Model of ice rubble pileup. *Journal of Engineering Mechanics*, 114, 149-160.

Timco, G.W. and M. Sayed 1986. Model tests of the ridge-building process of ice. Proc. of *IAHR Ice Symp.* Iowa City, Vol. 1, pp. 591-602.

Tuhkuri, J. and Lensu, M. 1998. Ice tank tests on ridging of non-uniform ice sheets. Espoo, *Helsinki University of Technology, Ship Laboratory*, Report M-236. 130 p.

Tuhkuri, J., Lensu, M. and Hopkins, M. 1998. Laboratory and field studies on ridging of an ice sheet. Proc. of the 14th International Ice Symposium, IAHR '98, Vol 1, Balkema, Rotterdam. pp. 397-404.

LIST OF POAC'99 PARTICIPANTS

Andersin John
Wärtsilä NSD
Finland

Arpiainen Matti
Kvaerner Masa-Yards
Finland

Backman Anders
Swedish Maritime Administration
Sweden

Baffer Bruce
Great Lakes Icebreaking Capability Project
US Coast Guard
USA

Betz Graden
Marathon Oil Company
USA

Bohle-Carbonell Martin
European Commission
Belgium

Bäckström Magnus
Kvaerner Masa-Yards
Finland

Cheng Bin
Finnish Institute of Marine Research
Finland

Dalen Øyvind
Nansen Environmental and Remote
Sensing Center
Norway

Dempsey John
Clarkson University
United States

Doble Martin
Scott Polar Research Institute
United Kingdom

Eronen Harri
ILS Oy
Finland

Evers Karl-Ulrich
Hamburgische Schiffbau-Versuchsanstalt
Germany

Forsén Ann-Christin
Kvaerner Masa-Yards
Finland

Fournier-Sicre Alain
European Space Agency Permanent
Mission in RF
Russia

Fransson Lennart
Luleå University of Technology
Sweden

Frederking Robert
Canadian Hydraulics Centre
National Research Council
Canada

Gagnon Robert
Institute for Marine Dynamics
Canada

Garipov Valery
Russian Federation Ministry of Fuel and
Energy
Russia

Gill Rashdal S.
Danish Meteorological Institute
Denmark

Goldstein Robert
Institute for Problems in Mechanics
Russian Academy of Sciences
Russia

Granfelt Peter
Helsinki University of Technology
Finland

Grönvall Hannu
Finnish Institute of Marine Research
Finland

Gudmestad Ove T.
Statoil
Norway

Gudoshnikov Yuri
Arctic and Antarctic Research Institute
Russia

Haapala Jari
University of Helsinki
Finland

Haapasaari Heli
Finnish Environment Institute
Finland

Haapio Antti
Meriturva Ship Simulation Unit
Finland

Haas Christian
Alfred Wegener Institute
Germany

Hagelstam Lennart
Finnish Maritime Administration
Finland

Hansen Edmond
Norwegian Polar Institute
Norway

Harjula Arjo
Finnish Maritime Administration
Finland

Haukioja Risto
Helsinki University of Technology
Finland

Hayward Richard
Germanisher Lloyd
Germany

Heideman Torsten
Kvaerner Masa-Yards
00560 Helsinki

Heinonen Jaakko
Helsinki University of Technology
Finland

Hellman Jens-Holger
Hamburg Ship Model Basin
Germany

Hietala Kaisa
Fortum Oil and Gas
Finland

Holttinen Hannele
VTT Energy
Finland

Hopkins Mark
US Army Cold Regions Research and
Engineering Laboratory
USA

Hoseth Knut Aune
Norwegian Water Resources and Energy
Directorate
Norway

Høyland Knut Vilhem
Norwegian University of Science and
Technology
Norway

Ivanov Ivan
Fortum Oil and Gas
Finland

Izumiyama Koh
Ship Research Institute
Japan

Jeffers Sharon
Canadian Ice Service
Canada

Jensen Arnor
Norwegian University of Science and Technology
Norway

Jevrejeva Svetlana
Estonian Meteorological and Hydrological Institute
Estonia

Johannessen Kenneth
Statoil
Norway

Johannessen Ola M.
Nansen Environmental and Remote Sensing Center
Norway

Juurmaa Kimmo
Kvaerner Masa-Yards
Finland

Kalliosaari Simo
Finnish Institute of Marine Research
Finland

Kannunikov Vjatsheslav
Gazprom
Russia

Karaminas Lefteris
Lloyd's Register of Shipping
United Kingdom

Karjalainen Markus
Fortum Oil and Gas Ltd
Finland

Karvonen Juha
Finnish Institute of Marine Research
Finland

Kasatkin Georgi
LUKoil
Russia

Kato Kazuyuki
Ishikawajina-Harima Heavy Industries Co. Ltd
Japan

Kioka Shinji
Hokkaido University
Japan

Kitagawa Hiromitsu
Hokkaido University
Japan

Kivimaa Seppo
VTT Manufacturing Technology
Finland

Korkiakoski Matti
Kamewa Finland Ltd
Finland

Koskinen Pekka
VTT Manufacturing Technology
Finland

Kotisalo Kimmo
Helsinki University of Technology
Finland

Kovacs Austin
Kovacs Enterprises
USA

Krjukov Anatoli
Sojuzmorgeo, Nilmorgeofizika
Russia

Kyröhonka Jukka
Kymenlaakso Polytechnics
Finland

Kyyrö Kari
Aker Finnyards Oy
Finland

Kämäräinen Jorma
Finnish Maritime Administration
Finland

Kärnä Tuomo
VTT Building Technology
Finland

Köhler Peter
Seatechnology Finland Ltd
Finland

Laasonen Juha
VTT Manufacturing Technology
Finland

Laiho Liisa
Ministry of Trade and Industry
Finland

Lehmus Eila
VTT Building Technology
Finland

Leiviskä Topi
Helsinki University of Technology
Finland

Lensu Mikko
Helsinki University of Technology
Finland

Leppäranta Matti
University of Helsinki
Finland

Li Zhijun
Dalian University of Technology
China

Liljeström Göran
Bureau ODEN AB
Sweden

Lindroos Harry
Wärtsilä NSD Corporation
Finland

Lohi Paavo
Aker Finnyards Oy
Finland

Lundqvist Jan-Eric
Swedish Metereological and Hydrological
Institut
Sweden

Lönnroth Nadja
University of Helsinki
Finland

Løset Sveinung
Norwegian University of Science and
Technology
Norway

Maddock William
Sandwell Engineering Inc.
Canada

Maillet André
Canadian Coast Guard
Canada

Makkonen Lasse
VTT Building Technology
Finland

Malovitski Jankif
Sojuzmorgeo
Russia

Matishov Gennadi
Murmansk Marine Biological Institute
Russia

Matskevitch Dmitri
Exxon Production Research Co.
United States

Mattila Markku
Kamewa Finland Ltd.
Finland

Mattsson Tom
Kvaerner Masa-Yards
Finland

Mazurkiewicz Boleslaw
Technical University of Gdansk
Poland

Mikhailichenko Vladimir
Ministry of Transport
Russia

Mironov Yevgeny
Arctic and Antarctic Research Insitute
Russia

Multala Jukka
Geological Survey of Finland
Finland

Mäkinen Eero
Kvaerner Masa-Yards
Finland

Mäkynen Marko
Helsinki University of Technology
Finland

Mälkki Pentti
Finnish Institute of Marine Research
Finland

Määttänen Mauri
Helsinki University of Technology
Finland

Naumov Alexei
Arctic and Antarctic Research Institute
Russia

Nemchinov Alexander
Kvaerner Masa-Yards, Moscow
Russia

Niini Mikko
Kvaerner Masa-Yards
Finland

Nortala-Hoikkanen Anita
Kvaerner Masa-Yards
Finland

Nyman Tapio
VTT Manufacturing Technology
Finland

Ohtsuka Natsuhiko
Hokkaido University
Japan

Okko Olli
VTT Communities and Infrastructure
Finland

Osipenko Nikolaj
Institute for Problems in Mechanics
Russian Academy of Sciences
Russia

Ovsienko Sergei
State Oceanographic Institute
Russia

Palaghian Liviu
Dunarea De Jos' University
Romania

Patey Matthew
Helsinki University of Technology
Finland

Pettersson Lasse H.
Nansen Environmental and Remote Sensing Center
Norway

Ple Olivier
Ecole Normale Supérieure de Cachan
France

Prinsenberg Simon
Bedford Institute of Oceanography
Canada

Pääkkö Kari
Ministry of Trade and Industry
Finland

Ranki Erkki
Kvaerner Masa-Yards
Finland

Riska Kaj
Helsinki University of Technology
Finland

Rybtshevski Igor
Minnauki
Russia

Rytkönen Jorma
VTT Manufacturing Technology
Finland

Saarinen Sami
Helsinki University of Technology
Finland

Sackinger William M.
Obelisk Hydrocarbons (Alaska) Ltd.
USA

Sandkvist Jim
SSPA Maritime Consulting Ab
Sweden

Savikurki Jarmo
Kamewa Finland Ltd.
Finland

Schwarz Joachim
Hamburgische Schiffbau-Versuchsanstalt
Germany

Seinä Ari
Finnish Institute of Marine Research
Finland

Sheinberg Rubin
Naval Architecture Branch
US Coast Guard
USA

Shkhinek Karl
St. Petersburg State Technical University
Russia

Shpigunov Gennadiy
Primorsk Shipping Corporation
Russia

Siirilä Timo
ILS Ltd
Finland

Smith Orson
University of Alaska Anchorage
United States

Soininen Harri
VTT Manufacturing Technology
Finland

Soldatov Juri
Rosshelf
Russia

Stanislav Rogachko
Moscow State University of Civil Engineering
Russia

Stepanov Igor
Arctic and Antarctic Research Institute
Russia

Suojanen Reko-Antti
Kvaerner Masa-Yards
Finland

Suslova Tatjana
European Space Agency Permanent Mission in RF
Russia

Tellefsen Terje P.
DSND
Norway

Tezov Dennis
Norwegian University of Science and Technology
Norway

Thor Sven-Erik
Aeronautical Research Institute of Sweden
Sweden

Timco Garry
Canadian Hydraulics Centre
National Research Council
Canada

Tshursina Natalia
Rosshelf
Russia

Tsoi Loly
Central Marine Research and Design Institute CNIIMF
Russia

Tuhkuri Jukka
Helsinki University of Technology
Finland

Usami Norihiro
Hokkaido University
Japan

Uto Shotaro
Ship Research Institute
Japan

Uuskallio Arto
ABB Azipod Oy
Finland

Vainio Jouni
Finnish Institute of Marine Research
Finland

Valanto Petri
Hamburgische Schiffbau-Versuchsanstalt
Germany

Weiss Jérôme
Laboratoire de Glaciologie et Géophysique de l'Environnement
CNRS
France

Veitch Brian
Memorial University of Newfoundland
Canada

Veldman Aalko
Wagenborg Kazakhstan B.V
Netherlands

Weydert Marco
European Commission
Belgium

Wilkman Göran
Kvaerner Masa-Yards
Finland

Voutilainen Esko
Fortum Oil and Gas
Finland

Yakovlev Anatoly
Central Marine Research and Design
Institute CNIIMF
Russia

Zubakin Gennadi
Arctic and Antarctic Research Institute
Russia

LIST OF CONTRIBUTIONS FROM THE LOLEIF PROJECT

The following papers presented at the POAC '99 Conference have been produced within the LOLEIF-Project in the framework of the EU-sponsored Marine Science and Technology (MAST III) Programme under Contract No. MAS3-CT-97-0078:

1. "Monitoring and observation of the formation of a first-year ice ridge field" by Høyland, K.V. and Løset, S.

2. "Experiments and preliminary simulations of the consolidation of a first-year sea ice ridge" by Høyland, K.V. and Løset, S.

3. "The ductile behaviour of damaged ice under compression" by Weiss, J.

4. "Non-universal scaling of arctic fractures" by Dempsey, J.P. and Palmer, A.C.

5. "An overview of the influence of structure width and ice thickness on the global ice load" by Løset, S., Shkhinek, K. and Uvarova, E.

6. "Numerical simulation of the ice failure process" by Shkhinek, K., Kapustiansky, S., Jilenkov, A. and Kärnä, T.

7. "An analysis of crack nucleation during creep of S2 columnar ice under uniaxial compression" by Meyssonnier, J. and Plé, O.

8. "Simulating ridge keel failure with finite element method" by Heinonen, J.

Dr. Joachim Schwarz
Coordinator of the LOLEIF project.

Jens–Holger Hellmann (left), Karl–Ulrich Evers, Stephanie Collatz, Teresa Sheinberg

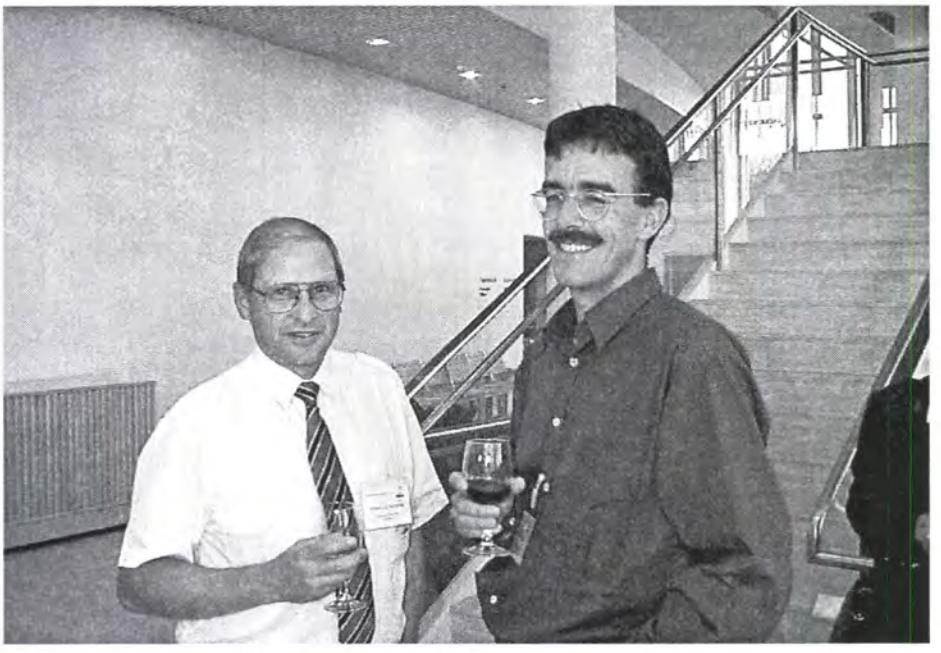

Göran Liljeström (left) and Christian Haas

Joachim Schwarz (left), Igor Stepanov, Yevgeny Mironov

Graden Betz (left), Bill Maddock, Lefteris Karaminas, Mikko Niini

Jarmo Savikurki (left) and Rubin Sheinberg

Torsten Heidemann (left), Kaj Riska, Eero Mäkinen

Nadja Lönnroth (left), Jan–Eric Lundqvist, Simo Kalliosaari, Jouni Vainio, Rashdal Gill

Lasse Makkonen (left), Sharon Jeffers, Robert Frederking

Richard Hayward (left), Orson Smith, Rashdal Gill, Simon Prinsenberg, André Maillet, Eila Lehmus, Mikko Lensu

Esko Voutilainen (left), Pekka Koskinen, Jorma Kämäräinen, Brian Veitch, Petri Valanto

Aino Laasonen (left), Juha Laasonen, Bin Cheng, Zhijun Li

Edmond Hansen (left), Jukka Kyröhonka, Jari Haapala